Slaviša Tomić

Master of Science

Target Localization and Tracking in Wireless Sensor Networks

Thesis submitted in partial fulfillment
of the requirements for the degree of

Doctor of Philosophy in
Electrical and Computer Engineering

Adviser:	Prof. Dr. Marko Beko, Professor Associado, ULHT
Co-adviser:	Prof. Dr. Rui Dinis, Professor Associado com Agregação, FCT-UNL

Examination Committee

Chairperson:	Prof. Dr. Paulo da Fonseca Pinto, FCT-UNL
Raporteurs:	Prof. Dr. Luís Cruz, FCT-UC
	Prof. Dr. João Pedro Gomes, IST-UL
Members:	Prof. Dr. Fernando Duarte Nunes, IST-UL
	Prof. Dr. Paulo Montezuma-Carvalho, FCT-UNL

FACULDADE DE CIÊNCIAS E TECNOLOGIA
UNIVERSIDADE NOVA DE LISBOA

Monte de Caparica, May 2017

Target Localization and Tracking in Wireless Sensor Networks

This document was created using the (pdf)LaTeX processor, based in the "unlthesis" template[1], developed at the Dep. Informática of FCT-NOVA [2].
[1] https://github.com/joaomlourenco/unlthesis [2] http://www.di.fct.unl.pt

To my nephews, Filip and David Kopanja. I hope that your future achievements will exceed by far those of your uncle.

Acknowledgements

I wish to express my sincere gratitude to my adviser, Professor Marko Beko, who brought me to FCT-UNL and gave me a chance to work in this excellent environment. Thank you for your guidance, motivation and support throughout my research career at FCT-UNL, but most of all thank you for being there for me whenever I needed your advice or a friendly talk. I have learned a lot from you, not only professionally, but also in my personal life.

I would also like to thank to my co-adviser, Professor Rui Dinis, for his constructive comments and opinions which helped improve the quality of this research work in a great deal. I was very fortunate to work with you.

Also, my sincere gratitude goes to Professor João Xavier and Professor Dragana Bajović, from whom I have learned a lot about non-linear optimization.

I would also like to thank to Professor Dragos Niculescu, Professor John-Austen Francisco and Maria Beatriz Quintino Ferreira for sharing unselfishly their experimental data with me. I know that you put in a lot of effort to carry out your experiments, and I am in debt with you for letting me use your data to test my algorithms with real indoor data.

There are many friends who enriched my life at FCT-UNL and Portugal. I have to emphasize the help I received from Miguel Luís and Francisco Ganhão, to whom I remain in eternal debt since the very first day I came to Portugal. I would also like to say thank you to my other dear officemates: Miguel Pereira, Filipe Ribeiro, João Guerreiro, António Furtado and Luís Irio. Furthermore, I thank to all my dear friends: Filipa Silva, Patrícia Duarte, Marta Soares, Luís Brazão, Carlos Dias, Pedro Domingos, André Falcão and Sérgio Carvalho, as well as to Filipe Dias, Mariana Oliveira, Sérgio Dias, Hugo Lopes and João Costa. Also, I thank to my dear roommates Hanson Tam, Tobias Linzmaier and Nils Bastek. Moreover, without listing names and taking the risk to forget someone, I would like to thank my dear friends from Angola and Portugal, with whom I have spent all these years playing sports and whose company I truly enjoyed. You all made me feel welcome in Portugal. Thank you!

Lastly, I would like to thank my family and friends from Serbia. Your love and support means a lot to me, and I would not be here without you. A special thanks to my dear friends Duško Linjak, Goran Radeka, Vladimir Nikolić, Darko Abramović, Ivana Vujičić, Jovana Ristić, Tijana Radivojević and Slobodan Radosavljević.

This research was supported by Fundação para a Ciência e a Tecnologia under the grant SFRH/BD/91126/2012.

Abstract

This thesis addresses the target localization problem in wireless sensor networks (WSNs) by employing statistical modeling and convex relaxation techniques. The first and the second part of the thesis focus on received signal strength (RSS)- and RSS-angle of arrival (AoA)-based target localization problem, respectively. Both non-cooperative and cooperative WSNs are investigated and various settings of the localization problem are of interest (*e.g.* known and unknown target transmit power, perfectly and imperfectly known path loss exponent). For all cases, maximum likelihood (ML) estimation problem is first formulated. The general idea is to tightly approximate the ML estimator by another one whose global solution is a *close* representation of the ML solution, but is easily obtained due to greater smoothness of the derived objective function. By applying certain relaxations, the solution to the derived estimator is readily obtained through general-purpose solvers. Both centralized (assumes existence of a central node that collects all measurements and carries out all necessary processing for network mapping) and distributed (each target determines its own location by iteratively solving a local representation of the derived estimator) algorithms are described. More specifically, in the case of centralized RSS-based localization, second-order cone programming (SOCP) and semidefinite programming (SDP) estimators are derived by applying SOCP and SDP relaxation techniques in non-cooperative and cooperative WSNs, respectively. It is also shown that the derived SOCP estimator can be extended for distributed implementation in cooperative WSNs. In the second part of the thesis, derivation procedure of a weighted least squares (WLS) estimator by converting the centralized non-cooperative RSS-AoA localization problem into a generalized trust region sub-problem (GTRS) framework, and an SDP estimator by applying SDP relaxations to the centralized cooperative RSS-AoA localization problem are described. Furthermore, a distributed SOCP estimator is developed, and an extension of the centralized WLS estimator for non-cooperative WSNs to distributed conduction in cooperative WSNs is also presented. The third part of the thesis is committed to RSS-AoA-based target tracking problem. Both cases of target tracking with fixed/static anchors and mobile sensors are investigated. First, the non-linear measurement model is *linearized* by applying Cartesian to polar coordinates conversion. Prior information extracted from target transition model is then added to the derived model, and by following maximum *a posteriori* (MAP)

criterion, a MAP algorithm is developed. Similarly, by taking advantage of the derived model and the prior knowledge, Kalman filter (KF) algorithm is designed. Moreover, by allowing sensor mobility, a simple navigation routine for sensors' movement management is described, which significantly enhances the estimation accuracy of the presented algorithms even for a reduced number of sensors.

The described algorithms are assessed and validated through simulation results and real indoor measurements.

Keywords: Target localization, target tracking, wireless sensor network, received signal strength (RSS), angle of arrival (AoA), convex optimization, maximum likelihood (ML) estimation, second-order cone programming (SOCP) problem, semidefinite programming (SDP) problem, generalized trust region sub-problem (GTRS), maximum *a posteriori* (MAP) estimator, Kalman filter (KF).

Resumo

Esta tese considera o problema de localização em redes sensoriais sem fios através do uso de modelos estatistícos e técnicas de optimização convexa. A primeira e segunda partes da tese são dedicadas ao problema de localização usando a potência do sinal recebido (RSS do Inglês Received Signal Strength) e RSS combinado com o âgulo do sinal recibido (AoA do Inglês Angle of Arrival), respectivamente. São consideradas redes cooperativas e não-cooperativas, bem como vários tipos de problemas de localização (*e.g.*, potência do sinal transmitido conhecida e desconhecida, conhecimento perfeito e imperfeito do factor de decaímento). Para todos os casos, começamos pela formulação do problema de máxima verosimilhança (ML do Inglês Maximum Likelihood). A ideia geral é aproximar o estimador de ML por um outro estimador cuja solução global é próxima da de ML, mas é obtida facilmente dada a natureza da sua função objetiva derivada. Aplicando certas relaxações, a solução do estimador derivado é obtida imediatamente através de algoritmos de uso propósito geral. São descritos algoritmos para as abordagens centralizada (assume existência de um nó central que combina todas as medições e implementa todo o processamento necessário para o posicionamento da rede) e distribuida (cada nó determina a sua própria posição resolvendo iterativamente um problema de posicionamento ao nível local). Mais especificamente, no caso de localização centralizada através da RSS, são derivados estimadores de programação cónica de segunda ordem (SOCP do Inglês Second-Order Cone Programming) e semi-definida (SDP do Inglês Semidefinite Programming), aplicando técnicas de relaxação SOCP e SDP em redes não-cooperativas e cooperativas, respectivamante. Também é mostrado que o estimador derivado SOCP pode ser generalizado para implementação distributiva em redes cooperativas. Na segunda parte da tese, é desenvolvido um estimador de mínimos quadrados ponderado (WLS do Inglês Weighted Least Squares), transformando o problema centralizado não-cooperativo baseado na RSS e AoA num subproblema generalizado de região de confiança (GTRS do Inglês Generalized Trust Region Sub-Problem), bem como um estimador SDP aplicando uma técnica de relaxação SDP ao problema centralizado cooperativo. Além disso, é descrito um estimador distributivo SOCP, tal como a extensão do estimador centralizado WLS para uma execução distributiva em redes cooperativas. A terceira parte da tese é dedicada ao problema de seguimento do alvo usando medições RSS e AoA. Os dois casos do problema do seguimento, com âncoras

fixas/estáticas e sensores móveis, são investigados. Para o efeito, começa-se por linearizar o modelo não-linear das medições, alterando entre coordenadas Cartesianas e polares. A informação prévia extraída dum modelo de transição do alvo é combinada ao modelo linearizado, e segundo o criterio de máxima probabilidade à posteriori (MAP do Inglês maximum a posteriori), dando origem a um estimador MAP. De igual modo, usando o modelo derivado e o conhecimento prévio, é desenvolvido um algoritmo baseado em filtragem de Kalman (KF do Inglês Kalman Filter). Além disso, é desenvolvido um algoritmo simples para gerir os movimentos dos sensores, permitindo lidar com a sua mobilidade. Esta rotina melhora significativamente a precisão de estimação dos algoritmos apresentados, mesmo para um número reduzido dos sensores.

Os algoritmos descritos são avaliados e validados através dos resultados de simulações e medições reais em ambientes interiores.

Palavras-chave: Localização de alvo, seguimento de alvo, redes sensoriais sem fios, potência de sinal recebido, ângulo de chegada de sinal recebido, optimização convexa, estimação máxima de verosimilhança, programação cónica de segunda ordem, programação semidefinida, sub-problema generalizado de região de confiança, máxima probabilidade à posteriori, filtragem Kalman.

Contents

List of Figures

List of Tables

Acronyms

AoA	angle of arrival.
BS	base station.
CDF	cumulative distribution function.
CRB	Cramer-Rao lower bound.
FIM	Fisher information matrix.
GNSS	global navigation satellite system.
GPS	global positioning system.
GTRS	generalized trust region sub-problem.
KF	Kalman filter.
LAN	local area network.
LE	localization error.
LoS	line-of-sight.
LS	least squares.
MAC	medium access control.
MAP	maximum *a posteriori*.

MDS	multidimensional scaling.
ME	mean error.
MEMS	micro-electro-mechanical systems.
ML	maximum likelihood.
NLoS	non-line-of-sight.
NRMSE	normalized root mean square error.
PDF	probability density function.
PF	particle filter.
PLE	Path loss exponent.
RF	radio frequency.
RMSE	root mean square error.
RSS	received signal strength.
RSSD	received signal strength difference.
RTT	round-trip time.
SDC	semidefinite cone.
SDP	semidefinite programming.
SoA	state of the art.
SOC	second-order cone.

SOCC	second-order cone constraint.
SOCP	second-order cone programming.
SR	squared range.
STD	standard deviation.
TDoA	time-difference of arrival.
ToA	time of arrival.
ToF	time of flight.
UT	unscented transformation.
WLAN	wireless local area network.
WLS	weighted least squares.
WSN	Wireless sensor network.

Nomenclature

For reference purposes, some of the most common symbols used throughout the thesis are listed below. Throughout the thesis, upper-case bold type, lower-case bold type and regular type are used for matrices, vectors and scalars, respectively.

$\mathbb{R}$	the set of real numbers
$\mathbb{R}^n$	n-dimensional real vectors
$\mathbb{R}^{m\times n}$	$m \times n$ real matrices
$[\boldsymbol{A}]_{ij}$	the ij-th element of $\boldsymbol{A}$
$\boldsymbol{A}^T$	the transpose of $\boldsymbol{A}$
$\boldsymbol{A}^{-1}$	the inverse of $\boldsymbol{A}$
$\mathrm{tr}(\boldsymbol{A})$	the trace of $\boldsymbol{A}$
$\boldsymbol{A} \succeq \boldsymbol{B}$	the matrix $\boldsymbol{A} - \boldsymbol{B}$ is positive semidefinite
$\boldsymbol{A} \otimes \boldsymbol{B}$	the Kronecker product of $\boldsymbol{A}$ and $\boldsymbol{A}$
$\boldsymbol{I}_n$	the $n \times n$ identity matrix
$\boldsymbol{0}_{m\times n}$	the $m \times n$ matrix of all zero entries
$\boldsymbol{1}_n$	the n-dimensional column vector with all entries equal to one
$\boldsymbol{e}_i$	the i-column of an identity matrix
$\mathrm{diag}(\boldsymbol{x})$	the square diagonal matrix with the elements of vector $\boldsymbol{x}$ as its main diagonal, and zero elements outside the main diagonal
$\|\boldsymbol{x}\|$	the Euclidean norm of vector $\boldsymbol{x}$; $\|\boldsymbol{x}\| = \sqrt{\boldsymbol{x}^T\boldsymbol{x}}$, where $\boldsymbol{x} \in \mathbb{R}^n$ is a column vector
$p(\cdot)$	probability density function
$\mathcal{N}(\boldsymbol{\mu}, \boldsymbol{\Sigma})$	real-valued Gaussian distribution with mean vector $\boldsymbol{\mu}$ and covariance matrix $\boldsymbol{\Sigma}$

$\sim$	distributed according to
$\approx$	approximately equal to
$\log_a(x)$	the base-a logarithm of x; when a is omitted it denotes the natural algorithm

CHAPTER 1

Introduction

1.1 Motivation

Wireless sensor network (WSN) generally refers to a wireless communication network which is composed of a number of devices, called sensors, allocated over a monitored region in order to measure some local quantity of interest [1]. Due to their autonomy in terms of human interaction and low device costs, WSNs find application in various areas, like event detection (fires, floods, hailstorms) [2], monitoring (industrial, agricultural, health care, environmental) [3, 4], energy-efficient routing [5], exploration (deep water, underground, outer space) [6], and surveillance [7] to name a few. Recent advances in radio frequency (RF) and micro-electro-mechanical systems (MEMS) permit the use of large-scale networks with hundreds or thousands of nodes [1].

In many practical applications (such as search and rescue, target tracking and detection, cooperative sensing and many more), data acquired inside a WSN are only relevant if the referred location is known. Moreover, accurate localization of people and objects in both indoor and outdoor environments enables new applications in emergency and commercial services (*e.g.* location-aware vehicles [8], asset management in warehouses [9], navigation [10–13], *etc.*) that can improve safety and efficiency in everyday life, since each individual device in the network can respond faster and *better* to the changes in the environment [14]. Therefore, accurate information about sensors' locations is a valuable resource, which offers additional knowledge to the user.

However, sensors are small, low cost and low power nodes commonly deployed in a large number over a region of interest with limited to non-existing control of their location in space, *e.g.* thrown out of an aeroplane for sensing in hostile environments [15]. Besides sensing, sensors have a limited (due to their battery life) capability of communicating and processing the acquired data. Installing a global positioning system (GPS) receiver in

each sensor is a possible solution, but it would severely augment the network costs and restrict its applicability [16]. Besides, GPS is ineffective in indoor, dense urban and forest environments or canyons [17]. In order to maintain low implementation costs, only a small fraction of sensors are equipped with GPS receivers (called anchors), while the remaining ones (called targets) determine their locations by using a kind of localization scheme that takes advantage of the known anchor locations [18]. Since the sensors have minimal processing capabilities, the key requirement is to develop localization algorithms that are fast, scalable and abstemious in their computational and communication requirements. Also, making use of existing technologies (such as terrestrial RF sources) when providing a solution to the object localization problem is strongly encouraged. Nevertheless, WSNs are subject to changes in topology (*e.g.* node mobility, adding nodes, node and/or link failures), which aggravates the development of even the simplest algorithms.

The idea of wireless positioning was initially conceived for cellular networks, since it invokes many innovative applications and services for its users. Nowadays, rapid increase of heterogeneous smart-devices (mobile phones, tablets) which offer self-sustained applications and seamless interfaces to various wireless networks is pushing the role of the location information to become a crucial component for mobile context-aware applications [18]. Even though we limit our discussion to sensor localization in WSN here, it is worth noting that, in practice, a base station (BS) or an access point in local area network (LAN) can be considered as an anchor, while other devices such as cell phones, laptops, tags, *etc.*, can be considered as targets.

1.2 Localization Schemes

Nowadays, RF signals come from a wide variety of sources and technologies, and they can be used for localization purpose. Location information can be obtained by range-based or range-free measurements. Here, the focus is on the former ones exclusively, since they provide higher estimation accuracy in general. Hence, the locations of the targets in a WSN are determined by using a kind of localization scheme that relies on the known locations of the anchors and range measurements between targets and anchors. Range measurements can be extracted from different characteristics of the radio signal, such as time of arrival (ToA) [19], time-difference of arrival (TDoA) [20], round-trip time (RTT), time of flight (ToF) [21], angle of arrival (AoA) [22] or received signal strength (RSS) [23, 24], depending on the available hardware. The trade-off between the localization accuracy and the implementation complexity of each technique is a very important factor when deciding which method to employ. For example, localization based on ToA or TDoA (including the GPS) gives high estimation accuracy, but requires a very complex process of timing and synchronization, thus making the localization cost-expensive [25]. Although less accurate than the localization using ToA, TDoA or AoA information, localization based on the RSS measurements requires no specialized hardware, less processing and communication (and consequently, lower energy), thus making it an attractive low-cost

solution for the localization problem [1, 16]. Another attractive low-cost approach might be exploiting RTT measurements, which are easily obtained in wireless local area network (WLAN) systems by using a simple device such as a printed circuit board [26]. Even though RTT systems circumvent the problem of clock synchronization between nodes, the major drawback of this approach is the need for double signal transmission in order to perform a single measurement [27].

Recently, hybrid systems that fuse two measurements of the radio signal have been investigated [26, 28–38]. Hybrid systems profit by exploiting the benefits of combined measurements (more available information), taking advantage of the strongest points of each technique and minimizing their drawbacks. On the other hand, the price to pay for using such systems is the increased complexity of network devices, which increases the network implementation costs [1, 16].

In order to acquire the necessary measurements, node communication is required, which can be non-cooperative or cooperative [18]. The former one allows targets to communicate with the anchors exclusively, Fig. 1.1a, while the latter one allows targets to communicate with all sensors inside their communication range, whether they are anchors or targets, Fig. 1.1b.

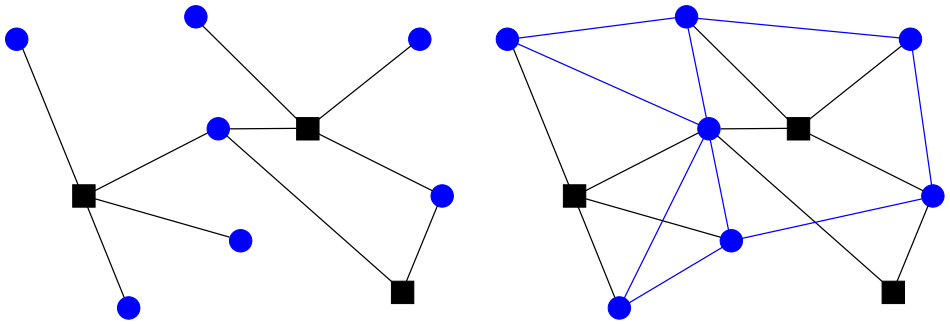

(a) Non-cooperative WSN (b) Cooperative WSN

Figure 1.1: Example of a WSN with three anchors (black squares) and seven targets (blue circles).

Typically, data processing inherent to localization schemes can be performed in a centralized (network-centric positioning) or a distributed (self-positioning) fashion [18]. On the one hand, existence of a central processor (sensor or a BS) is required for the former approach. Central processor gathers all measurements via wireless transmissions and produces a map of the entire network [30]-[33]. This approach is characterized by fundamental optimality and stability [18]. However, in large-scale networks, a high energy drain is likely to occur at and near the central processor, caused by bottlenecks [16]. Likewise, computational complexity of a centralized approach depends highly on the network size. In many applications a central processor (or one with enough computational capacity) is not available. Furthermore, confidentiality may prevent sharing objective functions between

sensors in some practical applications [39]. On the other hand, the latter approach is distinguished by low computational complexity and high-scalability, which makes it a preferable solution for large-scale and highly-dense networks [18]. However, distributed algorithms are executed iteratively, which makes them sensitive to error propagation and raises energy consumption. When determining which approach to use for a given application, one has to take into consideration all of the above properties, but if often comes down to efficiency comparison in terms of energy consumtpion. In general, when the average number of hops to the central processor is higher than the necessary number of iterations required for convergence, the distributed approach is likely to be more energy-efficient and vice versa [1].

1.2.1 Overview of Localization Techniques

A detailed survey on localization algorithms can be found in [40], and a brief overview of the state of the art (SoA) related with each chapter's discussion will be provided at the beginning of each chapter. Here, a general overview of the most commonly used localization techniques is presented.

Range-free Localization

The most commonly used range-free localization technique is fingerprinting. Generally, it can be described as a multiple hypothesis testing decision problem, where the objective is to deduce the best hypothesis (location of the target) based on previously acquired observations, *i.e.*, fingerprints. In practice, a fingerprinting localization method requires two phases: the training and the localization phase. During the training phase, fingerprints are collected at all sample locations [41]. During the localization phase, an obtained radio measurement is compared with all observations collected at sample locations, and the best fit sample location is taken as the estimated target location.

On the one hand, the main advantage of this technique is the flexibility to any radio interface. On the other hand, the localization accuracy depends on the reliability (quantity and up-to-date) of the training data, the error in the synthesis of the fingerprint parameters, and the sensitivity of the algorithm to changes of the environment.

To improve the robustness of the location estimation with respect to the inaccuracy of training data, several techniques are proposed in the literature. For instance, in [42] statistical learning is used to design an algorithm based on support vector machine.

Range-based Localization

Range-based localization technique is widely used nowadays owing to its potentially high accuracy, applicability to different radio technologies and ease of implementation. Within this approach, one can distinguish between range and range-difference based methods. Some of the most popular range-based localization techniques are briefly described in the following text.

Global Navigation Satellite System. A very popular way for determining target's location nowadays is through a global navigation satellite system (GNSS). It can deliver to its user the latitude and longitude position in real-time [1]. GNSS utilizes satellites orbiting the Earth, which broadcast signals using very precise frequencies and highly-accurate atomic clocks for time measurements. Any receiver on the ground can pick up the GNSS signal as long they are codded to read its signal. As the GNSS signals travel through the Earth's atmosphere, they can become distorted, leading to a reduced positional accuracy delivered to the receiver. Also, GNSS signals that are low on the horizon, *i.e.*, the ones that have low zenith are more likely to deliver error because they are traveling through more atmosphere. GNSS uses groups of satellites, called constellations, for their systems, see Fig. 1.2. For a receiver to establish its location, it must be able to pick up a signal from at least four of the satellites [43]. Currently, there are two globally operational GNSSs: American GPS (constellation of 32 satellites, fully operational since 1995) and Russian GLONASS (constellation of 24 satellites, restored in 2011). Also, The European Union's Galileo GNSS, as well as China's BeiDou-2 GNSS are scheduled to be fully operational by 2020. These systems can be used for providing location, navigation or for tracking the location of a receiver. The signals also allow the electronic receiver to calculate the current local time to high precision, which allows time synchronization. Although technologies like telephonic or internet reception could be used to further enhance the localization performance of GNSSs, they usually operate independently of any of them. Also, even though these systems represent today a standard solution for outdoor localization, they have very limited or no functionality in harsh propagation environments, such as dense urban, underground, underwater and indoor to name a few [43].

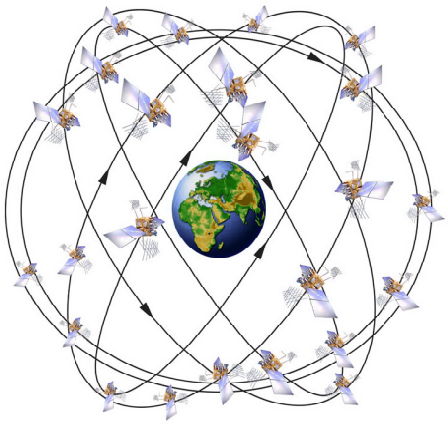

Figure 1.2: Example of a GNSS constellation.

Geometric-based Techniques. In the case where the noise is absent and the number of anchors is low, geometric-based techniques are appealing owing to their simplicity. Some basic and intuitive geometric methods are trilateration, triangulation and multilateration. Trilateration technique makes use of distance measurement and known location of anchor to describe a circle around the anchor with the radius equal to distance measurement [44].

Then, by using at least three anchors in 2-dimensional space, it locates the target by calculating the intersection of the circles based on simultaneous range measurements from anchors, Fig.1.3a. Triangulation is used when the direction of target instead of the distance is estimated, Fig.1.3b. The target location is determined by using the trigonometry laws of sine and cosine [45]. Multilateration is a technique based on the measurement of the difference in distance to two or more anchors which form a hyperbolic curve [46]. The intersection of the hyperbolas, corresponding to the TDoA measurements, determines the position of the target, Fig.1.3c.

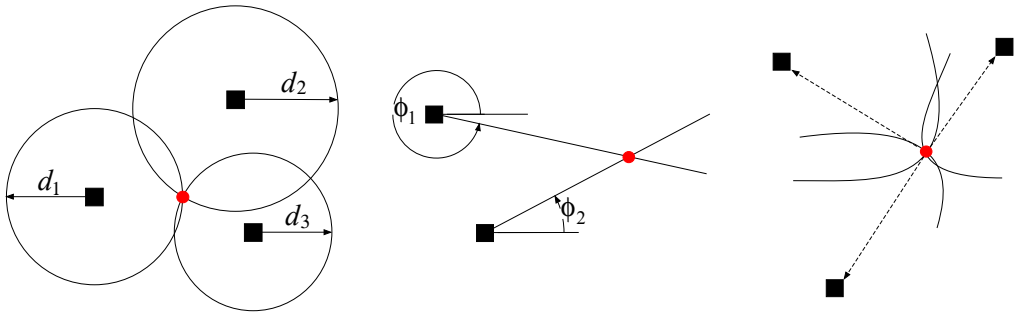

(a) Trilateration (b) Triangulation (c) Multilateration

Figure 1.3: Illustration of geometric localization techniques.

In practice however, due to noise in radio measurements, the position lines intersect at multiple points instead of a single one. In this case, geometric approach does not provide a useful insight as to which intersection point to choose as the location of the target.

Optimization-based Techniques. If data are known to be well described by a certain statistical model, then the maximum likelihood (ML) estimator can be derived and implemented. This is because the variance of these estimators approaches asymptotically (as the signal-to-noise ratio goes high) a lower bound given by the Cramer-Rao lower bound (CRB) [47]. Typically, ML solutions are obtained as the global minimum of the non-convex objective function which is directly derived from the likelihood function of the problem. Even though a closed form ML solution is not possible because of non-linear dependence between the measurements and the unknown parameters, approximate and iterative ML techniques can be derived.

Recursive methods, such as Newton's method, combined with gradient descent method, are often used [47]. However, the objective function may have many local optima, and local search methods may easily get trapped in a local optimum. To overcome this difficulty, and possibly provide a good initial point (close to the global minimum) for the iterative algorithms, approaches such as grid search methods, linear estimators, and convex relaxation techniques have been introduced to address the ML problem [48–56]. Grid search methods solve the localization problem by forming a grid and pasing each point of the grid through the ML objective function to find the one resulting in its minimum value. These methods are time-consuming, their accuracy and computational complexity are directly

proportional to the grid size and require a huge amount of memory when the number of the unknown parameters is too large. Linear estimators are very efficient in the sense of time-consumption and computational complexity, but they are derived based on many approximations which may severely affect their performance, especially in the case when the noise is large [52]. Convex relaxation techniques overcome the difficulties in the ML problem by transforming the original non-convex and non-linear problem into a convex one. The advantage of this approach is that the convergence to the globally optimal solution is guaranteed. However, due to application of relaxation techniques, the solution of a convex problem does not necessarily correspond to the solution of the original ML problem [57].

1.3 Research Question and General Approach

In this thesis, we investigate both RSS- and combined RSS-AoA-based target localization problems in non-cooperative and cooperative WSNs, and we consider both centralized and distributed types of algorithm execution. Furthermore, we also study the target tracking problem by taking advantage of coupled, RSS and AoA, measurements for both cases of fixed anchors and mobile sensors. In addition, various settings of the localization problem are of interest, such as:

- Only target's coordinates are not known;
- Target's coordinates and transmit power are simultaneously not known;
- Path loss exponent (PLE) is perfectly and imperfectly known;
- Synchronous node communication managed by a central node or by a kind of medium access control (MAC) protocol;
- Distinct target trajectories in the case of target tracking;
- Different velocities of the mobile sensors.

Moreover, in practice, WSNs are subject to changes in topology (*e.g.*, node and/or link failure) and in indoor and highly dense urban environments, mixture of line-of-sight (LoS) and non-line-of-sight (NLoS) links is likely to occur. Also, energy resources are often limited by sensor's battery, and the quality of the measurements by hardware imperfections and noise.

These advents and restrictions aggravate considerably the development of even the simplest algorithms. Therefore, by taking all of the mentioned challenges into consideration, the main research question of this thesis is:

> *How to design an efficient (highly accurate and computationally low-complex) localization algorithm, robust to network topology and channel characteristics, easily adaptable to different settings of the localization problem, applicable in real-time?*

To address the above research question, the research presented in the thesis commenced from the following hypothesis.

> *An efficient localization algorithm can be developed by using statistical modelling and convex optimization tools in order to tightly approximate the original non-linear and non-convex localization problem into a convex one. In addition, node cooperation and MAC schemes can be exploited in order to obtain a sufficient amount of information and prevent message collision (re-transmission), respectively. Also, by careful development of weighting strategy, the influence of potentially bad links can be minimized and the influence of potentially good ones enhanced. Furthermore, by integrating prior knowledge within an estimator and by designing a sensors navigation routine, the performance of an estimator can be improved significantly.*

Simulation and experimental results provided within the thesis, as well as a notable number of publications that have arisen from it, verify the probity of the above hypothesis.

1.4 Thesis Outline and Contributions

The thesis is organized into 4 chapters. We summarize the content of each chapter, besides the current one which gives the motivation and outline of this dissertation. Since the thesis is based on ardent and dedicated research which resulted in several publications in international journals and conferences, and book chapters, for each chapter, we also refer the publications (journal papers (J), books (B), book chapters (BC), conference papers (C), and patents (P)) that it has given rise.

In more detail, the outline and the original contributions of this thesis are as follows.

> *Chapter 2. RSS-based Target Localization*: In this chapter, RSS-based target localization problem for both non-cooperative and cooperative scenarios is considered. To solve original non-linear and non-convex localization problem, a sub-optimal approach that provides efficient solution is applied. More specifically, a non-convex least squares (LS) estimator which tightly approximates the ML one for small noise, but represents a smoother and simpler problem in comparison to the ML problem is introduced. By applying appropriate convex relaxations to the derived non-convex estimator, a second-order cone programming (SOCP) and mixed semidefinite programming (SDP)/SOCP estimators are developed for non-cooperative and cooperative localization cases, respectively. Our approach offers advantage over the existing ones as it allows straightforward adaptation to different scenarios of the RSS localization problem, thereby significantly reducing the estimation error. In Section 2.3, the centralized SOCP estimator is extended to distributed execution by letting each target to localize itself with the use of local information only. Consensus algorithm for finding an estimate of the transmit power and a simple coloring scheme for avoiding

message re-transmission are applied. Finally, a heuristic approach which improves the convergence rate of the new algorithm is discussed.

Publications. The results of this work have been published in:

J1 S. Tomic, M. Beko, and R. Dinis, "Distributed RSS-Based Localization in Wireless Sensor Networks Based on Second-Order Cone Programming," *Sensors*, vol. 14, no. 10, pp. 18410–18432, Oct. 2014.

J2 S. Tomic, M. Beko, and R. Dinis, "RSS-based Localization in Wireless Sensor Networks Using Convex Relaxation: Noncooperative and Cooperative Schemes," *IEEE Trans. Veh. Technol.,* vol. 64, no. 5, pp. 2037–2050, May 2015.

C1 S. Tomic, M. Beko, R. Dinis, V. Lipovac, "RSS-based Localization in Wireless Sensor Networks using SOCP Relaxation," In Proc. *IEEE 14th Workshop on Signal Processing Advances in Wireless Communications (SPAWC)*, Darmstadt, Germany, June 16-19, 2013.

C2 S. Tomic, M. Beko, R. Dinis, V. Lipovac, G. Dimic, "RSS-based Localization in Wireless Sensor Networks with Unknown Transmit Power and Path Loss Exponent using SDP Relaxation," In Proc. *WSEAS International Conference on Applied Electromagnetics, Wireless and Optical Communications (ELECTROSCIENCE)*, Dubrovnik, Croatia, June 25-27, 2013.

C3 S. Tomic, M. Beko, R. Dinis, M. Raspopovic, "Distributed RSS-based Localization in Wireless Sensor Networks using Convex Relaxation," In Proc. *International Conference on Computing, Networking and Communications (ICCNC)*, Hawaii, USA, February 3-6, 2014.

C4 S. Tomic, M. Beko, R. Dinis, M. Raspopovic, "Distributed RSS-based Localization in Wireless Sensor Networks with Asynchronous Node Communication," In Proc. *5th Doctoral Conference on Computing, Electrical and Industrial Systems (DoCEIS)*, Caparica, Portugal, April 7-9, 2014.

C5 S. Tomic, M. Marikj, M. Beko, R. Dinis, M. Raspopovic, R.Sendelj, "Energy-efficient Distributed RSS-based Localization in Wireless Sensor Networks Using Convex Relaxation," In Proc. *6th International ICT Forum*, Nis, Serbia, October 14-16, 2014.

C6 S. Tomic, M. Beko, R. Dinis, G. Dimic, M. Tuba, "Distributed RSS-based Localization in Wireless Sensor Networks with Node Selection Mechanism," In Proc. *6th Doctoral Conference on Computing, Electrical and Industrial Systems (DoCEIS)*, Caparica, Portugal, April 13-15, 2015.

C7 S. Tomic, M. Beko, R. Dinis, V. Lipovac, "Efficient Estimator for Distributed RSS-based Localization in Wireless Sensor Networks," In Proc. *International Wireless Communications and Mobile Computing Conference (IWCMC)*, Dubrovnik, Croatia, August 24-28, 2015.

Chapter 3. RSS-AoA-based Target Localization: This chapter tackles the target localization problem by measurement fusion. More precisely, hybrid RSS and AoA measurements are integrated in order to enhance the estimation accuracy in comparison with *traditional* approach. By using the RSS propagation model and simple geometry, a novel objective function based on the LS criterion is derived. For non-cooperative and cooperative WSN, the objective function is then transformed into a generalized trust region sub-problem (GTRS) and an SDP framework, respectively. Moreover, the original non-convex target localization problem is broken down into local sub-problems, which are converted into convex problems by applying SOCP relaxation technique. By solving this tight approximation of the original problem, each target estimates its own location, resorting only to local information from one-hop neighbors by following our described iterative procedure. Besides excellent trade-off between accuracy and computational cost, the new algorithms have a big advantage over existing approaches as their adaptation to different settings of the localization problem is straightforward.

Publications. The results of this work have been published in:

J3 S. Tomic, M. Beko and R. Dinis, "3-D Target Localization in Wireless Sensor Network Using RSS and AoA Measurement," *IEEE Trans. Vehic. Technol.,* vol. 66, no. 4, pp. 3197-3210, Apr. 2017.

J4 S. Tomic, M. Beko, and R. Dinis, "Distributed RSS-AoA Based Localization with Unknown Transmit Powers," *IEEE Wirel. Commun. Letters*, vol. 5, no. 4, pp. 392–395, Aug. 2016.

J5 S. Tomic, M. Beko, and R. Dinis, "Distributed Algorithm for Target Localization in Wireless Sensor Networks Using RSS and AoA Measurements," *Elsevier Journal on Pervasive and Mobile Computing*, vol. 37, pp. 63–77, Jun. 2017.

J6 S. Tomic, M. Beko, and R. Dinis, "A Closed-form Solution for RSS/AoA Target Localization by Spherical Coordinates Conversion," *IEEE Wirel. Commun. Letters*, vol. 5, no. 6, pp. 680–683, Dec. 2016.

B1 S. Tomic, M. Beko, R. Dinis, M. Tuba, N. Bacanin. *RSS-AoA-based Target Localization and Tracking in Wireless Sensor Networks.* Forthcoming, River Publishers Series in Communications, River Publishers, ISBN: 9788793519886, June 2017.

B2 D. Vicente, S. Tomic, M. Beko. *Distributed Algorithms for Target Localization in WSNs Using RSS and AoA Measurement.* Forthcoming, Lambert Academic Publishing, ISBN: 9783330085107.

P1 M. Beko, S. Tomic, R. Dinis, and P. Montezuma, "Método de Geolocalização 3-D em Redes de Sensores sem Fio não Cooperativas," PT, no. 108735, 2015, pending; published in the Industrial Property Bulletin no. 21/2017.

P2 M. Beko, S. Tomic, R. Dinis, and P. Montezuma, "Método para Localização Tridimensional de Nós Alvo numa Rede de Sensores sem Fio Baseado em Medições de Potência Recebida e Angulos de Chegada do Sinal Recebido," PT, no. 108963, 2015, pending.

P3 M. Beko, S. Tomic, R. Dinis, and P. Montezuma, "Method for RSS/AoA Target 3-D Localization in Wireless Networks," USA, no. 15287880, 2016, pending.

BC1 S. Tomic, M. Beko, and R. Dinis, "Hybrid RSS/AoA-based Localization of Target Nodes in a 3-D Wireless Sensor Network," *Sensors & Signals*, Eds. S. Y. Yurish, A. D. Malayeri: pp. 71–85, ISBN: 978-84-608-2320-9, Book Series, IFSA Publishing, 2015.

BC2 S. Tomic, M. Beko, and R. Dinis, "Target Localization in Cooperative Wireless Sensor Networks Using Measurement Fusion," *Advances in Sensors: Reviews. Transducers, Signal Conditioning and Wireless Sensors Networks*, Ed. S. Y. Yurish: pp. 329–344, ISBN: 978-84-608-7705-9, Book Series, Vol. 3, IFSA Publishing, 2016.

BC3 S. Tomic, M. Beko, and R. Dinis, "Distributed Algorithm for Multiple Target Localization in Wireless Sensor Networks Using Combined Measurements," *Advances in Sensors: Reviews. Sensors and Applications in Measuring and Automation Control Systems*, Ed. S. Y. Yurish: pp. 263–275, ISBN: 978-84-617-7596-5, Book Series, Vol. 4, IFSA Publishing, 2017.

C8 S. Tomic, M. Marikj, M. Beko, R. Dinis, "Hybrid RSS-AoA Technique for 3-D Node Localization in Wireless Sensor Networks," In Proc. *International Wireless Communications and Mobile Computing Conference (IWCMC)*, Dubrovnik, Croatia, August 24-28, 2015.

C9 S. Tomic, M. Beko, R. Dinis, L. Berbakov, "Cooperative Localization in Wireless Sensor Networks Using Combined Measurements," In Proc. *Telecommunications Forum (TELFOR)*, Belgrade, Serbia, November 24-26, 2015.

C10 S. Tomic, M. Beko, R. Dinis, M. Tuba, "A WLS Estimator for Target Localization in a Cooperative Wireless Sensor Network," In Proc. *7th Doctoral Conference on Computing, Electrical and Industrial Systems (DoCEIS)*, Caparica, Portugal, April 11-13, 2016.

C11 S. Tomic, M. Beko, R. Dinis, M. Tuba, N. Bacanin, "An Efficient WLS Estimator for Target Localization in Wireless Sensor Networks," In Proc. *Telecommunications Forum (TELFOR)*, Belgrade, Serbia, November 22-23, 2016.

Chapter 4. RSS-AoA-based Target Tracking: In this chapter, RSS-AoA-based target tracking problem is investigated. By applying Bayesian approach, prior knowledge given by state transition model is combined with observations, and the tracking problem via maximum *a posteriori* (MAP) criterion is formulated. Novel relationships

between the unknown target location and gathered measurements are established by applying Cartesian to polar coordinates conversion, which results in efficient *linearization* of the highly non-linear observation model. By taking advantage of the *linearized* observation model and following the MAP criterion and Kalman filter (KF) recipe, novel MAP and KF algorithms are derived which efficiently solve the target tracking problem with static anchors. The target tracking problem is then extended to the case where the target transmit power is not known. Also, the case where sensors' mobility is granted is studied, and a simple navigation routine is developed, which additionally betters the estimation accuracy, even for lower number of sensors.

Publications. The results of this work have been submitted to:

J7 S. Tomic, M. Beko, and R. Dinis, "Bayesian Methodology for Target Tracking Using RSS and AoA Measurements," Submitted to *Elsevier Journal on Ad Hoc Networks,* Dec. 2016.

J8 S. Tomic, M. Beko, and R. Dinis, "Target Tracking With Sensor Navigation Using Coupled RSS and AoA Measurements," Submitted to *Elsevier Journal on Signal Processing,* Dec. 2016.

C12 S. Tomic, M. Beko, R.Dinis, M. Tuba, and N.Bacanin, "MAP Estimator for Target Tracking in Wireless Sensor Networks for Unknown Transmit Power," In Proc. *8th Doctoral Conference on Computing, Electrical and Industrial Systems (DoCEIS)*, Caparica, Portugal, May 03-05, 2017.

C13 S. Tomic, M. Beko, R.Dinis, M. Tuba, and N.Bacanin, "Kalman Filter for Target Tracking Using Combined RSS and AoA Measurements," To appear in *13th International Wireless Communications and Mobile Computing Conference (IWCMC)*, Valencia, Spain, June 26-30, 2017.

Chapter 5. Conclusions and Future Work: This chapter concludes the thesis, by summarizing the main obtained results and enumerating the future lines of work.

CHAPTER 2

RSS-based Target Localization

2.1 Chapter Summary

This chapter addresses the problem of target localization by using RSS measurements. It is organized into two main sections in which we investigate both centralized, Section 2.2, and distributed, Section 2.3, localization problem, respectively. More specifically, the remainder of the chapter is organized as follows.

Section 2.2.1 offers an overview of the related work in the area of RSS-based target localization, as well as our contributions in that area. In Section 2.2.2, the RSS measurement model for locating a single target is introduced, centralized target localization problem is formulated for the case of known target transmit power and development of our centralized SOCP estimator is presented. We then extend this approach for the case where P_T, and P_T and PLE are simultaneously unknown. Section 2.2.3 introduces the RSS measurement model for the cooperative localization where multiple targets are located simultaneously. We provide a formulation of the centralized cooperative localization problem and provide details about the development of our SDP estimators for both cases of known and unknown target transmit power. The complexity analysis is summarized in Section 2.2.4. In Section 2.2.5 we provide both complexity and simulation results to compare the performance of our estimators with existing ones. Finally, in Section 2.2.6 we summarize the main conclusions regarding the centralized RSS-based localization problem.

Section 2.3.1 relates the SoA of the distributed RSS-based localization problem, and sums up our contributions in the area. In Section 2.3.2 the local ML optimization problem for locating multiple targets is formulated. Section 2.3.3 provides details about the development of our distributed SOCP estimator for both cases of known and unknown P_T. Computational complexity and energy consumption analysis are summarized in Section 2.3.4. In Section 2.3.5 we provide computational complexity, energy consumption and

simulation results to compare the performance of our distributed estimator with existing ones. Finally, in Section 2.3.6 we summarize the main conclusions regarding the distributed RSS-based localization problem.

2.2 Centralized RSS-based Target Localization

2.2.1 Related Work

Target localization based on the RSS measurements has recently attracted much attention in the wireless communications community [48–56]. The most popular estimator used in practice is the ML estimator, since it is asymptotically efficient (for large enough data records) [47]. However, solving the ML estimator of the RSS-based localization problem is a very difficult task, because it is highly non-linear and noncovex [16], hence it may have multiple local optima. In this case, search for the globally optimal solution is very hard via iterative algorithms, since they may converge to a local minimum or a saddle point resulting in a large estimation error. To overcome this difficulty, and possibly provide a good initial point (close to the global minimum) for the iterative algorithms, approaches such as grid search methods, linear estimators, and convex relaxation techniques have been introduced to address the ML problem [48–56]. The grid search methods are time-consuming and require huge amount of memory when the number of the unknown parameters is too large. Linear estimators are very efficient in the sense of time-consumption, but they are derived based on many approximations which may affect their performance, especially in the case when the noise is large [52]. In convex relaxation techniques such as the ones of [50]-[56], the difficulties in the ML problem are overcome by transforming the original non-convex and non-linear problem into a convex one. The advantage of this approach is that the convergence to the globally optimal solution is guaranteed. However, due to the use of relaxation techniques, the solution of a convex problem does not necessarily correspond to the solution of the original ML problem [57].

In [48], different weighting schemes for multidimensional scaling (MDS) formulation were presented and compared. It was shown that the solution of the MDS can be used as the initial value for iterative algorithms, which then converge faster and attain higher accuracy when compared with random initial values. Convex SDP estimators were proposed in [50] to address the non-convexity of the ML estimator, for both non-cooperative and cooperative localization problems with known target transmit power, P_T. The authors in [50] reformulate the localization problem by eliminating the logarithms in the ML formulation and approaching the localization problem as a minimax optimization one, which is then relaxed as an SDP. Even though the approach described in [50] provides good estimation results, especially for the case of cooperative localization, it has high computational complexity, which might restrict its application in large scale WSNs. In [51], the RSS-based localization problem for known P_T was formulated as a weighted least squares (WLS) problem, based on unscented transformation (UT). It was shown that for

the cooperative localization, the WLS formulation can be relaxed as a mixed SDP/SOCP, whereas for the non-cooperative localization, the WLS problem can be solved by a bisection method. In [54], Wang *et al.* addressed the non-cooperative RSS localization problem for the case of unknown P_T and the PLE. For the case of unknown P_T, based on the UT, a WLS formulation of the problem is derived, which was solved by the bisection method. When both P_T and PLE are not known, an alternating estimation procedure is introduced. However, both [51] and [54] have the assumption of perfect knowledge of the noise standard deviation (STD). This might not be the case in practice, especially in low-cost systems such as RSS where calibration is avoided due to maintaining low system costs [1, 16]. In [56], Vaghefi *et al.* addressed the RSS cooperative localization problem for unknown P_T. The case where the targets have different P_T (*e.g.*, due to different antenna gains) was considered in [56]. The authors solved the localization problem by applying an SDP relaxation technique, and converting the original ML problem into a convex one. Furthermore, in [56] the authors examined the effect of imperfect knowledge of the PLE on the performance of the SDP algorithm, and used an iterative procedure to solve the problem when P_T and PLE are simultaneously unknown.

Contributions

In this thesis, the RSS-based target localization problem for both non-cooperative and cooperative scenarios is considered. Instead of solving the ML problem, which is highly non-convex and computationally exhausting to solve globally, we propose a suboptimal approach that provides efficient solution. Hence, we introduce a new non-convex LS estimator which tightly approximates the ML one for small noise. This estimator represents a smoother and simpler localization problem in comparison with the ML one. Applying appropriate convex relaxations to the derived non-convex estimator, novel SOCP and novel mixed SDP/SOCP estimators are proposed for non-cooperative and cooperative localization cases, respectively.

The proposed approach offers an advantage over the existing ones as it allows straightforward adaptation to different scenarios of the RSS localization problem, thereby significantly reducing the estimation error. In both non-cooperative and cooperative scenarios, we first consider the simplest case of the localization problem where P_T is known at the anchors. Next, we consider a more realistic scenario in which we assume that P_T is an unknown parameter and we generalize our approaches for this setting. Finally, we investigate the most challenging scenario of the localization problem when P_T and PLE are simultaneously unknown at the anchors. In this case, for the non-cooperative localization, we apply an iterative procedure based on the proposed SOCP method in order to estimate all unknown parameters. We also provide details about the computational complexity of the considered algorithms.

In contrast to [50, 51], where the authors consider the localization problem for the case when P_T is known, here we address a more challenging scenario when both P_T and PLE are

not known. In [51, 54] the authors assume that the accurate knowledge of the noise STD is available, which might not be a valid assumption in some practical scenarios. Hence, we consider a more realistic scenario in which the noise STD is not available. In contrast to [56] where an SDP estimator is derived for the case of unknown P_T, we derive our estimators by using SOCP relaxation for the non-cooperative case and mixed SDP/SOCP relaxation for the cooperative case.

2.2.2 Non-cooperative Localization via SOCP relaxation

Let us consider a WSN with N anchors and one target, where the locations of the anchors are respectively denoted by $\boldsymbol{a}_1$, $\boldsymbol{a}_2$, ..., $\boldsymbol{a}_N$ and the location of the unknown target is denoted by $\boldsymbol{x}$. Without loss of generality, this section focuses on the 2-D scenario, *i.e.*, $\boldsymbol{x}, \boldsymbol{a}_1, \boldsymbol{a}_2, ..., \boldsymbol{a}_N \in \mathbb{R}^2$ (the extension for a 3-D scenario is straightforward). For the sake of simplicity, we assume that all anchors are equipped with omnidirectional antennas and connected to the target. Further, it is assumed that the anchor locations are known. The RSS model between the target and the i-th anchor is defined as [58, 59]

$$P_i(\text{dBm}) = P_0 - 10\gamma \log_{10} \frac{\|\boldsymbol{x} - \boldsymbol{a}_i\|}{d_0} + v_i, \text{ for } i = 1, ..., N, \tag{2.1}$$

where P_0 (dBm) represents the power received at a short reference distance d_0 ($d_0 \leq \|\boldsymbol{x} - \boldsymbol{a}_i\|$), γ is the PLE, and v_i is the log-normal shadowing term modeled as a zero-mean Gaussian random variable with variance σ_i^2, *i.e.*, $v_i \sim \mathcal{N}(0, \sigma_i^2)$. The model has been validated by a variety of measurement results [59]-[60].

Based on the measurements in (2.1) and Gaussian noise assumption, the ML estimator is found by solving the non-linear and non-convex LS problem when the noise is Gaussian

$$\hat{\boldsymbol{x}} = \arg\min_{\boldsymbol{x}} \sum_{i=1}^{N} \frac{1}{\sigma_i^2} \left[P_i - P_0 + 10\gamma \log_{10} \frac{\|\boldsymbol{x} - \boldsymbol{a}_i\|}{d_0} \right]^2. \tag{2.2}$$

To solve (2.2), recursive methods, such as Newton's method, combined with gradient descent method, are often used [47]. However, the objective function may have many local optima, and local search methods may easily get trapped in a local optimum. Hence, in this thesis, we employ convex relaxation to address the non-convexity of the localization problem.

In the remainder of this section, we deal with the case where P_T is known, with the case where P_T is considered to be an unknown parameter that needs to be estimated, and a more general problem when P_T and PLE are simultaneously unknown.

Non-cooperative scenario with known P_T

The target might be designed to measure and report its own calibration data to the anchors, in which case it is reasonable to assume that the target transmission power is known [16]. This corresponds to the case when the reference power P_0, which depends on P_T [58], is known.

For the sake of simplicity, in the rest of the section, we assume that $\sigma_i^2 = \sigma^2$, for $i = 1, ..., N$. When the noise term is sufficiently small, from (2.1) we get

$$\alpha_i \|\boldsymbol{x} - \boldsymbol{a}_i\| \approx d_0, \tag{2.3}$$

where $\alpha_i = 10^{\frac{P_i - P_0}{10\gamma}}$. One way for estimating the target location $\boldsymbol{x}$ is via the minimization of the LS criterion. Thus, according to (2.3), the least squares estimation problem can be formulated as[1]

$$\hat{\boldsymbol{x}} = \arg\min_{\boldsymbol{x}} \sum_{i=1}^{N} (\alpha_i \|\boldsymbol{x} - \boldsymbol{a}_i\| - d_0)^2 . \tag{2.4}$$

Even though problem in (2.4) is non-convex, when $\alpha_i = d_0$, for $i = 1, ..., N$, it can be accurately solved by the SCLP method presented in [61][2]. In the further text, we will present a novel approach to solve the problem defined in (2.4).

Defining auxiliary variables $\boldsymbol{z} = [z_1, ..., z_N]^T$, where $z_i = \alpha_i g_i - d_0$ and $g_i = \|\boldsymbol{x} - \boldsymbol{a}_i\|$, from (2.4) we get

$$\underset{\boldsymbol{x}, \boldsymbol{g}, \boldsymbol{z}}{\text{minimize}} \ \|\boldsymbol{z}\|^2$$

subject to

$$g_i = \|\boldsymbol{x} - \boldsymbol{a}_i\|, \ z_i = \alpha_i g_i - d_0, \ i = 1, ..., N. \tag{2.5}$$

Introducing an epigraph variable t, and relaxing the non-convex constraint $g_i = \|\boldsymbol{x} - \boldsymbol{a}_i\|$ as $g_i \geq \|\boldsymbol{x} - \boldsymbol{a}_i\|$, yields the following SOCP problem

$$\underset{\boldsymbol{x}, \boldsymbol{g}, \boldsymbol{z}, t}{\text{minimize}} \ t$$

subject to

$$\|[2\boldsymbol{z}; t-1]\| \leq t+1, \ \|\boldsymbol{x} - \boldsymbol{a}_i\| \leq g_i,$$

$$z_i = \alpha_i g_i - d_0, \ i = 1, ..., N. \tag{2.6}$$

Problem (2.6) can be efficiently solved by `CVX` [62], and we will refer to it as "SOCP1" in the further text[3].

[1] A justification for dropping the shadowing term in the propagation model is provided in the following text. We can rewrite (2.1) as $\frac{P_0 - P_i}{10\gamma} = \log_{10} \frac{\|\boldsymbol{x} - \boldsymbol{a}_i\|}{d_0} + \frac{v_i}{10\gamma}$, which corresponds to $\alpha_i \|\boldsymbol{x} - \boldsymbol{a}_i\| = d_0 10^{\frac{v_i}{10\gamma}}$. For sufficiently small noise, the first-order Taylor series expansion to the right-hand side of the previous expression is given by $\alpha_i \|\boldsymbol{x} - \boldsymbol{a}_i\| = d_0(1 + \frac{\ln 10}{10\gamma} v_i)$, *i.e.*, $\alpha_i \|\boldsymbol{x} - \boldsymbol{a}_i\| = d_0 + \epsilon_i$, where $\epsilon_i = d_0 \frac{\ln 10}{10\gamma} v_i$ is the zero-mean Gaussian random variable with the variance $d_0^2 \frac{(\ln 10)^2}{100\gamma^2} \sigma^2$. Clearly, the corresponding LS estimator is given by (2.4). Similar has been done in [56].

[2] It is possible to generalize the SCLP method to the weighted case, *i.e.*, to the case when $\alpha_i \neq d_0$ for some i. However, the algorithm of [61] yields a meaningless solution. This is due to the fact that the *almost convexity* property of the resulting constraints is not preserved.

[3] It is worth noting that "SOCP1" approach can be modified to solve the localization problem in a distributed fashion.

Non-cooperative scenario with unknown P_T

The assumption that the anchors know the actual target transmission power may be too strong in practice since it would require additional hardware in both target and anchors [16]. In this section, a more realistic and challenging scenario where the anchors are not aware of the target transmission power is considered, thus, P_0 is assumed to be unknown and has to be estimated. The joint ML estimation of $\boldsymbol{x}$ and P_0 can be formulated as

$$\hat{\boldsymbol{\theta}} = \underset{\boldsymbol{\theta}=[\boldsymbol{x}\,;P_0]}{\arg\min} \sum_{i=1}^{N} \frac{1}{\sigma^2} \left[P_i - \boldsymbol{l}^T\boldsymbol{\theta} + 10\gamma \log_{10} \frac{\|\boldsymbol{A}^T\boldsymbol{\theta} - \boldsymbol{a}_i\|}{d_0} \right]^2, \tag{2.7}$$

where $\boldsymbol{l} = [\boldsymbol{0}_{2\times 1}\,; 1]$ and $\boldsymbol{A} = [\boldsymbol{I}_2\,; \boldsymbol{0}_{1\times 2}]$.

In (2.3), we assumed that P_T, *i.e.*, P_0 is known. Assuming that P_0 is unknown, we can rewrite (2.3) as

$$\psi_i \|\boldsymbol{x} - \boldsymbol{a}_i\| \approx \eta\, d_0, \tag{2.8}$$

where $\psi_i = 10^{\frac{P_i}{10\gamma}}$ and $\eta = 10^{\frac{P_0}{10\gamma}}$. By following a procedure similar to the one in Section 2.2.2 for known P_T, we obtain the following SOCP problem

$$\underset{\boldsymbol{x},\boldsymbol{g},\boldsymbol{z},\eta,t}{\text{minimize}}\ t$$

subject to

$$\begin{aligned} \|[2\boldsymbol{z}; t-1]\| \le t+1,\ \|\boldsymbol{x} - \boldsymbol{a}_i\| \le g_i, \\ z_i = \psi_i\, g_i - \eta\, d_0,\ i = 1, ..., N. \end{aligned} \tag{2.9}$$

Even though the approach in (2.9) efficiently solves (2.7), we can further improve its performance. To do so, we will exploit the estimate of P_0, $\widehat{P}_0$, which we get by solving (2.9), and solve another SOCP problem. This SOCP approach will be described in the further text.

Introducing auxiliary variables $r_i = \|\boldsymbol{x} - \boldsymbol{a}_i\|$ and $\gamma_i = r_i^2$, expanding (2.4) and dropping the term d_0^2 which has no effect on the minimization, yields

$$\begin{aligned} \underset{\boldsymbol{x},\boldsymbol{\gamma},\boldsymbol{r}}{\text{minimize}} \sum_{i=1}^{N} \left(\widehat{\alpha}_i^2 \gamma_i - 2 d_0 \widehat{\alpha}_i r_i \right) \\ \text{subject to } \gamma_i = r_i^2,\ r_i = \|\boldsymbol{x} - \boldsymbol{a}_i\|,\ i = 1, ..., N, \end{aligned} \tag{2.10}$$

where $\widehat{\alpha}_i = 10^{\frac{\widehat{P}_0 - P_i}{10\gamma}}$. One can relax (2.10) to a convex optimization problem as follows. The non-convex constraint $\gamma_i = r_i^2$ will be replaced by the second-order cone constraint (SOCC) $r_i^2 \le \gamma_i$. Actually, the inequality constraint $r_i^2 \le \gamma_i$ will be satisfied as an equality since γ_i and r_i will decrease and increase in the minimization, respectively. Further, define an auxiliary variable $y = \|\boldsymbol{x}\|^2$. The constraint $y = \|\boldsymbol{x}\|^2$ is relaxed to a convex constraint $y \ge \|\boldsymbol{x}\|^2$ which is evidently a SOCC. With the use of all developed constraints, the problem (2.10) is approximated as a convex, SOCP, optimization problem:

$$\underset{\boldsymbol{x},\boldsymbol{\gamma},\boldsymbol{r},y}{\text{minimize}} \sum_{i=1}^{N} \left(\widehat{\alpha}_i^2 \gamma_i - 2 d_0 \widehat{\alpha}_i r_i \right)$$

subject to

$$\|[2\boldsymbol{x}; y-1]\| \leq y+1,\ \|[2r_i; \gamma_i-1]\| \leq \gamma_i+1,$$
$$\gamma_i = y - 2\boldsymbol{a}_i^T\boldsymbol{x} + \|\boldsymbol{a}_i\|^2,\ i=1,...,N. \tag{2.11}$$

In summary, the proposed procedure for solving (2.7) is given below:

Step 1) Solve (2.9) to obtain the initial estimate of $\boldsymbol{x}$, $\hat{\boldsymbol{x}}'$.

Step 2) Use $\hat{\boldsymbol{x}}'$ to compute the ML estimate of P_0, $\widehat{P}_0'$, from (2.7) as:

$$\widehat{P}_0' = \frac{\sum_{i=1}^{N}\left(P_i + 10\gamma\log_{10}\frac{\|\hat{\boldsymbol{x}}'-\boldsymbol{a}_i\|}{d_0}\right)}{N}; \tag{2.12}$$

Step 3) Use $\widehat{P}_0'$ to solve the SOCP in (2.11) and obtain the new target position estimate $\boldsymbol{x}$, $\hat{\boldsymbol{x}}''$. Compute the ML estimate of P_0, $\widehat{P}_0''$, from (2.12), by using $\hat{\boldsymbol{x}}''$.

The main reason for applying this simple procedure is that, we observed in our simulations that after solving (2.9) we obtain an excellent ML estimation of P_0, $\widehat{P}_0'$, which is very close to the true value of P_0. This motivated us to take advantage of this estimated value and solve another SOCP problem (2.11), as if P_T, *i.e.*, P_0 is known. In Section 2.2.5 we will see remarkable improvements in the estimation accuracy of both $\boldsymbol{x}$ and P_0 by employing the above procedure. We denote this three-step procedure as "SOCP2".

Non-cooperative scenario with unknown P_T and γ

Signal attenuation may be caused by many effects, such as multipath fading, diffraction, reflection, environment and weather conditions characteristics, etc. Thus, it is reasonable to assume that PLE, *i.e.*, γ is not known at the anchors. In this subsection we investigate the case where P_T and γ are simultaneously unknown at the anchors. The joint ML estimation of $\boldsymbol{x}$, P_0 and γ is written as

$$\hat{\boldsymbol{\theta}} = \underset{\boldsymbol{\theta}=[\boldsymbol{x};P_0;\gamma]}{\arg\min}\sum_{i=1}^{N}\frac{1}{\sigma_i^2}\left[P_i - \boldsymbol{h}^T\boldsymbol{\theta} + 10\boldsymbol{g}^T\boldsymbol{\theta}\log_{10}\frac{\|\boldsymbol{C}^T\boldsymbol{\theta}-\boldsymbol{a}_i\|}{d_0}\right]^2, \tag{2.13}$$

where $\boldsymbol{h} = [\boldsymbol{0}_{2\times1}; 1; 0]$, $\boldsymbol{g} = [\boldsymbol{0}_{3\times1}; 1]$ and $\boldsymbol{C} = [\boldsymbol{I}_2; \boldsymbol{0}_{2\times2}]$. Problem (2.13) is non-convex and has no closed form solution. To tackle (2.13), we employ a standard alternating procedure explained below (see also [54] and the references therein):

Step 1) Instead of blind estimation, use empirical values, *e.g.*, [58], and set the initial estimate of γ, $\hat{\gamma}^0 \in [\gamma_{\min}, \gamma_{\max}]$, and solve (2.9) to find the initial estimate of $\boldsymbol{x}$, $\hat{\boldsymbol{x}}^0$. Use $\hat{\gamma}^0$ and $\hat{\boldsymbol{x}}^0$ to calculate the ML estimate of P_0, $\widehat{P}_0^0$. Compute the value of the objective function, f_0, by plugging $\{\hat{\boldsymbol{x}}^0, \widehat{P}_0^0, \hat{\gamma}^0\}$ into (2.13). Set $k=1$;

Step 2) Use $\hat{\boldsymbol{x}}^{k-1}$ and $\widehat{P}_0^{k-1}$ to find the ML estimate of γ, $\widehat{\gamma}^k$, as:

$$\widehat{\gamma}^k = \frac{\sum_{i=1}^{N} 10\log_{10}\frac{\|\hat{\boldsymbol{x}}^{k-1}-\boldsymbol{a}_i\|}{d_0}\left(\widehat{P}_0^{k-1}-P_i\right)}{\sum_{i=1}^{N}\left(10\log_{10}\frac{\|\hat{\boldsymbol{x}}^{k-1}-\boldsymbol{a}_i\|}{d_0}\right)^2}.$$

If $\widehat{\gamma}^k \in [\gamma_{\min}, \gamma_{\max}]$ go to step 3); else stop;

Step 3) Use $\widehat{\gamma}^k$ and $\widehat{P}_0^{k-1}$ to solve (2.11), obtain the estimate of $\boldsymbol{x}$, $\hat{\boldsymbol{x}}^k$, and update the ML estimate of P_0, $\widehat{P}_0^k$. Plug $\{\hat{\boldsymbol{x}}^k, \widehat{P}_0^k, \hat{\gamma}^k\}$ into (2.13) and compute the value of the objective function, f_k. If $\frac{|f_k - f_{k-1}|}{f_{k-1}} < \epsilon$ (ϵ is a small positive number) or $k > K_{\max}$ ($K_{\max}$ is the maximum number of iteration) stop; otherwise let $k = k+1$ and go to step 2).

We refer to the above described iterative procedure as "SOCP3" in this thesis.

2.2.3 Cooperative Localization via SDP relaxation

Consider now a WSN with N anchor and M targets, where, as before the locations of the anchors $\boldsymbol{a}_1, \boldsymbol{a}_2, ..., \boldsymbol{a}_N$ are known, and the locations of the targets are $\boldsymbol{x}_1, \boldsymbol{x}_2, ..., \boldsymbol{x}_M$ (where $\boldsymbol{x}_i, \boldsymbol{a}_j \in \mathbb{R}^2$, for $i = 1, ..., M$ and $j = 1, ..., N$). Due to the limited communication range, R, or other physical limitations, only some targets can directly connect to the anchors, making the information gathered inside the network insufficient to perform a good estimation. To overcome this problem, sensor cooperation is required. Sensor cooperation allows direct communication between any two sensors in a WSN which are within the communication range of each other. This means that the targets also perform RSS measurements, *i.e.*, they play a role of the anchors, which number is scarce, in order to acquire adequate amount of information. After the RSS measurements are collected, all locations of the targets are estimated simultaneously. This kind of localization is called cooperative localization [18].

For ease of expression, matrix $\boldsymbol{X}$ is built such that it contains the positions of all targets, *i.e.*, $\boldsymbol{X} = [\boldsymbol{x}_1, \boldsymbol{x}_2, ..., \boldsymbol{x}_M]$ ($\boldsymbol{X} \in \mathbb{R}^{2\times M}$). Furthermore, sets $\mathcal{A} = \{(i,j) : \|\boldsymbol{x}_i - \boldsymbol{a}_j\| \leq R,\ i = 1, ..., M,\ j = 1, ..., N\}$ and $\mathcal{B} = \{(i,k) : \|\boldsymbol{x}_i - \boldsymbol{x}_k\| \leq R,\ i, k = 1, ..., M,\ i \neq k\}$ denote the existence of the target/anchor and the target/target connections, respectively. For the sake of simplicity, we assume that all targets radiate with the same power P_T, *i.e.*, P_0 and R are the same for all targets.

According to the radio propagation path loss model in [58], the RSS measurement for the cooperative localization can be formulated as

$$P_{ij}^{\mathcal{A}} = P_0 - 10\gamma\log_{10}\frac{\|\boldsymbol{x}_i - \boldsymbol{a}_j\|}{d_0} + v_{ij},\ (i,j) \in \mathcal{A},$$

$$P_{ik}^{\mathcal{B}} = P_0 - 10\gamma\log_{10}\frac{\|\boldsymbol{x}_i - \boldsymbol{x}_k\|}{d_0} + w_{ik},\ (i,k) \in \mathcal{B}, \tag{2.14}$$

where v_{ij} and w_{ik} are the log-normal shadowing terms modeled as zero-mean Gaussian random variables with variances $\sigma_{v_{ij}}^2$ and $\sigma_{w_{ik}}^2$, *i.e.*, $v_{ij} \sim \mathcal{N}(0, \sigma_{v_{ij}}^2)$ and $w_{ik} \sim \mathcal{N}(0, \sigma_{w_{ik}}^2)$.

We assume that the target/target path loss measurements are symmetric, *i.e.*, $P_{ik}^{\mathcal{B}} = P_{ki}^{\mathcal{B}}$ for $i \neq k$.

As in (2.1), the path loss approach and the measurements in (2.14) lead to the ML estimator, corresponding to solving the non-linear and non-convex LS problem

$$\hat{\boldsymbol{X}} = \arg\min_{\boldsymbol{X}} \sum_{(i,j):(i,j)\in\mathcal{A}} \frac{1}{\sigma_{v_{ij}}^2}\left[\left(P_{ij}^{\mathcal{A}} - P_0\right) + 10\gamma\log_{10}\frac{\|\boldsymbol{x}_i - \boldsymbol{a}_j\|}{d_0}\right]^2 + \sum_{(i,k):(i,k)\in\mathcal{B}} \frac{1}{\sigma_{w_{ik}}^2}\left[\left(P_{ik}^{\mathcal{B}} - P_0\right) + 10\gamma\log_{10}\frac{\|\boldsymbol{x}_i - \boldsymbol{x}_k\|}{d_0}\right]^2. \tag{2.15}$$

The problem defined in (2.15) is non-convex and non-linear, and, to the best of our knowledge, has no closed form solution. As before, from (2.15), we distinguish two different cases. In the first case, P_T (*i.e.*, P_0) is assumed to be known, whereas in the second case P_T is considered to be an unknown parameter which has to be estimated.

Cooperative scenario with known P_T

For the sake of simplicity, we assume that $\sigma_{v_{ij}}^2 = \sigma_{w_{ik}}^2 = \sigma^2$ in the remainder of this section. Following procedures similar to the ones in the non-cooperative localization problem, a convex estimator for cooperative localization is derived by applying semidefinite relaxation to the non-convex problem (2.15).

As in Section 2.2.2, we can approximate (2.14) as

$$\alpha_{ij}^{\mathcal{A}\,2}\|\boldsymbol{x}_i - \boldsymbol{a}_j\|^2 \approx d_0^2,\ \alpha_{ik}^{\mathcal{B}\,2}\|\boldsymbol{x}_i - \boldsymbol{x}_k\|^2 \approx d_0^2, \tag{2.16}$$

where $\alpha_{ij}^{\mathcal{A}} = 10^{\frac{P_{ij}^{\mathcal{A}} - P_0}{10\gamma}}$ and $\alpha_{ik}^{\mathcal{B}} = 10^{\frac{P_{ik}^{\mathcal{B}} - P_0}{10\gamma}}$. From (2.16), the following LS minimization problem is derived

$$\underset{\boldsymbol{X}}{\text{minimize}} \sum_{(i,j):(i,j)\in\mathcal{A}} \left(\alpha_{ij}^{\mathcal{A}\,2}\|\boldsymbol{x}_i - \boldsymbol{a}_j\|^2 - d_0^2\right)^2 + \sum_{(i,k):(i,k)\in\mathcal{A}} \left(\alpha_{ik}^{\mathcal{B}\,2}\|\boldsymbol{x}_i - \boldsymbol{x}_k\|^2 - d_0^2\right)^2. \tag{2.17}$$

Next, define the vector $\boldsymbol{y} = \text{vec}(\boldsymbol{X})$, where $\text{vec}(\boldsymbol{X})$ denotes the column-wise vectorization of $\boldsymbol{X}$. Then, (2.17) can be written as

$$\underset{\boldsymbol{y}}{\text{minimize}} \sum_{(i,j):(i,j)\in\mathcal{A}} \left(\alpha_{ij}^{\mathcal{A}\,2}\|\boldsymbol{E}_i^T\boldsymbol{y} - \boldsymbol{a}_j\|^2 - d_0^2\right)^2 + \sum_{(i,k):(i,k)\in\mathcal{B}} \left(\alpha_{ik}^{\mathcal{B}\,2}\|\boldsymbol{E}_i^T\boldsymbol{y} - \boldsymbol{E}_k^T\boldsymbol{y}\|^2 - d_0^2\right)^2, \tag{2.18}$$

where $\boldsymbol{E}_i = [\boldsymbol{e}_{2i-1}, \boldsymbol{e}_{2i}]$, and $\boldsymbol{e}_i$ represents the i-th column of the identity matrix $\boldsymbol{I}_{2M}$. Introducing an epigraph variable t and auxiliary variables $\boldsymbol{Y} = \boldsymbol{y}\boldsymbol{y}^T$ and $\boldsymbol{z} = [z_{ij}^{\mathcal{A}}, z_{ik}^{\mathcal{B}}]^T$, where $z_{ij}^{\mathcal{A}} = \alpha_{ij}^{\mathcal{A}\,2}\|\boldsymbol{E}_i^T\boldsymbol{y} - \boldsymbol{a}_j\|^2 - d_0^2$, for $(i,j) \in \mathcal{A}$, and $z_{ik}^{\mathcal{B}} = \alpha_{ik}^{\mathcal{B}\,2}\|\boldsymbol{E}_i^T\boldsymbol{y} - \boldsymbol{E}_k^T\boldsymbol{y}\|^2 - d_0^2$, for $(i,k) \in \mathcal{B}$, together with the convex relaxation $\boldsymbol{Y} \succeq \boldsymbol{y}\boldsymbol{y}^T$, the following convex epigraph form is obtained from (2.18)

$$\underset{\boldsymbol{y},\boldsymbol{Y},\boldsymbol{z},t}{\text{minimize}}\ t$$

subject to

$$z_{ij}^{\mathcal{A}} = {\alpha_{ij}^{\mathcal{A}}}^2\Big(\mathrm{tr}\Big(\boldsymbol{E}_i^T\boldsymbol{Y}\boldsymbol{E}_i\Big) - 2s_j^T\boldsymbol{E}_i^T\boldsymbol{y} + \|s_j\|^2\Big) - d_0^2, \text{ for } (i,j) \in \mathcal{A},$$

$$z_{ik}^{\mathcal{B}} = {\alpha_{ik}^{\mathcal{B}}}^2\Big(\mathrm{tr}\Big(\boldsymbol{E}_i^T\boldsymbol{Y}\boldsymbol{E}_i\Big) - 2\mathrm{tr}\Big(\boldsymbol{E}_i^T\boldsymbol{Y}\boldsymbol{E}_{\boldsymbol{k}}\Big) + \mathrm{tr}\Big(\boldsymbol{E}_k^T\boldsymbol{Y}\boldsymbol{E}_k\Big)\Big) - d_0^2, \text{for } (i,k) \in \mathcal{B},$$

$$\|[2\boldsymbol{z}; t-1]\| \leq t+1, \ \Big[\boldsymbol{Y}\ \boldsymbol{y}; \boldsymbol{y}^T\ 1\Big] \succeq \boldsymbol{0}_{2M+1}. \tag{2.19}$$

The above problem is an SDP (more precisely, it is a mixed SDP/SOCP), which can be readily solved by `CVX` [62]. If $\mathrm{rank}(\boldsymbol{Y}) = 1$, then the constraint $\boldsymbol{Y} \succeq \boldsymbol{y}\boldsymbol{y}^T$ is satisfied as an equality [57]. Note that we applied the Schur complement to rewrite $\boldsymbol{Y} \succeq \boldsymbol{y}\boldsymbol{y}^T$ into a semidefinite cone constraint form [57]. Note also that, in huge contrast to the existing SDP-based approaches [50], [51], [54], [56], which consider the unknown parameters as a matrix, here we consider them as a vector. In the remainder of the thesis, we will denote the above approach as "SDP1".

Cooperative scenario with unknown P_T

The joint ML estimation of $\boldsymbol{X}$ and P_0 is given by

$$\hat{\boldsymbol{\theta}} = \underset{\boldsymbol{\theta}=[\boldsymbol{x}_1^T,\ldots,\boldsymbol{x}_M^T,P_0]^T}{\arg\min} \sum_{(i,j):(i,j)\in\mathcal{A}} \frac{1}{\sigma^2}\left[\Big(P_{ij}^{\mathcal{A}} - \boldsymbol{q}^T\boldsymbol{\theta}\Big) + 10\gamma\log_{10}\frac{\|\boldsymbol{A}_i^T\boldsymbol{\theta} - \boldsymbol{a}_j\|}{d_0}\right]^2$$

$$+ \sum_{(i,k):(i,k)\in\mathcal{B}} \frac{1}{\sigma^2}\left[\Big(P_{ik}^{\mathcal{B}} - \boldsymbol{q}^T\boldsymbol{\theta}\Big) + 10\gamma\log_{10}\frac{\|\boldsymbol{A}_i^T\boldsymbol{\theta} - \boldsymbol{A}_k^T\boldsymbol{\theta}\|}{d_0}\right]^2, \tag{2.20}$$

where $\boldsymbol{q} = [\boldsymbol{0}_{2M\times 1}; 1]$, and $\boldsymbol{A}_i = [\boldsymbol{r}_{2i-1}, \boldsymbol{r}_{2i}]$, $\boldsymbol{r}_i$ represents the i-th column of the identity matrix $\boldsymbol{I}_{2M+1}$.

To solve (2.20) we will use a similar idea as in "SDP1" approach. We can rewrite (2.16) as

$$\beta_{ij}^{\mathcal{A}}\|\boldsymbol{x}_i - \boldsymbol{a}_j\|^2 \approx \eta d_0^2, \ \beta_{ik}^{\mathcal{B}}\|\boldsymbol{x}_i - \boldsymbol{x}_k\|^2 \approx \eta d_0^2, \tag{2.21}$$

where $\beta_{ij}^{\mathcal{A}} = 10^{\frac{P_{ij}^{\mathcal{A}}}{5\gamma}}$, $\beta_{ik}^{\mathcal{B}} = 10^{\frac{P_{ik}^{\mathcal{B}}}{5\gamma}}$ and $\eta = 10^{\frac{P_0}{5\gamma}}$. Following the steps highlighted in the previous section, the following convex problem is obtained

$$\underset{\boldsymbol{y},\boldsymbol{Y},\boldsymbol{z},t,\eta}{\text{minimize}}\ t$$

subject to

$$z_{ij}^{\mathcal{A}} = \beta_{ij}^{\mathcal{A}}\Big(\mathrm{tr}\Big(\boldsymbol{E}_i^T\boldsymbol{Y}\boldsymbol{E}_i\Big) - 2s_j^T\boldsymbol{E}_i^T\boldsymbol{y} + \|s_j\|^2\Big) - \eta d_0^2, \text{for} (i,j) \in \mathcal{A},$$

$$z_{ik}^{\mathcal{B}} = \beta_{ik}^{\mathcal{B}}\Big(\mathrm{tr}\Big(\boldsymbol{E}_i^T\boldsymbol{Y}\boldsymbol{E}_i\Big) - 2\mathrm{tr}\Big(\boldsymbol{E}_i^T\boldsymbol{Y}\boldsymbol{E}_k\Big) + \mathrm{tr}\Big(\boldsymbol{E}_k^T\boldsymbol{Y}\boldsymbol{E}_k\Big)\Big) - \eta d_0^2, \text{ for } (i,k) \in \mathcal{B},$$

$$\|[2\boldsymbol{z}; t-1]\| \leq t+1, \ \Big[\boldsymbol{Y}\ \boldsymbol{y}; \boldsymbol{y}^T\ 1\Big] \succeq \boldsymbol{0}_{2M+1}. \tag{2.22}$$

Even though the approach in (2.22) efficiently solves (2.20), we can further improve its performance. As in the case of non-cooperative localization where P_T was not known, we propose a simple three-step procedure:

Step 1) Solve (2.22) to obtain the initial estimate of $\boldsymbol{y}$, $\hat{\boldsymbol{y}}'$.

Step 2) Use $\hat{\boldsymbol{y}}'$ to compute the ML estimate of P_0, $\widehat{P}_0'$, from (2.20) as:

$$\widehat{P}_0' = \frac{\sum\limits_{(i,j):(i,j)\in\mathcal{A}} \left(P_{ij}^{\mathcal{A}} + 10\gamma \log_{10} \frac{\|\boldsymbol{E}_i^T \hat{\boldsymbol{y}}' - \boldsymbol{a}_j\|}{d_0} \right)}{|\mathcal{A}| + |\mathcal{B}|} + \frac{\sum\limits_{(i,k):(i,k)\in\mathcal{B}} \left(P_{ik}^{\mathcal{B}} + 10\gamma \log_{10} \frac{\|\boldsymbol{E}_i^T \hat{\boldsymbol{y}}' - \boldsymbol{E}_k^T \hat{\boldsymbol{y}}'\|}{d_0} \right)}{|\mathcal{A}| + |\mathcal{B}|}, \tag{2.23}$$

where $|\mathcal{A}|$ and $|\mathcal{B}|$ represent the cardinalities of the sets $\mathcal{A}$ and $\mathcal{B}$.

Step 3) Use $\widehat{P}_0'$ to solve (2.19) and obtain the new estimate of $\boldsymbol{y}$, $\hat{\boldsymbol{y}}''$. Compute the ML estimate of P_0, $\widehat{P}_0''$, from (2.23), by using $\hat{\boldsymbol{y}}''$.

We will refer to the above three-step procedure as "SDP2".

2.2.4 Complexity Analysis

The trade-off between the estimation accuracy and the computational complexity is one of the most important features of any method since it defines its applicability potential. This is the reason why, apart from the performance, we are interested in comparing the complexity of the proposed and the existing approaches as well.

The formula for computing the worst case complexity of a mixed SDP/SOCP [63], given below, is used to analyze the complexities of the considered algorithms in this thesis

$$\mathcal{O}\left(\sqrt{L}\left(m\sum_{i=1}^{N_{sd}} n_i^{sd^3} + m^2\sum_{i=1}^{N_{sd}} n_i^{sd^2} + m^2\sum_{i=1}^{N_{soc}} n_i^{soc} + \sum_{i=1}^{N_{soc}} n_i^{soc^2} + m^3\right)\right), \tag{2.24}$$

where L is the iteration complexity of the algorithm, m is the number of equality constraints, n_i^{sd} and n_i^{soc} are the dimensions of the i-th semidefinite cone (SDC) and the i-th second-order cone (SOC), respectively, and N_i^{sd} and N_i^{soc} are the number of SDC and SOC constraints, respectively. The formula (2.24) was derived by integrating the formulas for computing the worst case computational complexity of an SDP and an SOCP [63]. It corresponds to the formula for computing the complexity of an SDP for the case when we have no second-order cone constraint (SOCC) (in which case L is the dimension of the SDP cone, given as a result of accumulating all SDP cones), and vice versa (in which case L is the total number of SOCCs) [63].

We investigated the worst case asymptotic complexity of the algorithms, *i.e.*, we present only the dominating elements, which are expressed as a function of N and M. Since the worst case complexity is considered, we assumed that the network is fully connected, *i.e.*, the total number of connections in the network is $K = |\mathcal{A}| + |\mathcal{B}|$, where $|\mathcal{A}| = MN$ and $|\mathcal{B}| = \frac{M(M-1)}{2}$.

It should be pointed out that the algorithms mentioned here for solving the target localization are not uniquely defined in a clear primal or dual form, thus, we can interpret them in the form that is more suitable for the solver [64]. For example, if we interpret the cooperative localization problem defined in [50], in the dual form, we get $\frac{(M+2)(M+3)}{2} + K$ variables, which corresponds to $\frac{(M+2)(M+3)}{2} + K$ equality constraints in the primal form. In contrast, if we interpret the same problem in the primal form we get $4K + 3$ equality constraints, corresponding to the same number of variables in the dual form. While performing the simulations, we have experienced that the latter interpretation is computationally more efficient, thus, the complexity analysis is performed based on the primal form representation only.

To provide a more complete overview of the algorithm's performance to the reader, we present the complexity results together with the simulations results in the following section.

2.2.5 Performance Results

In this section we present a set of performance results to compare the proposed approaches with the existing ones, for both non-cooperative and cooperative localization with known and unknown P_T. All of the presented algorithms were solved by using the MATLAB package `CVX` [62], where the solver is SeDuMi [65].

Non-cooperative Localization

To generate the RSS measurements, the propagation model (2.1) is used. Extensive simulations have been carried out to compare the performance of the proposed methods in Section 2.2.2 with the existing ones for the cases of known and unknown target transmit power. Unless stated otherwise, in all simulations presented here, the number of Monte Carlo runs is $M_c = 10000$, the path loss exponent is $\gamma = 3$, the reference distance $d_0 = 1$ m and the reference power $P_0 = -10$ dBm. The anchors are uniformly distributed at a circle with the center at the origin, and the radius of the circle $r = 20$ m. A target is randomly distributed inside the square region $\{(x, y) \,|\, -B \leq x \leq B, -B \leq y \leq B\}$, where B will be defined below, and it is able to communicate with all anchors. The performance metric is the root mean square error (RMSE), defined as

$$\text{RMSE} = \sqrt{\sum_{i=1}^{M_c} \frac{\|\boldsymbol{x}_i - \widehat{\boldsymbol{x}}_i\|^2}{M_c}},$$

where $\widehat{\boldsymbol{x}}_i$ denotes the estimate of the true target location, $\boldsymbol{x}_i$, in the i-th Monte Carlo run for a specific noise realization. The CRB offers a lower bound on the RMSE of any unbiased estimator is employed as a performance benchmark; see Appendix A for more details.

Known P_T. Table 2.1 gives an overview of the considered algorithms in this subsection, together with their complexities. In [50], [51], the authors have considered both indoor

Table 2.1: Summary of the Considered Algorithms in Section 2.2.2 for known P_T

Algorithm	**Description**	**Complexity**
SDP_{RSS}	The SDP estimator in [50]	$\mathcal{O}(N^{4.5})$
WLS-1	The WLS estimator in [51]	$\mathcal{O}(N)$
SOCP1	The proposed SOCP estimator in (2.34)	$\mathcal{O}(N^{3.5})$

and outdoor localization scenarios. Our simulation results show that, for the chosen scenario, the proposed approach exhibits just a marginal gain when compared to the existing approaches. Thus, for the non-cooperative scenario when P_T is known we focus on indoor localization only.

- *Indoor Localization:* In Appendix B we give more details about the indoor propagation model. The simulation results for indoor localization are presented in Fig. 2.1. The scenario described in [51] is used to execute the comparison of the performances. Fig. 2.1 clearly demonstrates the superiority of the proposed approach over the existing ones for the whole range of σ. To illustrate this fact, consider the cases when $\sigma = 1$ dB and $\sigma = 6$ dB. For the former case, "SOCP1" shows a gain of approximately 0.2 m when compared to the existing approaches. For the latter case, "SOCP1" outperforms "WLS-1" and "SDP_{RSS}" approaches by 0.3 m and 0.5 m, respectively. In summary, the proposed approach outperforms the existing ones in terms of the estimation accuracy with an average error reduction of about 15%, whereas in terms of the computational complexity it represents a solid alternative.

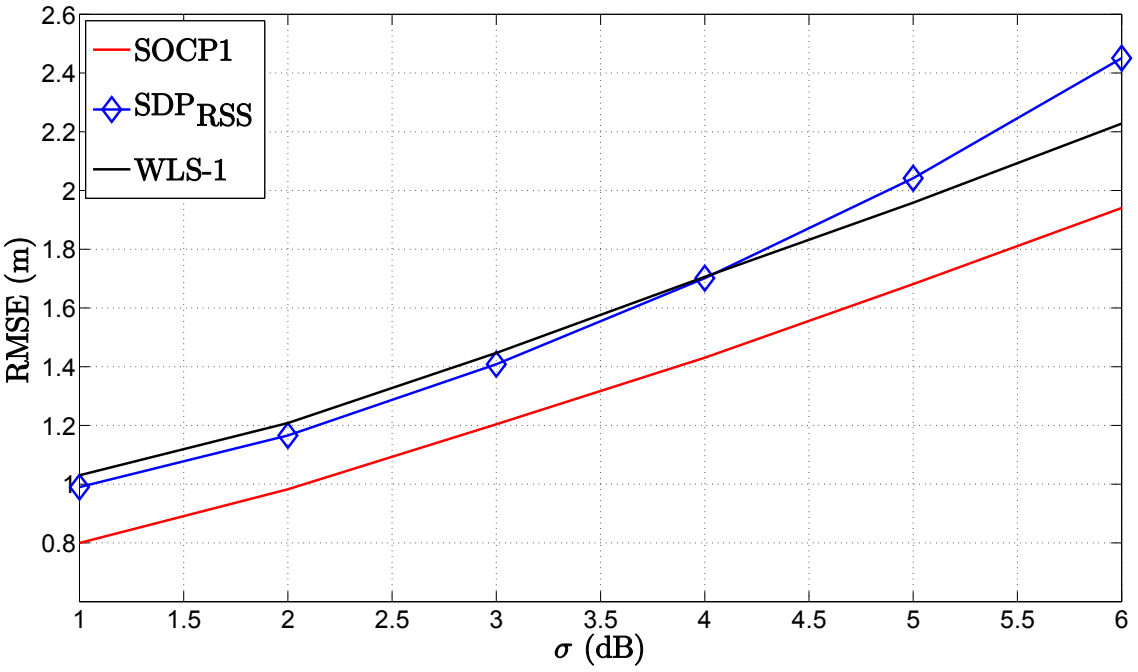

Figure 2.1: Simulation results for non-cooperative localization in indoor environment when P_0 is known: RMSE (m) versus σ (dB) when $N = 9$, $U = 5$ dB, $\gamma = 2.4$, $\gamma_w = 4$ dB, $d_0 = 1$ m, $P_0 = -10$ dBm, $M_c = 50000$.

Unknown P_T. Table 2.2 gives an overview of the considered algorithms in this subsection,

Table 2.2: Summary of the Considered Algorithms in Section 2.2.2 for unknown P_T

Algorithm	**Description**	**Complexity**
WLS-2	The WLS estimator in [54]	$\mathcal{O}(N)$
SDP-URSS	The SDP estimator in [56]	$\mathcal{O}(N^{3.5})$
SOCP2	The proposed SOCP estimator for unknown P_T	$2 \cdot \mathcal{O}(N^{3.5})$

Table 2.3: P_0 Estimation Analysis for "SOCP2" Approach

N	**After II - step**		**After III - step**	
	$\mathbf{RMSE}_{P_0}$	$\mathbf{Bias}_{P_0}$	$\mathbf{RMSE}_{P_0}$	$\mathbf{Bias}_{P_0}$
3	4.0639	1.8360	3.0967	0.4366
6	2.2483	0.3557	2.0541	0.0642
9	1.7591	0.1344	1.6997	0.0260
12	1.4582	0.0450	1.4476	0.0116
15	1.3135	0.0500	1.3029	0.0238
18	1.1836	0.0432	1.1774	0.0288
21	1.1097	0.0084	1.1072	0.0004

together with their complexities. Fig. 2.2 illustrates the comparison of the RMSE versus N for $\sigma = 5$ dB, $B = 15$ m and $r = 20$ m. From Fig. 2.2 we observe that the estimation error decreases as N is increased, as expected. Furthermore, we observe the superior RMSE performance of "SOCP2" approach for all chosen N. Fig. 2.2 also shows that the performance margin between the proposed and the existing approaches grows as N is increased; *e.g.*, for $N = 24$, "SOCP2" outperforms the existing ones for more than 0.5 m, which is a relatively large gain considering that when $N = 24$ the amount of information gathered in the network is significant. This can be explained, to some extent, by the fact that our approach has somewhat higher computational complexity than the existing ones, and the use of the proposed three-step procedure. When N increases we can obtain a better estimate of P_T, *i.e.* P_0, in the first step of our procedure, which then allows us to achieve high estimation accuracy in the second step with respect to (w.r.t.) $\boldsymbol{x}$; we refer the reader to the Table 2.3 for more details. As it can be seen, after the second step of our procedure we obtain an excellent estimate of P_0, which we then employ in the third step. From Table 2.3 we observe that as N is increased the estimation of P_0 is improved. Even though the estimation of P_0 in the second step is not perfect, the simulation results in Fig. 2.2 confirm the robustness of our SOCP approach to the imperfect knowledge of P_0.

From Fig. 2.2 we can see that the new approach is biased for small N. This is not surprising since it is known that RSS based algorithms are generally biased [1]. For the sake of completeness, we also compared the considered approaches in terms of bias. The bias is defined as $\text{Bias} = \| \frac{1}{M_c} \sum_{i=1}^{M_c} (\boldsymbol{x}_i - \hat{\boldsymbol{x}}_i) \|_1$, where $\| \bullet \|_1$ represents the l_1 norm. In our simulations, we have observed that all approaches are slightly biased. However, the bias

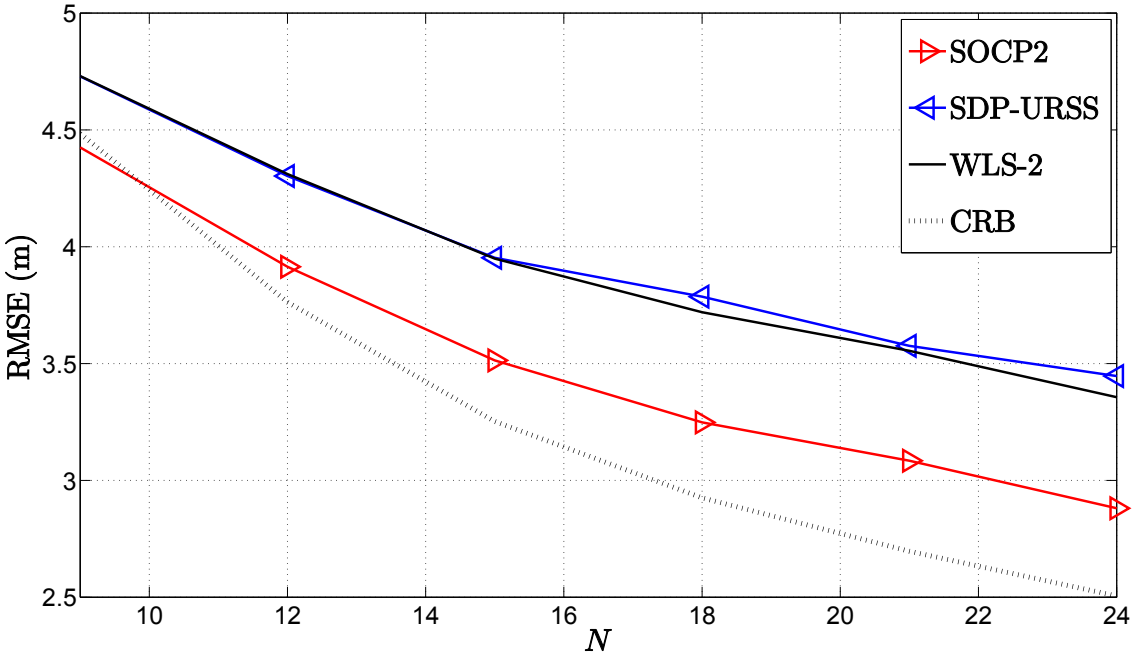

Figure 2.2: Simulation results for non-cooperative localization when P_0 is not known: RMSE (m) versus N when $\sigma = 5$ dB, $B = 15$ m, $r = 20$ m, $P_0 = -10$ dBm, $\gamma = 3$, $d_0 = 1$ m, $M_c = 10000$.

error is less than 0.14 m for all estimators, which is a relatively small error in the case when the RMSE error is of the order of few meters.

It is also worth mentioning that an estimate of P_0 can be obtained directly from η after solving (2.9) as $\hat{P}_0 = 10\gamma \log_{10} \eta$, in the first step of the proposed procedure. However, the localization problem is very difficult to solve on its own, even for known P_0. Not knowing P_0 further aggravates the situation, and hence, we believe that it comes natural that P_0 estimates obtained directly from the proposed algorithms would not be as reliable as the ML ones. Our intuition was confirmed in simulations, and we present the results in Fig. 2.3. In Fig. 2.3, the mean of the estimated value is represented by a red cross and a blue circle for direct and ML estimates of P_0 respectively, and their standard deviations are given by a line with the respective color. From the figure, one can see that more reliable and accurate solutions are obtained from the ML estimate of P_0, which justifies our choice of estimating P_0 through this approach in our proposed procedure.

Unknown P_T and γ. Table 2.4 gives an overview of the considered algorithms in this subsection, together with their complexities. The results in [66] imply that better estimation accuracy w.r.t. $\boldsymbol{x}$ is attained by choosing the initial value of the PLE, $\hat{\gamma}^0$, to be greater than the true value of γ. This motivated us to investigate the influence of the choice of $\hat{\gamma}^0$ on the estimation accuracy of the remaining unknown parameters. Our analysis showed that the influence of the choice of $\hat{\gamma}^0$ on the estimation accuracy of the target positions is significant. We present some of these results in Table 2.5. Note that the average number of iterations for an algorithm to converge is denoted by "Av. iter.". Generally, the best

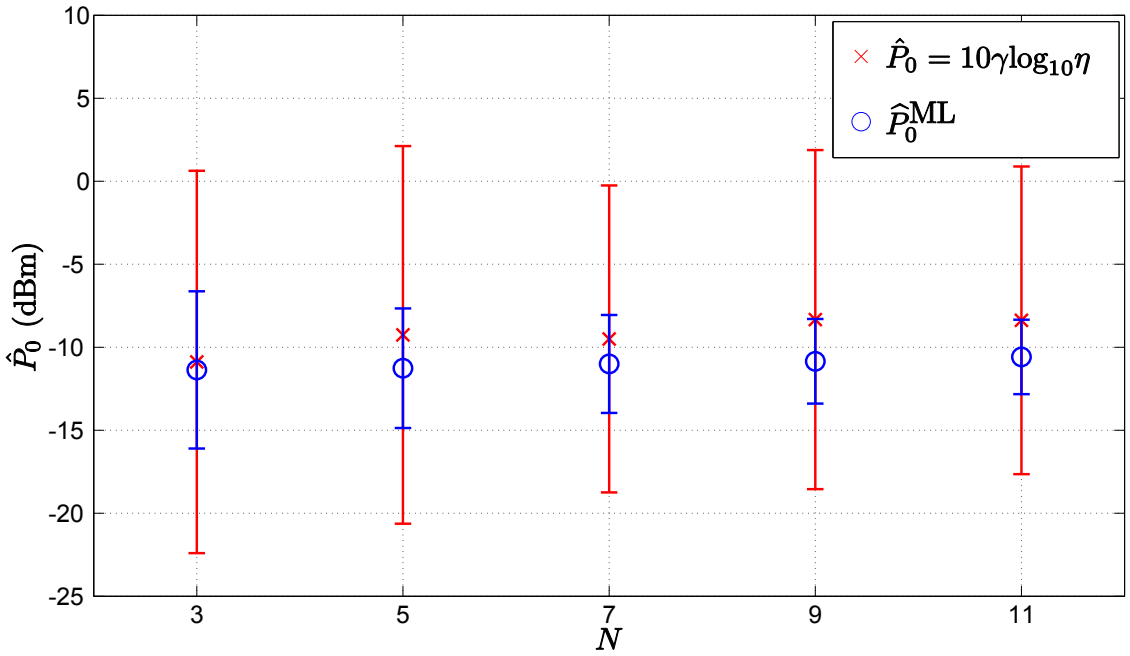

Figure 2.3: Simulation results for non-cooperative localization when P_0 is not known: $\hat{P}_0$ (dBm) versus N when $\sigma = 6$ dB, $B = 15$ m, $P_0 = -10$ dBm, $\gamma = 2.5$, $d_0 = 1$ m, $M_c = 1000$.

Table 2.4: Summary of the Considered Algorithms in Subsection 2.2.2 for unknown P_T and γ

Algorithm	**Description**	**Complexity**
WLS-3	The WLS estimator in [54]	$K_{\max} \cdot \mathcal{O}(N)$
SOCP3	The proposed SOCP estimator for unknown P_T and PLE	$K_{\max} \cdot \mathcal{O}\left(N^{3.5}\right)$

estimation accuracy w.r.t. $\boldsymbol{x}$ is achieved for $\hat{\gamma}^0 = \gamma_{\max}$. However, when the key requirement is to estimate P_0 or γ, then a random choice of $\hat{\gamma}^0 \in [\gamma_{\min}, \gamma_{\max}]$ is by far the best choice. The price to pay for this choice of $\hat{\gamma}^0$ is somewhat slower convergence, in comparison to the choice $\hat{\gamma}^0 = \gamma_{\max}$.

Fig. 2.4 illustrates the comparison of the RMSE versus N for $\sigma = 5$ dB, $B = 15$ m, and $r = 20$ m. In this figure, we represent a curve for the proposed approach for a random choice of $\hat{\gamma}^0 \in [\gamma_{\min}, \gamma_{\max}]$. Fig. 2.4 confirms the efficiency of the iterative procedure. It shows that the proposed approach is robust to the imperfect knowledge of the PLE, since it suffers only a small deterioration of the performance when both P_T and PLE are not known, compared to the case when only P_T is unknown. Furthermore, Fig. 2.4 shows the superior RMSE performance of the proposed approach for all chosen N. We observe that the performance margin between "SOCP3" and "WLS-3" increases as N increases. To illustrate this fact consider $N = 9$ and $N = 24$. In the former case "SOCP3" approach outperforms "WLS-3" for roughly 0.3 m, while in the latter case it shows a gain of roughly 0.5 m. From Fig. 2.4 it can be seen that "SOCP3" achieves the value RMSE = 4 m with

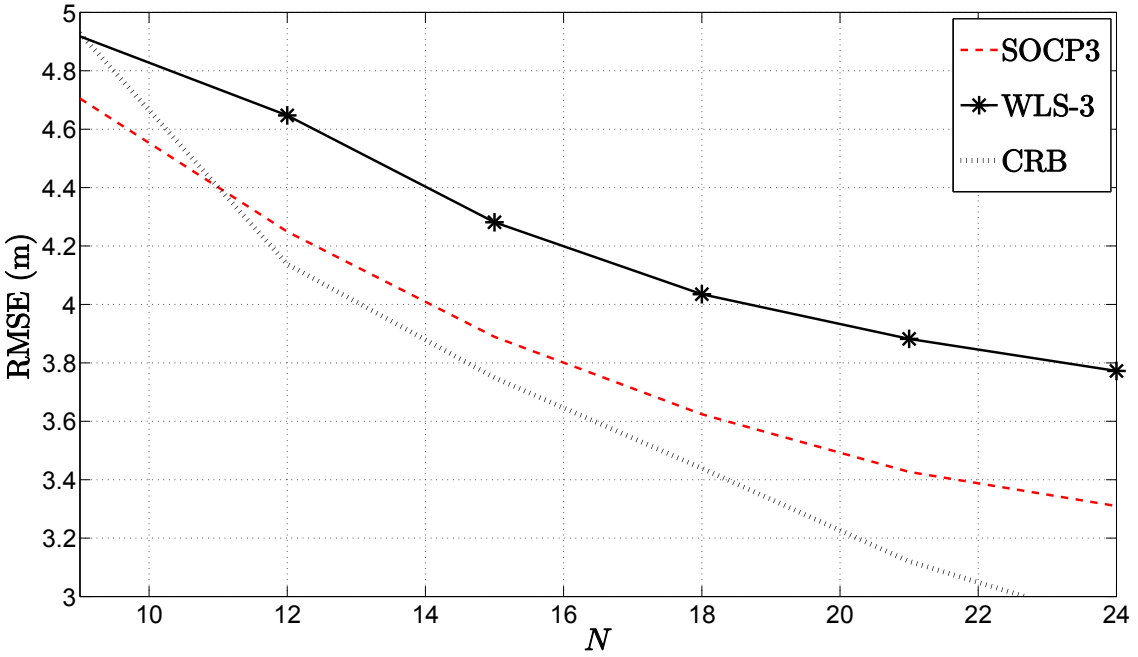

Figure 2.4: Simulation results for non-cooperative localization when P_0 and γ are not known: RMSE (m) versus N when $\sigma = 5$ dB, $B = 15$ m, $r = 20$ m, $P_0 = -10$ dBm, $d_0 = 1$ m, $K_{\max} = 30$, $\gamma_{\min} = 2$, $\gamma_{\max} = 4$, $\epsilon = 10^{-3}$ and $M_c = 10000$.

Table 2.5: Unknown Parameter Estimation Analysis for a Random Choice of $\hat{\gamma}_0 \in [\gamma_{\min}, \gamma_{\max}]$

N	$\hat{\gamma}_0 \in [\gamma_{\min}, \gamma_{\max}]$						
	RMSE$_{\boldsymbol{x}}$ (m)	**Bias$_{\boldsymbol{x}}$** (m)	**RMSE$_{P_0}$** (dBm)	**Bias$_{P_0}$** (dBm)	**RMSE$_{\gamma}$**	**Bias$_{\gamma}$**	**Av. iter.**
3	9.7700	0.0401	8.6155	0.1203	0.5715	0.0152	18.9713
6	5.6250	0.0531	7.8665	1.2038	0.5742	0.1042	11.9949
9	4.7049	0.1396	7.4599	0.7406	0.5540	0.0624	10.2199
12	4.2493	0.0366	7.3174	0.7629	0.5500	0.0634	9.1817
15	3.8891	0.0207	7.2133	0.6421	0.5448	0.0531	8.4968
18	3.6239	0.0422	7.1992	0.6195	0.5455	0.0492	7.9642
21	3.4266	0.0181	7.1175	0.4674	0.5388	0.0390	7.5611

4 anchors less than "WLS-3", which can reduce the cost of the network implementation in practice. Note that this gain comes at a cost of increased complexity.

Cooperative Localization

This subsection presents the simulation results for the cooperative localization problem. The performance of the proposed approaches in Section 2.2.3 will be compared with the existing algorithms for the cases of known and unknown P_T. In all simulation results presented here, the number of Monte Carlo runs is $M_c = 10000$, the path loss exponent is $\gamma = 3$, the reference distance $d_0 = 1$ m and the reference power $P_0 = -10$ dBm. Unless stated otherwise, the anchors are fixed at the positions (B, B), $(0, B)$, $(-B, B)$, $(-B, 0)$,

Table 2.6: Summary of the Considered Algorithms in Section 2.2.3 for known P_T

Algorithm	**Description**	**Complexity**
SDP_{RSS}	The SDP estimator in [50]	$\mathcal{O}\left(M^{0.5}\left(48M^4\left(N+\frac{M}{2}\right)^4\right)\right)$
SD/SOCP-1[4]	The mixed SDP/SOCP estimator in [51]	$2\cdot\mathcal{O}\left(M^{0.5}\left(M^4\left(N+\frac{M}{2}\right)^2\right)\right)$
SDP1	The proposed SDP estimator in (2.19)	$\mathcal{O}\left(\sqrt{2}M^{0.5}\left(4M^4\left(N+\frac{M}{2}\right)^2\right)\right)$

$(-B,-B)$, $(0,-B)$, $(B,-B)$, $(B,0)$, and $(0,0)$, where B will be defined below. Targets are randomly deployed inside the convex hull of the anchors, and due to the limited communication range only some of them can directly connect to the anchors. The performance metric is the normalized root mean square error (NRMSE), defined as

$$\text{NRMSE} = \sqrt{\frac{1}{M}\sum_{i=1}^{M_c}\sum_{j=1}^{M}\frac{\|\boldsymbol{x}_{ij}-\hat{\boldsymbol{x}}_{ij}\|}{M_c}},$$

where $\widehat{\boldsymbol{x}}_{ij}$ denotes the estimate of the true location of the j-th target, $\boldsymbol{x}_{ij}$, in the i-th Monte Carlo run for a specific noise realization.

Known P_T. Table 2.6 gives an overview of the considered algorithms in this subsection, together with their complexities. We observe from Table 2.6 that the proposed SDP approach has somewhat higher computational complexity than "SD/SOCP-1" approach and lower complexity than "SDP_{RSS}" approach. Although somewhat more complex than "SD/SOCP-1" approach, the proposed approach has the lowest running time, as one can see from Table 2.7a. This is due to the fact that for cooperative localization when P_T is known we solve only one SDP, while "SD/SOCP-1" involves solving two SDP problems.

Fig. 2.5 illustrates the comparison of the NRMSE versus M, for $N = 9$, $R = 6$ m, $\sigma = 5$ dB and $B = 15$ m. We observe that, as M increases the estimation accuracy of all algorithms improves, which is intuitive since more information is collected inside the network. Furthermore, from Fig. 2.5 it can be seen that the proposed approach outperforms the existing ones for all values of M, with the biggest improvement for medium-to-high M. The proposed approach outperforms on average "SD/SOCP-1" for roughly 0.5 m, even though "SD/SOCP-1" solves two SDP problems. Moreover, the new approach improves the estimation accuracy on average for about 0.25 m in comparison to "SDP_{RSS}", although "SDP_{RSS}" is more computationally complex. In short, albeit "SDP_{RSS}" is more computationally complex than the new approach and "SD/SOCP-1" solves two SDP problems which increases its execution time, the new approach outperforms both of them for all M.

Unknown P_T. Table 2.8 gives an overview of the considered algorithms in this subsection, together with their complexities. From Table 2.8 it can be seen that the proposed approach

[4]It should be noted that in [51], Wang *et al.* introduce a three-step algorithm for solving the problem of cooperative target localization. By solving the problem according to these steps, one is actually solving two SDP problems, which doubles the computational time of this algorithm.

Table 2.7: The Average Running Time of the Considered Algorithms for the Cooperative Localization. $N = 8$, $M = 20$, $R = 6$ m. CPU: Intel(R)Core(TM)i7-363QM 2.40 GHz.

Algorithm	**Time** (s)
SDP_{RSS}	1.5539
SD/SOCP-1	0.9680
SDP1	0.8691

(a) P_T is known

Algorithm	**Time** (s)
SD/SOCP-2	1.0898
SDP-URSS	0.7232
SDP2	1.7949

(b) P_T is not known

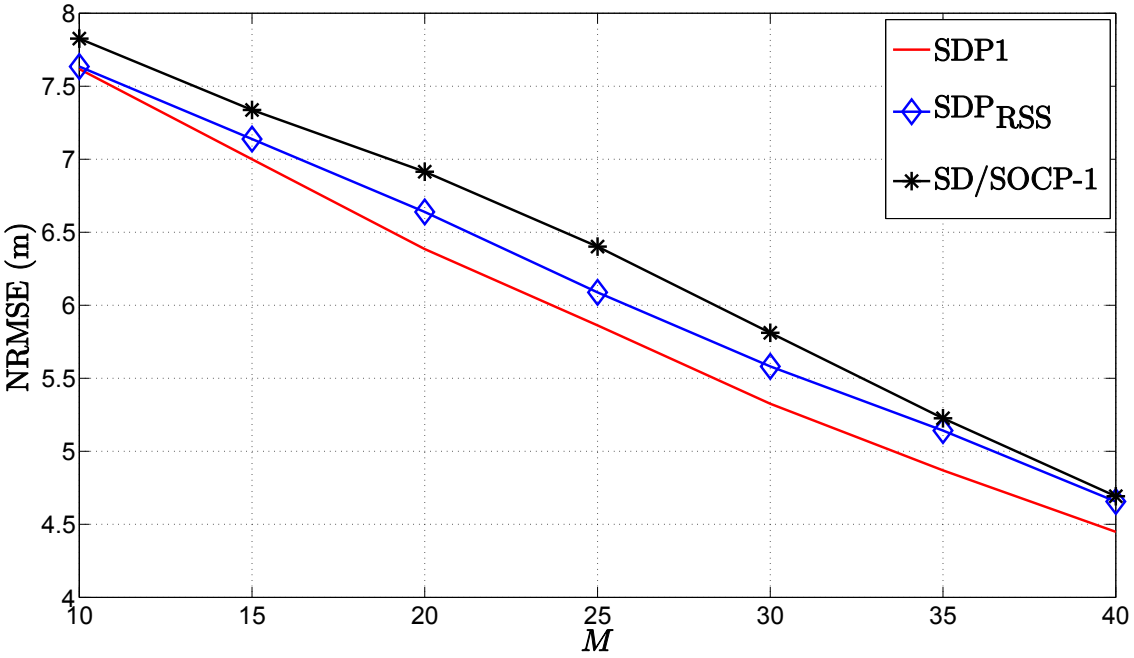

Figure 2.5: Simulation results for cooperative localization when P_0 is known: NRMSE (m) versus M when $N = 9$, $\sigma = 5$ dB, $B = 15$ m, $P_0 = -10$ dBm, $\gamma = 3$, $d_0 = 1$ m, $M_c = 10000$.

Table 2.8: Summary of the Considered Algorithms in Section 2.2.3 for unknown P_T

Algorithm	**Description**	**Complexity**
SD/SOCP-2	The mixed SDP/SOCP estimator in [54]	$2 \cdot \mathcal{O}\left(M^{0.5}\left(M^4\left(N+\frac{M}{2}\right)^2\right)\right)$
SDP-URSS	The SDP estimator in [56]	$\mathcal{O}\left(M^{0.5}\left(M^4\left(N+\frac{M}{2}\right)^2\right)\right)$
SDP2	The proposed SDP estimator for unknown P_T and PLE	$2 \cdot \mathcal{O}\left(\sqrt{2}M^{0.5}\left(4M^4\left(N+\frac{M}{2}\right)^2\right)\right)$

has the highest computational complexity. This was confirmed in our simulations; see Table 2.7b for more details.

In Fig. 2.6 we present one possible network configuration and the estimation accuracy of the target positions accomplished by the "SDP2" approach, for $N = 9$, $M = 40$, $R = 6$ m, $\sigma = 5$ dB and $B = 15$ m. From Fig. 2.6 one can see that better estimation accuracy is achieved for targets with higher number of connections (neighbors), as anticipated.

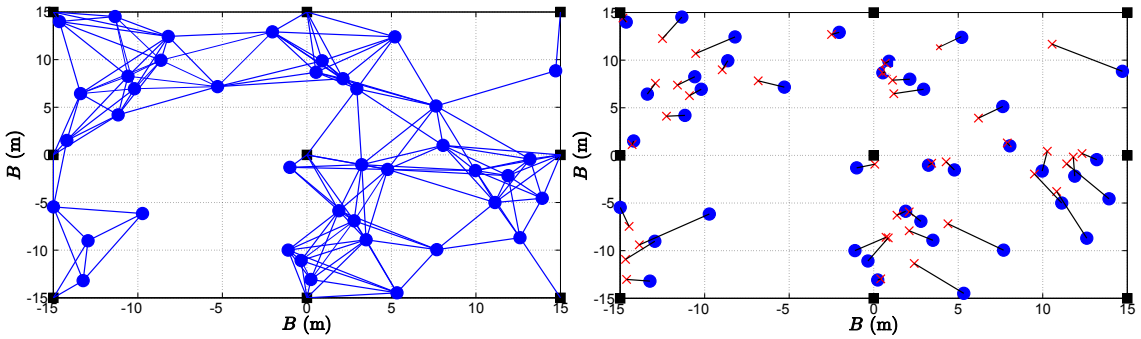

(a) A network configuration

(b) Estimation accuracy results for the "SDP2" approach

Figure 2.6: Example of (a) a network configuration and (b) estimation accuracy results for the "SDP2" approach. Black squares represent the locations of the anchors, blue circles represents the true locations of the targets and red symbols "X" represent the estimated targets.

Fig. 2.7 illustrates the NRMSE performance of the considered approaches for different M, when $N = 9$, $R = 6$ m, $\sigma = 5$ dB and $B = 15$ m. We can see that the estimation accuracy improves as M is increased, as expected. Fig. 2.7 confirms the superiority of our approach, since it outperforms the existing ones for all choices of M, with an average gain of about 0.5 m. When the information gathered by the network is not enough (low M) our approach outperforms "SD/SOCP-2" and "SDP-URSS" for roughly 2 m and 1 m, respectively. As M increases, the performance margin between all approaches decreases, as anticipated, since the information inside the network becomes sufficient to allow good performance for all estimators. Finally, from Figs. 2.5 and 2.7 it can be seen that the new approach suffers only a marginal deterioration in the performance for the scenario where P_T is not known.

Fig. 2.8 illustrates the NRMSE performance of the considered approaches for different R, when $N = 9$, $M = 15$, $\sigma = 5$ dB and $B = 15$ m. As anticipated, the estimation error decreases when R is increased. From Fig. 2.8 it is clear that the proposed approach outperforms the existing ones for all choices of R, with an average gain of more than 1 m and 0.5 m compared to "SD/SOCP-2" and "SDP-URSS", respectively. An important practical scenario would be the case where R is chosen to be low, due to the need to preserve low energy consumption in the network. In this case, our approach reduces the estimation error by about 2 m and 0.5 m, compared to "SD/SOCP-2" and "SDP-URSS", respectively. Intuitively, as R is increased, all methods are expected to perform good, since the information gathered by the network becomes sufficient enough. However, one can see form Fig. 2.8 that the performance gains between the proposed approach and "SDP-URSS" increases with R; for $R = 10$ m the new approach outperforms "SDP-URSS" for almost 1 m. This result further confirms the superiority of the proposed approach over "SDP-URSS".

Fig. 2.9 illustrates the NRMSE performance of the considered approaches for different

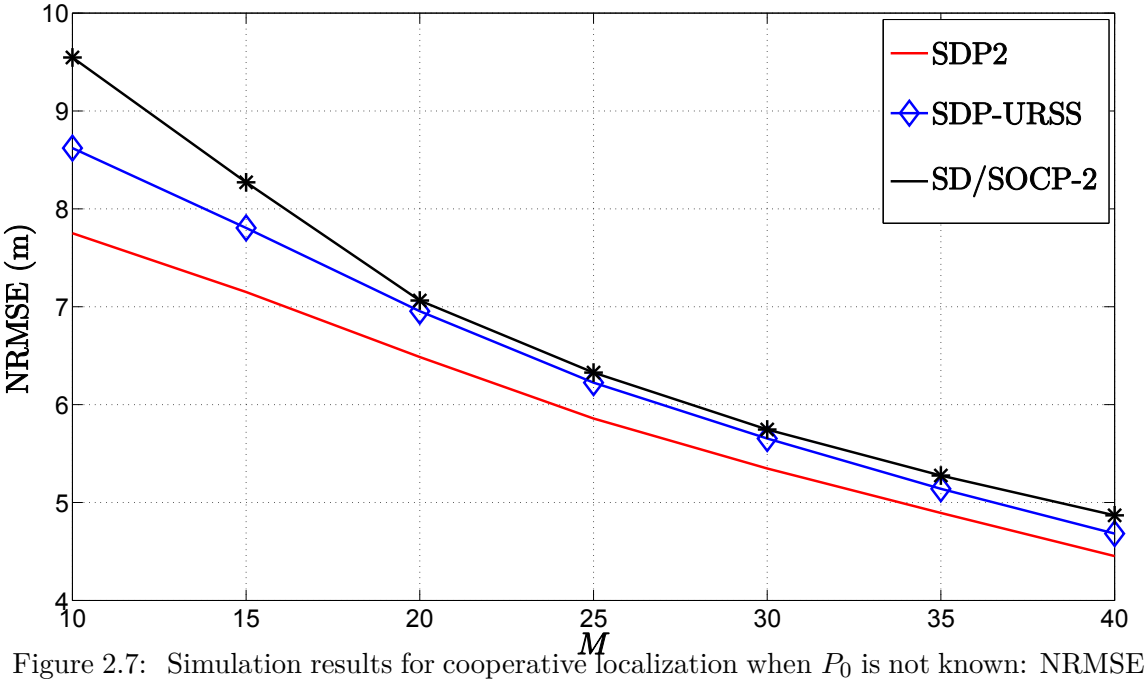

Figure 2.7: Simulation results for cooperative localization when P_0 is not known: NRMSE (m) versus M when $N = 9$, $R = 6$ m, $\sigma = 5$ dB, $B = 15$ m, $P_0 = -10$ dBm, $\gamma = 3$, $d_0 = 1$ m, $M_c = 10000$.

N, when $M = 15$, $R = 6$ m, $\sigma = 5$ dB and $B = 15$ m. Both anchor and targets were positioned randomly inside a square region of length $2B$. This scenario is of particular practical importance because a common requirement for a network is to be flexible and adaptable to different layouts. Fig. 2.9 shows that the estimation accuracy increases as N is increased, as predicted. One can see that our approach outperforms the existing ones for all choices of N, with an average gain of about 1 m and 0.5 m, compared to "SD/SOCP-2" and "SDP-URSS", respectively. Having less anchors in the network might reduce its implementation costs, since *e.g.*, they might be equipped with a GPS receiver in order to determine their own positions. Fig. 2.9 shows that the proposed approach needs on average 1 or 2 less anchors to achieve the same estimation accuracy as the SoA approaches[5].

To give an illustration of the quality of the ML estimate of P_0 versus direct estimate from η by solving (2.22), *i.e.*, estimating P_0 as $\hat{P}_0 = 10\gamma \log_{10} \eta$, we call the readers attention to Fig. 2.10. The mean of the estimated value is represented by a red cross and blue circle for direct and ML estimates of P_0 respectively, and their standard deviations are given by a line with the respective color. From Fig. 2.10, it can be seen that much more accurate estimates of P_0 are obtained through the ML approach, especially for large N.

Fig. 2.11 illustrates the cumulative distribution function (CDF) of mean error (ME) in the target position estimation of the considered approaches, for $N = 9$, $M = 15$, $R = 10$ m, $\sigma = 5$ dB and $B = 15$ m. The ME is defined as $\text{ME} = \sum_{i=1}^{M} \frac{\|\boldsymbol{x}_{ij} - \widehat{\boldsymbol{x}}_{ij}\|}{M}$ (m), for $j = 1, ..., M_c$, where $\boldsymbol{x}_{i,j}$ and $\hat{\boldsymbol{x}}_{i,j}$ denote the true and the estimated target positions of the i-th target

[5]The CRB was not presented in the Figs. 2.5, 2.7, 2.8 and 2.9, since the Fisher information matrix is singular for the chosen scenarios.

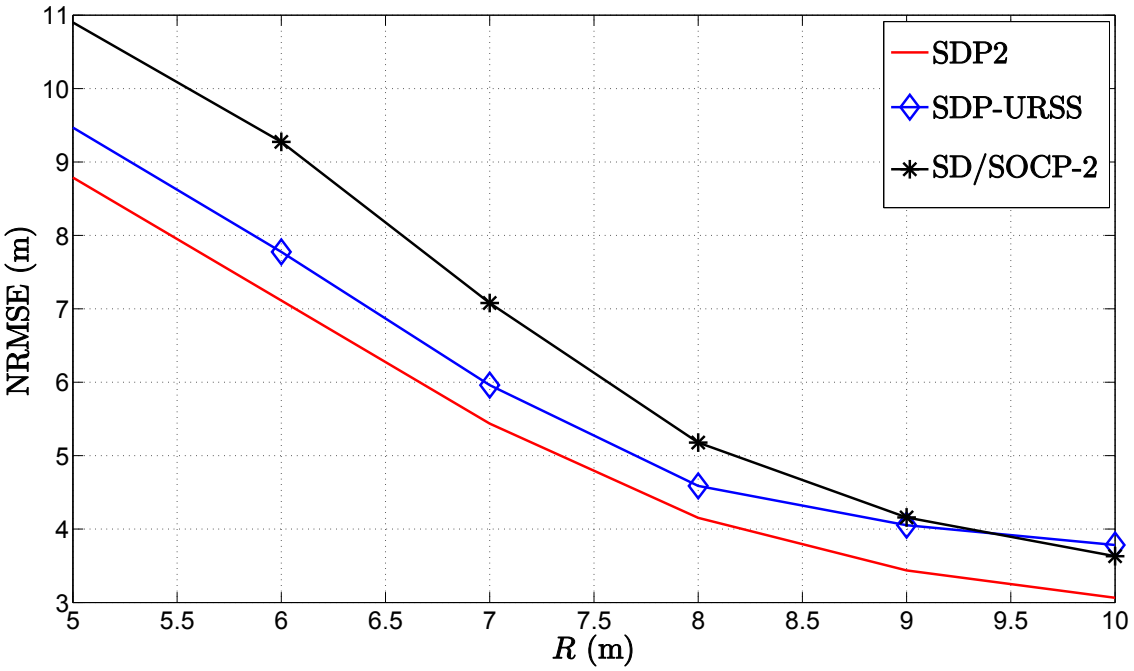

Figure 2.8: Simulation results for cooperative localization when P_0 is not known: NRMSE (m) versus R (m) when $N = 9$, $M = 15$, $\sigma = 5$ dB, $B = 15$ m, $P_0 = -10$ dBm, $\gamma = 3$, $d_0 = 1$ m, $M_c = 10000$.

in the j-th Monte Carlo run, respectively. Fig. 2.11 shows that the proposed approach outperforms the existing ones for all range of the ME, improving the estimation accuracy for more than 0.5 m on average. We can see that the new method achieves LE ≤ 3 m in 80% of the cases, while the existing ones attain the same value of the ME in less than 50% of the cases.

2.2.6 Conclusions

In this section we addressed the RSS-based target localization problem. Both non-cooperative and cooperative localization problems were investigated for both cases of known and unknown target transmit power, P_T.

In the case of the non-cooperative localization when P_T is known, we proposed the novel SOCP-based approach which has an excellent trade-off between the performance and the computational complexity, when compared to the existing approaches. For the case where P_T is not known, we introduced a simple three-step procedure based on the SOCP relaxation. The simulation results showed that the proposed approach provides not only a excellent estimation of the target positions, but also an excellent estimation of P_T. This motivated us to exploit the estimate of P_T and solve another SOCP problem as if P_T was known. The price we have to pay for applying this procedure was solving the problem two times. However, the simulation results confirm its effectiveness and show a remarkable improvement of the estimation accuracy. A gain of more than 15% was achieved, when comparing with the existing approaches, for the case where N is high. We concluded the

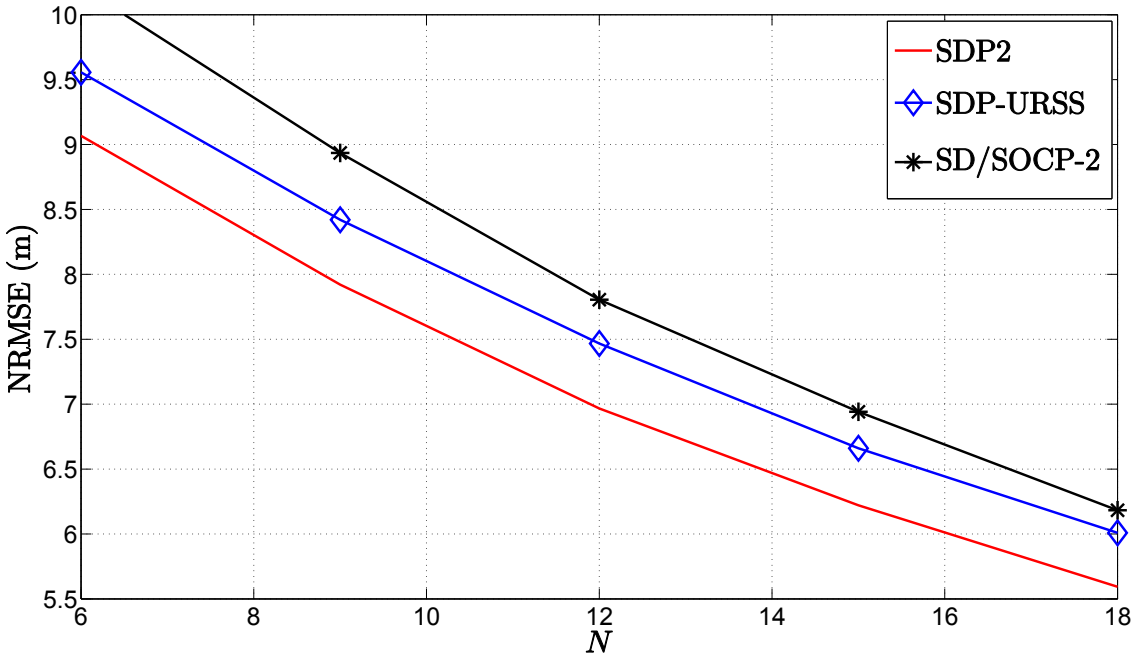

Figure 2.9: Simulation results for cooperative localization when P_0 is not known: NRMSE (m) versus N when $M = 15$, $R = 6$ m, $\sigma = 5$ dB, $B = 15$ m, $P_0 = -10$ dBm, $\gamma = 3$, $d_0 = 1$ m, $M_c = 10000$. Anchors and targets are randomly deployed inside the square region of length $2B$.

non-cooperative localization problem by investigating the case where both P_T and PLE are simultaneously unknown. By applying a standard iterative procedure, we showed that our method efficiently solves the most challenging scenario of the RSS localization problem and outperforms the existing one in terms of the estimation accuracy; the biggest gain was obtained for high N, where an improvement in the localization accuracy of about 15% was attained. Moreover, we have shown that our approach can be used to solve the non-cooperative localization problem in indoor environments. The new approach reduces the estimation error for more than 15% when compared to the SoA approaches.

In the case of the cooperative localization when P_T is known, we proposed a novel SDP-based approach. In huge contrast to the existing SDP approaches that consider the cooperative localization problem, in which the unknown variables are treated as a matrix, here we consider them as a vector. This approach implies a slight increase in the complexity in comparison to the SoA methods. However, the performance evaluation in Section 2.2.5 justifies the use of such an approach. For the case where P_T is known, the proposed approach outperforms the existing ones for all choices of M with the biggest margin for medium-to-high M. In the case where P_T is assumed to be not known, a simple three-step procedure based on SDP relaxation is applied. We have investigated the influence of different M and N, as well as different R on the estimation accuracy. For all the scenarios presented in this work, the new approach outperforms the SoA approaches with an increase in the accuracy between $15-20\%$ on average. Furthermore, the simulation results showed that our approach achieves a ME ≤ 3 m in 80% of the cases, while the

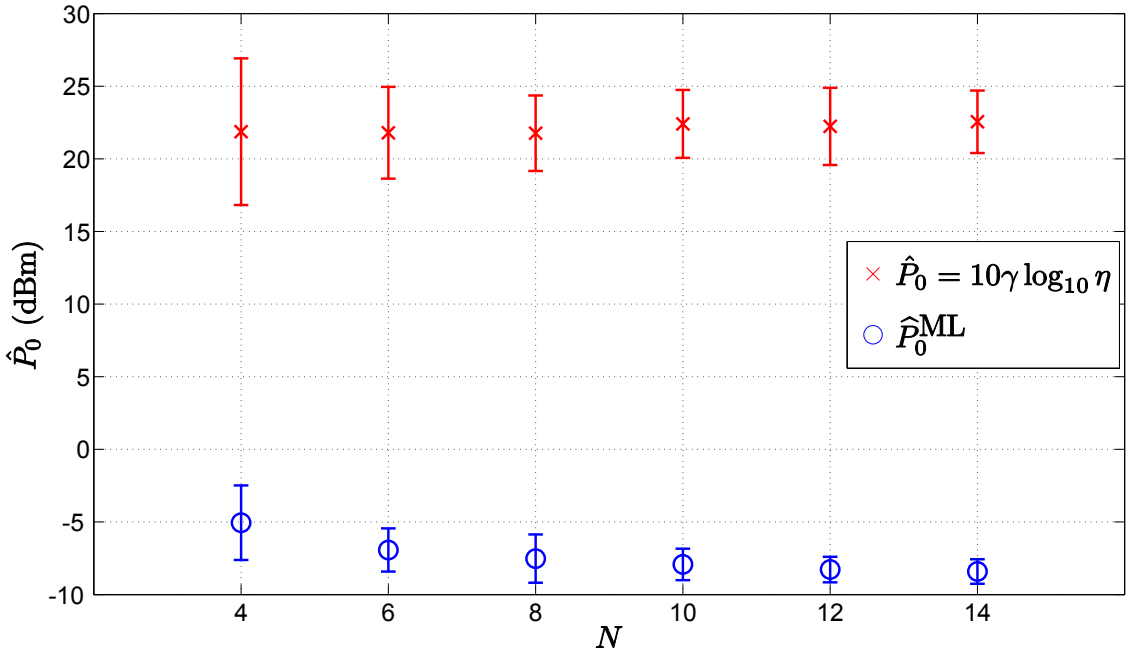

Figure 2.10: Simulation results for non-cooperative localization when P_0 is not known: $\hat{P}_0$ (dBm) versus N when $\sigma = 6$ dB, $B = 15$ m, $P_0 = -10$ dBm, $\gamma = 2.5$, $d_0 = 1$ m, $M_c = 1000$.

existing ones accomplish the same accuracy in less than 50% of the cases.

2.3 Distributed RSS-based Target Localization

2.3.1 Related Work

In [21], a distributed RSS-based localization algorithm for WSNs was presented. This algorithm was characterized by a spatial constraint that limits the solution space to a region around the current position estimate. Using discretization of the solution space, the authors in [21] found the position update of each sensor by minimizing a local objective function over the candidate set using direct substitution. Although the computational characteristics of such algorithms are excellent, their performance highly depends on good initialization, since the objective function is non-convex and the algorithm may get trapped into a local minimum or a saddle point, causing a large estimation error. Another distributed approach using consensus and convex optimization for sensor localization based on RSS measurements was introduced in [67]. This algorithm employed a semidefinite relaxation technique to transform the non-convex ML estimator into a convex one. Béjar and Zazo showed in [67] that applying a distributed algorithm based on an augmented Lagrangian approach using primal-dual decomposition to the derived convex estimator converges to the solution of the centralized approach. However, the approach in [67] deals only with a non-cooperative localization problem, where a single target emits beacon frames to all anchors in the network. In [68], a distributed cooperative localization algorithm that dynamically estimates the PLE by using RSS measurements was introduced. In

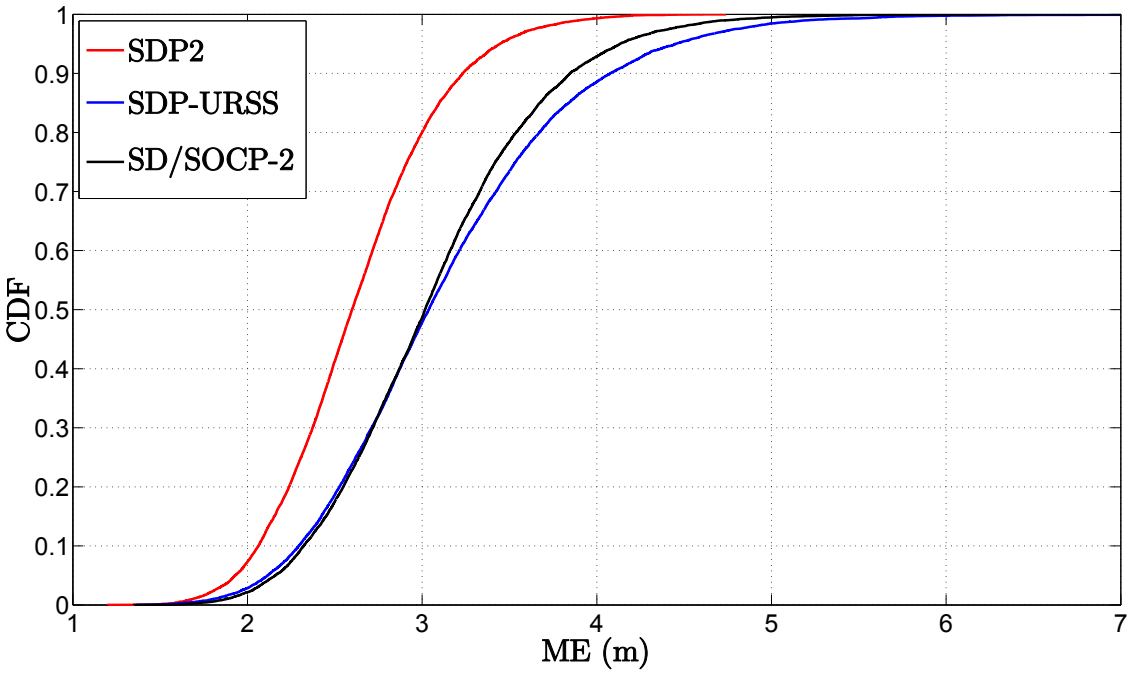

Figure 2.11: Simulation results for cooperative localization when P_0 is not known: CDF of ME (m) in target location estimation when $N = 9$, $M = 15$, $R = 10$ m, $\sigma = 5$ dB, $B = 15$ m, $P_0 = -10$ dBm, $\gamma = 3$, $d_0 = 1$ m, $M_c = 10000$.

order to reduce the energy consumption and possibly improve the estimation accuracy, the authors in [68] presented a node selection mechanism to limit the number of cooperating neighbors. Bel *et al.* used a Gauss-Seidel approach where the PLE is fixed first, and a gradient descent search is applied to estimate the target positions, which are then used to update the estimate of the PLE. This approach is efficient in the sense of computational complexity, but its performance highly depends on a good initialization and the step size of the search.

Contributions

All mentioned approaches deal only with the localization problem where the target's transmit power, P_T, is known. In this section, we design a novel distributed cooperative algorithm based on SOCP relaxation for sensor localization in WSNs using RSS measurements. In huge contrast to the existing work, we investigate both cases of known and unknown P_T. Hence, the main contribution of our work is twofold. In the case where P_T is known, the main contribution of our work is the reduction of the estimation error for more than 1.5 m in comparison to the SoA approaches. In the case where P_T is not known, to the best of authors' knowledge, there is no existing solution proposed to overcome the mentioned problem; hence, the main contribution of our work is a novel distributed SOCP-based algorithm for target localization in the presence of unknown P_T in a cooperative network. For both cases, we start by coloring the network to establish a working hierarchy inside the network. To color the network, we employ the second-order

coloring scheme [69], which implies that no node has the same color as any of its neighbors nor its neighbors' neighbors. This way we guarantee that our algorithm is completely distributed and efficient (collision-free and fast as nodes with the same color can work in parallel). Next, we break down the non-convex and computationally complex ML estimation problem into smaller sub-problems, *i.e.* we pose the local ML estimation problem for each target node. We derive a non-convex estimator which tightly approximates the local ML estimator for small noise. SOCP relaxation technique is applied to the derived non-convex estimator in order to form a convex one, which can be efficiently solved by interior-point algorithms [62]. Each target node obtains the solution locally, using an iterative procedure. In the case where P_T is not known, we propose a simple algorithm based on SOCP relaxation which can be described in four parts. First, target nodes obtain the estimates of their positions by iteratively solving the proposed SOCP problem for unknown P_T. Next, the position estimates are fixed and used to attain an estimation of P_T at each target node. Target nodes then obtain the average estimated value of P_T by means of average consensus. Finally, target nodes update their position estimates by solving the proposed SOCP problem for known P_T, by exploiting the consensus estimate of P_T. In addition, a possible improvement of the convergence properties of the proposed algorithm for known P_T is investigated, by allowing a first-degree memory in the nodes. We propose a simple heuristic approach which combines the previous and the new target position estimates in order to derive new estimates *closer* to the true target locations. At last, we provide details about the computational complexity and energy consumption of the considered algorithms.

2.3.2 Problem Formulation

We consider a large-scale WSN with M target and N anchors, randomly deployed over a region of interest. The considered network can be seen as a connected graph, $\mathcal{G}(\mathcal{V},\mathcal{E})$, with $|\mathcal{V}| = M+N$ vertices and $|\mathcal{E}|$ edges, where $|\bullet|$ represents the cardinality of a set. The set of targets and the set of anchors are labelled as $\mathcal{T} = \{t : t = 1,...,M\}$ and $\mathcal{A} = \{a : a = M+1,...,M+N\}$, respectively. Without loss of generality, this section focuses on a 2-D scenario (the extension to a 3-D scenario is straightforward), where the true locations of the sensors are denoted as $\boldsymbol{x}_i$ ($\boldsymbol{x}_i \in \mathbb{R}^2$), $\forall i \in \mathcal{V}$ ($\mathcal{V} = \mathcal{T} \cup \mathcal{A}$). Due to battery consumption (the lifetime of the network), it is assumed that all sensors have limited communication range, R (the generalization to other cases is straightforward). Hence, two sensors, i and j, can exchange information if and only if they are within the communication range of each other. The set of connections (edges) is defined as $\mathcal{E} = \{(i,j) : \|\boldsymbol{x}_i - \boldsymbol{x}_j\| \leq R,\ i \in \mathcal{T}, j \in \mathcal{V}, i \neq j\}$. Accordingly, the set of neighbors of target i is defined as $\mathcal{N}_i = \{j : (i,j) \in \mathcal{E}\}$.

For ease of expression, let us define $\boldsymbol{X} = [\boldsymbol{x}_1, \boldsymbol{x}_2, ..., \boldsymbol{x}_M]$ as the matrix of all target positions that need to be determined ($\boldsymbol{X} \in \mathbb{R}^{2\times M}$). We assume that the anchor positions are known *a priori*, while each target i is given an initial estimation of its position, $\hat{\boldsymbol{x}}_i^{(0)}$, $\forall i \in \mathcal{T}$; hence, $\hat{\boldsymbol{X}}^{(0)}$ contains all initial target position estimations. Furthermore, sets $\mathcal{U} =$

$\{(i,j):\ \|\boldsymbol{x}_i-\boldsymbol{x}_j\|\le R,\ \forall i\in\mathcal{T},\forall j\in\mathcal{A}\}$ and $\mathcal{W}=\{(i,k):\ \|\boldsymbol{x}_i-\boldsymbol{x}_k\|\le R,\ \forall i,k\in\mathcal{T},\ i\neq k\}$ denote the existence of the target/anchor and the target/target connections, respectively.

Under the log-normal shadowing and log-distance model, the received power, P_{ij} (dBm), between two sensors i and j at a distance $\|\boldsymbol{x}_i-\boldsymbol{x}_j\|$ from the transmitting sensor, can be modeled according to the following radio propagation model (in dBm) [58, 59]The

$$P_{ij}^{\mathcal{U}}=P_0-10\gamma\log_{10}\frac{\|\boldsymbol{x}_i-\boldsymbol{x}_j\|}{d_0}+v_{ij},\ (i,j)\in\mathcal{U},$$

$$P_{ik}^{\mathcal{W}}=P_0-10\gamma\log_{10}\frac{\|\boldsymbol{x}_i-\boldsymbol{x}_k\|}{d_0}+v_{ik},\ (i,k)\in\mathcal{W}, \tag{2.25}$$

where v_{ij} is the log-normal shadowing term between the i-th and j-th sensor, modeled as a zero-mean Gaussian random variable with variance σ_{ij}^2, *i.e.* $v_{ij}\sim\mathcal{N}\left(0,\sigma_{ij}^2\right)$. We assume that the target/target path loss measurements are symmetric, *i.e.*, $P_{ik}^{\mathcal{W}}=P_{ki}^{\mathcal{W}}$ for $i\neq k$.

Given the observation vector $\boldsymbol{P}=[P_{ij}]\,(\boldsymbol{P}\in\mathbb{R}^{|\mathcal{E}|})$, the probability density function (PDF) is

$$p(\boldsymbol{P}|\boldsymbol{X})=\prod_{(i,j):(i,j)\in\mathcal{U}}\frac{1}{\sqrt{2\pi\sigma_{ij}^2}}\exp\left\{-\frac{\left(P_{ij}^{\mathcal{U}}-P_0+10\gamma\log_{10}\frac{\|\boldsymbol{x}_i-\boldsymbol{x}_j\|}{d_0}\right)^2}{2\sigma_{ij}^2}\right\}$$

$$+\prod_{(i,k):(i,k)\in\mathcal{W}}\frac{1}{\sqrt{2\pi\sigma_{ik}^2}}\exp\left\{-\frac{\left(P_{ik}^{\mathcal{W}}-P_0+10\gamma\log_{10}\frac{\|\boldsymbol{x}_i-\boldsymbol{x}_k\|}{d_0}\right)^2}{2\sigma_{ik}^2}\right\} \tag{2.26}$$

The most common estimator used in practice is the ML estimator, since it has the property of being asymptotically efficient (for large enough data records) [47]. ML estimator forms its estimate as the matrix $\hat{\boldsymbol{X}}$, which maximizes the PDF in (2.26); hence, the ML estimator is obtained as

$$\hat{\boldsymbol{X}}=\arg\min_{\boldsymbol{X}}\sum_{(i,j):(i,j)\in\mathcal{U}}\frac{1}{\sigma_{ij}^2}\left[P_{ij}^{\mathcal{U}}-P_0+10\gamma\log_{10}\frac{\|\boldsymbol{x}_i-\boldsymbol{x}_j\|}{d_0}\right]^2$$

$$+\sum_{(i,k):(i,k)\in\mathcal{W}}\frac{1}{\sigma_{ik}^2}\left[P_{ik}^{\mathcal{W}}-P_0+10\gamma\log_{10}\frac{\|\boldsymbol{x}_i-\boldsymbol{x}_k\|}{d_0}\right]^2. \tag{2.27}$$

Even though the ML estimator is approximately the minimum variance unbiased (MVU) estimator [47], the LS problem in (2.27) is non-convex and has no closed-form solution. In the remainder of this thesis, we will show that the LS problem in (2.27) can be relaxed as a SOCP, which can be solved efficiently by interior-point algorithms [62].

Assumptions

Before we proceed, let us prompt some assumptions made about the considered WSN:

1) $\sigma_{ij}^2=\sigma^2,\ \forall(i,j)\in\mathcal{E}$;

2) *All sensors are equipped with omnidirectional antennas and have identical P_T;*

3) *The network is connected and it does not vary in time during the computational phase;*

4) *A coloring scheme of the network is available.*

Assumptions 1) and 2) are made for the sake of simplicity (without loss of generality). Assumption 2) implies that P_0 and R are equal for all sensors. In Assumption 3), a network is connected if and only if there exists a path between each sensors $i, j \in \mathcal{V}$. Finally, in Assumption 4), a coloring scheme is an assignment of colors (numbers) to the sensors in order to establish a working hierarchy in the network. In this thesis, we employ a second-order coloring scheme, meaning that no sensor has the same color (number) as any of its neighbors nor its neighbors' neighbors [69, 70], as illustrated in Fig. 2.12.

As one can see from Fig. 2.12, the blue sensors will be the first ones to estimate their positions, while all other sensors are in idle state. After the blue sensors finish working, they will broadcast the updated position to their neighbors. The red sensors will be the next ones to work, using the updated information from the blue sensors, and so on following the colors (numbers) in Fig. 2.12. Each sensor in the network needs to know only its own color and after which color (neighbor) is its turn to operate, rather than all the colors in the network. Note that, since we employed the second-order coloring scheme, sensors with the same color may work in parallel without a risk of message collision at the receiving end. According to Fig. 2.12, the execution time of the algorithm is decreased from the time needed to realize $|\mathcal{V}| = 13$ operations to $|\mathcal{C}| = 8$ operations by working in parallel, where $\mathcal{C}$ represents the set of colors of the sensors[6]. In wireless scenarios, coloring schemes are used in MAC protocols in order to achieve collision-free algorithms [70].

2.3.3 Distributed Approach Using SOCP Relaxation

Note that the objective function in (2.27) depends only on the positions and pairwise measurements between the adjacent sensors. Assuming that the initial position estimations of the target sensors are known, problem in (2.27) can be partitioned, *i.e.*, the minimization can be executed independently by each target, using only the information gathered from its neighbors. Hence, instead of solving (2.27), which can be computationally exhausting (in large-scale WSNs), we break down (2.27) into subproblems, which are solved locally (by each target) using iterative approach. Therefore, target i updates its position estimate by minimizing the following local ML problem:

$$\hat{\boldsymbol{x}}_i^{(k+1)} = \underset{\boldsymbol{x}_i}{\operatorname{argmin}} \sum_{j \in \mathcal{N}_i} \frac{1}{\sigma^2} \left[P_{ij} - P_0 + 10\gamma \log_{10} \frac{\|\boldsymbol{x}_i - \hat{\boldsymbol{x}}_j\|}{d_0} \right]^2, \ \forall i \in \mathcal{T}, \tag{2.28}$$

where $\hat{\boldsymbol{x}}_j$ denotes the last position update of the j-th neighbor (if the j-th neighbor is a target) or the true neighbor's position (if the j-th neighbor is an anchor) received by the i-th target. From (2.28) we distinguish two possible cases of the localization problem: P_T

[6]Note that the network coloring problem may be considered as an optimization problem where the goal is to minimize the number of different colors. Although interesting in its own right, we did not investigate this problem here, since it does not follow the main idea of this thesis.

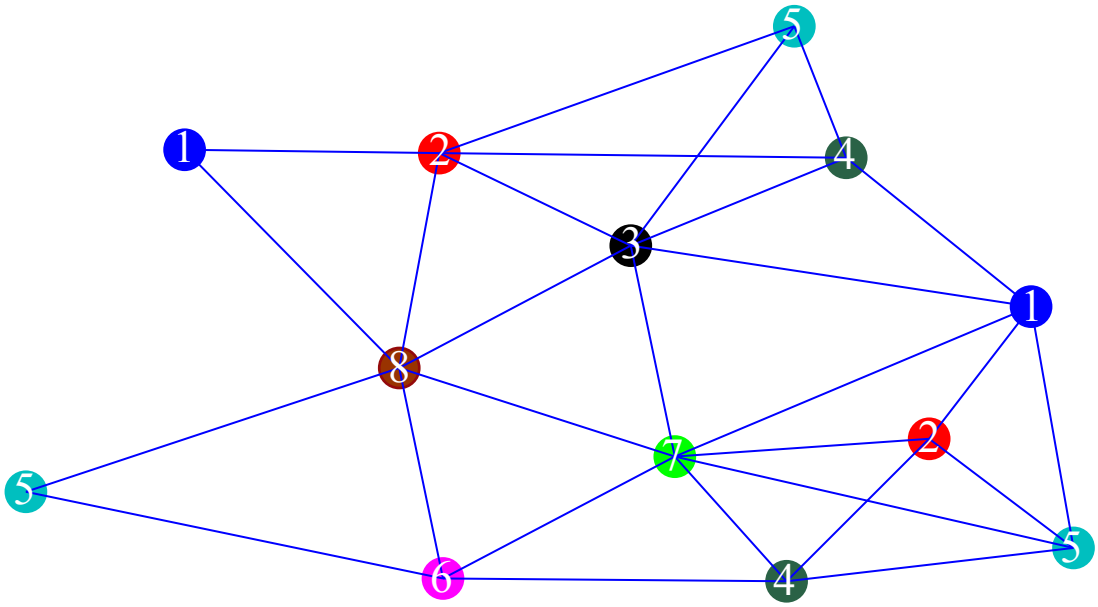

Figure 2.12: A possible second-order coloring scheme for a network with $|\mathcal{V}| = 13$ sensors.

of the transmitting sensor is known, and a more practical scenario where P_T is not known at the receiving end. In the following text we deal with these two cases and we propose a distributed solution based on the SOCP relaxation for both of them.

Transmit power is known

From the propagation model (2.25), the estimated distance between the i-th target and its j-th neighbor, $\hat{d}_{ij}$, is given by

$$\hat{d}_{ij} \approx d_0 10^{\frac{P_0 - P_{ij}}{10\gamma}}. \tag{2.29}$$

We can rewrite (2.29) as

$$\lambda_{ij}\hat{d}_{ij} \approx \alpha d_0, \tag{2.30}$$

where $\lambda_{ij} = 10^{\frac{P_{ij}}{10\gamma}}$ and $\alpha = 10^{\frac{P_0}{10\gamma}}$. Assuming that the initial target position estimates are available, from (2.30), the updated position of the i-th target, $\hat{\boldsymbol{x}}_i^{(k+1)}$, is found by

minimizing the following LS problem[7]:

$$\hat{\boldsymbol{x}}_i^{(k+1)} = \underset{\boldsymbol{x}_i}{\operatorname{argmin}} \sum_{j \in \mathcal{N}_i} \left(\lambda_{ij}\|\boldsymbol{x}_i - \hat{\boldsymbol{x}}_j\| - \alpha d_0\right)^2, \ \forall i \in \mathcal{T}. \tag{2.31}$$

LS problem in (2.31) is non-convex and has no closed-form solution. However, in the following text, we will show that (2.31) can be written as a convex optimization problem by using SOCP relaxation. First, define auxiliary variables $d_{ij} = \|\boldsymbol{x}_i - \hat{\boldsymbol{x}}_j\|$ and $\boldsymbol{z} = [z_{ij}]$, where $z_{ij} = \lambda_{ij} d_{ij} - \alpha d_0$, $\forall (i,j) \in \mathcal{E}$. We get

$$\underset{\boldsymbol{x}_i, d_{ij}, \boldsymbol{z}}{\text{minimize}} \sum_{j \in \mathcal{N}_i} z_{ij}^2$$

subject to

$$z_{ij} = \lambda_{ij} d_{ij} - \alpha d_0, \ d_{ij} = \|\boldsymbol{x}_i - \hat{\boldsymbol{x}}_j\|. \tag{2.32}$$

Introduce an epigraph variable, t. By using the second-order cone constraint (SOCC) relaxation, we obtain the following convex optimization problem:

$$\underset{\boldsymbol{x}_i, d_{ij}, \boldsymbol{z}, t}{\text{minimize}} \ t$$

subject to

$$\|\left[2\boldsymbol{z}; t-1\right]\| \leq t+1, \ z_{ij} = \lambda_{ij} d_{ij} - \alpha d_0, \ \|\boldsymbol{x}_i - \hat{\boldsymbol{x}}_j\| \leq d_{ij}. \tag{2.33}$$

Problem (2.33) is a SOCP problem, which can be efficiently solved by `CVX` package [62] for specifying and solving convex programs. Note that by applying the SOCC relaxation, the original set of feasible points is enlarged, which means that the optimal solution of (2.33), $\boldsymbol{x}_i^\star$, might not be the optimal solution of (2.31). However, if the SOCC of the form $\|\boldsymbol{p}\| \leq q$ is satisfied as an equality, we have that the SOCC relaxation is not a relaxation at all, and that $\boldsymbol{x}_i^\star$ of (2.33) is also the optimal solution of (2.31).

In summary, the derivation of the above SOCP approach can be described in two parts. In the first part, the local non-convex ML estimator in (2.28) is approximated by a different non-convex estimator in (2.31). The use of the objective function in (2.31) is motivated by the fact that we get a much smoother surface in comparison to (2.28), at a cost of introducing some bias with respect to the ML solution (see Fig. 2.13). If the bias effect is small, we might reach the ML solution by employing a local search around the solution of (2.31). In the second part of our approach, we convert (2.31) into a convex problem by applying SOCP relaxation.

[7] Another possible explanation with more theoretical justification leading to (2.31) is as follows. We can rewrite (2.25) as $\frac{P_0 - P_i}{10\gamma} = \log_{10} \frac{\|\boldsymbol{x}_i - \boldsymbol{x}_j\|}{d_0} + \frac{v_{ij}}{10\gamma}$, which corresponds to $\lambda_{ij}\|\boldsymbol{x}_i - \boldsymbol{x}_j\| = \alpha d_0 10^{\frac{v_{ij}}{10\gamma}}$. For sufficiently small noise, the first-order Taylor series expansion to the right-hand side of the previous expression is given by $\lambda_{ij}\|\boldsymbol{x}_i - \boldsymbol{x}_j\| = \alpha d_0 (1 + \frac{\ln 10}{10\gamma} v_{ij})$, *i.e.*, $\lambda_{ij}\|\boldsymbol{x}_i - \boldsymbol{x}_j\| = \alpha d_0 + \epsilon_{ij}$, where $\epsilon_{ij} = \alpha d_0 \frac{\ln 10}{10\gamma} v_{ij}$ is the zero-mean Gaussian random variable with the variance $\alpha^2 d_0^2 \frac{(\ln 10)^2}{100\gamma^2}\sigma^2$. Clearly, the corresponding LS estimator is given by (2.31). Similar has been done in [56]. Even though our estimator is derived under the assumption that the noise is small, it works excellent in the case where this assumption does not hold, as we will see in Section 2.3.5.

Fig. 2.13 illustrates a realization of the objective functions in (2.28) and (2.31), for the case where the true sensor positions are used (Figs. 2.13a and 2.13b) and a realization of (2.31) when the estimated positions of the targets, obtained by solving (2.33), are used: after the first and the tenth iteration (Figs. 2.13c and 2.13d), respectively. We randomly placed $M = 50$ target and $N = 25$ anchors inside a square region of the size $30 \times 30\,\mathrm{m}^2$. The i-th target is located at $[12.8; 23.0]$, and has 5 anchor and 5 targets as its neighbors. All targets were given an initial guess of their positions in the center of the mentioned area. The rest of the parameters are set to: $P_0 = -10$ dBm, $\sigma = 0$ dB, $\gamma = 3$, and the objective functions are plotted versus x and y coordinates (the step in the mesh grid is 0.1 m). Fig. 2.13a shows that the objective function in (2.28), given the true positions of the targets, has a global minimum at $[12.8; 23]$, and some local minima and saddle points. Fig. 2.13b shows that the objective function in (2.31), given the true positions of the targets, has a global minimum at $[12.8; 23.1]$, and is much smoother than (2.28). We can see that the objective functions (2.28) and (2.31) have similar behavior: both monotonically increase and decrease in the same regions. In Fig. 2.13c one can see that the global minimum has shifted to $[14.4; 17.3]$. Furthermore, it can be seen that the shape of this objective function does not coincide with the objective function in Fig. 2.13b. This is due to the fact that in the first iteration targets broadcast their initial position guess to their neighbors, which results in high estimation error. However, as the number of iterations is increased the estimation accuracy betters, as shown in Fig. 2.13d, where the global minimum is located at $[12.8; 23]$. From Fig. 2.13, it is clear that the objective function in (2.31) is an excellent approximation of the objective function in (2.28).

Algorithm 1 summarizes the proposed distributed SOCP approach for known P_T. Algorithm 1 is distributed in the sense that no central node coordinates the network, all communication occur exclusively between two incident sensors, and the data associated with each sensor is processed locally. Lines 5-7 are executed simultaneously by all sensors $i \in \mathcal{C}_c$, which may decrease the execution time of the algorithm. The only information exchange occurs in Line 7, when the sensors broadcast their position updates $\hat{\boldsymbol{x}}_i^{(k+1)}$ to their neighbors. Since $\hat{\boldsymbol{x}}_i^{(k+1)} \in \mathbb{R}^2$, we can conclude that the proposed algorithm requires at most a broadcast of $2K_{\max}M$ real values.

Transmit power is not known

In order to minimize the expenses and achieve a low-cost localization system, testing and calibration of the devices are usually not the priority in practice [1]. This means that the sensor's transmit power, P_T, is not calibrated, *i.e.*, not known. Not knowing P_T corresponds to not knowing P_0 in the used model; hence, in this subsection, P_0 is considered to be an unknown parameter that also needs to be estimated. Adaptation of the SOCP approach for known P_0 is straightforward for the case where P_0 is not known:

$$\underset{\boldsymbol{x}_i, d_{ij}, \boldsymbol{z}, t, \alpha}{\text{minimize}}\ t$$

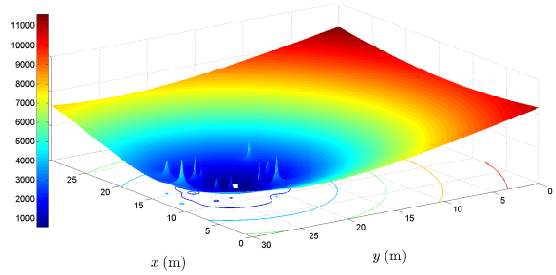

(a) Objective function in (2.28) using the true target positions

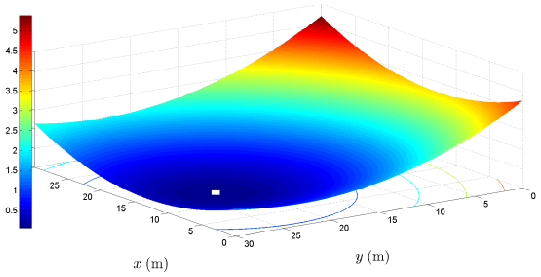

(b) Objective function in (2.31) after one iteration using the true target positions

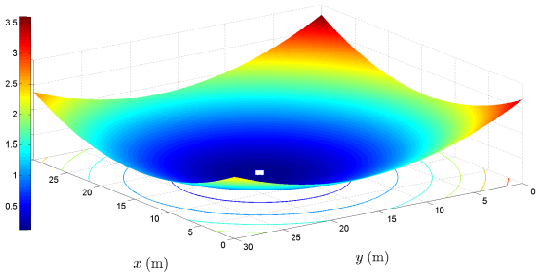

(c) Objective function in (2.31) after one iteration using estimated target positions

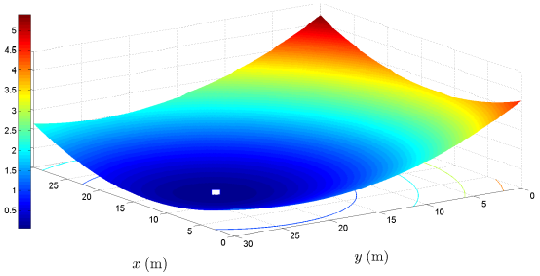

(d) Objective function in (2.31) after ten iterations using estimated target positions

Figure 2.13: Illustration of the cost functions (2.28) and (2.31) versus x and y coordinates (target location); the minimum of the cost function is indicated by a white square.

Algorithm 1 "SOCP1" - The proposed distributed SOCP algorithm for known P_T

Require: $\hat{\boldsymbol{X}}^{(0)}$, $K_{\max}$, $\mathcal{C}$, $\boldsymbol{x}_a$, $\forall a \in \mathcal{A}$

Initialize: $k \leftarrow 1$
repeat
  for $c = 1,...,\mathcal{C}$ **do**
    for all $i \in \mathcal{C}_c$ (in parallel) **do**
      Collect $\hat{\boldsymbol{x}}_j$ from $j \in \mathcal{N}_i$
      $\hat{\boldsymbol{x}}_i^{(k)} \leftarrow$ solve (2.33)
      Broadcast $\hat{\boldsymbol{x}}_i^{(k)}$ to $j \in \mathcal{N}_i$
    end for
  end for
  $k \leftarrow k+1$
until $k \leq K_{\max}$

subject to

$$\| [2\boldsymbol{z}; t-1] \| \leq t+1,\ z_{ij} = \lambda_{ij} d_{ij} - \alpha d_0,\ \|\boldsymbol{x}_i - \hat{\boldsymbol{x}}_j\| \leq d_{ij}. \tag{2.34}$$

Algorithm 2 summarizes the proposed distributed SOCP approach for unknown P_T. This algorithm can be easily explained in four parts. The first part includes lines 1-12, where we estimate the targets' positions by solving the SOCP problem described in (2.34), $K_{1\max}$ number of times. In order to minimize the oscillations in the position estimates, we employ a weight, w, in Line 7 of our algorithm. Although the difference in the performance is marginal, according to our simulations, the best choice of the weight is $w = \frac{1}{\sqrt{k}}$. Then, in lines 13-17, we use the estimates obtained in the $K_{1\max}$-th iteration to find the estimate of P_0, $\widehat{P}_{0i}$, at each target. Since we assumed that P_0 is identical for all sensors, an average consensus is executed next in order to reach the average estimated value of P_0, $\widehat{P}_0$; lines 18-20. To realize the average consensus, we employ the local-degree weights method [71], since it is particularly suitable for distributed implementation and guarantees convergence (if the graph is not bipartite). The final part of our algorithm involves lines 21-31, which are executed $K_{2\max}$ number of times. Here, we take advantage of $\widehat{P}_0$, and obtain the targets' position estimates by solving (2.33) as if P_0 is known, *i.e.*, we calculate $\hat{\alpha} = 10^{-\frac{\widehat{P}_0}{10\gamma}}$. Concerning the information exchange of the proposed algorithm, it is easy to see that it requires at most a broadcast of $(2(K_{1\max} + K_{2\max}) + D_{\max})M$ real values, given that $D_{\max}$ is the maximum number of communications between sensors in order to reach consensus.

2.3.4 Energy Consumption Analysis

To evaluate the overall performance of an algorithm, besides the estimation accuracy, it is also important to assess its energy consumption. The trade-off between the estimation accuracy and the energy consumption determines the applicability potential of an algorithm, thus, it is its key feature.

To prolong the lifetime of a network, *i.e.*, to maintain the lifetime of sensors' battery, it is very important to mitigate the energy depletion in a WSN. Two major energy-consuming phases of an algorithm are: data processing and data communication. In the following text we provide an analysis of these two phases. However, in order to provide a more complete overview of the algorithms' performance, we present the results of the analysis together with the simulation results in Section 2.3.5.

Data Processing

As we mentioned earlier, data collected inside the network is processed locally by each target in a distributed approach. In order to evaluate the efficiency of an approach, in terms of data processing, we have to determine its computational complexity. The formula for computing the worst case computational complexity of an SOCP problem [63], given

Algorithm 2 "SOCP2" - The proposed distributed SOCP algorithm for unknown P_T

Require: $\hat{\boldsymbol{X}}^{(0)}$, $K_{1\max}$, $K_{2\max}$, $\mathcal{C}$, $\boldsymbol{x}_a$, $\forall a \in \mathcal{A}$
Initialize: $k \leftarrow 1$
repeat
  for $c = 1, ..., \mathcal{C}$ **do**
    for all $i \in \mathcal{C}_c$ (in parallel) **do**
      Collect $\hat{\boldsymbol{x}}_j$ from $j \in \mathcal{N}_i$
      $\hat{\boldsymbol{x}}_{i\text{socp}}^{(k)} \leftarrow$ solve (2.34)
      $\hat{\boldsymbol{x}}_i^{(k)} \leftarrow (1-w)\hat{\boldsymbol{x}}_i^{(k-1)} + w\hat{\boldsymbol{x}}_{i\text{socp}}^{(k)}$
      Broadcast $\hat{\boldsymbol{x}}_i^{(k)}$ to $j \in \mathcal{N}_i$
    end for
  end for
  $k \leftarrow k+1$
until $k \leq K_{1\max}$
for $c = 1, ..., \mathcal{C}$ **do**
  for all $i \in \mathcal{C}_c$ (in parallel) **do**
    $\widehat{P}_{0i} \leftarrow \frac{\sum_{j\in\mathcal{N}_i} P_{ij} + 10\gamma \log_{10} \frac{\|\hat{\boldsymbol{x}}_i^{(k)} - \hat{\boldsymbol{x}}_j^{(k)}\|}{d_0}}{|\mathcal{N}_i|}$
  end for
end for
begin **consensus**
$\widehat{P}_0 \leftarrow \frac{1}{M}\sum_{i=1}^{M} \widehat{P}_{0i}$
end **consensus**
$k \leftarrow K_{1\max} + 1$
repeat
  for $c = 1, ..., \mathcal{C}$ **do**
    for all $i \in \mathcal{C}_c$ (in parallel) **do**
      Collect $\hat{\boldsymbol{x}}_j$ from $j \in \mathcal{N}_i$
      $\hat{\boldsymbol{x}}_i^{(k)} \leftarrow$ solve (2.33) by using $\widehat{P}_0$
      Broadcast $\hat{\boldsymbol{x}}_i^{(k)}$ to $j \in \mathcal{N}_i$
    end for
  end for
  $k \leftarrow k+1$
until $k \leq K_{1\max} + K_{2\max}$

below, is used to calculate the complexity of the proposed approach:

$$\mathcal{O}\left(\sqrt{L}\left(m^2\sum_{i=1}^{L}n_i+\sum_{i=1}^{L}n_i^2+m^3\right)\right), \tag{2.35}$$

where L is the number of the second-order cone constraints, m is the number of the equality constraints, and n_i is the dimension of the i-th second-order cone.

Let us assume that we can always equalize the energy consumption of two algorithms in the data processing phase through voltage adjustment [72]. Energy depletion of two algorithms is then compared through the execution time of the algorithms, meaning that a more energy-efficient algorithm is the more time-efficient one.

Data Communication

After processing the data in order to update its position estimate, a sensor immediately broadcasts this estimate to its neighbors. This phase of the algorithm is the most expensive - regarding the energy-consumption - since the energy required to transmit one bit could be used to execute thousands of instructions, depending on the hardware and the range [1, 16].

The formula for computing the total amount of energy consumed by the network in the communication phase, given below, is employed:

$$E_{\text{com}}=\left(E_{T_x}M+E_{R_x}\sum_{i=1}^{M}|\mathcal{N}_i|\right)K_{\text{req}}, \tag{2.36}$$

where E_{T_x} and E_{R_x} denote the energy consumed by a sensor for broadcasting and receiving data, respectively, and K_{req} is the number of iterations required for an algorithm to converge.

2.3.5 Performance Results

In this section, computer simulations are performed in order to compare the performance of the proposed approaches with the SoA. The proposed algorithms were solved by using the MATLAB package `CVX` [62], where the solver is SeDuMi [65].

A random deployment of M targets and N anchors inside a square region of length B in each Monte Carlo (M_c) run is considered. Random deployment of the sensors is of particular interest, since a common practical requirement for a WSN is that it is flexible in topology; hence, the localization algorithms need to be robust to various scenarios. In order to make the comparison of the considered approaches as fair as possible, we first obtained $M_c = 500$ targets' and anchors' positions, as well as noise realizations between sensors $(i,j)\in\mathcal{E}$ in each M_c run. Furthermore, we made sure that the network graph is connected in each M_c run. We then solved the localization problem with the considered approaches for those scenarios. In all simulations presented here, the path loss exponent is set to $\gamma = 3$, the reference distance $d_0 = 1$ m, the reference power $P_0 = -10$ dBm, and

the communication range of a sensor is $R = B/5$ m. We assumed that the initial guess of the target positions, $\hat{\boldsymbol{X}}^{(0)}$, is in the intersection of the diagonals of the square area, since the biggest possible error for this case is half of the diagonal of the area. In the case of known P_T, the maximum number of iterations is set to $K_{\max} = 200$, while for unknown P_T, $K_{1\max} = 10$ and $K_{2\max} = 25$, unless stated otherwise. The performance metric is the NRMSE, defined as

$$\text{NRMSE} = \sqrt{\frac{1}{MM_c}\sum_{i=1}^{M_c}\sum_{j=1}^{M}\|\boldsymbol{x}_{ij} - \widehat{\boldsymbol{x}}_{ij}\|^2},$$

where $\widehat{\boldsymbol{x}}_{ij}$ denotes the estimate of the true location of the j-th target, $\boldsymbol{x}_{ij}$, in the i-th Monte Carlo run.

In Table 2.9, we provide an overview of the considered algorithms in this section, together with their worst case computational complexities. To the best of authors' knowledge, the SoA algorithms for the case where P_T is known are described in [21, 68], whereas for the case when P_T is not known, there is no existing work.

From Table 2.9, it is clear that the computational complexity of the distributed algorithms mainly depends on the size of the neighborhood fragments, rather than the total number of sensors in the WSN. Although it is theoretically possible to have that $\max_i\{|\mathcal{N}_i|\} = M+N-1$, for $i = 1, ..., M$, in practice, the size of the neighborhood fragments are much smaller, due to limited R. For example, in our simulations, the majority of sensors had very few neighbors, and the average size of fragments was well below 10. Increasing the number of sensors in the network does not necessarily impact the neighborhood fragments (or not significantly), which is why the distributed algorithms are preferable in large-scale and highly-dense WSNs in contrast to the centralized ones. Table 2.9 also reveals that the proposed algorithms are computationally the most demanding, in comparison to the existing ones. However, this fact is justified by their superior performance in the estimation accuracy, as we will see in the following text. Additionally, it is important to stress that the communication process is much more energy-consuming than the computation one [1, 16].

In [21], the authors proposed a discretization of the search region over 5×5 resolution grid, since it represents the best trade-off between accuracy and computational complexity. In all scenarios considered here, for the approach in [21], we have discretized the search region with $F = 100$ randomly generated points in order to achieve higher estimation accuracy for this approach. The approach in [68] considers the localization problem where the PLE is not known. However, it is straightforward to adapt it for the case of known PLE, by using the true value of the PLE instead of the estimated one. In all considered scenarios, for the approach in [68], the step size of the gradient descent method is set to $\gamma_x = 10^{-3}$, while the required number of iterations are set to $t_{\text{iter1}} = K_{\max}$ and $t_{\text{iter2}} = 5$. Although in [68] the authors consider node selection mechanisms in order to determine the optimum number of cooperating sensors and obtain a good trade-off in terms of position accuracy versus energy consumption, we do not employ it here. The reason is that, for the

Table 2.9: Summary of the Considered Algorithms

Algorithm	Description	Complexity
DSCL	The spatially constrained algorithm in [21]	$K_{\max} \times M \times F \times \mathcal{O}\left(\max_i\{\lvert\mathcal{N}_i\rvert\}\right)$
LS	The least squares algorithm in [68]	$K_{\max} \times M \times t_{\text{iter2}} \times \mathcal{O}\left(\max_i\{\lvert\mathcal{N}_i\rvert\}\right)$
SOCP1	The proposed Algorithm 1 for known P_T	$K_{\max} \times M \times \mathcal{O}\left(\left(\max_i\{\lvert\mathcal{N}_i\rvert\}\right)^{3.5}\right)$
SOCP2	The proposed Algorithm 2 for unknown P_T	$(K_{1\max} + K_{2\max}) \times M \times \mathcal{O}\left(\left(\max_i\{\lvert\mathcal{N}_i\rvert\}\right)^{3.5}\right) + M \times D_{\max}$

chosen scenarios, the number of neighbors is below the optimum value for a majority of the targets; therefore, we allow targets to cooperate with all neighboring sensors, independent of the fragment size.

Known P_T

Fig. 2.14 illustrates the NRMSE versus k performance of the considered approaches for different N. From Fig. 2.14 we can see that the estimation accuracy of all approaches betters as k and/or N increases, as anticipated. Moreover, it can be seen that the proposed approach outperforms the existing ones in both estimation accuracy and convergence sense. In terms of the estimation accuracy, the new approach reduces the estimation error on average for about $1.5-2$ m, when compared to the existing ones. In terms of convergence, one can see that the proposed approach requires only $k=20$ iterations to converge, while the SoA approaches do not converge even after $k=200$ iterations. This result is very important in the sense of energy conservation, since the proposed approach may be stopped after only $k=15$ iterations, while the existing ones require much more iterations. Finally, it is worth mentioning that the "LS" approach outperforms the "DSCL" and the proposed one in the first iteration. This is due to the fact that the "LS" approach uses a weighted mean of the coordinates of the n nearest anchors to determine the initial guess of the targets' positions. This method, as well as the other ones, such as MDS [48], can also be used to obtain an initial guess for the proposed approach. However, these methods increase the computational cost, and we do not use them for our approach.

Fig. 2.15 illustrates the NRMSE versus k performance of the considered approaches for different M. From Fig. 2.15 it can be seen that all approaches require slightly higher number of iterations when M is increased. However, the estimation accuracy of all approaches does not deteriorate when more targets are added in the network; the proposed approach performs even better when M increases. Additionally, Fig. 2.15 exhibits superior performance of the proposed approach in both estimation accuracy and convergence realizations, in comparison to the SoA. We can see that the new approach improves the

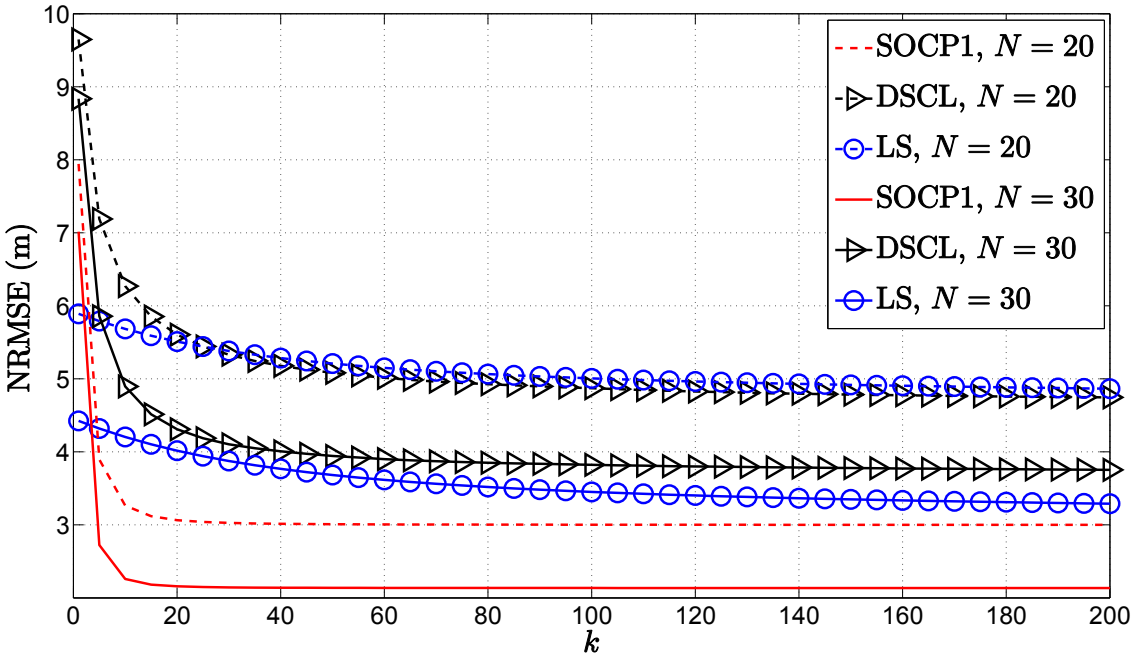

Figure 2.14: Simulation results for cooperative localization when P_0 is known: NRMSE (m) versus k comparison for different N, when $M = 50$, $\sigma = 0$ dB, $R = 6$ m, $B = 30$ m, $P_0 = -10$ dBm, $\gamma = 3$, $d_0 = 1$ m, $M_c = 500$.

estimation accuracy for more than 1.5 m, thereby requiring not more than $k = 20$ iterations to converge, while the existing methods require at least $k = 120$ iterations to converge.

In Figs. 2.14 and 2.15, we investigated the case where the wireless channel is noise-free. In practice however, the channel is prone to noise influence which can severely impact algorithm's performance. Hence, in Fig. 2.16 we investigate the influence of noise on the performance of the considered algorithms.

Fig. 2.16 illustrates the NRMSE versus k performance of the considered approaches for $\sigma = 6$ dB. As the performance benchmark, we employ the simulation results of the considered methods when the channel is noise-free, *i.e.*, $\sigma = 0$ dB in this figure. From Fig. 2.16 one can see that as σ increases, the performance of all approaches deteriorate for approximately 0.5 m. Moreover, we can see that the new approach converges after only $k = 20$ iterations for both choices of σ, while the existing approaches do not converge after $k = K_{\max}$ number of iterations. Finally, Fig. 2.16 shows that the proposed approach outperforms the SoA in terms of the estimation accuracy, achieving a gain of more than 1.5 m for both choices of σ.

From Figs. 2.14, 2.15 and 2.16, one can conclude that perhaps it is not necessary for an algorithm to perform all $K_{\max}$ number of iterations, since we might preserve energy if less iterations are performed. Thus, in Fig. 2.17 we illustrate the NRMSE performance of the considered approaches for different σ, as well as the average number of required iteration, $\bar{k}$, when a stopping criterion, $\|\hat{\boldsymbol{x}}_i^{(k+1)} - \hat{\boldsymbol{x}}_i^{(k)}\| \leq \epsilon$, is introduced. This stopping criterion implies that a target will stop calculating its position estimate if two consecutive

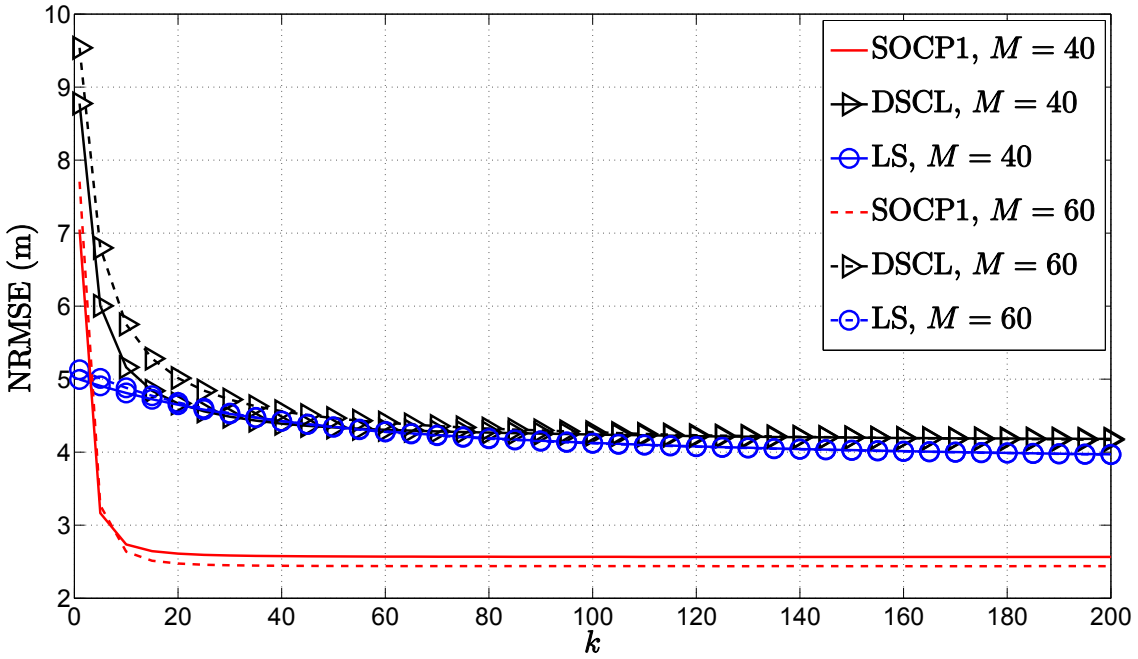

Figure 2.15: Simulation results for cooperative localization when P_0 is known: NRMSE (m) versus k comparison for different M, when $N = 25$, $\sigma = 0$ dB, $R = 6$ m, $B = 30$ m, $P_0 = -10$ dBm, $\gamma = 3$, $d_0 = 1$ m, $M_c = 500$.

estimations of its position are sufficiently close to each other. Once this condition is met by all targets, the network will stop working in order to save energy.

In Fig. 2.17, blue solid lines represent the NRMSE performance (left y-axis), and red solid lines represent $\bar{k}$ performance (right y-axis) of the considered approaches for different σ, when $K_{\max} = 100$ and $\epsilon = 10^{-3}$. As it can be seen from Fig. 2.17, the new approach outperforms the SoA for more than 1.5 m for all range of σ. Furthermore, we can see that the proposed approach also outperforms the existing ones in terms of convergence. Our approach requires on average about $\bar{k} = 42$ iterations to converge, while the existing approaches do not meet the stopping condition in $K_{\max}$ number of iterations.

Let us interpret the above result in terms of energy consumption. In Table 2.10, we represent the average running time per sensor per M_c run of the considered algorithms for $M_c = 100$ runs, which we will use to analyse the energy consumption of the algorithms.

Table 2.10: The Average Running Time Per Sensor Per M_c Run of the Considered Algorithms for known P_T, when $N = 25$, $M = 50$, $\sigma = 0$ dB, $R = 6$ m, $M_c = 100$. CPU: Intel(R)Core(TM)i7-363QM 2.40 GHz.

Algorithm	**Time** (s)
DSCL	0.0013
LS	0.0004
SOCP1	0.36

Assuming that E_{proc} is the total energy required for processing the data, E_p is the

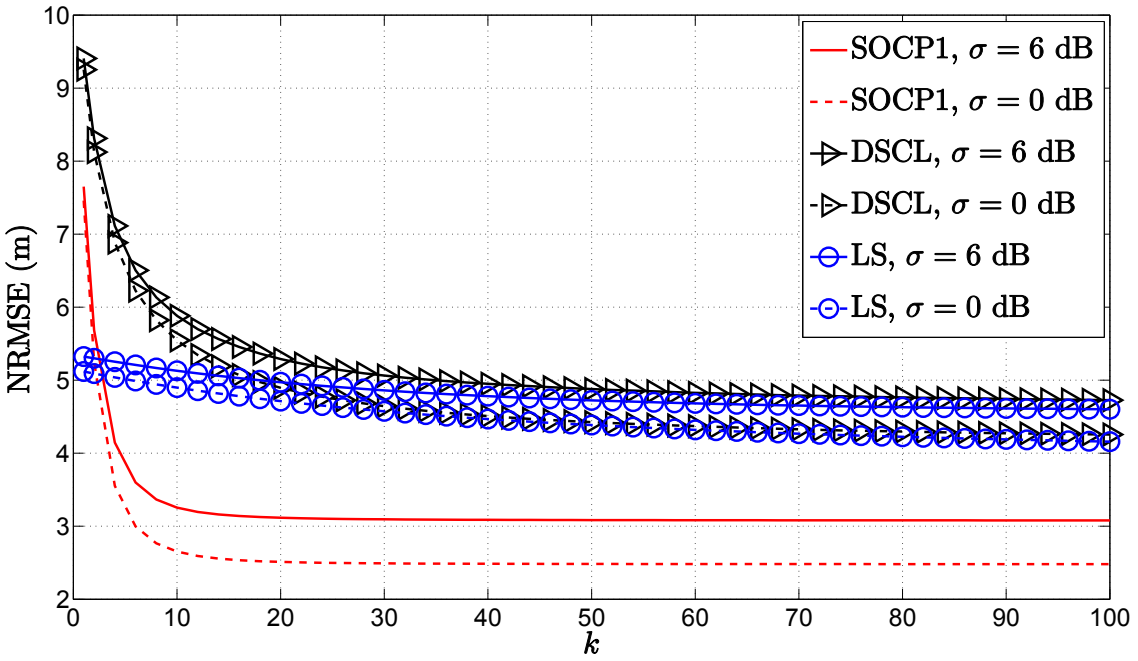

Figure 2.16: Simulation results for cooperative localization when P_0 is known: NRMSE (m) versus k comparison for different σ (dB), when $N = 25$, $M = 50$, $R = 6$ m, $B = 30$ m, $P_0 = -10$ dBm, $\gamma = 3$, $d_0 = 1$ m, $K_{\max} = 100$, $M_c = 500$.

energy spent per working second in data processing phase, t is the average running time of an algorithm, $K_{\text{req}} = \bar{k}$, $E_c = E_{T_x} M + E_{R_x} \sum_{i=1}^{M} |\mathcal{N}_i|$ is the energy spent per iteration in data communication phase, we present the results for the energy depletion of the considered algorithms in Table 2.11.

Table 2.11: The Average Energy Depletion of the Considered Algorithms for Known P_T, when $N = 25$, $M = 50$, $\sigma = 0$ dB, $R = 6$ m, $M_c = 100$.

Algorithm	E_{proc} (J)	E_{com} (J)	E_{tot} (J) $= E_{\text{proc}} + E_{\text{com}}$
DSCL	$E_p \times t \times M \times K_{\text{req}}$	$E_c \times K_{\text{req}}$	$63.4E_p + 100E_c$
LS	$E_p \times t \times M \times K_{\text{req}}$	$E_c \times K_{\text{req}}$	$21.7E_p + 100E_c$
SOCP1	$E_p \times t \times M \times K_{\text{req}}$	$E_c \times K_{\text{req}}$	$746.48E_p + 42E_c$

From Table 2.11, one can see that the proposed approach is the most energy-consuming in the data processing phase. This result is expected, since the proposed approach is more computationally complex, in comparison to the existing ones. Also, we can see that our approach preserves almost 60% of energy in the communication phase, in comparison to the SoA. Since the communication phase is much more energy-expensive than the data processing one [1, 16], *i.e.*, $E_c \gg E_p$, we can conclude that the proposed approach is likely to preserve energy for all values of σ. Moreover, since our approach requires a significantly lower number of signal transmissions, the utilization efficiency of the radio spectrum can be enhanced. This result is important because radio spectrum is a precious resource for wireless communications.

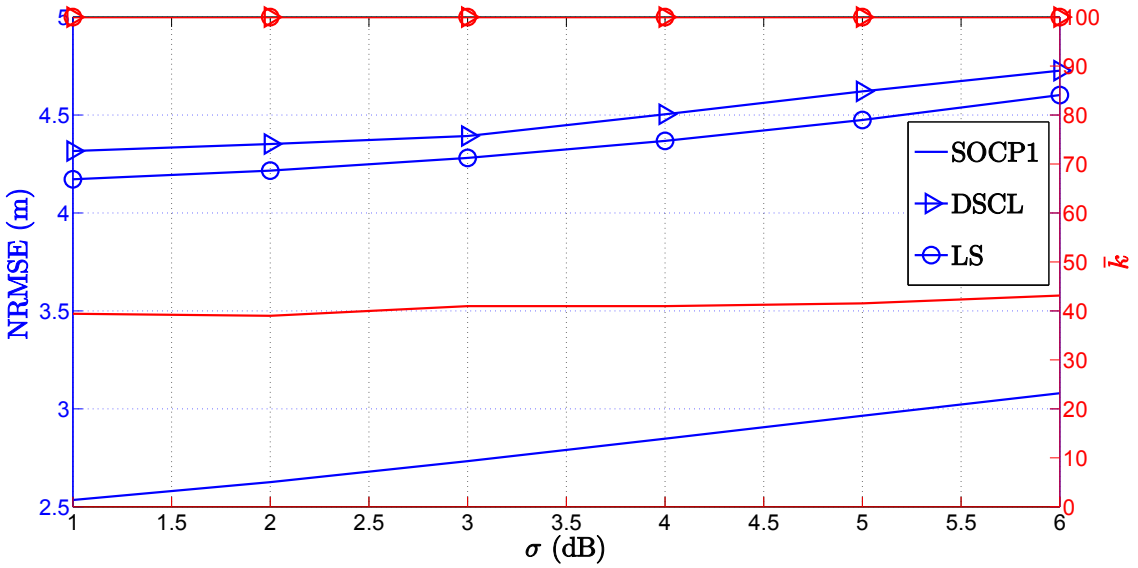

Figure 2.17: Simulation results for cooperative localization when P_0 is known: NRMSE and $\bar{k}$ versus σ comparison, when $N = 25$, $M = 50$, $R = 6$ m, $B = 30$ m, $P_0 = -10$ dBm, $\gamma = 3$, $d_0 = 1$ m, $K_{\max} = 100$, $\epsilon = 10^{-3}$, $M_c = 500$.

Heuristic approach for improving the convergence of the proposed algorithm

Although the proposed algorithm converges in less iterations than the existing ones, we have observed in our simulations that it still has potential for further improvement. In the following text we give a short overview of the proposed heuristic approach which improves the convergence of the proposed algorithm for known P_T, without a significant increase in the computational complexity.

Target i first obtains a solution of the SOCP problem in (2.33), $\hat{\boldsymbol{x}}_{i\text{socp}}^{(k+1)}$. Then, the target takes an additional step from the point $\hat{\boldsymbol{x}}_{i\text{socp}}^{(k+1)}$ in the direction $\overrightarrow{\hat{\boldsymbol{x}}_i^{(k)}\hat{\boldsymbol{x}}_{i\text{socp}}^{(k+1)}}$. The size of the step taken is $w\delta_i^{(k+1)}$, where w is the weight used to avoid oscillations in the position estimates and

$$\delta_i^{(k+1)} = \frac{\sum_{j\in\mathcal{N}_i} |r_{ij} - \|\hat{\boldsymbol{x}}_i^{(k)} - \hat{\boldsymbol{x}}_j\||}{|\mathcal{N}_i|},$$

given that $r_{ij} = d_0 10^{\frac{P_0 - P_{ij}}{10\gamma}}$. The motivation for calculating the step size in this way is that by improving the position estimates in every iteration, we are also minimizing the difference between the measured and the Euclidean distances; therefore, we are decreasing the step size in each iteration. Hence, an intermediate estimate is obtained as

$$\hat{\boldsymbol{x}}_{i\text{imp}}^{(k+1)} = \hat{\boldsymbol{x}}_{i\text{socp}}^{(k+1)} + \delta_i^{(k+1)}[\cos(\alpha_i); \sin(\alpha_i)],$$

where α_i is the angle between points $\hat{\boldsymbol{x}}_i^{(k)}$ and $\hat{\boldsymbol{x}}_{i\text{socp}}^{(k+1)}$. At last, target i determines its updated position estimate as

$$\hat{\boldsymbol{x}}_i^{(k+1)} = (1-w)\hat{\boldsymbol{x}}_{i\text{socp}}^{(k+1)} + w\hat{\boldsymbol{x}}_{i\text{imp}}^{(k+1)},$$

and immediately broadcasts this estimate to its neighbors.

In Fig. 2.18 we have investigated the influence of the chosen weight on the estimation accuracy of the proposed approach. Note that the choice $w = 0$ corresponds to the case where $\hat{\boldsymbol{x}}_i^{(k+1)} = \hat{\boldsymbol{x}}_{i\text{socp}}^{(k+1)}$, *i.e.*, no additional step is taken after the SOCP solution is attained. Fig. 2.18 shows that a considerable gain in the estimation accuracy is achieved in the first few iterations by taking the additional step. Moreover, it can be seen that the new approach converges after only $k = 5$ iterations for the choice $w \neq 0$, whereas $k = 15$ iterations are necessary for $w = 0$. Finally, even though the difference in the performance is marginal, based on our simulations, we have concluded that the best choice of the weight is $w = \frac{1}{k}$ in general.

Figs. 2.19b and 2.19c illustrate an example of the estimation process in the first ten iterations for the proposed approach, when $w = 0$ and $w = \frac{1}{k}$, respectively. In Fig. 2.19a we show the network layout considered for this particular example. Comparing Figs. 2.19b and 2.19c one can see that, in general, by making an additional step of the length $\delta_i^{(k)}$ in the first iteration pushes the estimates much closer to the true target positions. As the number of iterations increases, the step size, *i.e.*, w decreases, giving more importance to the solution obtained with the proposed SOCP approach. Additionally, from Fig. 2.19 we can see that the target which has no anchors as its neighbors (upper right corner) suffers the lowest, while the target closest to $\hat{\boldsymbol{x}}_i^{(0)}$ experiences the highest estimation accuracy in these few iterations. Although we cannot guarantee that our approach will converge under all conditions, our simulation results show that it is a good heuristic.

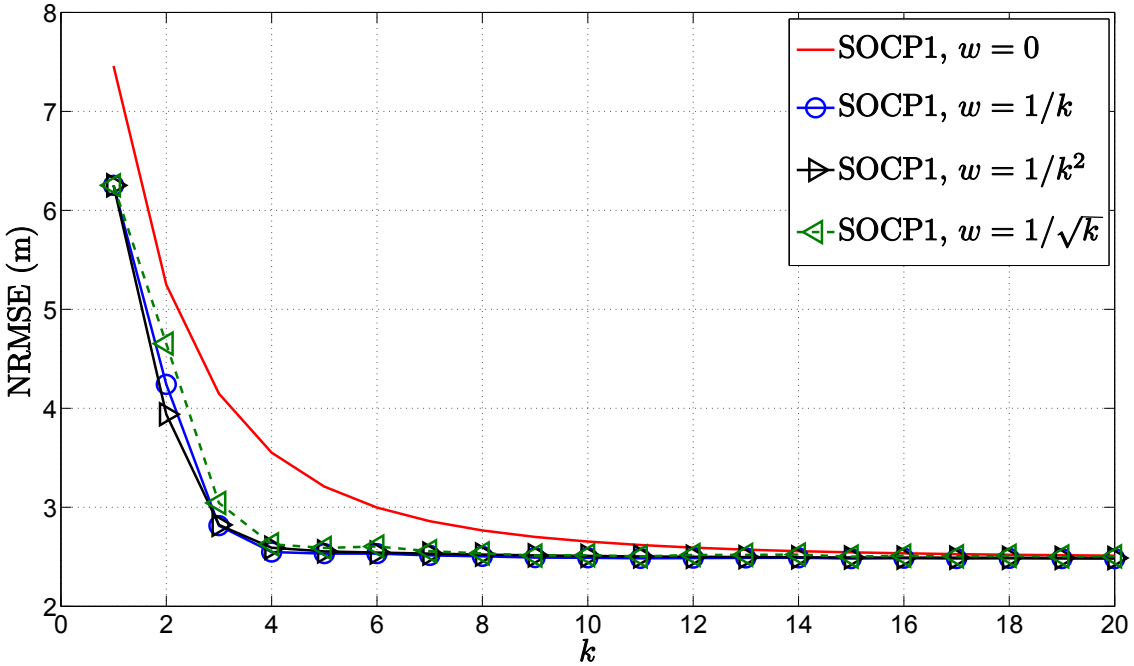

Figure 2.18: NRMSE (m) versus number of iterations comparison of the proposed approach for different choices of w.

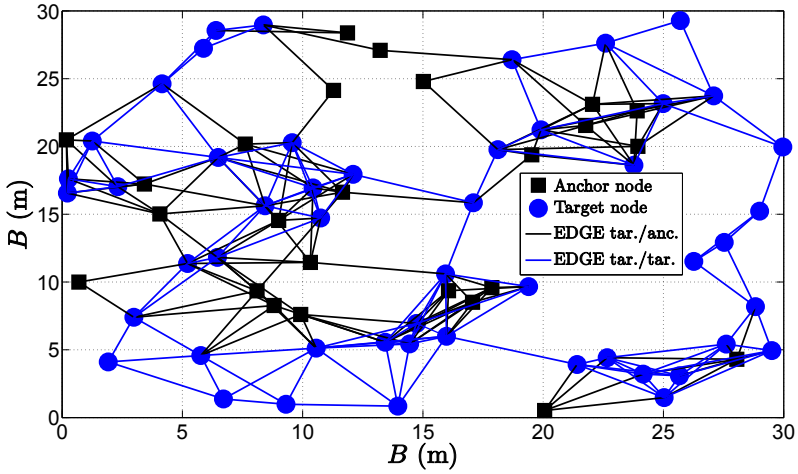

(a) Network configuration

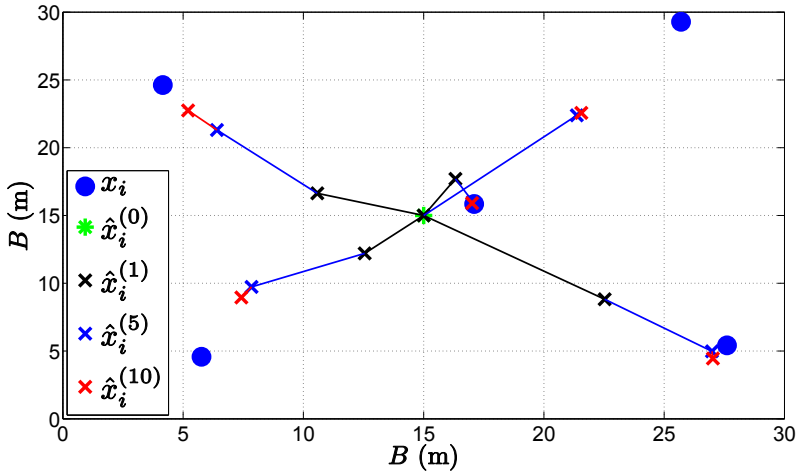

(b) SOCP1 approach, $w = 0$

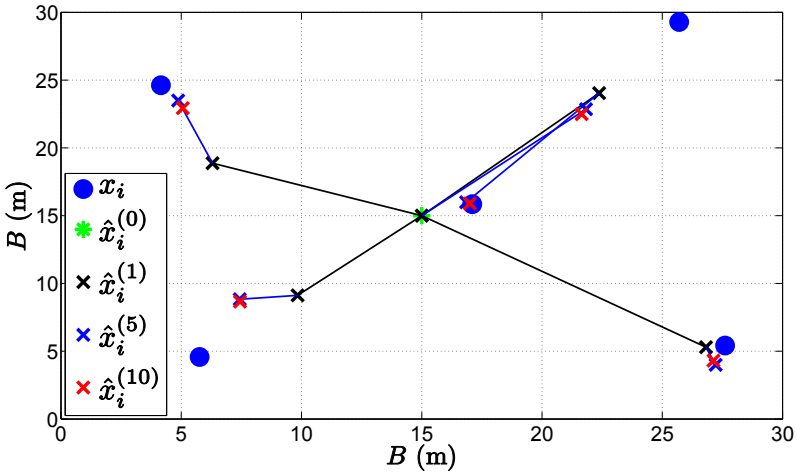

(c) SOCP1 approach, $w = \frac{1}{k}$

Figure 2.19: Estimation process of the proposed approach in the first 10 iterations.

Unknown P_T

Fig. 2.20 illustrates the NRMSE versus k performance of the proposed approach for unknown P_T. As the performance benchmark, we employ the proposed approach when P_T is known in this figure, since we are not aware of any existing work that addresses the distributed localization problem for the case when P_T is not known. From Fig. 2.20, it can be seen that the proposed approach reduces the estimation error as k increases, as expected. Also, the saddle point at $k = 10$ is observed. This is because in this point we obtain an estimate of P_T, and we proceed with our algorithm as if P_T is known, using its estimated value. From Fig. 2.20, we can conclude that the proposed approach provides excellent estimation accuracy, since it attains the lower bound given by the results of the proposed approach for known P_T.

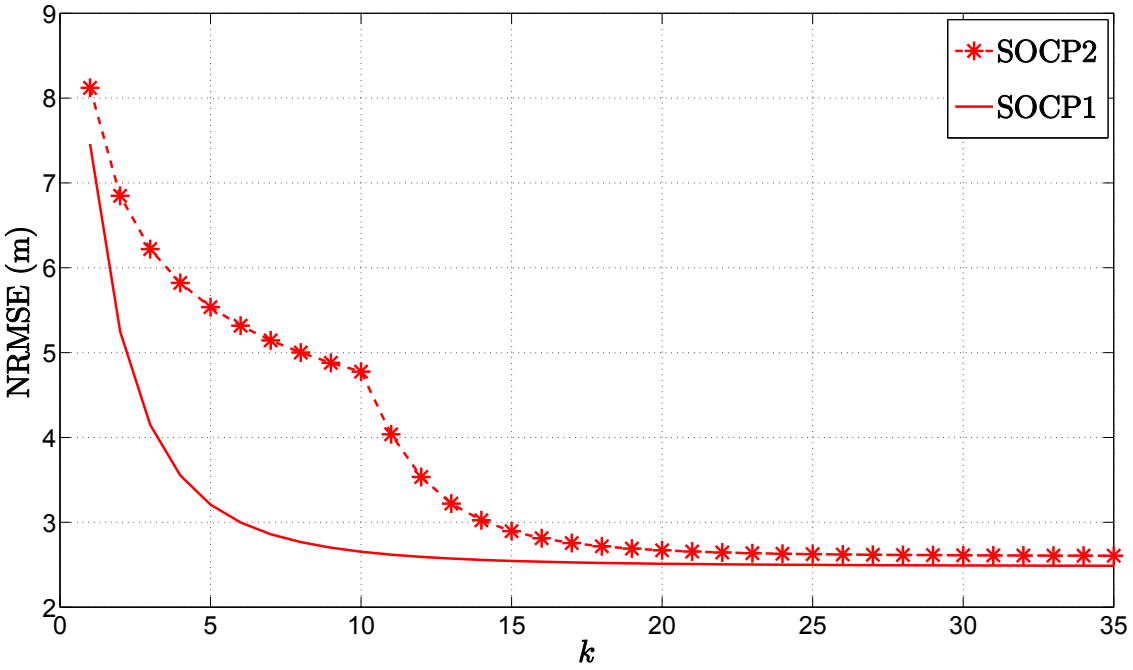

Figure 2.20: Simulation results for cooperative localization for known and unknown P_0: NRMSE versus k comparison, when $N = 25$, $M = 50$, $\sigma = 0$ dB, $R = 6$ m, $B = 30$ m, $P_0 = -10$ dBm, $\gamma = 3$, $d_0 = 1$ m, $M_c = 500$.

2.3.6 Conclusions

In this section, the RSS-based target localization problem in a cooperative WSN was addressed. A novel distributed cooperative algorithm based on SOCP relaxation was presented, for both cases of known and unknown target transmit power, P_T. For both scenarios, we started with the network coloring to ensure a completely distributed and collision-free algorithm. We derived the ML estimation problem to localize all targets simultaneously, and we broke it down into local ML problems for each target. The local ML estimator was tightly approximated by another non-convex estimator for small noise.

The derived non-convex estimator allowed the use of convex optimization tools in order to convert the estimation problem into a convex one. Hence, appropriate convex relaxations were applied to the derived non-convex estimator and novel SOCP estimators were proposed to solve the target localization problem for known and unknown P_T. As we considered a distributed implementation of the proposed algorithms, they were executed iteratively. In the case of unknown P_T, we solved the localization problem $K_{1\max}$ number of times, after which we attained the ML estimate of P_T by fixing the target estimates. We then took advantage of this estimate in order to further improve the estimation accuracy of the proposed approach; hence, we proceeded in our algorithm as if P_T is known. Additionally, we proposed a simple heuristic approach to further improve the convergence of the proposed approach for known P_T which requires a first-degree memory in the targets. Moreover, we provided details about the computational complexity and energy consumption of the considered algorithms. The simulation results confirmed the effectiveness of the proposed algorithms, showing a remarkable improvement in the estimation accuracy of more than 1.5 m in the case of known P_T, in comparison with the SoA. The new approach requires less number of iterations to converge, and is likely to preserve energy in all scenarios presented in this work. When P_T was not known, the simulation results certified excellent performance of our approach, attaining the lower bound defined by the new approach for known P_T.

CHAPTER 3

RSS-AoA-based Target Localization

3.1 Chapter Summary

This chapter addresses the problem of target localization by using combined RSS and AoA measurements. It is organized into two main sections in which we study both centralized, Section 3.2, and distributed, Section 3.3, localization problems, respectively. More specifically, the remainder of the chapter is organized as follows.

Section 3.2.1 describes the SoA of the centralized RSS-AoA localization problem, and presents our contribution in that area. In Section 3.2.2, the RSS and AoA measurement models are introduced and the centralized target localization problem is formulated. Section 3.2.3 presents the development of our estimators in the case of non-cooperative localization for both known and unknown P_T. In Section 3.2.4 we describe the derivation of our centralized estimators in the case of cooperative localization for both known and unknown P_T. In Sections 3.2.5 and 3.2.6, complexity and performance analysis are presented respectively, together with the relevant results in order to compare the performance of our estimators with the SoA. Finally, Section 3.2.7 summarizes the main conclusions regarding the centralized RSS-AoA-based localization problem.

Section 3.3.1 gives an overview of the related work in the area of distributed RSS-AoA localization problem, and summarizes our contributions. In Section 3.3.2, the distributed target localization problem is formulated. Section 3.3.3 presents the development of our distributed estimators. In Section 3.3.4 we provide analysis about the computational complexity, while in Section 3.3.5 we discuss the performance of our algorithms. Finally, Section 3.3.6 summarizes the main conclusions regarding the distributed RSS-AoA-based localization problem.

3.2 Centralized RSS-AoA-based Target Localization

3.2.1 Related Work

The approaches in [50, 51, 54, 56, 73], and [74] consider both non-cooperative and cooperative target localization problem, but the estimators are founded on RSS and distance measurements only. The approaches in [26]-[29] are based on the fusion of RSS and ToA measurements. A hybrid system that merges range and angle measurements was investigated in [30]. The authors in [30] proposed two estimators to solve the non-cooperative target localization problem in a 3-D scenario: linear LS and optimization based. The LS estimator is a relatively simple and well known estimator, while the optimization based estimator was solved by Davidon-Fletcher-Powell algorithm [75]. In [31], the authors derived an LS and an ML estimator for a hybrid scheme that combines received signal strength difference (RSSD) and AoA measurements. Non-linear constrained optimization was used to estimate the target's location from multiple RSS and AoA measurements. Both LS and ML estimators in [31] are λ-dependent, where λ is a non-negative weight assigned to regulate the contribution from RSS and AoA measurements. A selective WLS estimator for RSS/AoA localization problem was proposed in [32]. The authors determined the target location by exploiting weighted ranges from the two *nearest* anchor measurements, which were combined with the serving base station AoA measurement. In [31]-[32], authors investigated the non-cooperative hybrid RSS/AoA localization problem for a 2-D scenario only. A WLS estimator for a 3-D RSSD/AoA non-cooperative localization problem when the transmit power is unknown was presented in [33]. However, the authors in [33] only investigated a small-scale WSN, with extremely low noise power. An estimator based on SDP relaxation technique for cooperative target localization problem was proposed in [76]. The authors in [76] extended their previous SDP algorithm for pure range information into a hybrid one, by adding angle information for a triplets of points. However, due to the consideration of triplets of points, the computational complexity of the SDP approach increases rather substantially with the network size.

Contribution

In this work, we investigate the target localization problem in both non-cooperative and cooperative 3-D WSN. In the case of non-cooperative WSN, we assume that all targets communicate exclusively with anchors, and a single target is located at a time. In the case of cooperative WSN, we assume that all targets communicate with any sensor within their communication range (whether it is an anchor or a target), and that all targets are located simultaneously. For both cases, a hybrid system that fuses distance and angle measurements, extracted from RSS and AoA information respectively, is employed. By using the RSS propagation model and simple geometry, we derive a novel objective function based on the LS criterion. For the case of non-cooperative WSN, based on the squared range (SR) approach we show that the derived non-convex objective function can be transformed

into a GTRS framework, which can be solved exactly by a bisection procedure [28]. For the case of cooperative localization, we show that the derived objective function can be transformed into a convex function by applying SDP relaxation technique. Finally, we show that the generalization of the proposed estimators to the case where, alongside with the targets' locations, the transmit power, P_T, is also unknown, is straightforward for both non-cooperative and cooperative localization.

Thus, the main contribution of our work is threefold. First, by using RSS and AoA measurement models, we derive a novel non-convex objective function based on the LS criterion which tightly approximates the ML one for small noise. In the case of non-cooperative localization, we propose two novel estimators that significantly reduce the estimation error, compared with the SoA. Finally, in the case of cooperative localization, we present the first hybrid RSS/AoA estimators for target localization in a 3-D cooperative WSN.

3.2.2 Problem Formulation

We consider a WSN with N anchors and M targets, where the known locations of anchors are respectively denoted by $\boldsymbol{a}_1, \boldsymbol{a}_2, ..., \boldsymbol{a}_N$, and the unknown locations of targets are denoted by $\boldsymbol{x}_1, \boldsymbol{x}_2, ..., \boldsymbol{x}_M$ ($\boldsymbol{x}_i, \boldsymbol{a}_j \in \mathbb{R}^3$, $i = 1, ..., M$ and $j = 1, ..., N$). For ease of expression, let us define a vector $\boldsymbol{x} = [\boldsymbol{x}_1^T, \boldsymbol{x}_2^T, ..., \boldsymbol{x}_M^T]^T$ ($\boldsymbol{x} \in \mathbb{R}^{3M \times 1}$) as the vector of all unknown target locations, such that $\boldsymbol{x}_i = \boldsymbol{E}_i^T \boldsymbol{x}$, where $\boldsymbol{E}_i = \boldsymbol{e}_i \otimes \boldsymbol{I}_3$, and $\boldsymbol{e}_i$ is the i-th column of the identity matrix I_M. We determine these locations by using a hybrid system that fuses range and angle measurements. Combining two measurements of the radio signal provides more information to the user, and it is likely to enhance the estimation accuracy, as shown in Fig. 3.1.

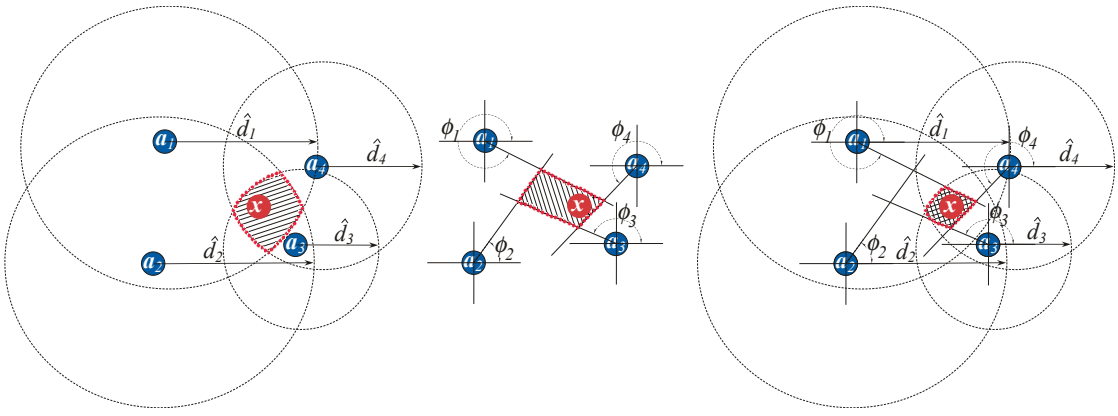

(a) Range-based Localization (b) Angle-based Localization (c) Hybrid Localization

Figure 3.1: Illustration of different localization systems in a 2-D space.

Fig. 3.1 illustrates how does a (a) range-based, (b) angle-based and (c) hybrid (range and angle) system operate for the case where $M = 1$ and $N = 4$. In the range-based

localization, each range measurement, $\hat{d}_i$, defines a circle as a possible location of the unknown target. Thus, a set of range measurements, $\{\hat{d}_1, \hat{d}_2, ..., \hat{d}_N\}$, defines multiple circles and the area determined by their intersection accommodates the target, Fig. 3.1(a). Similarly with the angle-based localization, where each angle measurement, ϕ_i, defines a line as the set of possible locations of the unknown target, Fig. 3.1(b). From Fig. 3.1(c), one can see that when the two measurements of the radio signal are integrated, the set of all possible solutions (the area determined by the intersection) is significantly reduced; hence, hybrid systems are more likely to improve the estimation accuracy.

Throughout this work, it is assumed that the range measurements are obtained from the RSS information exclusively, since ranging based on RSS requires the lowest implementation costs [1]. The RSS, P_{ij}, between two sensors i and j which are within the communication range of each other (from the transmitting sensor) can be written [58, 59] as:

$$P_{ij}^{\mathcal{A}} = P_0 - 10\gamma \log_{10} \frac{\|\boldsymbol{x}_i - \boldsymbol{a}_j\|}{d_0} + n_{ij}, \text{ for } (i,j) \in \mathcal{A}, \tag{3.1a}$$

$$P_{ik}^{\mathcal{B}} = P_0 - 10\gamma \log_{10} \frac{\|\boldsymbol{x}_i - \boldsymbol{x}_k\|}{d_0} + n_{ik}, \text{ for } (i,k) \in \mathcal{B}, \tag{3.1b}$$

where n_{ij} and n_{ik} are the log-normal shadowing terms modeled as $n_{ij} \sim \mathcal{N}(0, \sigma_{n_{ik}}^2)$, $n_{ik} \sim \mathcal{N}(0, \sigma_{n_{ik}}^2)$. Furthermore, the sets $\mathcal{A} = \{(i,j) : \|\boldsymbol{x}_i - \boldsymbol{a}_j\| \leq R, \text{for } i = 1, ..., M, j = 1, ..., N\}$ and $\mathcal{B} = \{(i,k) : \|\boldsymbol{x}_i - \boldsymbol{x}_k\| \leq R, \text{for } i,k = 1, ..., M, i \neq k\}$, where R is the communication range of a sensor, denote the existence of target/anchor and target/target connections, respectively.

To obtain the AoA measurements (both azimuth and elevation angles), we assume that either video cameras [77–79] or multiple antennas, or a directional antenna is implemented at anchors [30, 80, 81]. In order to make use of the AoA measurements from different sensors, the orientation information is required, which can be obtained by implementing a digital compass at each sensor [30, 80]. However, a digital compass introduces an error in the AoA measurements due to its static accuracy. For the sake of simplicity and without loss of generality, we model the angle measurement error and the orientation error as one random variable in the rest of this thesis.

Fig. 3.2 gives an illustration of a target and anchor locations in a 3-D space. As shown in Fig. 3.2, $\boldsymbol{x}_i = [x_{i1}, x_{i2}, x_{i3}]^T$ and $\boldsymbol{a}_j = [a_{j1}, a_{j2}, a_{j3}]^T$ are respectively the unknown coordinates of the i-th target and the known coordinates of the j-th anchor, while $d_{ij}^{\mathcal{A}}$, $\phi_{ij}^{\mathcal{A}}$ and $\alpha_{ij}^{\mathcal{A}}$ represent the distance, azimuth angle and elevation angle between the i-th target and the j-th anchor, respectively.

The ML estimate of the distance between two sensors can be obtained from the RSS measurement model (3.1) as follows [1]:

$$\hat{d}_{ij}^{\mathcal{A}} = d_0 10^{\frac{P_0 - P_{ij}^{\mathcal{A}}}{10\gamma}}, \text{ for } (i,j) \in \mathcal{A}, \tag{3.2a}$$

$$\hat{d}_{ik}^{\mathcal{B}} = d_0 10^{\frac{P_0 - P_{ik}^{\mathcal{B}}}{10\gamma}}, \text{ for } (i,k) \in \mathcal{B}. \tag{3.2b}$$

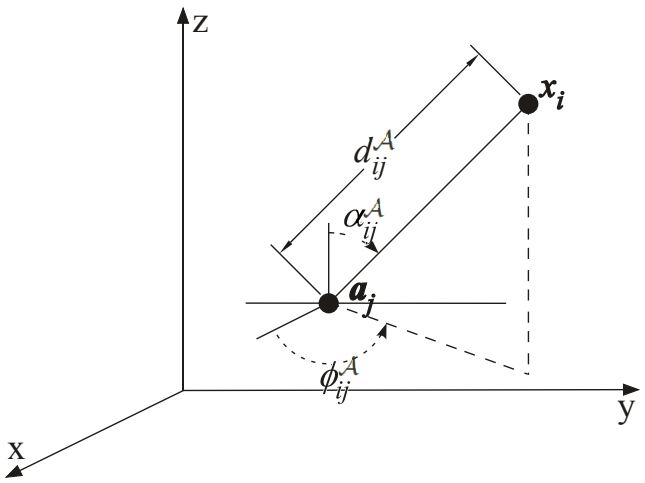

Figure 3.2: Illustration of a target and anchor locations in a 3-D space.

Applying simple geometry, azimuth and elevation angle measurements can be modeled as [30]:

$$\phi_{ij}^{\mathcal{A}} = \arctan\left(\frac{x_{i2} - a_{j2}}{x_{i1} - a_{j1}}\right) + m_{ij}, \text{ for } (i,j) \in \mathcal{A}, \tag{3.3a}$$

$$\phi_{ik}^{\mathcal{B}} = \arctan\left(\frac{x_{i2} - x_{k2}}{x_{i1} - x_{k1}}\right) + m_{ik}, \text{ for } (i,k) \in \mathcal{B}, \tag{3.3b}$$

and

$$\alpha_{ij}^{\mathcal{A}} = \arccos\left(\frac{x_{i3} - a_{j3}}{\|\boldsymbol{x}_i - \boldsymbol{a}_j\|}\right) + v_{ij}, \text{ for } (i,j) \in \mathcal{A}, \tag{3.4a}$$

$$\alpha_{ik}^{\mathcal{B}} = \arccos\left(\frac{x_{i3} - x_{k3}}{\|\boldsymbol{x}_i - \boldsymbol{x}_k\|}\right) + v_{ik}, \text{ for } (i,k) \in \mathcal{B}. \tag{3.4b}$$

respectively, where m_{ij}, m_{ik} and v_{ij}, v_{ik} are respectively the measurement errors of azimuth and elevation angles, modeled as $m_{ij} \sim \mathcal{N}(0, \sigma_{m_{ij}}^2)$, $m_{ik} \sim \mathcal{N}(0, \sigma_{m_{ik}}^2)$ and $v_{ij} \sim \mathcal{N}(0, \sigma_{v_{ij}}^2)$, $v_{ik} \sim \mathcal{N}(0, \sigma_{v_{ik}}^2)$.

Given the observation vector $\boldsymbol{\theta} = [\boldsymbol{P}^T, \boldsymbol{\phi}^T, \boldsymbol{\alpha}^T]^T$ ($\boldsymbol{\theta} \in \mathbb{R}^{3(|\mathcal{A}|+|\mathcal{B}|)}$), where $\boldsymbol{P} = [P_{ij}^{\mathcal{A}}, P_{ik}^{\mathcal{B}}]^T$, $\boldsymbol{\phi} = [\phi_{ij}^{\mathcal{A}}, \phi_{ik}^{\mathcal{B}}]^T$, $\boldsymbol{\alpha} = [\alpha_{ij}^{\mathcal{A}}, \alpha_{ik}^{\mathcal{B}}]^T$, and $|\bullet|$ denotes the cardinality of a set (the number of elements in a set), the PDF is given as:

$$p(\boldsymbol{\theta}|\boldsymbol{x}) = \prod_{i=1}^{3(|\mathcal{A}|+|\mathcal{B}|)} \frac{1}{\sqrt{2\pi\sigma_i^2}} \exp\left\{-\frac{(\theta_i - f_i(\boldsymbol{x}))^2}{2\sigma_i^2}\right\}, \tag{3.5}$$

where

$$\boldsymbol{f}(\boldsymbol{x}) = \begin{bmatrix} \vdots \\ P_0 - 10\gamma \log_{10} \frac{\|\boldsymbol{x}_i - \boldsymbol{a}_j\|}{d_0} \\ \vdots \\ P_0 - 10\gamma \log_{10} \frac{\|\boldsymbol{x}_i - \boldsymbol{x}_k\|}{d_0} \\ \vdots \\ \arctan\left(\frac{x_{i2}-a_{j2}}{x_{i1}-a_{j1}}\right) \\ \vdots \\ \arctan\left(\frac{x_{i2}-x_{k2}}{x_{i1}-x_{k1}}\right) \\ \vdots \\ \arccos\left(\frac{x_{i3}-a_{j3}}{\|\boldsymbol{x}_i - \boldsymbol{a}_j\|}\right) \\ \vdots \\ \arccos\left(\frac{x_{i3}-x_{k3}}{\|\boldsymbol{x}_i - \boldsymbol{x}_k\|}\right) \\ \vdots \end{bmatrix}, \boldsymbol{\sigma} = \begin{bmatrix} \vdots \\ \sigma_{n_{ij}} \\ \vdots \\ \sigma_{n_{ik}} \\ \vdots \\ \sigma_{m_{ij}} \\ \vdots \\ \sigma_{m_{ik}} \\ \vdots \\ \sigma_{v_{ij}} \\ \vdots \\ \sigma_{v_{ik}} \\ \vdots \end{bmatrix}.$$

The most common estimator used in practice is the ML estimator, since it has the property of being asymptotically efficient (for large enough data records) [47, 82]. The ML estimator forms its estimate as the vector $\hat{\boldsymbol{x}}$, which maximizes the PDF in (3.5); hence, the ML estimator is obtained as:

$$\hat{\boldsymbol{x}} = \arg\min_{\boldsymbol{x}} \sum_{i=1}^{3(|\mathcal{A}|+|\mathcal{B}|)} \frac{1}{\sigma_i^2} \left[\theta_i - f_i(\boldsymbol{x})\right]^2. \tag{3.6}$$

Even though the ML estimator is approximately the minimum variance unbiased estimator [47], the LS problem in (3.6) is non-convex and has no closed-form solution. In the remainder of this work, we will show that the LS problem in (3.6) can be solved efficiently by applying certain approximations. More precisely, for non-cooperative WSN, we propose a suboptimal estimator based on the GTRS framework leading to an SR-WLS estimator, which can be solved exactly by a bisection procedure [83]. For the case of cooperative WSN, we propose a convex relaxation technique leading to an SDP estimator which can be solved efficiently by interior-point algorithms [57]. Not only that the new approaches efficiently solve the traditional RSS/AoA localization problem, but they can also be used to solve the localization problem when P_T is not known, with straightforward generalization.

Assumptions

We outline here some assumptions for the WSN (made for the sake of simplicity and without loss of generality):

(1) The network is connected and it does not change during the computation time;

(2) Measurement errors for RSS and AoA model are independent, and $\sigma_{n_{ij}} = \sigma_n$, $\sigma_{m_{ij}} = \sigma_m$ and $\sigma_{v_{ij}} = \sigma_v$, $\forall (i,j) \in \mathcal{A} \cup \mathcal{B}$;

(3) The range measurements are extracted from the RSS information exclusively and all target/target measurements are symmetric;

(4) All sensors have identical P_T;

(5) All sensors are equipped with either multiple antennas or a directional antenna, and they can measure the AoA information.

In assumption (1), we assume that the sensors are static and that there is no node/link failure during the computation period, and all sensors can convey their measurements to a central processor. Assumptions (2) and (4) are made for the sake of simplicity. Assumption (3) is made without loss of generality; it is readily seen that, if $P_{ik}^{\mathcal{B}} \neq P_{ki}^{\mathcal{B}}$, then it serves to replace $P_{ik}^{\mathcal{B}} \leftarrow (P_{ik}^{\mathcal{B}} + P_{ki}^{\mathcal{B}})/2$ and $P_{ki}^{\mathcal{B}} \leftarrow (P_{ik}^{\mathcal{B}} + P_{ki}^{\mathcal{B}})/2$ when solving the localization problem. Assumption (4) implies that P_0 and R are identical for all sensors. Finally, assumption (5) is made for the case of cooperative localization, where only some targets are able to directly connect to anchors; thus, they are forced to cooperate with other targets within their communication range.

3.2.3 Non-cooperative Localization

By non-cooperative WSN, we imply a network comprising a number of targets and anchors where each target is allowed to communicate with anchors exclusively, and a single target is localized at a time. For such a setting, we can assume that the targets are passive nodes that only emit radio signals, and that all radio measurements are collected by anchors.

In the remainder of this section, we develop a suboptimal estimator to solve the non-cooperative localization problem in (3.6), whose *exact* solution can be obtained by a bisection procedure. We then show that its generalization for the case where P_T is not known is straightforward.

Non-cooperative localization with known P_T

Note that the targets communicate with anchors exclusively in a non-cooperative network; hence, the set $\mathcal{B}$ in the path loss model (3.1) is empty. Therefore, when the noise power is sufficiently small, from (3.1a) we have:

$$\lambda_{ij}^{\mathcal{A}} \|\boldsymbol{x}_i - \boldsymbol{a}_j\| \approx d_0 \text{ for } (i,j) \in \mathcal{A}, \tag{3.7}$$

where $\lambda_{ij}^{\mathcal{A}} = 10^{\frac{P_{ij}^{\mathcal{A}} - P_0}{10\gamma}}$. Similarly, from (3.3a) and (3.4a) we respectively get:

$$\boldsymbol{c}_{ij}^T(\boldsymbol{x}_i - \boldsymbol{a}_j) \approx 0, \tag{3.8}$$

and

$$\boldsymbol{k}_{ij}^T(\boldsymbol{x}_i - \boldsymbol{a}_j) \approx \|\boldsymbol{x}_i - \boldsymbol{a}_j\| \cos(\alpha_{ij}^{\mathcal{A}}), \tag{3.9}$$

where $\boldsymbol{c}_{ij} = [-\sin(\phi_{ij}^{\mathcal{A}}), \cos(\phi_{ij}^{\mathcal{A}}), 0]^T$ and $\boldsymbol{k}_{ij} = [0,0,1]^T$.

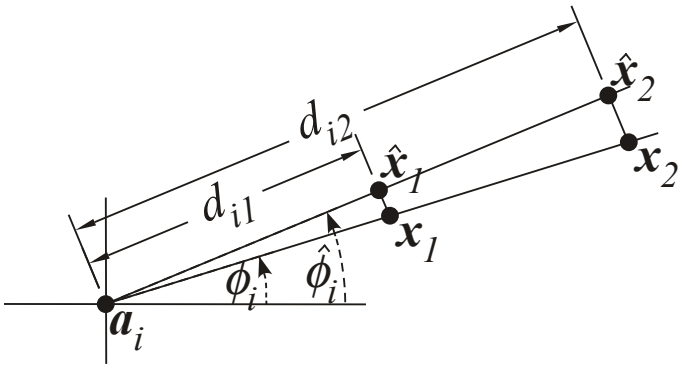

Figure 3.3: Illustration of azimuth angle measurements: short-range versus long-range.

Next, we can rewrite (3.7) as:

$$\lambda_{ij}^{\mathcal{A}\,2}\|\boldsymbol{x}_i - \boldsymbol{a}_j\|^2 \approx d_0^2. \tag{3.10}$$

Introduce weights, $\boldsymbol{w} = [\sqrt{w_{ij}}]$, where each w_{ij} is defined as

$$w_{ij} = 1 - \frac{\hat{d}_{ij}^{\mathcal{A}}}{\sum_{(i,j)\in\mathcal{A}} \hat{d}_{ij}^{\mathcal{A}}},$$

such that more importance is given to nearby links. The reason for defining the weights in this manner is because both RSS and AoA short-range measurements are trusted more than long ones. The RSS measurements have relatively constant standard deviation with distance [1]. This implies that multiplicative factors of RSS measurements are constant with range. For example, for a multiplicative factor of 1.5, at a range of 1 m, the measured range would be 1.5 m, and at an actual range of 10 m, the measured range would be 15 m, a factor of 10 times greater [1]. In the case of AoA measurements, the reason is more intuitive, and we call the reader's attention to Fig. 3.3.

In Fig. 3.3, an azimuth angle measurement made between an anchor and two targets located along the same line, but with different distances from the anchor is illustrated. The true and the measured azimuth angles between the anchor and the targets are denoted by ϕ_i and $\hat{\phi}_i$, respectively. Our goal is to determine the locations of the two targets. Based on the available information, the location estimates of the two targets are at points $\hat{\boldsymbol{x}}_1$ and $\hat{\boldsymbol{x}}_2$. However, from Fig. 3.3, we can see that the estimated location of the target physically closer to the anchor ($\hat{\boldsymbol{x}}_1$) is much closer to its true location than the one further away. In other words, for a given angle, the more two sensors are physically further apart the greater the set of all possible solutions will be (more likely to impair the localization accuracy).

Replace $\|\boldsymbol{x}_i - \boldsymbol{a}_j\|$ in (3.9) with $\hat{d}_{ij}^{\mathcal{A}}$ described in (3.2a), to obtain the following WLS problem according to (3.10), (3.8) and (3.9) as:

$$\begin{aligned}\hat{\boldsymbol{x}}_i = \arg\min_{\boldsymbol{x}_i} & \sum_{(i,j):(i,j)\in\mathcal{A}} w_{ij}\Big(\lambda_{ij}^{\mathcal{A}\,2}\|\boldsymbol{x}_i - \boldsymbol{a}_j\|^2 - d_0^2\Big)^2 + \sum_{(i,j):(i,j)\in\mathcal{A}} w_{ij}\Big(\boldsymbol{c}_{ij}^T(\boldsymbol{x}_i - \boldsymbol{a}_j)\Big)^2 \\ & + \sum_{(i,j):(i,j)\in\mathcal{A}} w_{ij}\Big(\boldsymbol{k}_{ij}^T(\boldsymbol{x}_i - \boldsymbol{a}_j) - \hat{d}_{ij}^{\mathcal{A}}\cos(\alpha_{ij}^{\mathcal{A}})\Big)^2.\end{aligned} \tag{3.11}$$

The above WLS estimator is non-convex and has no closed-form solution. However, we can express (3.11) as a quadratic programming problem whose *global* solution can be computed efficiently [83]. Using the substitution $\boldsymbol{y}_i = [\boldsymbol{x}_i^T, \|\boldsymbol{x}_i\|^2]^T$, the problem in (3.11) can be rewritten as:

$$\underset{\boldsymbol{y}_i}{\text{minimize}} \; \|\boldsymbol{W}(\boldsymbol{A}\boldsymbol{y}_i - \boldsymbol{b})\|^2$$

subject to

$$\boldsymbol{y}_i^T \boldsymbol{D} \boldsymbol{y}_i + 2\boldsymbol{l}^T \boldsymbol{y}_i = 0, \tag{3.12}$$

where $\boldsymbol{W} = \boldsymbol{I}_3 \otimes \text{diag}(\boldsymbol{w})$,

$$\boldsymbol{A} = \begin{bmatrix} \vdots & \vdots \\ -2\lambda_{ij}^{\mathcal{A}^2} \boldsymbol{a}_j^T & \lambda_{ij}^{\mathcal{A}^2} \\ \vdots & \vdots \\ \boldsymbol{c}_{ij}^T & 0 \\ \vdots & \vdots \\ \boldsymbol{k}_{ij}^T & 0 \\ \vdots & \vdots \end{bmatrix}, \boldsymbol{b} = \begin{bmatrix} \vdots \\ d_0^2 - \lambda_{ij}^{\mathcal{A}^2} \|\boldsymbol{a}_j\|^2 \\ \vdots \\ \boldsymbol{c}_{ij}^T \boldsymbol{a}_j \\ \vdots \\ \boldsymbol{k}_{ij}^T \boldsymbol{a}_j + \hat{d}_{ij}^{\mathcal{A}} \cos(\alpha_{ij}^{\mathcal{A}}) \\ \vdots \end{bmatrix},$$

$$\boldsymbol{D} = \begin{bmatrix} \boldsymbol{I}_3 & \boldsymbol{0}_{3\times 1} \\ \boldsymbol{0}_{1\times 3} & 0 \end{bmatrix}, \boldsymbol{l} = \begin{bmatrix} \boldsymbol{0}_{3\times 1} \\ -1/2 \end{bmatrix},$$

i.e., $\boldsymbol{A} \in \mathbb{R}^{3|\mathcal{A}|\times 4}$, $\boldsymbol{b} \in \mathbb{R}^{3|\mathcal{A}|\times 1}$, and $\boldsymbol{W} \in \mathbb{R}^{3|\mathcal{A}|\times 3|\mathcal{A}|}$.

The objective function and the constraint in (3.12) are both quadratic. This type of problem is known as GTRS [83, 84], and it can be solved exactly by a bisection procedure [83]. We denote (3.12) as "SR-WLS1" in the remaining text.

Non-cooperative localization with unknown P_T

To maintain low implementation costs, testing and calibration are not the priority in practice. Thus, sensors' transmit powers are often not calibrated, *i.e.*, not known. Not knowing P_T in the RSS measurement model corresponds to not knowing P_0 in the RSS model (3.1); see [16, 38] and the references therein.

The generalization of the proposed estimators for known P_0 is straightforward for the case where P_0 is not known. Notice that equation (3.7) can be rewritten as:

$$\beta_{ij}^{\mathcal{A}} \|\boldsymbol{x}_i - \boldsymbol{a}_j\| \approx \eta d_0, \text{ for } (i,j) \in \mathcal{A}, \tag{3.13}$$

where $\beta_{ij}^{\mathcal{A}} = 10^{\frac{P_{ij}^{\mathcal{A}}}{10\gamma}}$, and $\eta = 10^{\frac{P_0}{10\gamma}}$ is an unknown parameter that needs to be estimated.

Substitute $\|\boldsymbol{x}_i - \boldsymbol{a}_j\|$ with $\hat{d}_{ij}^{\mathcal{A}}$ in (3.9). Then, we can rewrite (3.9) as:

$$\beta_{ij}^{\mathcal{A}} \boldsymbol{k}_{ij}^T (\boldsymbol{x}_i - \boldsymbol{a}_j) \approx \eta d_0 \cos(\alpha_{ij}^{\mathcal{A}}). \tag{3.14}$$

In order to assign more importance to nearby links, introduce weights $\widetilde{\boldsymbol{w}} = [\sqrt{\widetilde{w}_{ij}}]$, where

$$\widetilde{w}_{ij} = \frac{P_{ij}^{\mathcal{A}}}{\sum_{(i,j)\in\mathcal{A}} P_{ij}^{\mathcal{A}}}.$$

By squaring (3.13), we can obtain the following WLS problem, according to (3.13), (3.8) and (3.14) as:

$$(\hat{\boldsymbol{x}}_i, \hat{\eta}) = \arg\min_{\boldsymbol{x}_i,\eta} \sum_{(i,j):(i,j)\in\mathcal{A}} \widetilde{w}_{ij} \left(\beta_{ij}^{\mathcal{A}^2}\|\boldsymbol{x}_i - \boldsymbol{a}_j\|^2 - \eta^2 d_0^2\right)^2 + \sum_{(i,j):(i,j)\in\mathcal{A}} \widetilde{w}_{ij}\Big(\boldsymbol{c}_{ij}^T(\boldsymbol{x}_i - \boldsymbol{a}_j)\Big)^2 + \sum_{(i,j):(i,j)\in\mathcal{A}} \widetilde{w}_{ij}\Big(\beta_{ij}^{\mathcal{A}}\boldsymbol{k}_{ij}^T(\boldsymbol{x}_i - \boldsymbol{a}_j) - \eta d_0\cos(\alpha_{ij}^{\mathcal{A}})\Big)^2.$$

Using the substitution $\widetilde{\boldsymbol{y}}_i = [\boldsymbol{x}_i^T, \|\boldsymbol{x}_i\|^2, \eta, \eta^2]^T$, we can rewrite (3.15) as a GTRS:

$$\underset{\widetilde{\boldsymbol{y}}_i}{\text{minimize}}\ \|\widetilde{\boldsymbol{W}}(\widetilde{\boldsymbol{A}}\widetilde{\boldsymbol{y}}_i - \widetilde{\boldsymbol{b}})\|^2$$

subject to

$$\widetilde{\boldsymbol{y}}_i^T\widetilde{\boldsymbol{D}}\widetilde{\boldsymbol{y}}_i + 2\widetilde{\boldsymbol{l}}^T\widetilde{\boldsymbol{y}}_i = 0, \tag{3.15}$$

where $\widetilde{\boldsymbol{W}} = \boldsymbol{I}_3 \otimes \mathrm{diag}(\widetilde{\boldsymbol{w}})$, $\widetilde{\boldsymbol{D}} = \mathrm{diag}([1,1,1,0,1,0])$, and

$$\widetilde{\boldsymbol{A}} = \begin{bmatrix} \vdots & \vdots & \vdots & \vdots \\ -2\beta_{ij}^{\mathcal{A}^2}\boldsymbol{a}_j^T & \beta_{ij}^{\mathcal{A}^2} & 0 & -d_0 \\ \vdots & \vdots & \vdots & \vdots \\ \boldsymbol{c}_{ij}^T & 0 & 0 & 0 \\ \vdots & \vdots & \vdots & \vdots \\ \beta_{ij}^{\mathcal{A}}\boldsymbol{k}_{ij}^T & 0 & -d_0\cos(\alpha_{ij}^{\mathcal{A}}) & 0 \\ \vdots & \vdots & \vdots & \vdots \end{bmatrix}, \widetilde{\boldsymbol{b}} = \begin{bmatrix} \vdots \\ -\beta_{ij}^{\mathcal{A}^2}\|\boldsymbol{a}_j\|^2 \\ \vdots \\ \boldsymbol{c}_{ij}^T\boldsymbol{a}_j \\ \vdots \\ \beta_{ij}^{\mathcal{A}}\boldsymbol{k}_{ij}^T\boldsymbol{a}_j \\ \vdots \end{bmatrix},$$

$$\widetilde{\boldsymbol{l}} = \left[\boldsymbol{0}_{1\times 3}, -\frac{1}{2}, 0, -\frac{1}{2}\right]^T,$$

i.e., $\widetilde{\boldsymbol{A}} \in \mathbb{R}^{3|\mathcal{A}|\times 6}$, $\widetilde{\boldsymbol{b}} \in \mathbb{R}^{3|\mathcal{A}|\times 1}$, and $\widetilde{\boldsymbol{W}} \in \mathbb{R}^{3|\mathcal{A}|\times 3|\mathcal{A}|}$.

Even though the approach in (3.15) efficiently solves (3.6) for unknown P_0, we can further improve its performance. To do so, we will first solve (3.15) to obtain the location estimate, and use this estimate to find the ML estimate of P_0, $\widehat{P}_0$. Then, we will take advantage of $\widehat{P}_0$ to solve another WLS problem as if P_0 is known. Hence, the proposed procedure for solving (3.6) when P_0 is not known is summarized below:

1. Solve (3.15) to obtain the initial estimate of $\boldsymbol{x}_i$, $\hat{\boldsymbol{x}}_i'$;

2. Use $\hat{\boldsymbol{x}}_i'$ to compute the ML estimate of P_0, $\widehat{P}_0$ as:

$$\widehat{P}_0 = \frac{\sum_{(i,j)\in\mathcal{A}}\left(P_{ij}^{\mathcal{A}} + 10\gamma\log_{10}\frac{\|\hat{\boldsymbol{x}}_i' - \boldsymbol{a}_j\|}{d_0}\right)}{|\mathcal{A}|};$$

3. Exploit $\widehat{P}_0$ to calculate $\hat{\lambda}_{ij}^{\mathcal{A}} = 10^{\frac{P_{ij}^{\mathcal{A}} - \widehat{P}_0}{10\gamma}}$, and use this estimated value to solve the SR-WLS in (3.12).

The main reason for applying this simple procedure is that we observed in our simulations that after solving (3.15) an excellent ML estimation of P_0, $\widehat{P}_0$, is obtained, very close to the true value of P_0. This motivated us to take advantage of this estimated value to solve another WLS problem (3.12), as if P_0 is known. We denote the above three-step procedure as "SR-WLS2" in the remaining text.

3.2.4 Cooperative Localization

By cooperative WSN, we imply a network consisting of a number of targets and anchors where a target can communicate with any sensor within its communication range, and all targets are localized simultaneously. A kind of node cooperation is required in networks with modest energy capabilities, where communication ranges are limited (in order to prolong the sensors' battery lives) and only some targets can communicate directly with the anchor nodes.

Throughout this section, we develop a convex estimator by using appropriate relaxation technique leading to an SDP estimator for 3-D localization. Moreover, we show that the generalization of the proposed estimator to the case of unknown P_0 is straightforward.

For sufficiently small noise, (3.1), (3.3) and (3.4) can be rewritten as:

$$\lambda_{ij}^{\mathcal{A}\,2} \|\boldsymbol{x}_i - \boldsymbol{a}_j\|^2 \approx d_0^2, \text{ for } (i,j) \in \mathcal{A}, \tag{3.16a}$$

$$\lambda_{ik}^{\mathcal{B}\,2} \|\boldsymbol{x}_i - \boldsymbol{x}_k\|^2 \approx d_0^2, \text{ for } (i,k) \in \mathcal{B}, \tag{3.16b}$$

$$\boldsymbol{c}_{ij}^T (\boldsymbol{x}_i - \boldsymbol{a}_j) \approx 0, \text{ for } (i,j) \in \mathcal{A}, \tag{3.17a}$$

$$\boldsymbol{c}_{ik}^T (\boldsymbol{x}_i - \boldsymbol{x}_k) \approx 0, \text{ for } (i,k) \in \mathcal{B}, \tag{3.17b}$$

and

$$\boldsymbol{k}_{ij}^T (\boldsymbol{x}_i - \boldsymbol{a}_j)(\boldsymbol{x}_i - \boldsymbol{a}_j)^T \boldsymbol{k}_{ij} \approx \|\boldsymbol{x}_i - \boldsymbol{a}_j\|^2 \cos^2(\alpha_{ij}^{\mathcal{A}}), \text{ for } (i,j) \in \mathcal{A}, \tag{3.18a}$$

$$\boldsymbol{k}_{ik}^T (\boldsymbol{x}_i - \boldsymbol{x}_k)(\boldsymbol{x}_i - \boldsymbol{x}_k)^T \boldsymbol{k}_{ik} \approx \|\boldsymbol{x}_i - \boldsymbol{x}_k\|^2 \cos^2(\alpha_{ik}^{\mathcal{B}}), \text{ for } (i,k) \in \mathcal{B}, \tag{3.18b}$$

where $\lambda_{ik}^{\mathcal{B}} = 10^{\frac{P_{ik}^{\mathcal{B}} - P_0}{10\gamma}}$, $\boldsymbol{c}_{ik} = [-\sin(\phi_{ik}^{\mathcal{B}}), \cos(\phi_{ik}^{\mathcal{B}}), 0]^T$, and $\boldsymbol{k}_{ik} = [0,0,1]^T$.

Following the LS principle, from (3.16), (3.17) and (3.18) we obtain the target location

estimates, $\hat{\boldsymbol{x}}$, by minimizing the objective function:

$$\begin{aligned}\hat{\boldsymbol{x}} = \arg\min_{\boldsymbol{x}} & \sum_{(i,j):(i,j)\in\mathcal{A}} \left(\lambda_{ij}^{\mathcal{A}\,2}\|\boldsymbol{x}_i-\boldsymbol{a}_j\|^2-d_0^2\right)^2+\sum_{(i,j):(i,j)\in\mathcal{A}}\left(\boldsymbol{c}_{ij}^T(\boldsymbol{x}_i-\boldsymbol{a}_j)\right)^2\\ &+\sum_{(i,j):(i,j)\in\mathcal{A}}\left(\boldsymbol{k}_{ij}^T(\boldsymbol{x}_i-\boldsymbol{a}_j)(\boldsymbol{x}_i-\boldsymbol{a}_j)^T\boldsymbol{k}_{ij}-\|\boldsymbol{x}_i-\boldsymbol{a}_j\|^2\cos^2(\alpha_{ij}^{\mathcal{A}})\right)^2\\ &+\sum_{(i,k):(i,k)\in\mathcal{B}}\left(\lambda_{ik}^{\mathcal{B}\,2}\|\boldsymbol{x}_i-\boldsymbol{x}_k\|^2-d_0^2\right)^2+\sum_{(i,k):(i,k)\in\mathcal{B}}\left(\boldsymbol{c}_{ik}^T(\boldsymbol{x}_i-\boldsymbol{x}_k)\right)^2\\ &+\sum_{(i,k):(i,k)\in\mathcal{B}}\left(\boldsymbol{k}_{ik}^T(\boldsymbol{x}_i-\boldsymbol{x}_k)(\boldsymbol{x}_i-\boldsymbol{x}_k)^T\boldsymbol{k}_{ik}-\|\boldsymbol{x}_i-\boldsymbol{x}_k\|^2\cos^2(\alpha_{ik}^{\mathcal{B}})\right)^2.\end{aligned} \tag{3.19}$$

Although the optimization problem in (3.19) is non-convex and has no closed-form solution, we will show in the following text that it can be converted into an SDP problem.

Cooperative localization with known P_T

A common approach in the literature (when dealing with cooperative localization) is to stack all unknowns in one big matrix variable $\boldsymbol{Y}=[\boldsymbol{x}_1,...,\boldsymbol{x}_M]$ ($\boldsymbol{Y}\in\mathbb{R}^{3\times M}$) [50]-[56]. However, this approach cannot be applied to solve (3.19) because of the vector outer product that appears in two sums with respect to the elevation angle. Instead, we assemble the unknowns in a vector, which allows us to cope effortlessly with the outer product.

Introduce auxiliary variable $\boldsymbol{X}=\boldsymbol{x}\boldsymbol{x}^T$ ($\boldsymbol{X}\in\mathbb{R}^{3M\times 3M}$). Moreover, introduce an auxiliary vector $\boldsymbol{z}=[z_{ij}^{\mathcal{A}},g_{ij}^{\mathcal{A}},p_{ij}^{\mathcal{A}},z_{ik}^{\mathcal{B}},g_{ik}^{\mathcal{B}},p_{ik}^{\mathcal{B}}]^T$ ($\boldsymbol{z}\in\mathbb{R}^{3(|\mathcal{A}|+|\mathcal{B}|)\times 1}$). Then, the problem in (3.19) can be rewritten as:

$$\underset{\boldsymbol{x},\boldsymbol{X},\boldsymbol{z}}{\text{minimize}}\ \|\boldsymbol{z}\|^2$$

subject to

$$z_{ij}^{\mathcal{A}}=\lambda_{ij}^{\mathcal{A}\,2}\left(\operatorname{tr}\left(\boldsymbol{E}_i^T\boldsymbol{X}\boldsymbol{E}_i\right)-2\boldsymbol{a}_j^T\boldsymbol{E}_i^T\boldsymbol{x}+\|\boldsymbol{a}_j\|^2\right)-d_0^2, \tag{3.20a}$$

$$g_{ij}^{\mathcal{A}}=\boldsymbol{c}_{ij}^T\left(\boldsymbol{E}_i^T\boldsymbol{x}-\boldsymbol{a}_j\right),\ \text{for}\ (i,j)\in\mathcal{A}, \tag{3.20b}$$

$$\begin{aligned}p_{ij}^{\mathcal{A}}=&\,\boldsymbol{k}_{ij}^T\left(\boldsymbol{E}_i^T\boldsymbol{X}\boldsymbol{E}_i-2\boldsymbol{E}_i^T\boldsymbol{x}\boldsymbol{a}_j^T+\boldsymbol{a}_j\boldsymbol{a}_j^T\right)\boldsymbol{k}_{ij}\\ &-\left(\operatorname{tr}\left(\boldsymbol{E}_i^T\boldsymbol{X}\boldsymbol{E}_i\right)-2\boldsymbol{a}_j^T\boldsymbol{E}_i^T\boldsymbol{x}+\|\boldsymbol{a}_j\|^2\right)\cos^2(\alpha_{ij}^{\mathcal{A}}),\end{aligned} \tag{3.20c}$$

$$z_{ik}^{\mathcal{B}}=\lambda_{ik}^{\mathcal{B}\,2}\left(\operatorname{tr}\left(\boldsymbol{E}_i^T\boldsymbol{X}\boldsymbol{E}_i\right)-2\operatorname{tr}\left(\boldsymbol{E}_i^T\boldsymbol{X}\boldsymbol{E}_k\right)+\operatorname{tr}\left(\boldsymbol{E}_k^T\boldsymbol{X}\boldsymbol{E}_k\right)\right)-d_0^2, \tag{3.20d}$$

$$g_{ik}^{\mathcal{B}}=\boldsymbol{c}_{ik}^T\left(\boldsymbol{E}_i^T\boldsymbol{x}-\boldsymbol{E}_k^T\boldsymbol{x}\right),\ \text{for}\ (i,k)\in\mathcal{B} \tag{3.20e}$$

$$\begin{aligned}p_{ik}^{\mathcal{B}}=&\,\boldsymbol{k}_{ik}^T\left(\boldsymbol{E}_i^T\boldsymbol{X}\boldsymbol{E}_i-2\boldsymbol{E}_i^T\boldsymbol{X}\boldsymbol{E}_k+\boldsymbol{E}_k^T\boldsymbol{X}\boldsymbol{E}_k\right)\boldsymbol{k}_{ik}\\ &-\left(\operatorname{tr}\left(\boldsymbol{E}_i^T\boldsymbol{X}\boldsymbol{E}_i\right)-2\operatorname{tr}\left(\boldsymbol{E}_i^T\boldsymbol{X}\boldsymbol{E}_k\right)+\operatorname{tr}\left(\boldsymbol{E}_k^T\boldsymbol{X}\boldsymbol{E}_k\right)\right)\cos^2(\alpha_{ik}^{\mathcal{B}}),\end{aligned} \tag{3.20f}$$

$$\boldsymbol{X}=\boldsymbol{x}\boldsymbol{x}^T. \tag{3.20g}$$

Defining an epigraph variable, t, together with the semidefinite and second-order cone relaxations of the form $\boldsymbol{X}\succeq\boldsymbol{x}\boldsymbol{x}^T$ and $\|\boldsymbol{z}\|^2\leq t$ respectively, the following convex epigraph form is obtained from the above problem:

$$\underset{\boldsymbol{x},\boldsymbol{X},\boldsymbol{z},t}{\text{minimize}}\ t$$

subject to (3.20a)-(3.20f),

$$\left\| \begin{bmatrix} 2\boldsymbol{z} \\ t-1 \end{bmatrix} \right\| \leq t+1, \ \begin{bmatrix} \boldsymbol{X} & \boldsymbol{x} \\ \boldsymbol{x}^T & 1 \end{bmatrix} \succeq \mathbf{0}_{3M+1}. \tag{3.21}$$

The above problem is an SDP (more precisely, it is a mixed SDP/SOCP), which can be readily solved by `CVX` [62]. It is worth mentioning that, if $\text{rank}(\boldsymbol{X}) = 1$, then the relaxed constraint $\boldsymbol{X} \succeq \boldsymbol{x}\boldsymbol{x}^T$ is satisfied as an equality [57]. Note also that we applied the Schur complement to rewrite $\boldsymbol{X} \succeq \boldsymbol{x}\boldsymbol{x}^T$ into a semidefinite cone constraint form. In the following text, we will denote (3.21) as "SDP1".

Cooperative localization with unknown P_T

The generalization of the proposed SDP estimator for known P_0 is straightforward for the case where P_0 is not known. From (3.16), we have that:

$$\beta_{ij}^{\mathcal{A}\,2} \|\boldsymbol{x}_i - \boldsymbol{a}_j\|^2 \approx \rho d_0^2, \text{ for } (i,j) \in \mathcal{A}, \tag{3.22a}$$

$$\beta_{ik}^{\mathcal{B}\,2} \|\boldsymbol{x}_i - \boldsymbol{x}_k\|^2 \approx \rho d_0^2, \text{ for } (i,k) \in \mathcal{B}, \tag{3.22b}$$

where $\beta_{ik} = 10^{\frac{P_{ik}^{\mathcal{B}}}{10\gamma}}$ for $(i,k) \in \mathcal{B}$ and $\rho = 10^{\frac{P_0}{5\gamma}}$. Therefore, according to (3.22), (3.17) and (3.18), the target location estimates are obtained by minimizing the following LS problem:

$$\begin{aligned}
(\hat{\boldsymbol{x}}, \hat{\rho}) = \arg\min_{\boldsymbol{x},\rho} & \sum_{(i,j):(i,j)\in\mathcal{A}} \left(\beta_{ij}^{\mathcal{A}\,2} \|\boldsymbol{x}_i - \boldsymbol{a}_j\|^2 - \rho d_0^2\right)^2 + \sum_{(i,j):(i,j)\in\mathcal{A}} \left(\boldsymbol{c}_{ij}^T (\boldsymbol{x}_i - \boldsymbol{a}_j)\right)^2 \\
& + \sum_{(i,j):(i,j)\in\mathcal{A}} \left(\boldsymbol{k}_{ij}^T (\boldsymbol{x}_i - \boldsymbol{a}_j)(\boldsymbol{x}_i - \boldsymbol{a}_j)^T \boldsymbol{k}_{ij} - \|\boldsymbol{x}_i - \boldsymbol{a}_j\|^2 \cos^2(\alpha_{ij}^{\mathcal{A}})\right)^2 \\
& + \sum_{(i,k):(i,k)\in\mathcal{B}} \left(\beta_{ik}^{\mathcal{B}\,2} \|\boldsymbol{x}_i - \boldsymbol{x}_k\|^2 - \rho d_0^2\right)^2 + \sum_{(i,k):(i,k)\in\mathcal{B}} \left(\boldsymbol{c}_{ik}^T (\boldsymbol{x}_i - \boldsymbol{x}_k)\right)^2 \\
& + \sum_{(i,k):(i,k)\in\mathcal{B}} \left(\boldsymbol{k}_{ik}^T (\boldsymbol{x}_i - \boldsymbol{x}_k)(\boldsymbol{x}_i - \boldsymbol{x}_k)^T \boldsymbol{k}_{ik} - \|\boldsymbol{x}_i - \boldsymbol{x}_k\|^2 \cos^2(\alpha_{ik}^{\mathcal{B}})\right)^2.
\end{aligned} \tag{3.23}$$

By following similar steps as described in the previous section, we obtain the SDP estimator defined below:

$$\underset{\boldsymbol{x},\rho,\boldsymbol{X},\boldsymbol{z},t}{\text{minimize}} \ t$$

subject to

$$\begin{aligned}
z_{ij}^{\mathcal{A}} &= \beta_{ij}^{\mathcal{A}\,2} \left(\text{tr}\left(\boldsymbol{E}_i^T \boldsymbol{X} \boldsymbol{E}_i\right) - 2\boldsymbol{a}_j^T \boldsymbol{E}_i^T \boldsymbol{x} + \|\boldsymbol{a}_j\|^2\right) - \rho d_0^2, \\
g_{ij}^{\mathcal{A}} &= \boldsymbol{c}_{ij}^T \left(\boldsymbol{E}_i^T \boldsymbol{x} - \boldsymbol{a}_j\right), \text{ for } (i,j) \in \mathcal{A}, \\
p_{ij}^{\mathcal{A}} &= \boldsymbol{k}_{ij}^T \left(\boldsymbol{E}_i^T \boldsymbol{X} \boldsymbol{E}_i - 2\boldsymbol{E}_i^T \boldsymbol{x}\boldsymbol{a}_j^T + \boldsymbol{a}_j\boldsymbol{a}_j^T\right) \boldsymbol{k}_{ij} \\
&\quad - \left(\text{tr}\left(\boldsymbol{E}_i^T \boldsymbol{X} \boldsymbol{E}_i\right) - 2\boldsymbol{a}_j^T \boldsymbol{E}_i^T \boldsymbol{x} + \|\boldsymbol{a}_j\|^2\right) \cos^2(\alpha_{ij}^{\mathcal{A}}), \\
z_{ik}^{\mathcal{B}} &= \beta_{ik}^{\mathcal{B}\,2} \left(\text{tr}\left(\boldsymbol{E}_i^T \boldsymbol{X} \boldsymbol{E}_i\right) - 2\,\text{tr}\left(\boldsymbol{E}_i^T \boldsymbol{X} \boldsymbol{E}_k\right) + \text{tr}\left(\boldsymbol{E}_k^T \boldsymbol{X} \boldsymbol{E}_k\right)\right) - \rho d_0^2, \\
g_{ik}^{\mathcal{B}} &= \boldsymbol{c}_{ik}^T \left(\boldsymbol{E}_i^T \boldsymbol{x} - \boldsymbol{E}_k^T \boldsymbol{x}\right), \text{ for } (i,k) \in \mathcal{B} \\
p_{ik}^{\mathcal{B}} &= \boldsymbol{k}_{ik}^T \left(\boldsymbol{E}_i^T \boldsymbol{X} \boldsymbol{E}_i - 2\boldsymbol{E}_i^T \boldsymbol{X} \boldsymbol{E}_k + \boldsymbol{E}_k^T \boldsymbol{X} \boldsymbol{E}_k\right) \boldsymbol{k}_{ik} \\
&\quad - \left(\text{tr}\left(\boldsymbol{E}_i^T \boldsymbol{X} \boldsymbol{E}_i\right) - 2\,\text{tr}\left(\boldsymbol{E}_i^T \boldsymbol{X} \boldsymbol{E}_k\right) + \text{tr}\left(\boldsymbol{E}_k^T \boldsymbol{X} \boldsymbol{E}_k\right)\right) \cos^2(\alpha_{ik}^{\mathcal{B}}),
\end{aligned}$$

$$\left\| \begin{bmatrix} 2\boldsymbol{z} \\ t-1 \end{bmatrix} \right\| \leq t+1, \ \begin{bmatrix} \boldsymbol{X} & \boldsymbol{x} \\ \boldsymbol{x}^T & 1 \end{bmatrix} \succeq \mathbf{0}_{3M+1}. \tag{3.24}$$

Although the above SDP estimator efficiently solves the target localization problem for the case of unknown P_0 in a cooperative WSN, we propose the following three-step procedure to further enhance the estimation accuracy:

1. Solve (3.24) to obtain the initial estimate of all target locations $\boldsymbol{x}$, $\hat{\boldsymbol{x}}'$;
2. Use $\hat{\boldsymbol{x}}'$ to compute the ML estimate of P_0, $\widehat{P}_0$ as:

$$\widehat{P}_0 = \frac{\sum\limits_{(i,j):(i,j)\in\mathcal{A}} \left(P_{ij}^{\mathcal{A}} + 10\gamma \log_{10} \frac{\|\boldsymbol{E}_i^T \hat{\boldsymbol{x}}' - \boldsymbol{a}_j\|}{d_0} \right)}{|\mathcal{A}|+|\mathcal{B}|} + \frac{\sum\limits_{(i,k):(i,k)\in\mathcal{B}} \left(P_{ik}^{\mathcal{B}} + 10\gamma \log_{10} \frac{\|\boldsymbol{E}_i^T \hat{\boldsymbol{x}}' - \boldsymbol{E}_k^T \hat{\boldsymbol{x}}'\|}{d_0} \right)}{|\mathcal{A}|+|\mathcal{B}|};$$

3. Exploit $\widehat{P}_0$ to calculate $\hat{\lambda}_{ij}^{\mathcal{A}} = 10^{\frac{P_{ij}^{\mathcal{A}} - \widehat{P}_0}{10\gamma}}$ $\forall (i,j) \in \mathcal{A}$ and $\hat{\lambda}_{ik}^{\mathcal{B}} = 10^{\frac{P_{ik}^{\mathcal{B}} - \widehat{P}_0}{10\gamma}}$ $\forall (i,k) \in \mathcal{B}$, and use these estimated values to solve the SDP in (3.21) as if P_0 is known.

We refer to the above three-step procedure as "SDP2" in the following text.

3.2.5 Complexity Analysis

The trade-off between the estimation accuracy and the computational complexity is one of the most important features of any algorithm since it defines its applicability potential. This is the reason why, apart from the performance, we also want to analyse the computational complexity of the considered approaches.

The formula (2.24) for computing the worst case computational complexity of a mixed SDP/SOCP [63] is used to analyse the complexities of the considered algorithms in this section. For completeness, we reproduce the formula below

$$\mathcal{O}\left(\sqrt{L} \left(m \sum_{i=1}^{N_{sd}} n_i^{sd^3} + m^2 \sum_{i=1}^{N_{sd}} n_i^{sd^2} + m^2 \sum_{i=1}^{N_{soc}} n_i^{soc} + \sum_{i=1}^{N_{soc}} n_i^{soc^2} + m^3 \right) \right),$$

where L is the iteration complexity of the algorithm, m is the number of equality constraints, n_i^{sd} and n_i^{soc} are respectively the dimensions of the i-th SDC and the i-th SOC, and N_i^{sd} and N_i^{soc} are the number of SDC and SOC constraints, respectively. Formula (2.24) corresponds to the formula for computing the complexity of an SDP for the case when we have no SOCCs (in which case L is the dimension of the SDC given as a result of accumulating all SDC), and vice versa (in which case L is the total number of SOC constraints) [63].

Since we are interested in analysing the worst case asymptotic computational complexity, we present only the dominating elements, which are expressed as a function of N

Table 3.1: Summary of the Considered Algorithms

Algorithm	Description	Complexity
SR-WLS1	The proposed SR-WLS estimator for non-cooperative localization when P_T is known (3.40)	$K_{\max} \cdot \mathcal{O}(N)$
LS	The LS estimator for non-cooperative localization when P_T is known in [30]	$\mathcal{O}(N)$
SR-WLS2	The proposed SR-WLS approach for non-cooperative localization in Section 3.2.3 for unknown P_T	$2 \cdot K_{\max} \cdot \mathcal{O}(N)$
SDP1	The proposed SDP estimator for cooperative localization when P_T is known in (3.21)	$\mathcal{O}\left(\sqrt{3M}\left(81M^4\left(N+\frac{M}{2}\right)^2\right)\right)$
SDP2	The proposed SDP approach for cooperative localization in Section 3.2.4 for unknown P_T	$2 \cdot \mathcal{O}\left(\sqrt{3M}\left(81M^4\left(N+\frac{M}{2}\right)^2\right)\right)$

and M. Therefore, we assume that the network is fully connected[1], *i.e.*, the total number of connections in the network is $C = |\mathcal{A}| + |\mathcal{B}|$, where $|\mathcal{A}| = MN$ and $|\mathcal{B}| = \frac{M(M-1)}{2}$. In the case of non-cooperative localization, each target is located at a time; hence, we can presume that $M = 1$ in this case.

Assuming that $K_{\max}$ is the maximum number of steps in the bisection procedure used to solve (3.12) and (3.15), Table 3.1 provides an overview of the considered algorithms together with their worst case computational complexities.

Table 3.1 reveals that the computational complexity of the considered approaches depends mainly on the network size, *i.e.*, the total number of sensors in the WSN. This property is consistent for algorithms executed in a centralized manner [18], where the acquired information is conveyed to a central processor that performs the necessary computations. As shown in Table 3.1, in the case of non-cooperative localization, the proposed estimators based on GTRS framework are slightly more complex than the existing one, due to the iterative bisection procedure. However, the higher computational complexity of the proposed estimators is justified by their superior performance in the sense of estimation accuracy, as we will see in Section 3.2.6. Finally, from Table 3.1 we can see that the proposed estimators for cooperative localization are computationally the most demanding. This is not surprising, since the cooperative localization problem is very challenging, and requires the use of sophisticated mathematical tools in order to be solved globally.

3.2.6 Performance Results

In this section, we present a set of performance results to compare the proposed approaches with the existing ones, for both non-cooperative and cooperative localization with known and unknown P_T. In order to demonstrate the benefit of fusing two radio measurements versus traditional localization systems, we present also the performance results of the proposed methods for known P_T when only RSS measurements are employed, called here

[1]In practice, however, the number of connections in the network is significantly smaller, due to energy restrictions, *i.e.*, limited R.

SR-WLS$_{\text{RSS}}$ and SDP$_{\text{RSS}}$ for non-cooperative and cooperative localization, respectively. Also, it is worth mentioning that for the sake of fairness, the range measurements for the LS method in [30], were acquired according to (3.2a). All of the presented algorithms were solved by using the MATLAB package `CVX` [62], where the solver is SeDuMi [65].

To generate the radio measurements, (3.1), (3.3) and (3.4) were used. We considered a random deployment of nodes inside a box with a length of the edges $B = 15$ m in each Monte Carlo (M_c) run. Random deployment of nodes is of practical interest, since the algorithms are tested against various network topologies. Unless stated otherwise, the reference distance is set to $d_0 = 1$ m, the reference power $P_0 = -10$ dBm, the maximum number of steps in the bisection procedure to $K_{\max} = 30$, and the PLE was fixed to $\gamma = 2.5$. However, in practice it is almost impossible to perfectly estimate the value of the PLE. Therefore, to account for a realistic measurement model mismatch and test the robustness of the considered approaches to imperfect knowledge of the PLE, the true PLE for each link was drawn from a uniform distribution on an interval $[2.2, 2.8]$, *i.e.*, $\gamma_{ij} \in [2.2, 2.8], \forall (i,j) \in \mathcal{A} \cup \mathcal{B}, i \neq j$.

Non-cooperative WSN

In a non-cooperative WSN, targets communicate exclusively with anchors and one target is located at a time; hence, without loss of generality, we can assume that $M = 1$. It was assumed that the RSS and AoA measurements were performed by anchors. As the main performance metric for the non-cooperative localization we used the RMSE, defined as

$$\text{RMSE} = \sqrt{\sum_{i=1}^{M_c} \frac{\|\boldsymbol{x}_i - \widehat{\boldsymbol{x}}_i\|^2}{M_c}},$$

where $\widehat{\boldsymbol{x}}_i$ denotes the estimate of the true target location, $\boldsymbol{x}_i$, in the i-th M_c run.

Fig. 3.4 illustrates the RMSE versus N comparison when $\sigma_{n_{ij}} = 6$ dB, $\sigma_{m_{ij}} = 10$ deg and $\sigma_{v_{ij}} = 10$ deg. Besides the considered algorithms, we also present the CRB in the figure (derivation of the CRB for the RSS-AoA-based localization is presented in Appendix C) As anticipated, Fig. 3.4 reveals that the performance of all algorithms improves as more anchors are added into the network, *i.e.*, as more reliable information is available. It also confirms the effectiveness of using the combined measurements in hybrid systems versus using only a single measurement like in traditional systems. Furthermore, one can see that the proposed estimators for both known and unknown P_T outperform significantly the existing one for all N. Additionally, it can be seen that "SR-WLS2" achieves the lower bound provided by its complement for known P_T, "SR-WLS1". We can also observe that the performance margin between the proposed estimators for known and unknown P_T decreases with the increase of N. This behaviour is intuitive, since with increased N we expect to obtain a better estimation of P_T (*closer* to its true value), which would allow us to enhance the estimation accuracy in the third step of our proposed procedure. Finally, although our estimators were based on the assumption that the noise is small, Fig. 3.4 reveals that they work excellent even for the cases where the noise power is high.

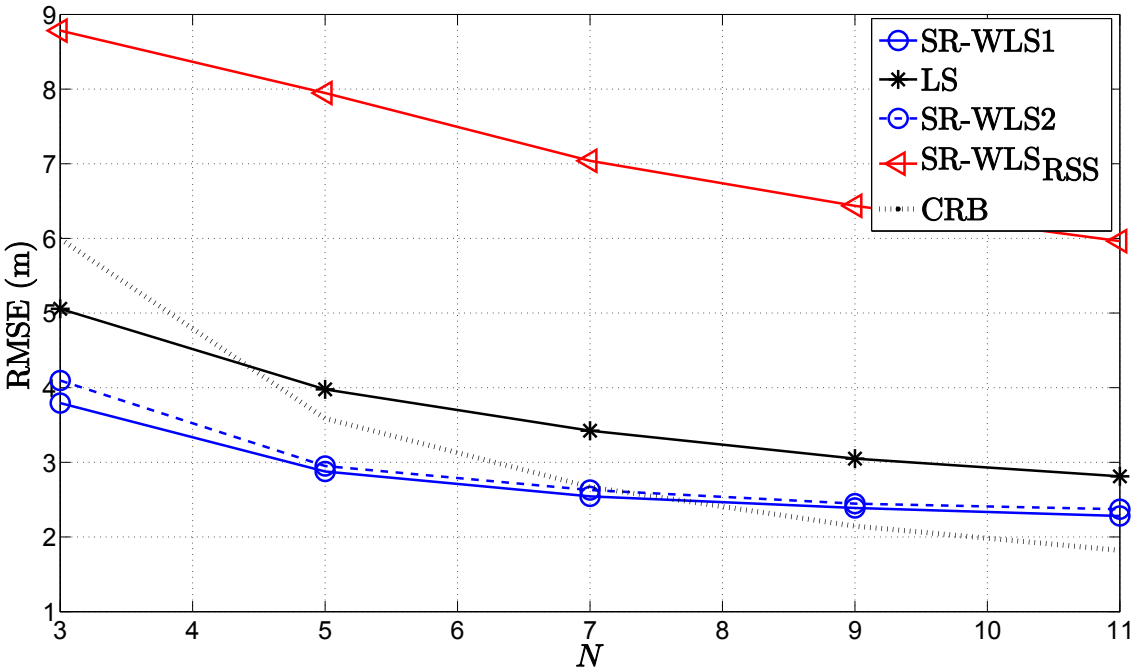

Figure 3.4: RMSE (m) versus N comparison, when $\sigma_{n_{ij}} = 6$ dB, $\sigma_{m_{ij}} = 10$ deg, $\sigma_{v_{ij}} = 10$ deg, $\gamma_{ij} \in [2.2, 2.8]$, $\gamma = 2.5$, $B = 15$ m, $P_0 = -10$ dBm, $d_0 = 1$ m, $M_c = 50000$.

In Figs. 3.5, 3.6 and 3.7 we investigate the influence of the quality of certain types of measurements on the performance of the considered approaches. More specifically, Figs. 3.5, 3.6 and 3.7 illustrate the RMSE (m) versus $\sigma_{n_{ij}}$ (dB), $\sigma_{m_{ij}}$ (deg) and $\sigma_{v_{ij}}$ (deg) comparison when $N = 4$, respectively. From these figures, one can observe that when the quality of a certain measurement drops, the performance of the considered algorithms worsens, as expected. Further, one can see that both the proposed and the existing approach suffer the biggest deterioration in the performance when the quality of the RSS measurements weakens. Also, while the quality of the azimuth angle measurements affect more the proposed approaches than the "LS" method, the error in the elevation angle measurements has very little effect on their performance. Furthermore, it can be seen that the proposed procedure for unknown P_T is robust to noise feature, since the performance margin between "SR-WLS1" and its counterpart for unknown P_T remains constant with the increase of noise, in general. Finally, Figs. 3.5, 3.6 and 3.7 exhibit superior performance of the proposed algorithms in comparison with the existing one, in general.

Cooperative WSN

This subsection presents the simulation results for the cooperative localization problem. As it was already mentioned, to the best of authors' knowledge, localization algorithms for hybrid RSS/AoA systems in cooperative 3-D WSNs are not available in the literature. Therefore, only the performance of the proposed approaches in Sections 3.2.4 for both cases of known and unknown P_T are analysed. In this section, it was assumed that the

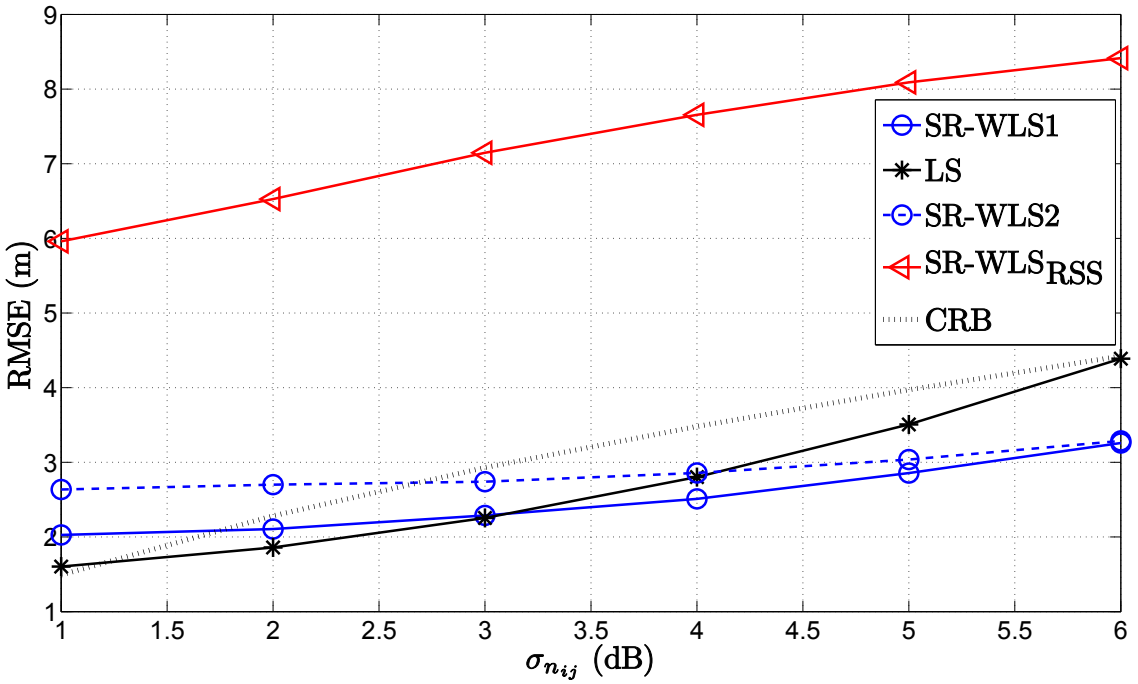

Figure 3.5: RMSE (m) versus $\sigma_{n_{ij}}$ (dB) comparison, when $N = 4$, $\sigma_{m_{ij}} = 10$ deg, $\sigma_{v_{ij}} = 10$ deg, $\gamma_{ij} \in [2.2, 2.8]$, $\gamma = 2.5$, $B = 15$ m, $P_0 = -10$ dBm, $d_0 = 1$ m, $M_c = 50000$.

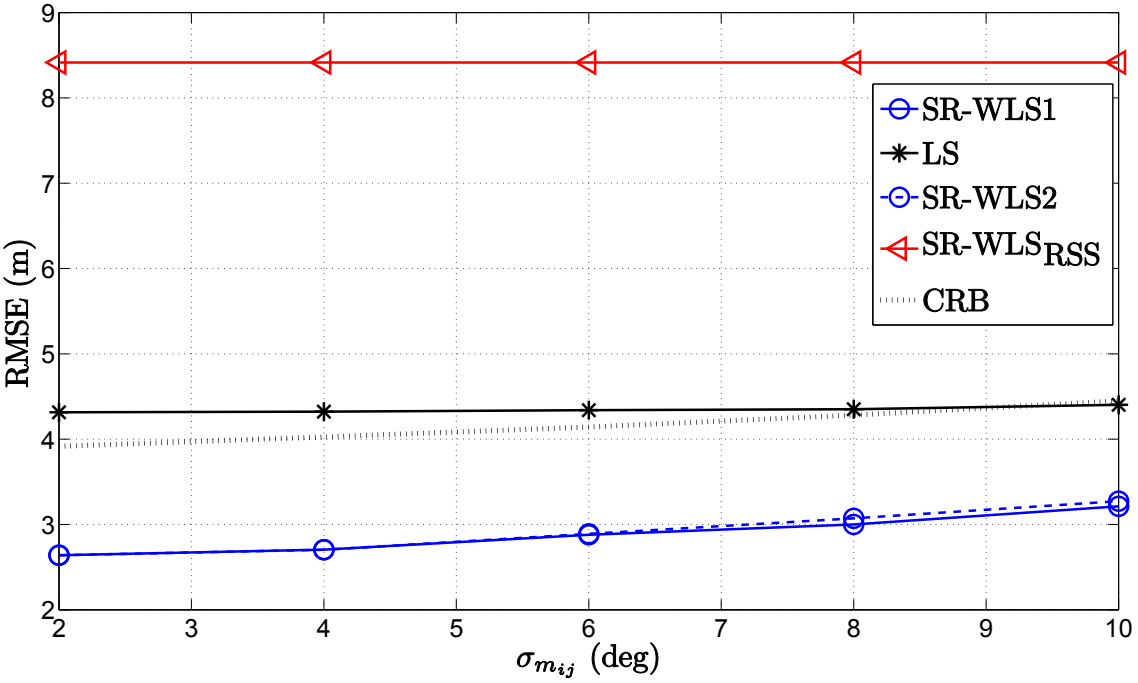

Figure 3.6: RMSE (m) versus $\sigma_{m_{ij}}$ (deg) comparison, when $N = 4$, $\sigma_{n_{ij}} = 6$ dB, $\sigma_{v_{ij}} = 10$ deg, $\gamma_{ij} \in [2.2, 2.8]$, $\gamma = 2.5$, $B = 15$ m, $P_0 = -10$ dBm, $d_0 = 1$ m, $M_c = 50000$.

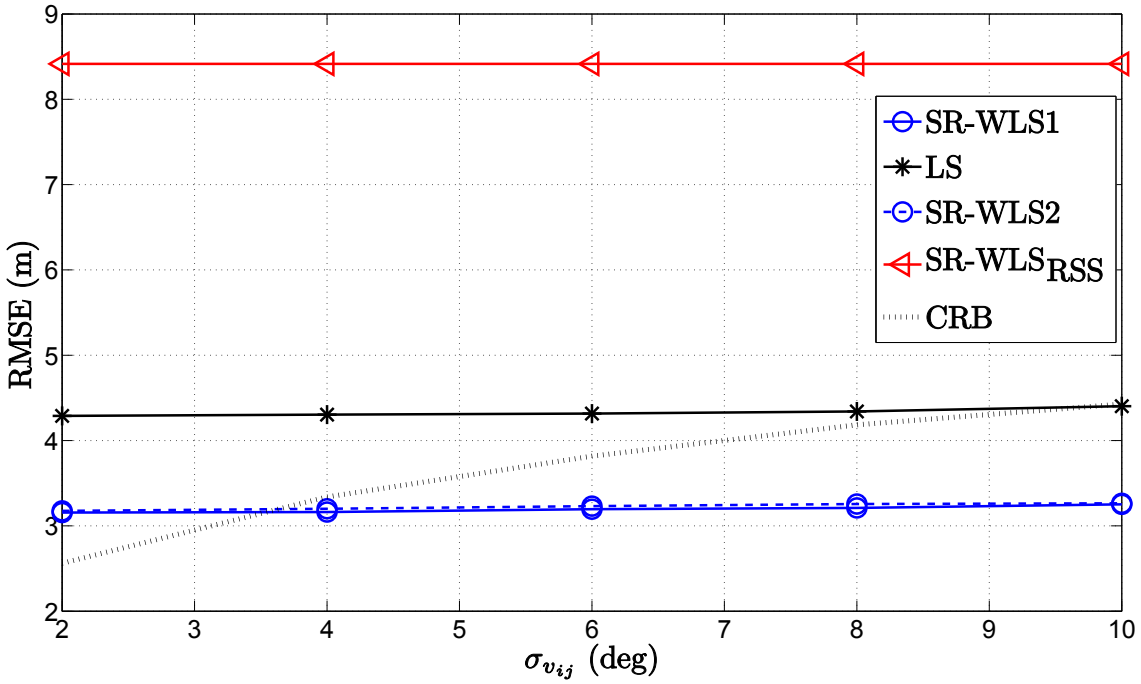

Figure 3.7: RMSE (m) versus $\sigma_{v_{ij}}$ (deg) comparison, when $N = 4$, $\sigma_{n_{ij}} = 6$ dB, $\sigma_{m_{ij}} = 10$ deg, $\gamma_{ij} \in [2.2, 2.8]$, $\gamma = 2.5$, $B = 15$ m, $P_0 = -10$ dBm, $d_0 = 1$ m, $M_c = 50000$.

signal measurements were performed by targets. As the main performance metric we used the NRMSE, defined as

$$\text{NRMSE} = \sqrt{\sum_{i=1}^{M_c} \sum_{j=1}^{M} \frac{\|\boldsymbol{x}_{ij} - \widehat{\boldsymbol{x}}_{ij}\|^2}{M\, M_c}},$$

where $\widehat{\boldsymbol{x}}_{ij}$ denotes the estimate of the true location of the j-th target, $\boldsymbol{x}_{ij}$, in the i-th M_c run.

Fig. 3.8 illustrates the NRMSE versus N comparison of the proposed estimators for both known and unknown P_T and the proposed SDP method for known P_T when only RSS measurements were used, for $M = 20$, $R = 8$ m, $\sigma_{n_{ij}} = 6$ dB, $\sigma_{m_{ij}} = 10$ deg and $\sigma_{v_{ij}} = 10$ deg. Fig. 3.4 confirms that adding more reliable information into the network boosts the performance of all considered estimators, and decreases the performance margin between "SDP1" and "SDP2". This behavior is not unusual since by increasing N we are expected to obtain a better estimation of P_T (*closer* to its true value) in the second step of our proposed procedure which would enhance the estimation accuracy in the final step of the procedure. Furthermore, Fig. 3.8 confirms that by fusing two radio measurements of the transmitted signal can significantly decrease the estimation error in comparison with using only one measurement.

Fig. 3.9 illustrates the NRMSE versus M comparison of the considered estimators, when $N = 8$, $R = 8$ m, $\sigma_{n_{ij}} = 6$ dB, $\sigma_{m_{ij}} = 10$ deg and $\sigma_{v_{ij}} = 10$ deg. One can notice from Fig. 3.9 that adding more targets into the network does not impair the performance of the

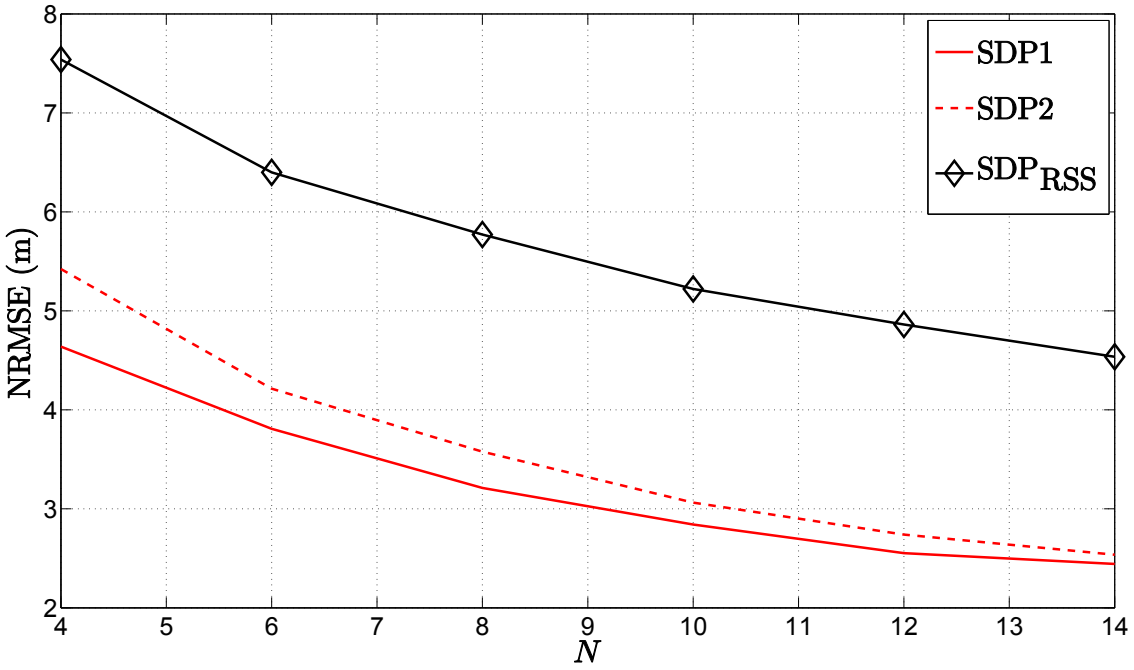

Figure 3.8: NRMSE (m) versus N comparison, when $M = 20$, $R = 8$ m, $\sigma_{n_{ij}} = 6$ dB, $\sigma_{m_{ij}} = 10$ deg, $\sigma_{v_{ij}} = 10$ deg, $\gamma_{ij} \in [2.2, 2.8]$, $\gamma = 2.5$, $B = 15$ m, $P_0 = -10$ dBm, $d_0 = 1$ m, $M_c = 1000$.

considered estimators. In fact, their performance betters as M increases. It also exhibits that the performance margin between "SDP1" and "SDP2" slowly grows with increase of M. This might be explained by the fact that when more targets are added in the network, more unreliable measurements are obtained (set $\mathcal{B}$ is enlarged) which might deteriorate the estimation of P_T and consequently the location estimation. Finally, although the measurement noise is high in Fig. 3.9, we can see that the proposed methods perform excellent.

Fig. 3.10 illustrates the NRMSE versus R comparison of the considered estimators, when $N = 8$, $M = 20$, $\sigma_{n_{ij}} = 6$ dB, $\sigma_{m_{ij}} = 10$ deg and $\sigma_{v_{ij}} = 10$ deg. Fig. 3.10 shows that the estimation error of the new estimators decreases as R increases. This behavior is anticipated, since when R grows, the acquired information inside the network also grows, as well as the probability that more target/anchor connections are established. One can observe that the performance margin between the hybrid methods and the RSS one increases as R grows. This is because when R is too low (*e.g.* $R = 5$ m) the amount of information obtained from sensors is insufficient, resulting in a poor estimation accuracy (NRMSE ≈ 8 m). Obviously, when R is expanded the proposed hybrid methods benefit more from the additional links than "SDP$_{\text{RSS}}$" method, since for each additional link two measurements (RSS and AoA) are performed. Note however that increasing R directly impacts the sensor's battery life, and that in practice we want to keep R as low as possible[2].

[2]The estimators in [31]-[32] and [76] were not considered here, since they were designed for 2-D scenarios, and a possible generalization to a 3-D scenario is not obvious. However, it is worth mentioning that, in our

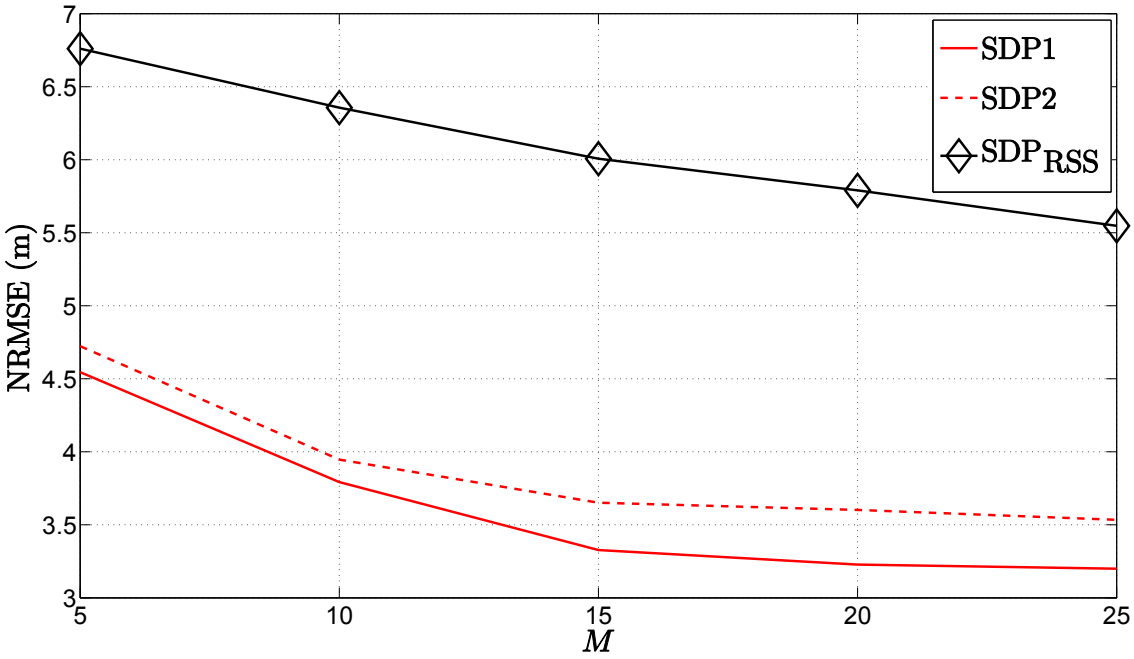

Figure 3.9: NRMSE (m) versus M comparison, when $N = 8$, $R = 8$ m, $\sigma_{n_{ij}} = 6$ dB, $\sigma_{m_{ij}} = 10$ deg, $\sigma_{v_{ij}} = 10$ deg, $\gamma_{ij} \in [2.2, 2.8]$, $\gamma = 2.5$, $B = 15$ m, $P_0 = -10$ dBm, $d_0 = 1$ m, $M_c = 1000$.

Real Indoor Experiment

In this section, we assess the performance of our SR-WLS2 algorithm that takes advantage of both RSS and AoA measurements through a real indoor experiment. Our experiment is based entirely on the measurements performed in [81]. Fig. 3.11 illustrates the 56 m $\times$25 m building in which the measurements were taken. In the figure, the true locations of the measurement points (targets) are indicated by blue circles and the true locations of the base stations (anchors) are indicated by black squares.

In [81], a regular 802.11 equipped laptop took four sets of measurements at each measurement point, one for each pose of the target (facing north, east, south, and west). No compass was used for orientation, and the target was set just by aiming to have the measurement laptop parallel with the walls. The location of the target was randomized in order to include in the measurements situations where both a human body and a laptop screen block the shortest path towards a base station. Although the polarization did not seem to matter, the authors in [81] performed all the measurements with 802.11 card kept in an horizontal plane, as is standard in most laptops. A measurement for a pose was in fact an average over three or four revolutions of the base station, in order to reduce the

simulations, the proposed algorithms outperformed the mentioned ones in terms of the estimation accuracy in 2-D scenarios. Note also that the WLS estimator in [33] for 3-D scenarios was omitted here. The reason is that this estimator did not exhibit acceptable performance in the investigated settings, where the area accommodating nodes and the noise power are much larger than it was considered in [33].

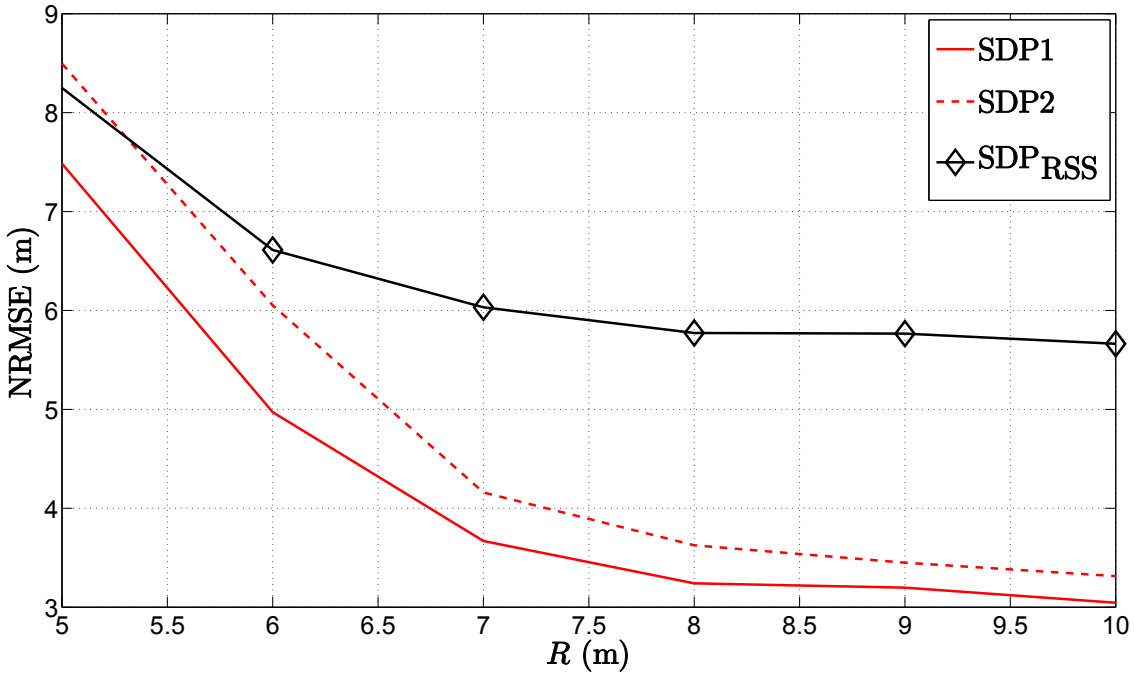

Figure 3.10: NRMSE (m) versus R (m) comparison, when $N = 8$, $M = 20$, $\sigma_{n_{ij}} = 6$ dB, $\sigma_{m_{ij}} = 10$ deg, $\sigma_{v_{ij}} = 10$ deg, $\gamma_{ij} \in [2.2, 2.8]$, $\gamma = 2.5$, $B = 15$ m, $P_0 = -10$ dBm, $d_0 = 1$ m, $M_c = 1000$

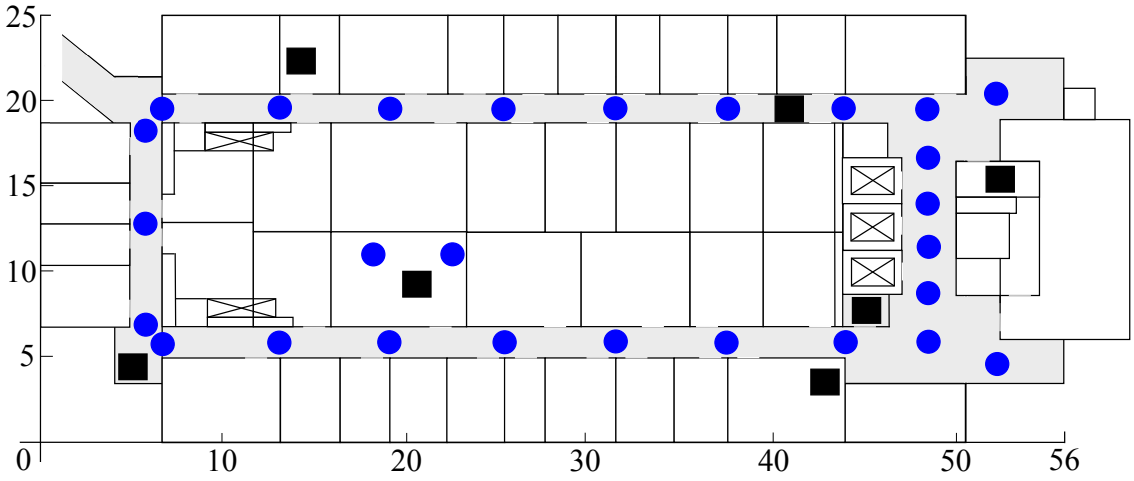

Figure 3.11: Experimental set-up with 7 anchors (black squares) and 27 targets (blue circles)

effect of temporary factors, such as open doors, or people passing by. Measurements were taken at various times of the day and night, including the busy morning and afternoon hours.

The way the authors in [81] managed to extract the AoA measurements on a 802.11 base station was to attach a directional antenna to a wireless access point. When this antenna was rotated, the RSS reported by the card was higher in the direction of the measurement point in general, see Fig. 3.12. To automatize this measurement of the angle, the authors mounted a small Toshiba Libretto 70ct laptop on a record player (turntable). In order to obtain higher difference in the maximums, they chose an antenna that is highly directional. The Lucent 2 Mbps 802.11 card was linked to a Hyperlink 14 dB gain directional antenna. The antenna was attached to the bottom of the laptop, so that it rotates in the horizontal plane.

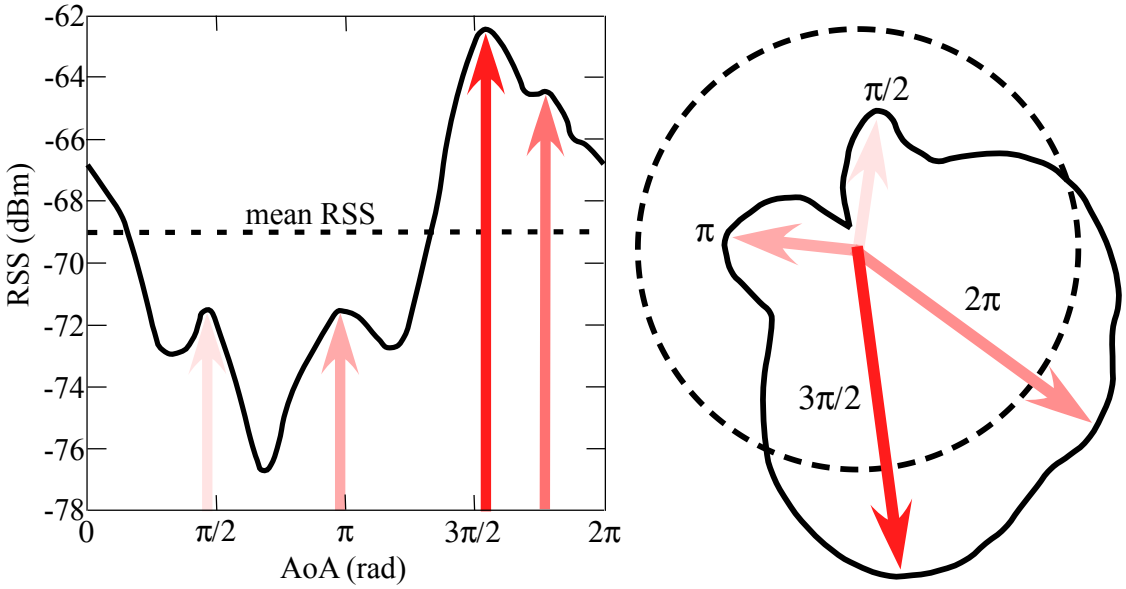

(a) Cartesian representation of RSS peak

(b) Polar representation of RSS peak

Figure 3.12: Illustration of the RSS peaks, indicating a possible direction of the target.

In Fig. 3.12, one can see that there is more than one peak in the RSS measurements, each one indicating a possible direction of the target. Obviously, choosing the right peak is a critical element of the measurement procedure, since failing to do so might result in large errors. However, the results in [81] indicate that the best measured AoA comes either from the first or the second RSS peak in 90% of the cases. Such results are not surprising in indoor environments, where a mixture of LoS and NLoS links exist, since in such environments it is expected to get one peak in the RSS from a signal propagating through a corridor and the other one from a signal passing through walls, the so-called quasi LoS [85]. Nevertheless, there still remain 10% of the cases in which the right direction comes from other RSS peaks. To resolve this issue, in this thesis, we have exploited our knowledge about the building configuration and the known locations of the anchors in

order to eliminate those AoA measurements that do not make any sense. For example, it only made sense that the anchor physically closest to the origin and the one furthest away in the y-axis direction could only obtain AoA measurements in the I and IV, and in the III and IV quadrants of a Cartesian coordinate system, respectively. Therefore, if the first peak resulted in a direction outside these quadrants, we have disregarded it and chose the second one, and so on.

By using the measurements in [81], we first applied a linear regression method to obtain $\gamma = 3.4$. For such an experimental setup, we compared the performance of our SR-WLS2 algorithm with the LS method used in [81]. We present the CDF of the localization error (LE), where LE $= \|\boldsymbol{x}_i - \widehat{\boldsymbol{x}}_i\|$ (m), for $i = 1, ..., M_c$, in Fig. 3.13 for different number of *closest* anchors utilized. The figure shows that as N is increased, the performance of both methods betters in general, as anticipated. Still, the figure shows that the obtained results are not always better for larger N. Such a behaviour can be explained to some extent by the fact that the experimental setup perhaps was not ideally balanced in the sense of anchors' locations, resulting in considerable difference between links' length. This might produce *bad* links (very distant from the source), which, when taken into consideration, can have negative impact on the estimation accuracy of an algorithm. Furthermore, one can see that both estimators perform well in the considered scenario, since the median error for $N = 7$ is pretty much the same for both estimators, just above 2 m. However, it can be seen that the performance of the SR-WLS2 is more stable, as it produces a ME ≤ 4 m in more than 80% of the cases. This is somewhat expected and can be explained to some extent by the fact that our SR-WLS2 method is executed iteratively, which raises its computational complexity. Nevertheless, Fig. 3.13 exhibits a superior performance of our SR-WLS2 method for low N, in general.

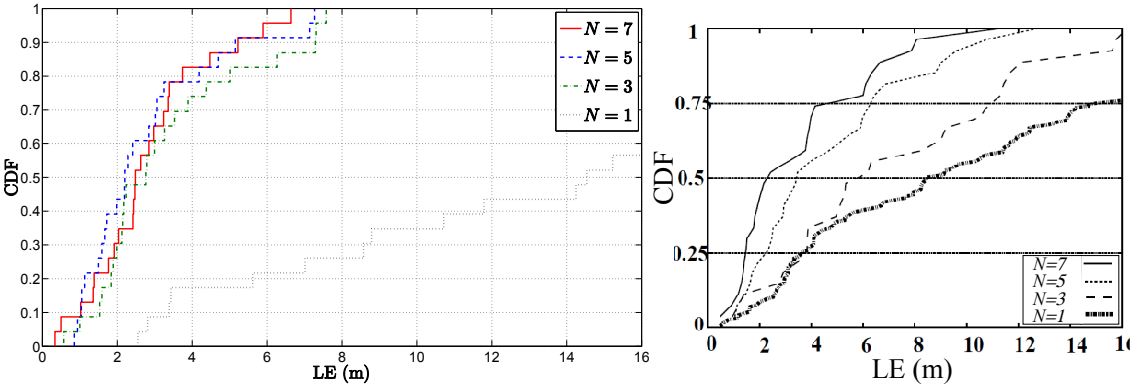

(a) SR-WLS2 (b) The approach in [81]

Figure 3.13: CDF of the LE (m).

In favor of testing the hypothesis that hybrid methods perform better than *traditional* ones, we present also the RMSE (m) versus N performance comparison of our SR-WLS2 estimator in the case where we used RSS only and combined RSS and AoA measurements

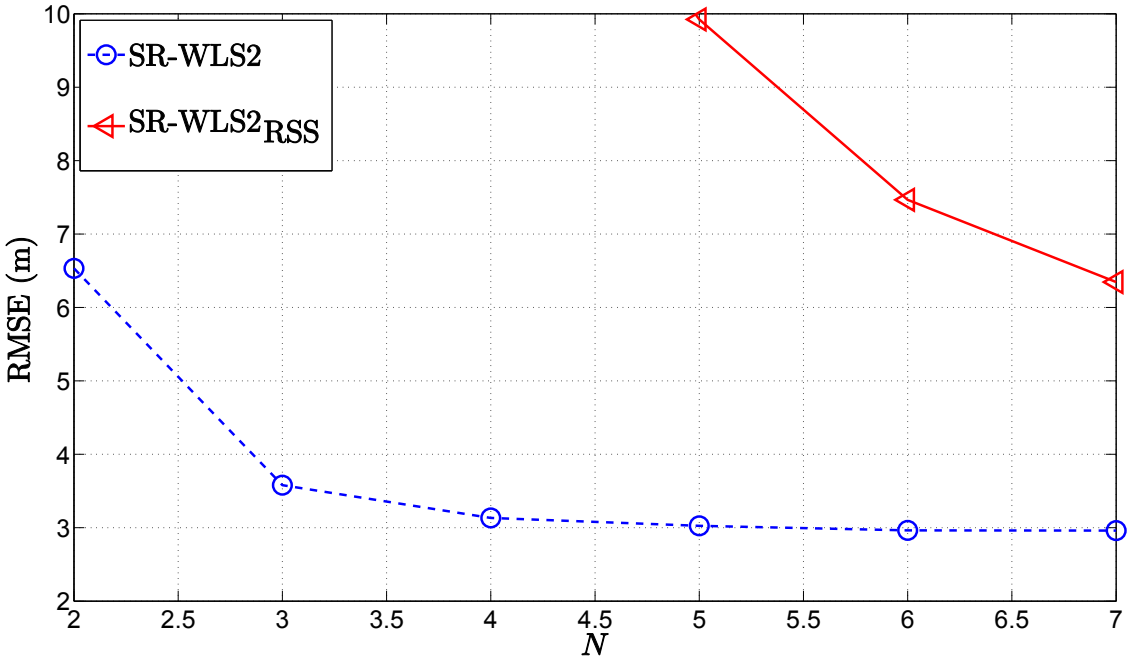

Figure 3.14: RMSE (m) versus N performance comparison in the considered experimental setup.

in Fig. 3.14. It can be seen that the performance of both approaches betters when N grows. Furthermore, the figure confirms the superiority of the hybrid approach, showing significant error reduction in the case where measurements are combined. However, the performance margin between the considered approaches reduces as N is increased, as expected. Nevertheless, the advantage of the hybrid approach over the *traditional* one is significant (more than 3 m) even for $N = 7$.

Finally, although the indoor localization scenario is very challenging, based on the results obtained in the considered indoor experiment, we can conclude that our method performs well in such a surrounding.

3.2.7 Conclusions

In this section, we addressed the hybrid RSS/AoA target localization problem in both non-cooperative and cooperative 3-D WSN, for both cases of known and unknown P_T. We first developed a novel non-convex objective function from the RSS and AoA measurement models. For the case of non-cooperative localization, we showed that the derived objective function can be transformed into a GTRS framework, by following the SR approach. Moreover, we showed that the derived non-convex objective function can be transformed into a convex one, by applying SDP relaxation technique in the case of cooperative localization. For the case where P_T is not known, we proposed a three-step procedure in order to enhance the estimation accuracy of our algorithms. The simulation results confirmed the effectiveness of the new algorithms in a variety of settings. For the case of non-cooperative

localization, the simulation results show that the proposed approaches significantly outperform the existing one, even for the case where the proposed estimators have no knowledge about P_T. For the case of cooperative localization, we have investigated the influence of N, M and R on the estimation accuracy. For all considered scenarios, the new estimators exhibited excellent performance, and robustness to not knowing P_T.

3.3 Distributed RSS-AoA-based Target Localization

3.3.1 Related Work

Localization of a sensor network with small number of anchors using graph theory and binary data has drawn much attention recently [86]-[87]. In [88] a study of traditional non-cooperative RSS- and AoA-based localization methods for visible light communication systems was presented. The approaches in [26]-[29] are based on the fusion of RSS and ToA measurements. The works [30–33] already described in Section 3.2.1 deal only with non-cooperative target localization problem, where a single target is located at a time. Also, most of these techniques are for 2-dimensional space only. Two estimators for 3-dimensional non-cooperative RSS/AoA localization problem based on convex optimization and squared-range approach were proposed in [34]. The work in [35] addressed an RSS/AoA non-cooperative localization problem in 2-D non-line of sight environments. The authors in [35] proposed an alternating optimization algorithm, composed of fixing the value of the scatter orientation and solving the SDP representation of the localization problem and later using the obtained location estimate to update the value of the scatter orientation, for localizing a mobile target in a WSN. An estimator based on SDP relaxation technique for cooperative target localization problem was proposed in [76]. The authors in [76] extended their previous SDP algorithm for pure range information into a hybrid one, by adding angle information for a triplets of points. However, due to the consideration of triplets of points, the computational complexity of the SDP approach increases rather substantially with the network size. In [36], a cooperative RSS/AoA localization problem was investigated. The authors in [36] proposed an SDP estimator to simultaneously localize multiple targets. However, the proposed algorithm is for centralized applications only, and its computational complexity depends highly on the network size. Convex optimization techniques were employed in [38] to solve the cooperative RSS/AoA target localization problem with unknown transmit powers in a distributed manner.

Contribution

Apart from [36] and [38], all mentioned approaches investigate non-cooperative localization problem only, where the location of a single target, which communicates with anchors exclusively, is determined at a time. Contrary to these approaches, in this thesis we investigate the target localization problem in a large-scale WSN, where the number of anchors is scarce and the communication range of all sensors is restricted (*e.g.*, to prolong

sensor's battery life). In such settings, only some targets can directly communicate with anchors; therefore, cooperation between any two sensors within the communication range is required in order to acquire sufficient amount of information to perform localization. We design novel distributed hybrid localization algorithms based on SOCP relaxation and GTRS framework that take advantage of combined RSS/AoA measurements with known transmit power to estimate the locations of all targets in a WSN. The proposed algorithms are distributed in the sense that no central sensor coordinates the network, all communications occur exclusively between two incident sensors and the data associated with each sensor are processed locally. First, the non-convex and computationally complex ML estimation problem is broken down into smaller sub-problems, *i.e.*, the local ML estimation problem for each target is posed. By using the RSS propagation model and simple geometry, we derive a novel local non-convex estimator based on the LS criterion, which tightly approximates the local ML one for small noise levels. Then, we show that the derived non-convex estimator can be transformed into a convex SOCP estimator that can be solved efficiently by interior-point algorithms [57]. Furthermore, following the SR approach, we propose a suboptimal SR-WLS estimator based on the GTRS framework, which can be solved exactly by a bisection procedure [83]. We then generalize the proposed SOCP estimator for known transmit powers to the case where the target transmit powers are different and not known.

3.3.2 Problem Formulation

Consider a large-scale WSN with M targets and N anchors, randomly deployed over a region of interest. The considered network can be seen as a connected graph, $\mathcal{G}(\mathcal{V},\mathcal{E})$, with $|\mathcal{V}| = M+N$ vertices and $|\mathcal{E}|$ edges, where $|\bullet|$ represents the cardinality (the number of elements in a set) of a set. The set of targets and the set of anchors are respectively labeled as $\mathcal{T}$ ($|\mathcal{T}| = M$) and $\mathcal{A}$ ($|\mathcal{A}| = N$), and their locations are denoted by $\boldsymbol{x}_1, \boldsymbol{x}_2, ..., \boldsymbol{x}_M$ and $\boldsymbol{a}_1, \boldsymbol{a}_2, ..., \boldsymbol{a}_N$ ($\boldsymbol{x}_i, \boldsymbol{a}_j \in \mathbb{R}^3$, $\forall i \in \mathcal{T}$ and $\forall j \in \mathcal{A}$), respectively. To save power (battery duration conditions the lifetime of a network), it is assumed that all sensors have limited communication range, R. Thus, two sensors, i and j, can exchange information if and only if they are within the communication range of each other. The sets of all target/anchor and target/target connections (edges) are defined as $\mathcal{E}_{\mathcal{A}} = \{(i,j) : \|\boldsymbol{x}_i - \boldsymbol{a}_j\| \leq R, \forall i \in \mathcal{T}, \forall j \in \mathcal{A}\}$ and $\mathcal{E}_{\mathcal{T}} = \{(i,k) : \|\boldsymbol{x}_i - \boldsymbol{x}_k\| \leq R, \forall i,k \in \mathcal{T}, i \neq k\}$, respectively.

For ease of expression, let us define a matrix $\boldsymbol{X} = [\boldsymbol{x}_1, \boldsymbol{x}_2, ..., \boldsymbol{x}_M]$ ($\boldsymbol{X} \in \mathbb{R}^{3\times M}$) as the matrix of all unknown target locations. We determine these locations by using a hybrid system that fuses range and angle measurements.

Throughout this work, it is assumed that the range measurements are obtained from the RSS information exclusively, since ranging based on RSS requires the lowest implementation costs [1]. The RSS between two sensors i and j which are within the communication

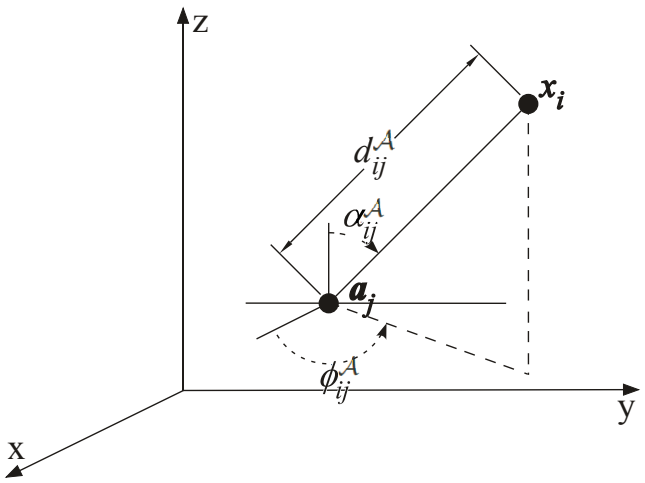

Figure 3.15: Illustration of a target and anchor locations in a 3-D space.

range of each other (from the transmitting sensor), P_{ij} (dBm), is modeled as:

$$P_{ij}^{\mathcal{A}} = P_{0i} - 10\gamma \log_{10} \frac{\|\boldsymbol{x}_i - \boldsymbol{a}_j\|}{d_0} + n_{ij}, \forall (i,j) \in \mathcal{E}_{\mathcal{A}}, \tag{3.25a}$$

$$P_{ik}^{\mathcal{T}} = P_{0i} - 10\gamma \log_{10} \frac{\|\boldsymbol{x}_i - \boldsymbol{x}_k\|}{d_0} + n_{ik}, \forall (i,k) \in \mathcal{E}_{\mathcal{T}}, \tag{3.25b}$$

(see [58, 59]), where n_{ij} and n_{ik} are the log-normal shadowing terms modeled as $n_{ij} \sim \mathcal{N}(0, \sigma_{n_{ij}}^2)$, $n_{ik} \sim \mathcal{N}(0, \sigma_{n_{ik}}^2)$. We assume that the target/target RSS measurements are symmetric[3], *i.e.*, $P_{ik}^{\mathcal{T}} = P_{ki}^{\mathcal{T}}, \forall (i,k) \in \mathcal{E}_{\mathcal{T}}, i \neq k$.

To obtain the AoA measurements (both azimuth and elevation angles), we assume that either antenna arrays or a directional antenna is implemented at anchors [30, 80, 81, 89, 90], or that the anchors are equipped with video cameras [77–79]. In order to make use of the AoA measurements from different anchors, the orientation information is required, which can be obtained by implementing a digital compass at each anchor [30, 80]. However, a digital compass introduces an error in the AoA measurements due to its static accuracy. For the sake of simplicity and without loss of generality, we model the angle measurement error and the orientation error as one random variable in the rest of this work.

Fig. 3.15 gives an illustration of a target and an anchor locations in a 3-D space. As shown in Fig. 3.15, $\boldsymbol{x}_i = [x_{i\mathrm{x}}, x_{i\mathrm{y}}, x_{i\mathrm{z}}]^T$ and $\boldsymbol{a}_j = [a_{j\mathrm{x}}, a_{j\mathrm{y}}, a_{j\mathrm{z}}]^T$ are respectively the unknown coordinates of the i-th target and the known coordinates of the j-th anchor, while $d_{ij}^{\mathcal{A}}$, $\phi_{ij}^{\mathcal{A}}$ and $\alpha_{ij}^{\mathcal{A}}$ represent the distance, azimuth angle and elevation angle between the i-th target and the j-th anchor, respectively. The ML estimate of the distance between two sensors can be obtained from the RSS measurement model (3.25) as follows [1]:

$$\widehat{d}_{ij} = \begin{cases} d_0 10^{\frac{P_{0i} - P_{ij}^{\mathcal{A}}}{10\gamma}}, & \text{if } j \in \mathcal{A}, \\ d_0 10^{\frac{P_{0i} - P_{ij}^{\mathcal{T}}}{10\gamma}}, & \text{if } j \in \mathcal{T}. \end{cases} \tag{3.26}$$

[3]This assumption is made without loss of generality; it is readily seen that, if $P_{ik}^{\mathcal{T}} \neq P_{ki}^{\mathcal{T}}$, then it is enough to replace $P_{ik}^{\mathcal{T}} \leftarrow (P_{ik}^{\mathcal{T}} + P_{ki}^{\mathcal{T}})/2$ and $P_{ki}^{\mathcal{T}} \leftarrow (P_{ik}^{\mathcal{T}} + P_{ki}^{\mathcal{T}})/2$ when solving the localization problem.

Applying simple geometry, azimuth and elevation angle measurements[4] can be modeled respectively as [30]:

$$\phi_{ij}^{\mathcal{A}} = \arctan\left(\frac{x_{i\mathrm{y}} - a_{j\mathrm{y}}}{x_{i\mathrm{x}} - a_{j\mathrm{x}}}\right) + m_{ij}, \text{ for } (i,j) \in \mathcal{E}_{\mathcal{A}}, \tag{3.27}$$

and

$$\alpha_{ij}^{\mathcal{A}} = \arccos\left(\frac{x_{i\mathrm{z}} - a_{j\mathrm{z}}}{\|\boldsymbol{x}_i - \boldsymbol{a}_j\|}\right) + v_{ij}, \text{ for } (i,j) \in \mathcal{E}_{\mathcal{A}}, \tag{3.28}$$

where m_{ij} and v_{ij} are the measurement errors of azimuth and elevation angles, respectively, modeled as $m_{ij} \sim \mathcal{N}(0, \sigma_{m_{ij}}^2)$ and $v_{ij} \sim \mathcal{N}(0, \sigma_{v_{ij}}^2)$.

Given the observation vector $\boldsymbol{\theta} = [\boldsymbol{P}^T, \boldsymbol{\phi}^T, \boldsymbol{\alpha}^T]^T$ ($\boldsymbol{\theta} \in \mathbb{R}^{3|\mathcal{E}_{\mathcal{A}}|+|\mathcal{E}_{\mathcal{T}}|}$), where $\boldsymbol{P} = [P_{ij}^{\mathcal{A}}, P_{ik}^{\mathcal{T}}]^T$, $\boldsymbol{\phi} = [\phi_{ij}^{\mathcal{A}}]^T$, $\boldsymbol{\alpha} = [\alpha_{ij}^{\mathcal{A}}]^T$, the PDF is given as:

$$p(\boldsymbol{\theta}|\boldsymbol{X}) = \prod_{i=1}^{3|\mathcal{E}_{\mathcal{A}}|+|\mathcal{E}_{\mathcal{T}}|} \frac{1}{\sqrt{2\pi\sigma_i^2}} \exp\left\{-\frac{(\theta_i - f_i(\boldsymbol{X}))^2}{2\sigma_i^2}\right\}, \tag{3.29}$$

where

$$\boldsymbol{f}(\boldsymbol{X}) = \begin{bmatrix} \vdots \\ P_{0i} - 10\gamma \log_{10} \frac{\|\boldsymbol{x}_i - \boldsymbol{a}_j\|}{d_0} \\ \vdots \\ P_{0i} - 10\gamma \log_{10} \frac{\|\boldsymbol{x}_i - \boldsymbol{x}_k\|}{d_0} \\ \vdots \\ \arctan\left(\frac{x_{i\mathrm{y}} - a_{j\mathrm{y}}}{x_{i\mathrm{x}} - a_{j\mathrm{x}}}\right) \\ \vdots \\ \arccos\left(\frac{x_{i\mathrm{z}} - a_{j\mathrm{z}}}{\|\boldsymbol{x}_i - \boldsymbol{a}_j\|}\right) \\ \vdots \end{bmatrix}, \boldsymbol{\sigma} = \begin{bmatrix} \vdots \\ \sigma_{n_{ij}} \\ \vdots \\ \sigma_{n_{ik}} \\ \vdots \\ \sigma_{m_{ij}} \\ \vdots \\ \sigma_{v_{ij}} \\ \vdots \end{bmatrix}.$$

Maximizing the log of the likelihood function (3.29) with respect to $\boldsymbol{X}$ gives us the ML estimate, $\hat{\boldsymbol{X}}$, of the unknown locations [47], as:

$$\hat{\boldsymbol{X}} = \arg\min_{\boldsymbol{X}} \sum_{i=1}^{3|\mathcal{E}_{\mathcal{A}}|+|\mathcal{E}_{\mathcal{T}}|} \frac{1}{\sigma_i^2} [\theta_i - f_i(\boldsymbol{X})]^2. \tag{3.30}$$

Asymptotically (for large data records) the ML estimator in (3.30) is the minimum variance unbiased estimator [47]. However, finding the ML estimate directly from (3.30) is not possible, since (3.30) is non-convex and has no closed-form solution. Nevertheless, in the remainder of this work we will show that the LS problem in (3.30) can be solved in a distributed manner by applying certain approximations. More precisely, we propose a convex relaxation technique leading to a distributed SOCP estimator that can be solved

[4]Note that we consider here the case where only anchors have the necessary equipment to perform the respective angle measurements. An alternative approach would be to provide the necessary equipment to all sensors. However, our simulations showed that there is no gain for such a setting, and it would severely raise the overall network implementation costs.

efficiently by interior-point algorithms [57], and a suboptimal estimator based on the GTRS framework leading to a distributed SR-WLS estimator, which can be solved *exactly* by a bisection procedure [83]. We also show that the proposed SOCP estimator can be generalized to solve the localization problem in (3.30) where, besides the target locations, their transmit powers are different and unknown.

Assumptions

We outline here some assumptions for the WSN (made for the sake of simplicity and without loss of generality):

(1) The network is connected and it does not change during the computation period;

(2) Measurement errors for RSS and AoA models are independent, and $\sigma_{n_{ij}} = \sigma_n$, $\sigma_{m_{ij}} = \sigma_m$ and $\sigma_{v_{ij}} = \sigma_v$, $\forall (i,j) \in \mathcal{E}_{\mathcal{A}} \cup \mathcal{E}_{\mathcal{T}}$;

(3) The necessary equipment for collecting the AoA measurements is installed at anchors exclusively;

(4) A coloring scheme of the network is available.

In assumption (1), we assume that the sensors are static and that there is no sensor/link failure during the computation period, and that there exists a path between any two sensors $i, j \in \mathcal{V}$. Assumption (2) is made for the sake of simplicity. Assumption (3) indicates that only anchors are suitably equipped to acquire the AoA measurements (*e.g.* with directional antenna or antenna array [30, 80, 89], or video cameras [77, 78]), due to network costs. Finally, assumption (4) implies that a coloring scheme is available in order to color (number) the sensors and establish a working hierarchy in the network. More precisely, we assume that a second-order coloring scheme is employed, meaning that no sensor has the same color (number) as any of its one-hop neighbors nor its two-hop neighbors [23, 69, 70]. In this way, we avoid message collision and reduce the execution time of the algorithm, since sensors with the same color can work in parallel.

3.3.3 Distributed Localization

Notice that the problem in (3.30) is dependent on the locations and pairwise measurements between the adjacent sensors only. Thus, having the initial location estimations of the targets, $\hat{\boldsymbol{X}}^{(0)}$, at hand, the problem in (3.30) can be divided, *i.e.*, the minimization can be performed independently by each target using only the information gathered from its neighbors. Hence, rather than solving (3.30), which can be computationally exhausting (in large-scale WSNs), we break down (3.30) into sub-problems, which we solve locally (by each target) using iterative approach. Consequently, target i updates its location estimate

in each iteration, t, by solving the following local ML problem:

$$\hat{\boldsymbol{x}}_i^{(t+1)} = \arg\min_{\boldsymbol{x}_i} \sum_{j=1}^{3|\mathcal{E}_{\mathcal{A}_i}|+|\mathcal{E}_{\mathcal{T}_i}|} \frac{1}{\sigma_j^2} \left[\theta_j - f_j(\boldsymbol{x}_i)\right]^2, \forall i \in \mathcal{T}, \tag{3.31}$$

where $\mathcal{E}_{\mathcal{A}_i} = \{j : (i,j) \in \mathcal{E}_{\mathcal{A}}\}$ and $\mathcal{E}_{\mathcal{T}_i} = \{k : (i,k) \in \mathcal{E}_{\mathcal{T}}, i \neq k\}$ represent the set of all anchor and all target neighbors of the target i respectively, and the first $|\mathcal{E}_{\mathcal{A}_i}| + |\mathcal{E}_{\mathcal{T}_i}|$ elements of $f_j(\boldsymbol{x}_i)$ are given as:

$$f_j(\boldsymbol{x}_i) = P_{0i} - 10\gamma \log_{10} \frac{\|\boldsymbol{x}_i - \hat{\boldsymbol{a}}_j\|}{d_0}, \text{ for } j = 1, ..., |\mathcal{E}_{\mathcal{A}_i}| + |\mathcal{E}_{\mathcal{T}_i}|,$$

with

$$\hat{\boldsymbol{a}}_j = \begin{cases} \boldsymbol{a}_j, & \text{if } j \in \mathcal{A}, \\ \hat{\boldsymbol{x}}_j^{(t)}, & \text{if } j \in \mathcal{T}. \end{cases}$$

Transmit Powers Are Known

Distributed SOCP Algorithm. Assuming that $\hat{\boldsymbol{X}}^{(0)}$ is given, when the noise power is sufficiently small, from (3.25) we can write:

$$\lambda_{ij} \|\boldsymbol{x}_i - \hat{\boldsymbol{a}}_j\| \approx d_0, \forall i \in \mathcal{T}, \forall j \in \mathcal{E}_{\mathcal{A}_i} \cup \mathcal{E}_{\mathcal{T}_i}, \tag{3.32}$$

where

$$\lambda_{ij} = \begin{cases} 10^{\frac{P_{ij}^{\mathcal{A}} - P_{0i}}{10\gamma}}, & \text{if } j \in \mathcal{A}, \\ 10^{\frac{P_{ij}^{\mathcal{T}} - P_{0i}}{10\gamma}}, & \text{if } j \in \mathcal{T}. \end{cases}$$

Similarly, from (3.27) and (3.28) we respectively get:

$$\boldsymbol{c}_{ij}^T (\boldsymbol{x}_i - \boldsymbol{a}_j) \approx 0, \forall i \in \mathcal{T}, \forall j \in \mathcal{E}_{\mathcal{A}_i} \tag{3.33}$$

and

$$\boldsymbol{k}_{ij}^T (\boldsymbol{x}_i - \boldsymbol{a}_j) \approx \|\boldsymbol{x}_i - \boldsymbol{a}_j\| \cos(\alpha_{ij}^{\mathcal{A}}), \forall i \in \mathcal{T}, \forall j \in \mathcal{E}_{\mathcal{A}_i} \tag{3.34}$$

where $\boldsymbol{c}_{ij} = [-\sin(\phi_{ij}^{\mathcal{A}}), \cos(\phi_{ij}^{\mathcal{A}}), 0]^T$ and $\boldsymbol{k}_{ij} = [0,0,1]^T$. According to the LS criterion and (3.32), (3.33) and (3.34) each target updates its location by solving the following problem:

$$\begin{aligned} \hat{\boldsymbol{x}}_i^{(t+1)} = \arg\min_{\boldsymbol{x}_i} & \sum_{j \in \mathcal{E}_{\mathcal{A}_i} \cup \mathcal{E}_{\mathcal{T}_i}} (\lambda_{ij} \|\boldsymbol{x}_i - \hat{\boldsymbol{a}}_j\| - d_0)^2 \\ + \sum_{j \in \mathcal{E}_{\mathcal{A}_i}} & \left(\boldsymbol{c}_{ij}^T (\boldsymbol{x}_i - \boldsymbol{a}_j)\right)^2 + \sum_{j \in \mathcal{E}_{\mathcal{A}_i}} \left(\boldsymbol{k}_{ij}^T (\boldsymbol{x}_i - \boldsymbol{a}_j) - \|\boldsymbol{x}_i - \boldsymbol{a}_j\| \cos(\alpha_{ij}^{\mathcal{A}})\right)^2. \end{aligned} \tag{3.35}$$

The LS problem in (3.35) is non-convex and has no closed-form solution. To convert (3.35) into a convex problem, we introduce auxiliary variables $r_{ij} = \|\boldsymbol{x}_i - \hat{\boldsymbol{a}}_j\|, \forall (i,j) \in \mathcal{E}_{\mathcal{A}} \cup \mathcal{E}_{\mathcal{T}}$, $\boldsymbol{z} = [z_{ij}]$, $\boldsymbol{g} = [g_{ij}]$, $\boldsymbol{p} = [p_{ij}]$, where $z_{ij} = \lambda_{ij}^{\mathcal{A}} r_{ij} - d_0, \forall (i,j) \in \mathcal{E}_{\mathcal{A}} \cup \mathcal{E}_{\mathcal{T}}$, $g_{ij} = \boldsymbol{c}_{ij}^T (\boldsymbol{x}_i - \boldsymbol{a}_j)$, and $p_{ij} = \boldsymbol{k}_{ij}^T (\boldsymbol{x}_i - \boldsymbol{a}_j) - r_{ij} \cos(\alpha_{ij}^{\mathcal{A}}), \forall (i,j) \in \mathcal{E}_{\mathcal{A}}$. We get:

$$\underset{\boldsymbol{x}_i, \boldsymbol{r}, \boldsymbol{z}, \boldsymbol{g}, \boldsymbol{p}}{\text{minimize}} \ \|\boldsymbol{z}\|^2 + \|\boldsymbol{g}\|^2 + \|\boldsymbol{p}\|^2$$

subject to

$$\begin{aligned} r_{ij} &= \|\boldsymbol{x}_i - \hat{\boldsymbol{a}}_j\|,\ \forall (i,j) \in \mathcal{E}_{\mathcal{A}} \cup \mathcal{E}_{\mathcal{T}}, \\ z_{ij} &= \lambda_{ij} r_{ij} - d_0,\ \forall (i,j) \in \mathcal{E}_{\mathcal{A}} \cup \mathcal{E}_{\mathcal{T}}, \\ g_{ij} &= \boldsymbol{c}_{ij}^T (\boldsymbol{x}_i - \boldsymbol{a}_j),\ \forall (i,j) \in \mathcal{E}_{\mathcal{A}}, \\ p_{ij} &= \boldsymbol{k}_{ij}^T (\boldsymbol{x}_i - \boldsymbol{a}_j) - r_{ij} \cos(\alpha_{ij}^{\mathcal{A}}),\ \forall (i,j) \in \mathcal{E}_{\mathcal{A}}. \end{aligned} \tag{3.36}$$

Introduce epigraph variables e_1, e_2 and e_3, and apply second-order cone constraint relaxation of the form $\|\boldsymbol{z}\|^2 \leq e_1$, to obtain:

$$\underset{\boldsymbol{x}_i, \boldsymbol{r}, \boldsymbol{z}, \boldsymbol{g}, \boldsymbol{p}, e_1, e_2, e_3}{\text{minimize}} \ e_1 + e_2 + e_3$$

subject to

$$\begin{aligned} \|\boldsymbol{x}_i - \hat{\boldsymbol{a}}_j\| &\leq r_{ij},\ \forall (i,j) \in \mathcal{E}_{\mathcal{A}} \cup \mathcal{E}_{\mathcal{T}}, \\ z_{ij} &= \lambda_{ij} r_{ij} - d_0,\ \forall (i,j) \in \mathcal{E}_{\mathcal{A}} \cup \mathcal{E}_{\mathcal{T}}, \\ g_{ij} &= \boldsymbol{c}_{ij}^T (\boldsymbol{x}_i - \boldsymbol{a}_j),\ \forall (i,j) \in \mathcal{E}_{\mathcal{A}}, \\ p_{ij} &= \boldsymbol{k}_{ij}^T (\boldsymbol{x}_i - \boldsymbol{a}_j) - r_{ij} \cos(\alpha_{ij}^{\mathcal{A}}),\ \forall (i,j) \in \mathcal{E}_{\mathcal{A}}, \\ \left\| \begin{bmatrix} 2\boldsymbol{z} \\ e_1 - 1 \end{bmatrix} \right\| &\leq e_1 + 1, \left\| \begin{bmatrix} 2\boldsymbol{g} \\ e_2 - 1 \end{bmatrix} \right\| \leq e_2 + 1, \left\| \begin{bmatrix} 2\boldsymbol{p} \\ e_3 - 1 \end{bmatrix} \right\| \leq e_3 + 1. \end{aligned} \tag{3.37}$$

The problem in (3.37) is an SOCP problem, which can be efficiently solved by the `CVX` package [62] for specifying and solving convex programs. In the further text, we will refer to (3.37) as "SOCP".

Distributed SR-WLS Algorithm. We can rewrite (3.32) as:

$$\lambda_{ij}^2 \|\boldsymbol{x}_i - \hat{\boldsymbol{a}}_j\|^2 \approx d_0^2,\ \forall (i,j) \in \mathcal{E}_{\mathcal{A}} \cup \mathcal{E}_{\mathcal{T}}. \tag{3.38}$$

In order to give more importance to the nearby links, introduce weights, $\boldsymbol{w} = [\sqrt{w_{ij}}]$, where

$$w_{ij} = 1 - \frac{\widehat{d}_{ij}}{\sum_{(i,j) \in \mathcal{E}_{\mathcal{A}} \cup \mathcal{E}_{\mathcal{T}}} \widehat{d}_{ij}}.$$

In (3.34), substitute $\|\boldsymbol{x}_i - \hat{\boldsymbol{a}}_j\|$ with $\widehat{d}_{ij}$ described in (3.26). According to the WLS criterion and (3.38), (3.33) and (3.34) each target updates its location by solving the following problem:

$$\begin{aligned} \hat{\boldsymbol{x}}_i^{(t+1)} = \arg\min_{\boldsymbol{x}_i} & \sum_{j \in \mathcal{E}_{\mathcal{A}_i} \cup \mathcal{E}_{\mathcal{T}_i}} w_{ij} \left(\lambda_{ij}^2 \|\boldsymbol{x}_i - \hat{\boldsymbol{a}}_j\|^2 - d_0^2 \right)^2 \\ + \sum_{j \in \mathcal{E}_{\mathcal{A}_i}} w_{ij} \left(\boldsymbol{c}_{ij}^T (\boldsymbol{x}_i - \boldsymbol{a}_j) \right)^2 & + \sum_{j \in \mathcal{E}_{\mathcal{A}_i}} w_{ij} \left(\boldsymbol{k}_{ij}^T (\boldsymbol{x}_i - \boldsymbol{a}_j) - \widehat{d}_{ij} \cos(\alpha_{ij}^{\mathcal{A}}) \right)^2. \end{aligned} \tag{3.39}$$

The above WLS estimator is non-convex and has no closed-form solution. However, we can express (3.39) as a quadratic programming problem whose *global* solution can be computed efficiently [83]. Using the substitution $\boldsymbol{y}_i = [\boldsymbol{x}_i^T, \|\boldsymbol{x}_i\|^2]^T, \forall i \in \mathcal{T}$, (3.39) can be rewritten as:

$$\hat{\boldsymbol{y}}_i^{(t+1)} = \arg\min_{\boldsymbol{y}_i} \|\boldsymbol{W}(\boldsymbol{A}\boldsymbol{y}_i - \boldsymbol{b})\|^2$$

subject to

$$\boldsymbol{y}_i^T \boldsymbol{D} \boldsymbol{y}_i + 2\boldsymbol{l}^T \boldsymbol{y}_i = 0, \tag{3.40}$$

where $\boldsymbol{W} = \text{diag}\left(\left[w_{ij\in\mathcal{E}_{\mathcal{A}_i}\cup\mathcal{E}_{\mathcal{T}_i}}, w_{ij\in\mathcal{E}_{\mathcal{A}_i}}, w_{ij\in\mathcal{E}_{\mathcal{A}_i}}\right]\right)$, *i.e.*, $\boldsymbol{W} \in \mathbb{R}^{3|\mathcal{E}_{\mathcal{A}_i}|+|\mathcal{E}_{\mathcal{T}_i}|\times 3|\mathcal{E}_{\mathcal{A}_i}|+|\mathcal{E}_{\mathcal{T}_i}|}$,

$$\boldsymbol{A} = \begin{bmatrix} \vdots & \vdots \\ -2\lambda_{ij}^2 \hat{\boldsymbol{a}}_j^T & \lambda_{ij}^2 \\ \vdots & \vdots \\ \boldsymbol{c}_{ij}^T & 0 \\ \vdots & \vdots \\ \boldsymbol{k}_{ij}^T & 0 \\ \vdots & \vdots \end{bmatrix}, \boldsymbol{b} = \begin{bmatrix} \vdots \\ d_0^2 - \lambda_{ij}^2 \|\hat{\boldsymbol{a}}_j\|^2 \\ \vdots \\ \boldsymbol{c}_{ij}^T \boldsymbol{a}_j \\ \vdots \\ \boldsymbol{k}_{ij}^T \boldsymbol{a}_j + \widehat{d}_{ij}^{\mathcal{A}} \cos(\alpha_{ij}^{\mathcal{A}}) \\ \vdots \end{bmatrix},$$

$$\boldsymbol{D} = \begin{bmatrix} \boldsymbol{I}_3 & \boldsymbol{0}_{3\times 1} \\ \boldsymbol{0}_{1\times 3} & 0 \end{bmatrix}, \boldsymbol{l} = \begin{bmatrix} \boldsymbol{0}_{3\times 1} \\ -1/2 \end{bmatrix},$$

i.e., $\boldsymbol{A} \in \mathbb{R}^{3|\mathcal{E}_{\mathcal{A}_i}|+|\mathcal{E}_{\mathcal{T}_i}|\times 4}$ and $\boldsymbol{b} \in \mathbb{R}^{3|\mathcal{E}_{\mathcal{A}_i}|+|\mathcal{E}_{\mathcal{T}_i}|\times 1}$.

The objective function and the constraint in (3.40) are both quadratic. This type of problem is known as GTRS [83, 84], and it can be solved *exactly* by a bisection procedure [83]. We denote (3.40) as "SR-WLS" in the remaining text.

In summary, the derivation of the above approaches can be described in two parts. In the first part, the local non-convex ML estimator in (3.31) is approximated by a different non-convex estimator, (3.35) and (3.39) respectively. The use of the objective functions in (3.35) and (3.39) is motivated by the fact that we get a much smoother surface in comparison to (3.31), at a cost of introducing some bias with respect to the ML solution (see Fig. 3.16). If the bias effect is small, we might reach the ML solution by employing a local search around the solution of (3.35) and (3.39). In the second part of our approach, we convert (3.35) and (3.39) into a convex problem and GTRS framework, by following the above procedures.

Fig. 3.16 illustrates a realization of the objective function in (3.31), for the case where the true sensors' locations were used and a realization of (3.35) and (3.39) after only one iteration, and (3.39) after three iterations, where the estimated targets' locations were used. The i-th target was located at $[2.0; 3.3]$, and it could directly communicate with its three anchor and three target neighbors. The noise STD of RSS measurements was set to $\sigma_{n_{ij}} = 2$ dB and the noise STD of angle measurements was set to $\sigma_{m_{ij}} = 3$ deg, and the rest of the parameters follow the set-up described in Section 3.3.5. On the one hand, in Fig. 3.16a, where the true sensors' locations were used, one can see that the objective function is highly non-convex and its global minimum is located at $[2.4; 3.5]$. Due to non-convexity of the problem, recursive algorithms, such as gradient search method, might get trapped into a local minimum, causing large error in the location estimation process. On the other hand, in Figs. 3.16b, 3.16c and 3.16d, where estimated targets' locations (obtained by solving the proposed "SOCP" and "SR-WLS" algorithm, respectively) were used, it can

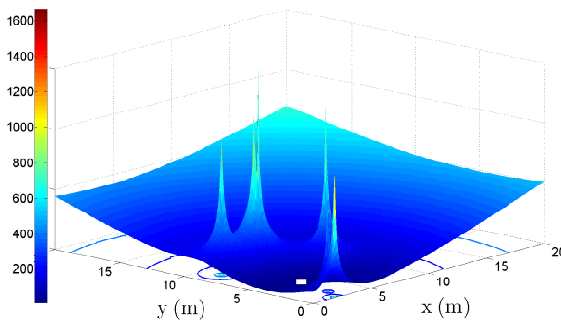

(a) Objective function in (3.31) using true sensors' locations

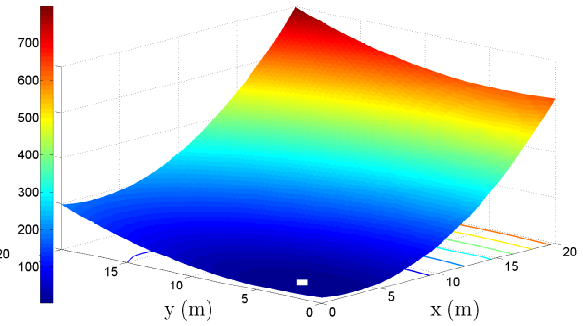

(b) Objective function in (3.35) after one iteration

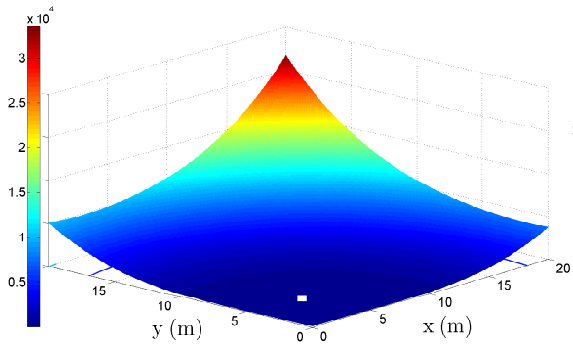

(c) Objective function in (3.39) after one iteration

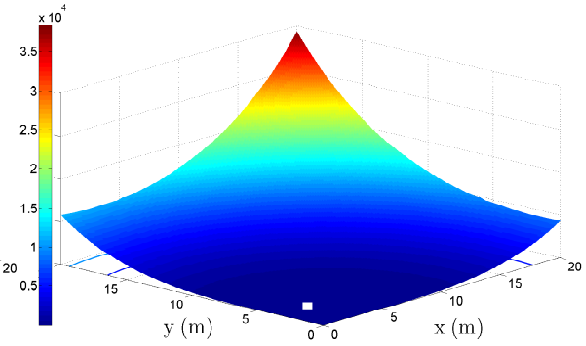

(d) Objective function in (3.39) after three iterations

Figure 3.16: Illustration of the objective functions in (3.31), (3.35) and (3.39) versus x (m) and y (m) coordinates (target location); the minimum of the objective function is indicated by a white square.

be seen that these objective functions are much smoother than the one in (3.31), and that the global minimum after only one iteration is located at $[2.5; 4.1]$ and $[4.3; 4.9]$ for (3.35) and (3.39), respectively and at $[2.4; 3.6]$ for (3.39) after three iterations. Because of the smoothness of the objective functions, the global minimum of the considered problems can be obtained uniquely and effortlessly for all targets via interior-point algorithms [57] and bisection procedure [83], by following the proposed procedures. However, the *quality* of the obtained solution will depend on the tightness of the performed relaxation. As we show in Section 3.3.5, the estimation accuracy betters as the number of iterations grows in general. Thus, we can conclude that the objective functions in (3.35) and (3.39) represent an excellent approximation of the original problem defined in (3.31).

Assuming that $\mathcal{C}$ represents the set of colors of the sensors, Algorithm 3 summarizes the proposed distributed SOCP and SR-WLS algorithms. Algorithm 3 is distributed in the sense that there is no central processor in the network, its coordination is carried out according to the applied coloring scheme, information exchange occurs between two incident sensors exclusively, and data processing is performed locally by each target. Lines $5-7$ are executed simultaneously by all targets $i \in \mathcal{C}_c$, which may decrease the execution time of the algorithm. At Line 6, we solve (3.37) if SOCP algorithm is employed, and (3.40) if

SR-WLS algorithm is employed. The only information exchange occurs at Line 7, when targets broadcast their location updates $\hat{\boldsymbol{x}}_i^{(t+1)}$ to their neighbors. Since $\hat{\boldsymbol{x}}_i^{(t+1)} \in \mathbb{R}^3$, we can conclude that the proposed algorithm requires at most a broadcast of $3 \times T_{\max} \times M$ real values. Depending on which estimator is employed, in the remaining text, we label Algorithm 3 either as "SOCP" or as "SR-WLS".

Algorithm 3 The proposed distributed SOCP/SR-WLS algorithm

Require: $\hat{\boldsymbol{X}}^{(0)}$, $T_{\max}$, $\mathcal{C}$, $\boldsymbol{a}_j$, $\forall j \in \mathcal{A}$
1: **Initialize:** $t \leftarrow 0$
2: **repeat**
3: **for** $c = 1, ..., \mathcal{C}$ **do**
4: **for all** $i \in \mathcal{C}_c$ (in parallel) **do**
5: Collect $\hat{\boldsymbol{a}}_j, \forall j \in \mathcal{E}_{\mathcal{A}_i} \cup \mathcal{E}_{\mathcal{T}_i}$
6: $\hat{\boldsymbol{x}}_i^{(t+1)} \leftarrow \begin{cases} \text{solve (3.37),if using SOCP algorithm,} \\ \text{solve (3.40),if using SR-WLS algorithm} \end{cases}$
7: Broadcast $\hat{\boldsymbol{x}}_i^{(t+1)}$ to $\hat{\boldsymbol{a}}_j, \forall j \in \mathcal{E}_{\mathcal{A}_i} \cup \mathcal{E}_{\mathcal{T}_i}$
8: **end for**
9: **end for**
10: $t \leftarrow t + 1$
11: **until** $t < T_{\max}$

Transmit Powers Are Not Known

Often in practice testing and calibration are not the priority in order to restrict the implementation costs. Moreover, due to battery exhaust over time, sensors' transmit powers, P_i's, might change over time. Therefore, P_i's are often not calibrated, *i.e.*, not known. Not knowing P_i implies that P_{0i} is not known in the RSS model (3.25); see [16] and the references therein.

The generalization of the proposed SOCP estimator for known P_{0i} is straightforward for the case where P_{0i} is not known. More specifically, we can rewrite (3.32) as follows:

$$\zeta_{ij} \|\boldsymbol{x}_i - \hat{\boldsymbol{a}}_j\| \approx \eta_i d_0, \forall i \in \mathcal{T}, \forall j \in \mathcal{E}_{\mathcal{A}} \cup \mathcal{E}_{\mathcal{T}}, \tag{3.41}$$

where $\eta_i = 10^{\frac{P_{0i}}{10\gamma}}$ and

$$\zeta_{ij} = \begin{cases} 10^{\frac{P_{ij}^{\mathcal{A}}}{10\gamma}}, & \text{if } j \in \mathcal{A}, \\ 10^{\frac{P_{ij}^{\mathcal{T}}}{10\gamma}}, & \text{if } j \in \mathcal{T}. \end{cases}$$

Following the LS concept and (3.41), (3.33) and (3.34), each target updates its location by solving the following problem:

$$\begin{aligned} \left(\hat{\boldsymbol{x}}_i^{(t+1)}, \eta_i\right) = \underset{\boldsymbol{x}_i, \eta_i}{\arg\min} \sum_{j \in \mathcal{E}_{\mathcal{A}_i} \cup \mathcal{E}_{\mathcal{T}_i}} (\zeta_{ij} \|\boldsymbol{x}_i - \hat{\boldsymbol{a}}_j\| - \eta_i d_0)^2 \\ + \sum_{j \in \mathcal{E}_{\mathcal{A}_i}} \left(\boldsymbol{c}_{ij}^T (\boldsymbol{x}_i - \boldsymbol{a}_j)\right)^2 + \sum_{j \in \mathcal{E}_{\mathcal{A}_i}} \left(\boldsymbol{k}_{ij}^T (\boldsymbol{x}_i - \boldsymbol{a}_j) - \|\boldsymbol{x}_i - \boldsymbol{a}_j\| \cos(\alpha_{ij}^{\mathcal{A}})\right)^2. \end{aligned} \tag{3.42}$$

By applying similar procedure as in the previous section, we obtain the following SOCP estimator:

$$\underset{\boldsymbol{x}_i,\eta_i,\boldsymbol{r},\boldsymbol{z},\boldsymbol{g},\boldsymbol{p},e_1,e_2,e_3}{\text{minimize}} \; e_1+e_2+e_3$$

subject to

$$\begin{gathered}
\|\boldsymbol{x}_i-\hat{\boldsymbol{a}}_j\|\leq r_{ij},\ \forall(i,j)\in\mathcal{E}_{\mathcal{A}}\cup\mathcal{E}_{\mathcal{T}},\\
z_{ij}=\zeta_{ij}r_{ij}-\eta_i d_0,\ \forall(i,j)\in\mathcal{E}_{\mathcal{A}}\cup\mathcal{E}_{\mathcal{T}},\\
g_{ij}=\boldsymbol{c}_{ij}^T(\boldsymbol{x}_i-\boldsymbol{a}_j),\ \forall(i,j)\in\mathcal{E}_{\mathcal{A}},\\
p_{ij}=\boldsymbol{k}_{ij}^T(\boldsymbol{x}_i-\boldsymbol{a}_j)-r_{ij}\cos(\alpha_{ij}^{\mathcal{A}}),\ \forall(i,j)\in\mathcal{E}_{\mathcal{A}},\\
\left\|\begin{bmatrix}2\boldsymbol{z}\\ e_1-1\end{bmatrix}\right\|\leq e_1+1,\left\|\begin{bmatrix}2\boldsymbol{g}\\ e_2-1\end{bmatrix}\right\|\leq e_2+1,\left\|\begin{bmatrix}2\boldsymbol{p}\\ e_3-1\end{bmatrix}\right\|\leq e_3+1.
\end{gathered}\tag{3.43}$$

The problem in (3.43) is a classical SOCP, where the objective function and equality constraints are affine, and the inequality constraints are second-order cone constraints [57].

Algorithm 4 outlines the proposed SOCP algorithm for unknown P_i's. Lines $5-10$ are performed concurrently by all targets $i\in\mathcal{C}_c$, which might reduce the running time of the algorithm. At Line 6, we solve (3.43) S number of times, after which we start calculating the ML estimate of P_{0i}, $\widehat{P}_{0i}$, and switch to solving (3.37) as if P_{0i} is known. Line 7 is introduced to avoid the oscillation in the location estimates. At Line 10, the location updates, $\hat{\boldsymbol{x}}_i^{(t+1)}\forall i\in\mathcal{T}$, are broadcasted to neighbors of i. In the remaining text, we label Algorithm 4 as "uSOCP".

3.3.4 Complexity Analysis

In order to evaluate the overall performance of a localization algorithm, it is necessary to analyze the trade off between the estimation accuracy and computational complexity. In this section, we investigate computational complexity of the considered algorithms. According to [63], the worst case computational complexity of an SOCP is:

$$\mathcal{O}\left(\sqrt{L}\left(m^2\sum_{i=1}^{L}n_i+\sum_{i=1}^{L}n_i^2+m^3\right)\right),\tag{3.44}$$

where L is the number of the second-order cone constraints, m is the number of the equality constraints, and n_i is the dimension of the i-th second-order cone.

Assuming that $N_{\max}$ is the maximum number of steps in the bisection procedure, Table 3.2 provides a summary of the worst case computational complexities of the considered algorithms. In Table 3.2, the labels "SDP" and "uSOCP2" are used to denote the centralized SDP algorithm in [36] and the distributed SOCP algorithm in [38], respectively, which will be used later on in Section 3.3.5 to offer a better understanding of the performance of the proposed algorithms.

Table 3.2 shows that the computational complexity of a distributed algorithm depends mainly on the size of neighborhood fragments, rather than the total number of sensors in a WSN. Theoretically, it is possible to have a fully connected network, *i.e.*, $|\mathcal{E}_{\mathcal{A}_i}|+|\mathcal{E}_{\mathcal{T}_i}|=M+N-1,\forall i\in\mathcal{T}$. However, in practice, the size of the neighborhood fragments are much

Algorithm 4 The proposed distributed uSOCP algorithm

Require: $\hat{\boldsymbol{x}}_i^{(0)}, \forall i \in \mathcal{T}$, $\boldsymbol{a}_j, \forall j \in \mathcal{A}$, $\mathcal{C}$, S, P_0^{Low}, P_0^{Up}, $T_{\max}$

Initialize: $t \leftarrow 0$
repeat
  for $c = 1, ..., \mathcal{C}$ **do**
    for all $i \in \mathcal{C}_c$ (in parallel) **do**
      Collect $\hat{\boldsymbol{a}}_j, \forall j \in \mathcal{E}_{\mathcal{A}_i} \cup \mathcal{E}_{\mathcal{T}_i}$
      $\hat{\boldsymbol{x}}_i^{(t+1)} \leftarrow \begin{cases} \text{solve (3.43)}, & \text{if} t < S, \\ \text{solve (3.37) using } \widehat{P}_{0i}, & \text{if} t \geq S \end{cases}$
      if $\frac{\|\hat{\boldsymbol{x}}_i^{(t+1)} - \hat{\boldsymbol{x}}_i^{(t)}\|}{\|\hat{\boldsymbol{x}}_i^{(t)}\|} > 1$ **then**
        $\hat{\boldsymbol{x}}_i^{(t+1)} \leftarrow \hat{\boldsymbol{x}}_i^{(t)}$
      end if
      Broadcast $\hat{\boldsymbol{x}}_i^{(t+1)}$ to $\hat{\boldsymbol{a}}_j, \forall j \in \mathcal{E}_{\mathcal{A}_i} \cup \mathcal{E}_{\mathcal{T}_i}$
    end for
  end for
  $t \leftarrow t + 1$
  if $t > S$ **then**
    for all $i \in \mathcal{T}$ (in parallel) **do**
      $\widehat{P}_{0i} \leftarrow \frac{\sum_{j \in \mathcal{E}_{\mathcal{A}_i} \cup \mathcal{E}_{\mathcal{T}_i}} P_{ij} + 10\gamma \log_{10} \frac{\|\hat{\boldsymbol{x}}^{(t)} - \hat{\boldsymbol{a}}_j\|}{d_0}}{|\mathcal{E}_{\mathcal{A}_i}| + |\mathcal{E}_{\mathcal{T}_i}|}$
      if $\widehat{P}_{0i} < P_0^{\text{Low}}$ **then**
        $\widehat{P}_{0i} \leftarrow P_0^{\text{Low}}$
      else if $\widehat{P}_{0i} > P_0^{\text{Up}}$ **then**
        $\widehat{P}_{0i} \leftarrow P_0^{\text{Up}}$
      end if
    end for
  end if
until $t < T_{\max}$

Table 3.2: Computational Complexity of the Considered Algorithms

Algorithm	Complexity
SOCP	$T_{\max} \times M \times \mathcal{O}\left(\left(\max_i \left\{3\lvert\mathcal{E}_{\mathcal{A}_i}\rvert + \lvert\mathcal{E}_{\mathcal{T}_i}\rvert\right\}\right)^{3.5}\right)$
SR-WLS	$T_{\max} \times M \times \mathcal{O}\left(N_{\max} \times \max_i \left\{3\lvert\mathcal{E}_{\mathcal{A}_i}\rvert + \lvert\mathcal{E}_{\mathcal{T}_i}\rvert\right\}\right)$
uSOCP	$T_{\max} \times M \times \mathcal{O}\left(\left(\max_i \left\{3\lvert\mathcal{E}_{\mathcal{A}_i}\rvert + \lvert\mathcal{E}_{\mathcal{T}_i}\rvert\right\}\right)^{3.5}\right)$
SDP	$\mathcal{O}\left(\sqrt{3M}\left(81M^4\left(N + \frac{M}{2}\right)^2\right)\right)$
uSOCP2	$T_{\max} \times M \times \mathcal{O}\left(\max_i \left\{\sqrt{3\lvert\mathcal{E}_{\mathcal{A}_i}\rvert + \lvert\mathcal{E}_{\mathcal{T}_i}\rvert}\left((3\lvert\mathcal{E}_{\mathcal{A}_i}\rvert)^2(3\lvert\mathcal{E}_{\mathcal{A}_i}\rvert + \lvert\mathcal{E}_{\mathcal{T}_i}\rvert) + (3\lvert\mathcal{E}_{\mathcal{A}_i}\rvert + \lvert\mathcal{E}_{\mathcal{T}_i}\rvert)^2\right)\right\}\right)$

smaller, due to energy restrictions (limited R). Therefore, distributed algorithms are a preferable solution in large-scale and highly-dense networks, since adding more sensors in the network will not have a severe impact on the size of neighborhood fragments. Table 3.2 also reveals that the proposed distributed SOCP algorithms are computationally more demanding than the proposed SR-WLS one. This result is not surprising, since the SOCP approach employs sophisticated mathematical tools, whereas the SR-WLS approach applies a bisection procedure to solve the localization problem. Nevertheless, higher complexity of the proposed SOCP algorithms is justified by their superior performance in terms of the estimation accuracy and convergence, as we will see in Section 3.3.5.

3.3.5 Performance Results

In this section, we present a set of results in order to assess the performance of the proposed approaches in terms of the estimation accuracy and convergence. All of the presented algorithms were solved by using the MATLAB package `CVX` [62], where the solver is SeDuMi [65]. In order to demonstrate the benefit of fusing two radio measurements versus traditional localization systems, we include also the performance results of the proposed methods when only RSS measurements are employed, called here "SOCP_{RSS}" and "$\text{SR-WLS}_{\text{RSS}}$". To provide a performance benchmark, we employ also the existing distributed SOCP approach for unknown P_i's [38] labelled as "uSOCP2", as well as the centralized cooperative approach described in [36] for known P_i's which is used as a lower bound on the performance of the distributed approaches, denoted as "SDP".

A random deployment of M targets and N anchors inside a cube region of length B in each Monte Carlo (M_c) run is considered. Random deployment of sensors is of particular interest, since the localization algorithms are tested against various network topologies in order to assess their robustness. In favor of making the comparison of the considered approaches as fair as possible, we first obtained $M_c = 500$ targets' and anchors' locations, as well as noise realizations between two sensors $\forall (i,j) \in \mathcal{E}_{\mathcal{A}} \cup \mathcal{E}_{\mathcal{T}}, i \neq j$, in each M_c run. Furthermore, we made sure that the network graph is connected in each M_c run. We then solved the localization problem with the considered approaches for those scenarios. In all simulations presented here, the reference distance was set to $d_0 = 1$ m, the communication range of a sensor to $R = 6.5$ m, the maximum number of steps in the bisection procedure to $N_{\max} = 30$ and the PLE was fixed to $\gamma = 3$. The true value of the reference power is drawn from a uniform distribution on an interval $[P_0^{\text{Low}}, P_0^{\text{Up}}]$, *i.e.*, $P_{0i} \in \mathcal{U}[P_0^{\text{Low}}, P_0^{\text{Up}}]$ dBm. Also, to account for a realistic measurement model mismatch and test the robustness of the new algorithms to imperfect knowledge of the PLE, the true PLE was drawn from $\gamma_{ij} \in \mathcal{U}[2.7, 3.3], \forall (i,j) \in \mathcal{E}_{\mathcal{A}} \cup \mathcal{E}_{\mathcal{T}}, i \neq j$. Finally, we assumed that the initial guess of the targets' locations, $\hat{\boldsymbol{X}}^{(0)}$, is in the intersection of the big diagonals of the cube area.

The performance metric is the NRMSE, defined as

$$\text{NRMSE} = \sqrt{\frac{1}{MM_c}\sum_{i=1}^{M_c}\sum_{j=1}^{M}\|\boldsymbol{x}_{ij} - \widehat{\boldsymbol{x}}_{ij}\|^2},$$

where $\widehat{\boldsymbol{x}}_{ij}$ denotes the estimate of the true location of the j-th target, $\boldsymbol{x}_{ij}$, in the i-th Monte Carlo run.

Fig. 3.17 illustrates the NRMSE versus t performance of the considered approaches when $N = 20$ and $M = 50$. From Fig. 3.17, we can see that the performance of all considered algorithms betters as t grows, as anticipated. Furthermore, it can be noticed that the "uSOCP" curve gets saturated at $t = 3$. Hence, at this point we start estimating P_{0i}'s, and continue our algorithm as if P_{0i}'s are known. This fact explains the sudden curve drop after $t = 3$. One can argue that the proposed "uSOCP" algorithm shows excellent performance, outperforming noticeably the existing "uSOCP2" approach and achieving the lower bound provided by its counterpart for known P_i's. Also, it can be seen that the proposed hybrid methods outperform considerably their traditional counterparts that utilize RSS measurements only. Moreover, the "SR-WLS" method performs better than the "SOCP_{RSS}" method in every iteration. This is important to note because the later method is computationally more demanding due to the use of sophisticated mathematical tools, which shows that even a simple algorithm such as the one based on bisection procedure can produce high estimation accuracy when two radio measurements are combined. One can perceive that all major changes in the performance for the considered algorithms take place in the first few iterations ($t \leq 10$ or $t \leq 20$), and that the performance gain is negligible afterwards. This result is very important because it shows that our approaches require a low number of signal transmissions, which might enhance the utilization efficiency of the radio spectrum, a precious resource for wireless communications. It also shows that our algorithms are energy efficient; the communication phase is much more expensive (in terms of energy) than the data processing one [1]. Finally, the proposed SOCP performs outstanding, very close to the lower bound provided by the centralized "SDP" approach in just a few iterations.

Fig. 3.18 illustrates the NRMSE versus t performance of the considered approaches when $N = 30$ and $M = 50$. Figs. 3.17 and 3.18 reveal that the performance of all algorithms improves significantly as more anchors are added into the network. This behavior is expected, since when N grows more reliable information and more AoA measurements are available in the network. Furthermore, Fig. 3.18 exhibits that the proposed hybrid algorithms outperform their RSS counterparts, and that they can be stopped after just $5 - 10$ iterations. Finally, although the new methods were derived under the assumption that the noise is small, we can see that they work excellent even when the assumption does not hold.

Fig. 3.19 illustrates the NRMSE versus t performance of the considered approaches when $N = 20$ and $M = 60$. From Figs. 3.17 and 3.19 it can be seen that the distributed

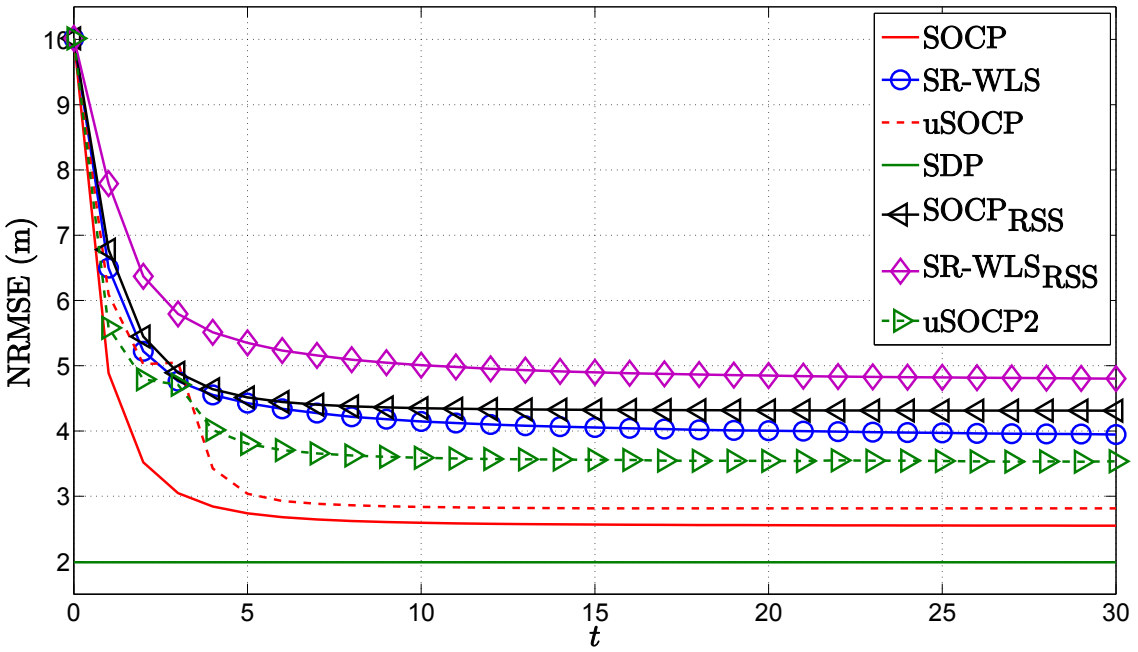

Figure 3.17: NRMSE (m) versus t comparison, when $N = 20$, $M = 50$, $R = 6.5$ m, $\sigma_{n_{ij}} = 3$ dB, $\sigma_{m_{ij}} = 6$ deg, $\sigma_{v_{ij}} = 6$ deg, $\gamma_{ij} \in \mathcal{U}[2.7, 3.3]$, $\gamma = 3$, $B = 20$ m, $P_{0i} \in \mathcal{U}[-12, -8]$ dBm, $d_0 = 1$ m, $M_c = 500$.

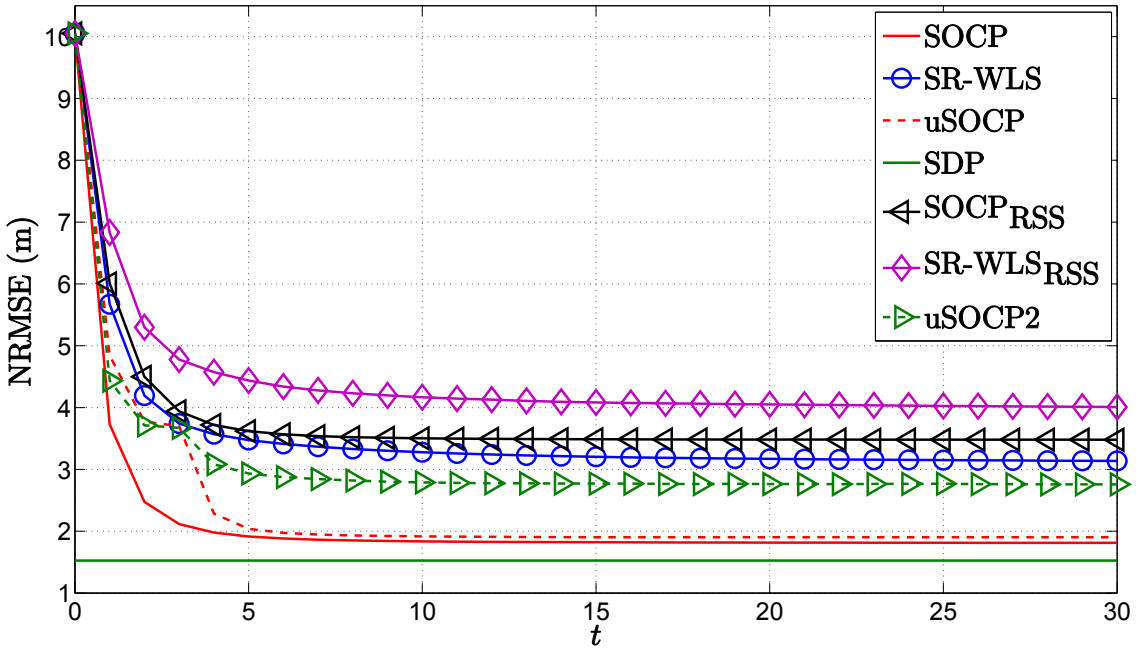

Figure 3.18: NRMSE (m) versus t comparison, when $N = 30$, $M = 50$, $R = 6.5$ m, $\sigma_{n_{ij}} = 3$ dB, $\sigma_{m_{ij}} = 6$ deg, $\sigma_{v_{ij}} = 6$ deg, $\gamma_{ij} \in \mathcal{U}[2.7, 3.3]$, $\gamma = 3$, $B = 20$ m, $P_{0i} \in \mathcal{U}[-12, -8]$ dBm, $d_0 = 1$ m, $M_c = 500$.

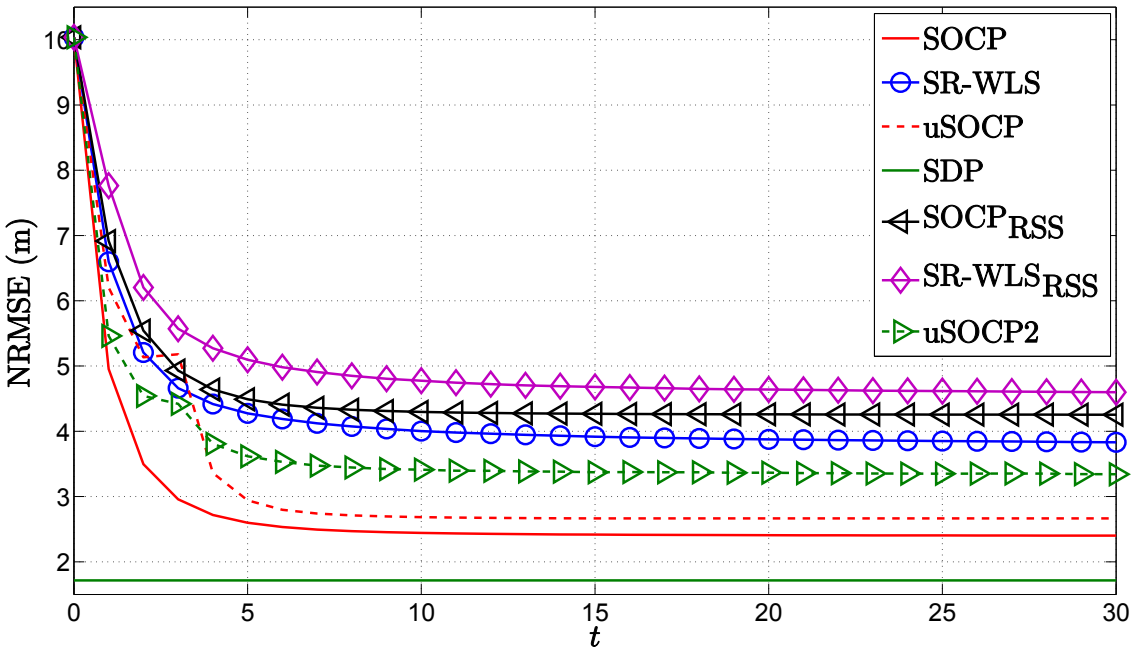

Figure 3.19: NRMSE (m) versus t comparison, when $N = 20$, $M = 60$, $R = 6.5$ m, $\sigma_{n_{ij}} = 3$ dB, $\sigma_{m_{ij}} = 6$ deg, $\sigma_{v_{ij}} = 6$ deg, $\gamma_{ij} \in \mathcal{U}[2.7, 3.3]$, $\gamma = 3$, $B = 20$ m, $P_{0i} \in \mathcal{U}[-12, -8]$ dBm, $d_0 = 1$ m, $M_c = 500$.

approaches require a slightly higher number of iterations to converge when M is increased. However, the estimation accuracy of the considered algorithms does not deteriorate when more targets are added in the network; it actually betters when M is increased. Finally, Fig. 3.19 confirms the effectiveness of using the combined measurements in hybrid systems in comparison with using only a single measurement[5].

In Figs. 3.20, 3.21 and 3.22 we investigate the impact of the quality of RSS and AoA measurements on the performance of the considered approaches. More precisely, Figs. 3.20, 3.21 and 3.22 respectively illustrate the NRMSE (m) versus $\sigma_{n_{ij}}$ (dB), $\sigma_{m_{ij}}$ (deg) and $\sigma_{v_{ij}}$ (deg) comparison, when $N = 20$, $M = 50$, $R = 6.5$ m, and $T_{\max} = 30$. In these figures, we can observe that the performance of all algorithms degrades as the quality of a certain measurement drops, as expected. It can also be seen that the quality of the RSS measurements has the most significant impact on the performance of the proposed algorithms, while the error in the azimuth and elevation angle measurements have marginal influence on the performance. This is not surprising, since the error of a few degrees in AoA measurements does not impair considerably their quality on a fairly short distance (communication range of all sensors is restricted to $R = 6.5$ m), as shown in Figs. 3.21 and 3.22. On the other hand, RSS measurements are notoriously unpredictable [1]. Nonetheless, we can see from Fig. 3.20 that the performance loss is lower than 15% for the "SOCP" and "uSOCP", and 10% for the "SR-WLS", which is

[5]Actually, in Figs. 3.17, 3.18 and 3.19 we have performed the simulations with $T_{\max} = 200$ iterations in order to make sure that the considered approaches converge. In favour of a better overview, here, we present only the results for the first $t = 30$ iterations.

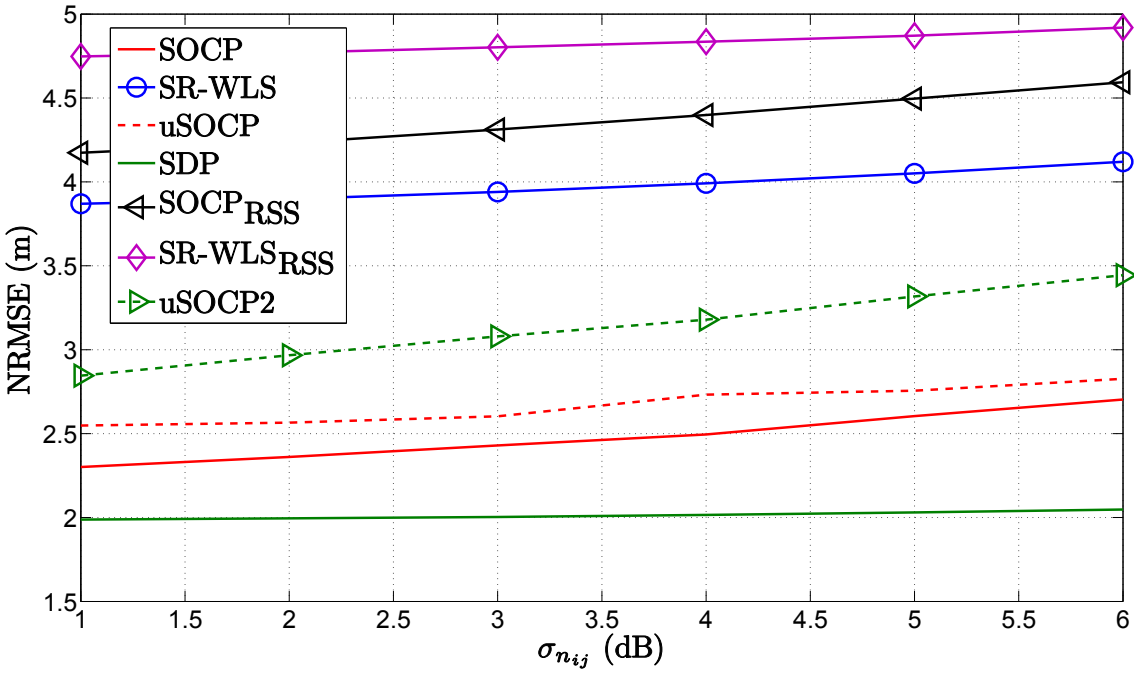

Figure 3.20: NRMSE (m) versus $\sigma_{n_{ij}}$ (dB) comparison, when $N = 20$, $M = 50$, $R = 6.5$ m, $\sigma_{m_{ij}} = 1$ deg, $\sigma_{v_{ij}} = 1$ deg, $\gamma_{ij} \in \mathcal{U}[2.7, 3.3]$, $\gamma = 3$, $T_{\max} = 30$, $B = 20$ m, $P_{0i} \in \mathcal{U}[-12, -8]$ dBm, $d_0 = 1$ m, $M_c = 500$.

relatively low for the considered error span. Finally, from the figures, we can see that the proposed "uSOCP" outperforms the existing "uSOCP2" for all settings.

3.3.6 Conclusions

In this section, we proposed two novel distributed algorithms to solve the RSS/AoA localization problem for known transmit powers based on SOCP relaxation technique and GTRS framework. The proposed SOCP algorithm provides exceptional localization accuracy in just a few iterations. Our algorithm based on GTRS framework is solved via a simple bisection procedure, and it represents an excellent alternative to our SOCP algorithm, since its somewhat lower accuracy is compensated with linear computational complexity. We also show that the proposed SOCP algorithm for known transmit power can be generalized to the case where the transmit powers are different and not known. Our simulation results show that all of the proposed algorithms efficiently solve the very challenging cooperative localization problem, both in terms of the estimation accuracy and the convergence; the SOCP-based algorithm achieves the lower bound provided by the centralized SDP algorithm in only a few iterations, and outperforms notably the existing distributed approach. Furthermore, the simulation results confirmed the robustness of the proposed algorithms to the imperfect knowledge of the PLE, which is a very important practical scenario.

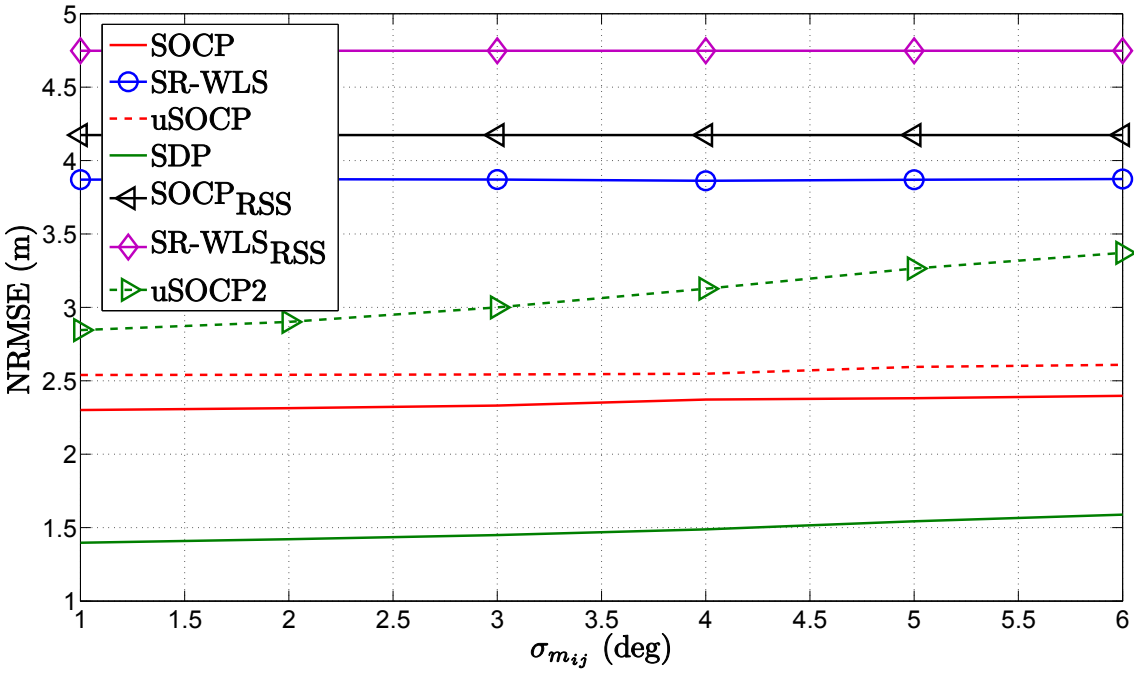

Figure 3.21: NRMSE (m) versus $\sigma_{m_{ij}}$ (deg) comparison, when $N = 20$, $M = 50$, $R = 6.5$ m, $\sigma_{n_{ij}} = 1$ dB, $\sigma_{v_{ij}} = 1$ deg, $\gamma_{ij} \in \mathcal{U}[2.7, 3.3]$, $\gamma = 3$, $T_{\max} = 30$, $B = 20$ m, $P_{0i} \in \mathcal{U}[-12, -8]$ dBm, $d_0 = 1$ m, $M_c = 500$.

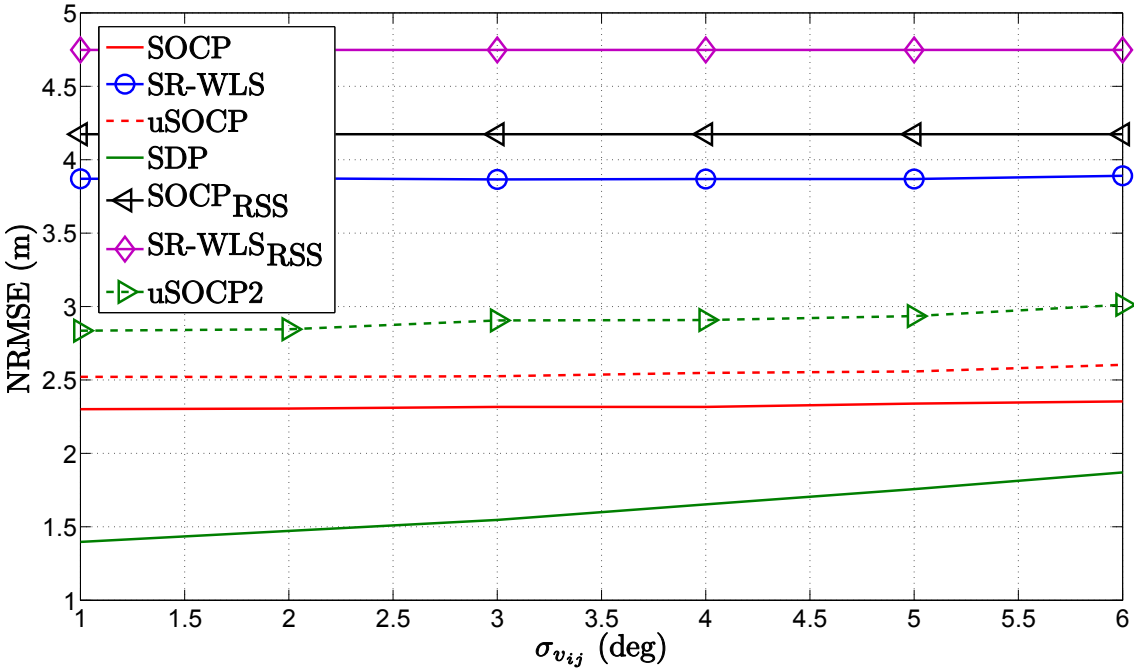

Figure 3.22: NRMSE (m) versus $\sigma_{v_{ij}}$ (deg) comparison, when $N = 20$, $M = 50$, $R = 6.5$ m, $\sigma_{n_{ij}} = 1$ dB, $\sigma_{m_{ij}} = 1$ deg, $\gamma_{ij} \in \mathcal{U}[2.7, 3.3]$, $\gamma = 3$, $T_{\max} = 30$, $B = 20$ m, $P_{0i} \in \mathcal{U}[-12, -8]$ dBm, $d_0 = 1$ m, $M_c = 500$.

CHAPTER 4

Target Tracking

4.1 Chapter Summary

This chapter addresses the problem of tracking of a moving target by using coupled RSS and AoA measurements. The remainder of the chapter is organized as follows.

Section 4.2 describes the existing work in the area of RSS-AoA-based target tracking problem, and highlights our contributions. In Section 4.3 we introduce the target state transition model as well as the measurement model, and we formulate the target tracking problem by using the Bayesian approach. Section 4.4 describes our technique used to *linearize* the measurement model. Section 4.5 present the derivation of our tracking algorithms, as well as our navigation routine for sensors' mobility management. In Section 4.6, simulation results are presented for two different target trajectories in order to validate the performance of our algorithms. Finally, Section 4.7 summarizes the main conclusions.

4.2 Introduction

The problem of accurate localization of a moving object in real-time has motivated a great deal of scientific research recently, owing to a constant growth of the range of enabling devices and technologies, and the requirement for seamless solutions in location-based services [16, 91–96]. In order to maintain low implementation costs, making use of existing technologies (such as terrestrial radio frequency sources) when providing a solution to the object tracking problem is strongly encouraged. These include for example, time of arrival, RSS, AoA, or a combination of them [20, 23, 36, 38, 73, 96–100].

4.2.1 Related Work

The authors in [20, 23, 36, 38, 73, 97, 98, 100] considered only the *classical* target localization problem, where they disregarded the prior knowledge and gave all importance to observations exclusively. The works in [92, 93] and [96], investigated the target tracking problem, where the observations were combined with some prior knowledge to enhance the estimation accuracy. However, they all examined pure RSS-based target tracking problem only. In [95], the authos investigated the target tracking problem by employing hybrid, RSS and AoA, measurements. Both KF and particle filter (PF) were proposed in [95], as well as a generalized pattern search method for estimating the PLE for each link in every time step. Nevertheless, the authors considered the tracking problem with static anchors only. The works presented in [11, 101], tackled the target tracking problem with mobile sensors navigation. Still, hybrid RSS-AoA target tracking problem was not a part of their study.

4.2.2 Contribution

In this work, the problem of tracking a mobile target by employing hybrid RSS-AoA measurements is considered. We assume that the target transmit power is unknown, and start by describing our *linearization* process of the highly non-linear observation model. Next, we combine the prior knowledge given by state transition model with the *linearized* model in order to enhance the estimation accuracy. Then, is it shown that the application of the MAP and the KF criterion is straightforward, resulting in a novel MAP and a novel KF algorithm. Finally, we propose a simple navigation routine to manage sensors' mobility, which leads to great improvement in the estimation accuracy, even for lower number of sensors. A realistic scenario where the PLE and the true sensors' locations are not perfectly known is also taken into consideration.

4.3 Problem Formulation

We consider a WSN[1] composed of N mobile sensors with known locations, $\boldsymbol{a}_{i,t} = [a_{\mathrm{ix},t}, a_{iy,t}]^T$ for $i = 1, ..., N$, and a moving target whose location, $\boldsymbol{x}_t = [x_{\mathrm{x},t}, x_{\mathrm{y},t}]^T$, we desire to determine at each time instant t. For simplicity, we assume a constant velocity target motion model (*e.g.*, perturbed only by wind gust) such that the velocity components in the x and y directions at time t are given by

$$\boldsymbol{v}_t = \boldsymbol{v}_{t-1} + \boldsymbol{r}_{v,t}, \tag{4.1}$$

where $\boldsymbol{r}_{v,t}$ represents the noise perturbations. Hence, from the equations of motion [47], the target location at time t is

$$\boldsymbol{x}_t = \boldsymbol{x}_{t-1} + \boldsymbol{v}_{t-1}\Delta + \boldsymbol{r}_{x,t}, \tag{4.2}$$

[1]For simplicity and without loss of generality, this thesis focuses on 2-dimensional scenario. The extension to 3-dimensional scenario is straightforward.

where Δ and $\boldsymbol{r}_{x,t}$ are the sampling interval between two consecutive time steps and location process noise, respectively. Now, if we describe the target state at t by its location and velocity, *i.e.*, $\boldsymbol{\theta}_t = [\boldsymbol{x}_t^T, \boldsymbol{v}_t^T]^T$, from (4.1) and (4.2) we get

$$\boldsymbol{\theta}_t = \boldsymbol{S}\,\boldsymbol{\theta}_{t-1} + \boldsymbol{r}_t, \tag{4.3}$$

where $\boldsymbol{r}_t = [\boldsymbol{r}_{x,t}^T, \boldsymbol{r}_{v,t}^T]^T$ is the state process noise [91–96], assumed to be zero-mean Gaussian with a covariance matrix $\boldsymbol{Q}$, *i.e.*, $\boldsymbol{r}_t \sim \mathcal{N}(\boldsymbol{0}, \boldsymbol{Q})$, where $\boldsymbol{Q}$ is defined as

$$\boldsymbol{Q} = q \begin{bmatrix} \frac{\Delta^3}{3} & 0 & \frac{\Delta^2}{2} & 0 \\ 0 & \frac{\Delta^3}{3} & 0 & \frac{\Delta^2}{2} \\ \frac{\Delta^2}{2} & 0 & \Delta & 0 \\ 0 & \frac{\Delta^2}{2} & 0 & \Delta \end{bmatrix},$$

with q denoting the state process noise intensity [91, 93, 102]. The symbol $\boldsymbol{S}$ in (4.3) stands for the state transition matrix, which models the state dynamics and is given by

$$\boldsymbol{S} = \begin{bmatrix} 1 & 0 & \Delta & 0 \\ 0 & 1 & 0 & \Delta \\ 0 & 0 & 1 & 0 \\ 0 & 0 & 0 & 1 \end{bmatrix}.$$

A detailed derivation of the state transition model, as well as the matrices $\boldsymbol{S}$ and $\boldsymbol{Q}$ is given in Appendix D.

At each time instant, the target emits a signal to sensors which withdraw the RSS and AoA information from it. Thus, the measurement equation can be formulated as

$$\boldsymbol{z}_t = \boldsymbol{h}(\boldsymbol{x}_t) + \boldsymbol{n}_t, \tag{4.4}$$

where $\boldsymbol{z}_t = [\boldsymbol{P}_t^T, \boldsymbol{\phi}_t^T]^T$ ($\boldsymbol{z}_t \in \mathbb{R}^{2N}$) is the observation vector comprising RSS, $\boldsymbol{P}_t = [P_{i,t}]^T$, and AoA, $\boldsymbol{\phi}_t = [\phi_{i,t}]^T$, measurements at time instant t. The function $\boldsymbol{h}(\boldsymbol{x}_t)$ in (4.4) is defined as $h_i(\boldsymbol{x}_t) = P_0 - 10\gamma \log_{10} \frac{\|\boldsymbol{x}_t - \boldsymbol{a}_{i,t}\|}{d_0}$ for $i = 1, ..., N$ [58], and $h_i(\boldsymbol{x}_t) = \tan^{-1}\left(\frac{x_{\mathrm{y},t} - a_{\mathrm{iy},t}}{x_{\mathrm{x},t} - a_{\mathrm{ix},t}}\right)$ for $i = N+1, ..., 2N$ [30]. The measurement noise, $\boldsymbol{n}_t$, is modeled as $\boldsymbol{n}_t \sim \mathcal{N}(\boldsymbol{0}, \boldsymbol{C})$, where the noise covariance is defined as $\boldsymbol{C} = \mathrm{diag}([\sigma_{n_i}^2, \sigma_{m_i}^2]) \otimes \boldsymbol{I}_4$, with σ_{n_i} (dB) and σ_{m_i} (rad) being the noise standard deviation of the RSS and AoA measurements, respectively, $\boldsymbol{I}_M$ denoting the identity matrix of size M and symbol $\otimes$ representing the Kronecker product.

In Bayesian estimation theory, the prior knowledge, obtained through the state transition model (4.3), is combined with the noisy observations (4.4) to obtain the marginal posterior PDF, $p(\boldsymbol{\theta}_t | \boldsymbol{z}_{1:t})$. Through $p(\boldsymbol{\theta}_t | \boldsymbol{z}_{1:t})$ we can quantify the belief we have in the values of the state $\boldsymbol{\theta}_t$ given all the past measurements $\boldsymbol{z}_{1:t}$ and obtain an estimate at any time instant we desire. The main steps of the Bayesian estimation are described below [91–96].

- *Initialization:* The marginal posterior PDF at $t = 0$ is set to the prior PDF $p(\boldsymbol{\theta}_0)$ of $\boldsymbol{\theta}_0$.

- *Prediction:* By using the state transition model (4.3), the predictive PDF of the state at t is given by

$$p(\boldsymbol{\theta}_t|\boldsymbol{z}_{1:t-1}) = \int p(\boldsymbol{\theta}_t|\boldsymbol{\theta}_{t-1})p(\boldsymbol{\theta}_{t-1}|\boldsymbol{z}_{1:t-1})d\boldsymbol{\theta}_{t-1}. \tag{4.5}$$

- *Update:* By following the Bayes' rule [91, 102], we have

$$p(\boldsymbol{\theta}_t|\boldsymbol{z}_{1:t}) = \frac{p(\boldsymbol{z}_t|\boldsymbol{\theta}_t)p(\boldsymbol{\theta}_t|\boldsymbol{z}_{1:t-1})}{p(\boldsymbol{z}_t|\boldsymbol{z}_{1:t-1})} \tag{4.6}$$

where $p(\boldsymbol{z}_t|\boldsymbol{\theta}_t)$ is the likelihood and $p(\boldsymbol{z}_t|\boldsymbol{z}_{1:t-1}) = \int p(\boldsymbol{z}_t|\boldsymbol{\theta}_t)p(\boldsymbol{\theta}_t|\boldsymbol{z}_{1:t-1})d\boldsymbol{\theta}_t$ is just a normalizing constant, independent of $\boldsymbol{\theta}_t$, needed to insure that $p(\boldsymbol{\theta}_t|\boldsymbol{z}_{1:t})$ integrates to 1 [47]. In general, the marginal PDF at $t-1$ cannot be calculated analytically, and the integral in (4.5) cannot be obtained analytically if the state model is non-linear. Therefore, some approximations are required in order to obtain $p(\boldsymbol{\theta}_t|\boldsymbol{z}_{1:t})$.

4.4 Linearization of the Measurement Model

In practice, network testing and calibration are often not the priority, especially in low-cost systems such as RSS [16]. Hence, some parameters, such as target transmit power, might not be calibrated, *i.e.*, not known beforehand. Not knowing the transmit power matches not knowing P_0 in (4.4) [16]. Therefore, in this section we will show how to *linearize* the measurement model for the case of unknown P_0.

Under the assumption that the noise power is small, by using Taylor series approximation from (4.4) we can write for the RSS model

$$\rho + \epsilon_i = \mu_{i,t}\|\boldsymbol{x}_t - \boldsymbol{a}_{i,t}\|, \text{ for } i = 1, ..., N, \tag{4.7}$$

where $\rho = \exp\left(\frac{P_0}{\eta\gamma}\right)$, $\eta = \frac{10}{\ln(10)}$, $\mu_{i,t} = \exp\left(\frac{P_{i,t}}{\eta\gamma}\right)$, and $\epsilon_i \sim \mathcal{N}(0, (\frac{\rho}{\eta\gamma}\sigma_{n_i})^2)$. By rearranging the terms and squaring (4.7), we get

$$\epsilon_i \approx \frac{\mu_{i,t}}{2}\|\boldsymbol{x}_t - \boldsymbol{a}_{i,t}\| - \frac{\rho}{2}, \tag{4.8}$$

where we disregarded the second-order noise terms. By converting from Cartesian to polar coordinates, we can express $\boldsymbol{x}_t - \boldsymbol{a}_{i,t} = r_{i,t}\boldsymbol{u}_{i,t} : r_{i,t} \geq 0, \|\boldsymbol{u}_{i,t}\| = 1$, where the unit vector can be obtained by employing the available AoA information, *i.e.*, $\boldsymbol{u}_i = [\cos(\phi_{i,t}), \sin(\phi_{i,t})]^T$. If we apply this conversion in (4.8) and multiply by $\boldsymbol{u}_{i,t}^T\boldsymbol{u}_{i,t}$ we get

$$\epsilon_i \approx \frac{\mu_{i,t}}{2}\boldsymbol{u}_{i,t}^T(\boldsymbol{x}_t - \boldsymbol{a}_{i,t}) - \frac{\rho}{2}. \tag{4.9}$$

Similarly, for the AoA model we can write from (4.4)

$$\boldsymbol{c}_{i,t}^T(\boldsymbol{x}_t - \boldsymbol{a}_{i,t}) \approx 0, \text{ for } i = N+1, ..., 2N, \tag{4.10}$$

where $\boldsymbol{c}_{i,t} = [-\sin(\phi_{i,t}), \cos(\phi_{i,t})]^T$.

Assuming that the noise term is sufficiently small and introducing weights, $\boldsymbol{w}_t = [\sqrt{w_{i,t}}]$, where $w_{i,t} = P_{i,t}/\sum_{i=1}^{N} P_{i,t}$, in (4.9) and (4.10) such that more importance is given to *nearby* links, gives

$$w_{i,t}\frac{\mu_{i,t}}{2}\boldsymbol{u}_{i,t}^T(\boldsymbol{x}_t - \boldsymbol{a}_{i,t}) \approx w_{i,t}\frac{\rho}{2}, \text{ for } i = 1, ..., N, \tag{4.11a}$$

$$w_{i,t}\boldsymbol{c}_{i,t}^T(\boldsymbol{x}_t - \boldsymbol{a}_{i,t}) \approx 0, \text{ for } i = N+1, ..., 2N. \tag{4.11b}$$

We can rewrite (4.11) in a linear vector form as

$$\boldsymbol{A}_t\boldsymbol{y}_t = \boldsymbol{b}_t, \tag{4.12}$$

where $\boldsymbol{y}_t = [\boldsymbol{x}_t^T, \rho]^T$, and

$$\boldsymbol{A}_t = \begin{bmatrix} \vdots & \vdots \\ w_{i,t}\frac{\mu_{i,t}}{2}\boldsymbol{u}_{i,t}^T & -\frac{w_{i,t}}{2} \\ \vdots & \vdots \\ w_{i,t}\boldsymbol{c}_i^T & 0 \\ \vdots & \vdots \end{bmatrix}, \boldsymbol{b}_t = \begin{bmatrix} \vdots \\ w_{i,t}\frac{\mu_{i,t}}{2}\boldsymbol{u}_{i,t}^T\boldsymbol{a}_{i,t} \\ \vdots \\ w_{i,t}\boldsymbol{c}_{i,t}^T\boldsymbol{a}_{i,t} \\ \vdots \end{bmatrix}.$$

By applying the LS criterion to the *linearized* measurement model in (4.12) we get

$$\hat{\boldsymbol{y}}_t = \underset{\boldsymbol{y}_t = [\boldsymbol{x}_t^T, \rho]^T}{\arg\min} \|\boldsymbol{A}_t\boldsymbol{y}_t - \boldsymbol{b}_t\|^2, \tag{4.13}$$

whose solution is readily obtained as $\hat{\boldsymbol{y}}_t = (\boldsymbol{A}_t^T\boldsymbol{A}_t)^{-1}(\boldsymbol{A}_t^T\boldsymbol{b}_t)$.

Subsequently, one could take advantage of the solution obtained through (4.13) to additionally improve its quality, *i.e.*, it could be exploited to find the ML estimate[2] of P_0, $\widehat{P}_0$, as

$$\widehat{P}_0 = \frac{\sum_{i=1}^{N} P_{i,t} + 10\gamma\log_{10}\frac{\|\hat{\boldsymbol{x}}_t - \boldsymbol{a}_{i,t}\|}{d_0}}{N} \tag{4.14}$$

and *linearize* the measurement model in a similar manner as before. First, calculate $\widehat{\rho} = \exp\left(\frac{\widehat{P}_0}{\eta\gamma}\right)$. Define weights $\widetilde{\boldsymbol{w}}_t = \sqrt{\widetilde{w}_{i,t}}$, where $\widetilde{w}_{i,t} = 1 - \frac{\widehat{d}_{i,t}}{\sum_{i=1}^{N}\widehat{d}_{i,t}}$ with $\widehat{d}_{i,t} = \exp\left(\frac{\widehat{P}_0 - P_{i,t}}{\eta\gamma}\right)$ being the ML estimate of the distance between the target and i-th anchor at time t. Then, by following similar steps as above, we can rewrite (4.9) and (4.10) in a vector form as

$$\widetilde{\boldsymbol{A}}_t\boldsymbol{x}_t = \widetilde{\boldsymbol{b}}_t, \tag{4.15}$$

where

$$\widetilde{\boldsymbol{A}}_t = \begin{bmatrix} \vdots \\ \widetilde{w}_{i,t}\frac{\mu_{i,t}}{2}\boldsymbol{u}_{i,t}^T \\ \vdots \\ \widetilde{w}_{i,t}\boldsymbol{c}_i^T \\ \vdots \end{bmatrix}, \widetilde{\boldsymbol{b}}_t = \begin{bmatrix} \vdots \\ \widetilde{w}_{i,t}(\frac{\mu_{i,t}}{2}\boldsymbol{u}_{i,t}^T\boldsymbol{a}_{i,t} + \frac{\widehat{\rho}}{2}) \\ \vdots \\ w_{i,t}\boldsymbol{c}_{i,t}^T\boldsymbol{a}_{i,t} \\ \vdots \end{bmatrix}.$$

[2]In the case where the true value of the transmit power is available beforehand, one would simply substitute $\widehat{P}_0$ by P_0 in the upcoming steps.

Hence, the localization problem can be posed in an LS form

$$\hat{\boldsymbol{x}}_t = \arg\min_{\boldsymbol{x}_t} \|\widetilde{\boldsymbol{A}}_t \boldsymbol{x}_t - \widetilde{\boldsymbol{b}}_t\|^2, \tag{4.16}$$

whose solution is obtained as $\hat{\boldsymbol{x}}_t = (\widetilde{\boldsymbol{A}}_t^T \widetilde{\boldsymbol{A}}_t)^{-1}(\widetilde{\boldsymbol{A}}_t^T \widetilde{\boldsymbol{b}}_t)$.

4.5 Target Tracking

4.5.1 Maximum A Posteriori Estimator

Within the Bayesian methodology, one of the most common criteria for determining a state estimate is the MAP criteria [47]. According to this estimation approach, we choose a state estimate, $\hat{\boldsymbol{\theta}}_{t|t}$, that maximizes the marginal PDF, *i.e.*,

$$\hat{\boldsymbol{\theta}}_{t|t} = \arg\max_{\boldsymbol{\theta}_t} p(\boldsymbol{\theta}_t|\boldsymbol{z}_{1:t}). \tag{4.17}$$

Based on (4.6), we observe that (4.17) is equivalent to maximization of $p(\boldsymbol{z}_t|\boldsymbol{\theta}_t)p(\boldsymbol{\theta}_t|\boldsymbol{z}_{1:t-1})$. This is evocative of the ML estimator except for the presence of the prior PDF. Consequently, the MAP estimator is

$$\hat{\boldsymbol{\theta}}_{t|t} = \arg\max_{\boldsymbol{\theta}_t} p(\boldsymbol{z}_t|\boldsymbol{\theta}_t)p(\boldsymbol{\theta}_t|\boldsymbol{z}_{1:t-1}) = \arg\max_{\boldsymbol{\theta}_t} [\ln p(\boldsymbol{z}_t|\boldsymbol{\theta}_t) + \ln p(\boldsymbol{\theta}_t|\boldsymbol{z}_{1:t-1})]. \tag{4.18}$$

The problem in (4.18) is highly non-convex and its analytical solution can not be obtained in general. As such, some approximations are required in order to obtain $\hat{\boldsymbol{\theta}}_{t|t}$.

First, we can approximate $p(\boldsymbol{\theta}_{t-1}|\boldsymbol{z}_{1:t-1})$ as a Gaussian distribution [102], *i.e.*, $p(\boldsymbol{\theta}_{t-1}|\boldsymbol{z}_{1:t-1}) \sim \mathcal{N}(\hat{\boldsymbol{\theta}}_{t-1|t-1}, \hat{\boldsymbol{\Sigma}}_{t-1|t-1})$. Then, according to (4.5) we get

$$p(\boldsymbol{\theta}_t|\boldsymbol{z}_{1:t-1}) \approx \frac{1}{k_1} \exp\left(-\frac{1}{2}(\boldsymbol{\theta}_t - \hat{\boldsymbol{\theta}}_{t|t-1})^T \hat{\boldsymbol{\Sigma}}_{t|t-1}^{-1}(\boldsymbol{\theta}_t - \hat{\boldsymbol{\theta}}_{t|t-1})\right), \tag{4.19}$$

where k_1 is a constant, and $\hat{\boldsymbol{\theta}}_{t|t-1}$ and $\hat{\boldsymbol{\Sigma}}_{t|t-1}$ are the mean and the covariance of the one-step predicted state acquired through (4.3) as

$$\hat{\boldsymbol{\theta}}_{t|t-1} = \boldsymbol{S}\,\hat{\boldsymbol{\theta}}_{t-1|t-1} \tag{4.20a}$$

$$\hat{\boldsymbol{\Sigma}}_{t|t-1} = \boldsymbol{S}\,\hat{\boldsymbol{\Sigma}}_{t-1|t-1}\,\boldsymbol{S}^T + \boldsymbol{Q}. \tag{4.20b}$$

The likelihood function can be written as

$$p(\boldsymbol{z}_t|\boldsymbol{\theta}_t) = \frac{1}{k_2} \exp\left(-\frac{1}{2}\,(\boldsymbol{z}_t - \boldsymbol{h}(\boldsymbol{x}_t))^T\,\boldsymbol{C}^{-1}\,(\boldsymbol{z}_t - \boldsymbol{h}(\boldsymbol{x}_t))\right), \tag{4.21}$$

where k_2 is a constant. Then, according to (4.18) we have

$$\hat{\boldsymbol{\theta}}_{t|t} = \arg\min_{\boldsymbol{\theta}_t}\ (\boldsymbol{z}_t - \boldsymbol{h}(\boldsymbol{x}_t))^T\,\boldsymbol{C}^{-1}\,(\boldsymbol{z}_t - \boldsymbol{h}(\boldsymbol{x}_t)) + (\boldsymbol{\theta}_t - \hat{\boldsymbol{\theta}}_{t|t-1})^T \hat{\boldsymbol{\Sigma}}_{t|t-1}^{-1}(\boldsymbol{\theta}_t - \hat{\boldsymbol{\theta}}_{t|t-1}). \tag{4.22}$$

We have shown in Section 4.4 how to tightly approximate the likelihood function. By following similar reasoning, we can rewrite (4.22) as

$$\hat{\boldsymbol{\theta}}_{t|t} = \arg\min_{\boldsymbol{\theta}_t} \|\boldsymbol{H}_t\boldsymbol{\theta}_t - \boldsymbol{f}_t\|^2, \tag{4.23}$$

where $\boldsymbol{H}_t = \left[\widetilde{\boldsymbol{A}}_t, \mathbf{0}_{2N\times 2}; \hat{\Sigma}_{t|t-1}^{-1/2}\right]$ ($\boldsymbol{H}_t \in \mathbb{R}^{(2N+4)\times 4}$), $\boldsymbol{f}_t = \left[\widetilde{\boldsymbol{b}}_t; \hat{\Sigma}_{t|t-1}^{-1/2}\hat{\boldsymbol{\theta}}_{t|t-1}\right]$ ($\boldsymbol{f}_t \in \mathbb{R}^{2N+4}$), and $\mathbf{0}_{D\times L}$ is a D by L matrix of all zeros. The solution of (4.23) is obtained as $\hat{\boldsymbol{\theta}}_{t|t} = (\boldsymbol{H}_t^T\boldsymbol{H}_t)^{-1}(\boldsymbol{H}_t^T\boldsymbol{f}_t)$.

The step by step proposed MAP-based algorithm[3] for the case where the target transmit power is not known (labelled here as "uMAP") is outlined in Algorithm 5.

Algorithm 5 uMAP Algorithm Description

Require: $\boldsymbol{z}_t$, for $t = 0,...,T-1$, $\boldsymbol{Q}$, $\boldsymbol{S}$

1: **Initialization:** $\hat{\boldsymbol{x}}_{0|0} \leftarrow$ (4.13), $\widehat{P}_0 \leftarrow$ (4.14), $\hat{\boldsymbol{\theta}}_{0|0} \leftarrow [\hat{\boldsymbol{x}}_{0|0}^T, 0, 0]^T$, $\hat{\Sigma}_{t|t} \leftarrow \boldsymbol{I}_4$ for $t = 0,...,T-1$

2: **for** $t = 1,...,T-1$ **do**

3: **Prediction:**

4: $-\ \hat{\boldsymbol{\theta}}_{t|t-1} \leftarrow$ (4.20a)
$-\ \hat{\Sigma}_{t|t-1} \leftarrow$ (4.20b)

5: **Update:**

6: $-\ \hat{\boldsymbol{\theta}}_{t|t} \leftarrow$ (4.23)
$-\ \widehat{P}_0 \leftarrow$ (4.14)

7: **end for**

4.5.2 Kalman Filter

The KF may be thought of as a generalized sequential minimum mean square estimator of a signal embedded in noise, where the unknown parameters are allowed to evolve in time according a given dynamical model [47]. If the state and the measurement models are linear and the noise is assumed to be zero-mean with finite covariance, the KF provides the optimal solution in the LS sense [91].

Even though the measurement model (4.4) is non-linear, we can *linearize* it as in (4.15). Therefore, by following the KF recipe [47], the mean and the covariance are updated as

$$\hat{\boldsymbol{\theta}}_{t|t} = \hat{\boldsymbol{\theta}}_{t|t-1} + \boldsymbol{K}_t(\widetilde{\boldsymbol{b}}_t - \boldsymbol{G}_t\hat{\boldsymbol{\theta}}_{t|t-1}), \tag{4.24a}$$

$$\hat{\Sigma}_{t|t} = (\boldsymbol{I}_4 - \boldsymbol{K}_t\boldsymbol{G}_t)\hat{\Sigma}_{t|t-1}, \tag{4.24b}$$

where $\boldsymbol{K}_t$ is the Kalman gain at time instant t, and $\boldsymbol{G}_t = [\widetilde{\boldsymbol{A}}_t, \mathbf{0}_{2N\times 2}]$ ($\boldsymbol{G}_t \in \mathbb{R}^{2N\times 4}$).

The step by step proposed KF algorithm for the case where the target transmit power is not known (denoted here as "uKF") is outlined in Algorithm 6.

[3]Notice that in Algorithm 5 we do not update the state covariance matrix. Although this update could be accomplished through $\hat{\boldsymbol{\theta}}_{t|t}$ and the use of Karush-Kuhn-Tucker optimality conditions together with certain approximations (*e.g.* see the approach in [102]), it does not bring any gain to our uMAP algorithm, and we do not apply it here.

Algorithm 6 uKF Algorithm Description

Require: $\boldsymbol{z}_t$, for $t = 0, ..., T-1$, $\boldsymbol{Q}$, $\boldsymbol{C}$, $\boldsymbol{S}$

1: **Initialization:** $\hat{\boldsymbol{x}}_{0|0} \leftarrow$ (4.13), $\widehat{P}_0 \leftarrow$ (4.14), $\hat{\boldsymbol{\theta}}_{0|0} \leftarrow [\hat{\boldsymbol{x}}_{0|0}^T, 0, 0]^T$, $\hat{\boldsymbol{\Sigma}}_{0|0} \leftarrow \boldsymbol{I}_4$

2: **for** $t = 1, ..., T-1$ **do**

3: **Prediction:**

4: $-\ \hat{\boldsymbol{\theta}}_{t|t-1} \leftarrow$ (4.20a)
$-\ \hat{\boldsymbol{\Sigma}}_{t|t-1} \leftarrow$ (4.20b)

5: $\boldsymbol{K}_t \leftarrow \hat{\boldsymbol{\Sigma}}_{t|t-1}\boldsymbol{G}_t^T(\boldsymbol{G}_t\hat{\boldsymbol{\Sigma}}_{t|t-1}\boldsymbol{G}_t^T + \boldsymbol{C})^{-1}$

6: **Update:**

7: $-\ \hat{\boldsymbol{\theta}}_{t|t} \leftarrow$ (4.24a)
$-\ \hat{\boldsymbol{\Sigma}}_{t|t} \leftarrow$ (4.24b)
$-\ \widehat{P}_0 \leftarrow$ (4.14)

8: **end for**

4.5.3 Sensor Navigation

Although the proposed algorithms described in Algorithm 5 and Algorithm 6 provide efficient solution to the target tracking problem, their estimation accuracy can be further enhanced. Until now, we have considered the sensors to be static, and only the target to be mobile. By allowing sensor mobility, such that they are permited to move in certain directions based on pre-established rules, we can not only improve the estimation accuracy of the proposed algorithms, but do so with a reduced number of sensors. The price to pay for applying such a routine is somewhat increased computational cost (required for determining the direction of sensor movement) and increased energy consumption (depleted in the process of the actual sensor movement), in comparison with the static sensors routine. Nevertheless, the interest for target tracking problem using navigated mobile sensors is growing rapidly, especially in areas such as autonomous surveillance, automated data collection and monitoring to name a few [11, 101].

The proposed routine for sensor navigation is described in Algorithm 7. It represents a universal addition to the proposed uMAP and uKF algorithms, which is realized by incorporating lines $3-13$ after line 6 in the uMAP, and after line 7 in the uKF. The basic idea of our navigation routine is to let the mobile sensors approach the target with the shortest possible path determined by the available information such as their estimated and the target's estimated location) at time instant t, until a certain threshold distance, τ. After the mobile sensors penetrate τ, our idea is to spread them around the target, so that we prevent possible sensor collision. More specifically, at line 4, each mobile sensor estimates its candidate location, $\breve{\boldsymbol{a}}_{i,t}$, by resorting only to its previous estimated location, the already available AoA measurement and its velocity, v_a. With this candidate location, the mobile sensors then estimate the possible distance from the estimated target location (as if they moved to the candidate location). If this estimated distance is not less than τ, the candidate location is accepted as the new estimated location of the mobile sensor, $\hat{\boldsymbol{a}}_{i,t}$, line 6; otherwise, the mobile sensors are spread around the target. To this end, we modify the angle measurement, $\breve{\phi}_{i,t-1}$ at line 9, and use this modified value to estimate the

updated location of the mobile sensors, line 10. However, to account for a realistic model mismatches, at lines 7 and 11, we include noise perturbations within the sensors' actual movements, which result in imperfect knowledge about the mobile sensors' locations.

Algorithm 7 Sensor Navigation Algorithm Description

Require: $\boldsymbol{a}_{i,0}$, $\phi_{i,t}$, for $i = 1, ..., N$, $t = 0, ..., T-1$, v_a, τ
1: **Initialization:** $\hat{\boldsymbol{a}}_{i,0} \leftarrow \boldsymbol{a}_{i,0}$
2: **for** $t = 1, ..., T-1$ **do**
3: **for** $i = 1, ..., N$ **do**
4: $\breve{\boldsymbol{a}}_{i,t} \leftarrow \hat{\boldsymbol{a}}_{i,t-1} + v_a \Delta[\cos(\phi_{i,t-1}), \sin(\phi_{i,t-1})]^T$
5: **if** $\|\breve{\boldsymbol{a}}_{i,t} - \hat{\boldsymbol{x}}_t\| \geq \tau$ **then**
6: $\hat{\boldsymbol{a}}_{i,t} \leftarrow \breve{\boldsymbol{a}}_{i,t}$
7: $\boldsymbol{a}_{i,t} \leftarrow \boldsymbol{a}_{i,t-1} + v_a \Delta[\cos(\phi_{i,t-1}), \sin(\phi_{i,t-1})]^T + \boldsymbol{r}_{x,t}$
8: **else**
9: $\breve{\phi}_{i,t} \leftarrow \phi_{i,t} + (-1)^i \pi/4$
10: $\hat{\boldsymbol{a}}_{i,t} \leftarrow \hat{\boldsymbol{a}}_{i,t-1} + v_a \Delta[\cos(\breve{\phi}_{i,t-1}), \sin(\breve{\phi}_{i,t-1})]^T$
11: $\boldsymbol{a}_{i,t} \leftarrow \boldsymbol{a}_{i,t-1} + v_a \Delta[\cos(\breve{\phi}_{i,t-1}), \sin(\breve{\phi}_{i,t-1})]^T + \boldsymbol{r}_{x,t}$
12: **end if**
13: **end for**
14: **end for**

4.6 Performance Results

4.6.1 Simulation Results

In this section, we validate the performance of the proposed algorithms through computer simulations. All of the presented algorithms were solved by using MATLAB. We consider two essentially different scenarios: one in which the target takes sharp manoeuvres and another one in which the target trajectory is more smooth; see Fig.4.1. The initial target location is at $[21, 20]^T$ (Fig,4.1a) and $[40, 15]^T$ (4.1b). The target state changes according to the state transition model (4.3), and at each time instant the radio measurements are generated in concordance with (4.4). Unless stated otherwise, the reference power is set to $P_0 = -10$ dBm, the initial location of $N = 3$ sensors is fixed at $\boldsymbol{a}_{i,0} = [[70, 10]^T, [40, 70]^T [10, 40]^T]$ and the PLE is set to $\gamma = 3$. However, to account for a more realistic measurement model mismatch, the true value of the PLE for each link was drawn from a uniform distribution on an interval $[2.7, 3.3]$, *i.e.*, $\gamma_{i,t} \sim \mathcal{U}[2.7, 3.3]$, at every time instant. A sample is taken every $\Delta = 1$ s during $T = 150$ s trajectory duration in each Monte Carlo, $M_c = 1000$, run. In the case where sensor mobility is allowed, we set the threshold distance[4] to $\tau = 5$ m. Furthermore, $\sigma_{n_i} = 9$ dB, $\sigma_{m_i} = 4\pi/180$ rad,

[4] In our simulations, we have also studied the influence of this parameter on the performance of the proposed algorithms. It was concluded that it has no significant impact on the performance, since similar results were attained for different values of τ (*e.g.*, $\tau = 10$ m or $\tau = 0$ m). However, we chose this particular value because it seems a reasonable practical threshold, keeping in mind the estimation error and noise influence to prevent sensor collision.

and $q = 2.5 \times 10^{-3}$ m^2/s^3. The performance metric used here is the RMSE, defined as $\text{RMSE}_t = \sqrt{\sum_{i=1}^{M_c} \frac{\|\boldsymbol{x}_{i,t} - \widehat{\boldsymbol{x}}_{i,t}\|^2}{M_c}}$, where $\widehat{\boldsymbol{x}}_{i,t}$ denotes the estimate of the true target location, $\boldsymbol{x}_{i,t}$, in the i-th M_c run at time instant t.

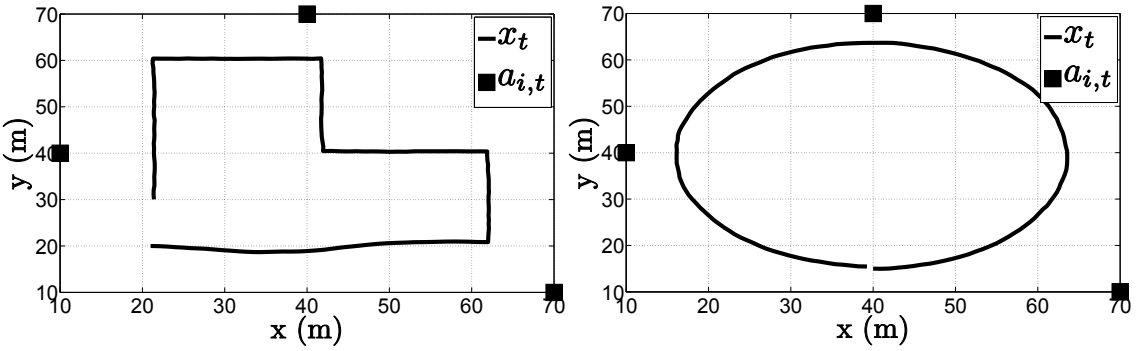

(a) Scenario 1 (b) Scenario 2

Figure 4.1: True target trajectory and mobile sensors' initial locations.

The performance of the proposed uMAP and uKF algorithms is compared with the existing KF in [95], where the initial target state was obtained by solving the LS method used in [95] to linearize the observation model[5]. Moreover, in favour of testing the belief that the Bayesian approaches (which integrate the prior knowledge with observations) outperform the *classical* ones (which disregard the prior knowledge and are based merely on observations), we show here the results for the sequential localization method in (4.16) with perfect knowledge about the target transmit power and PLE, denoted here by "WLS". Finally, to offer a lower bound on the performance of the proposed algorithms their counterparts for known target transmit power are also included, labelled here as "MAP" and "KF".

Fig. 4.2 illustrates the RMSE (m) versus t (s) comparison of all considered approaches in the first scenario, for the static sensors case, *i.e.*, $v_a = 0$ m/s. From it, we can observe that all algorithms suffer deteriorations at each sharp manoeuvre of the target, especially in the proximity of the sensors. This is somewhat anticipated, since the role of the prior knowledge is cancelled out with each sharp manoeuvre, and the vicinity of the target and any of the sensors creates a dis-balance between the significance of that particular measurement and all of other ones. Nonetheless, all algorithms recover fairly quickly from these impairments. Furthermore, the figure shows that the proposed algorithms outperform the existing KF in [95] in general, as well as the *classical* approach for all t. Moreover, it is worth mentioning that our algorithms show robustness to not knowing the target transmit power, since they achieve their lower bounds given by their equivalents for known transmit power. Finally, the new algorithms behave excellent even for the case where the PLE is not perfectly known.

[5]Since the authors in [95] proposed also a method for PLE estimation, in order to make the comparison fair, the true value of the PLE for every link is considered perfectly known for the KF [95] at any time step.

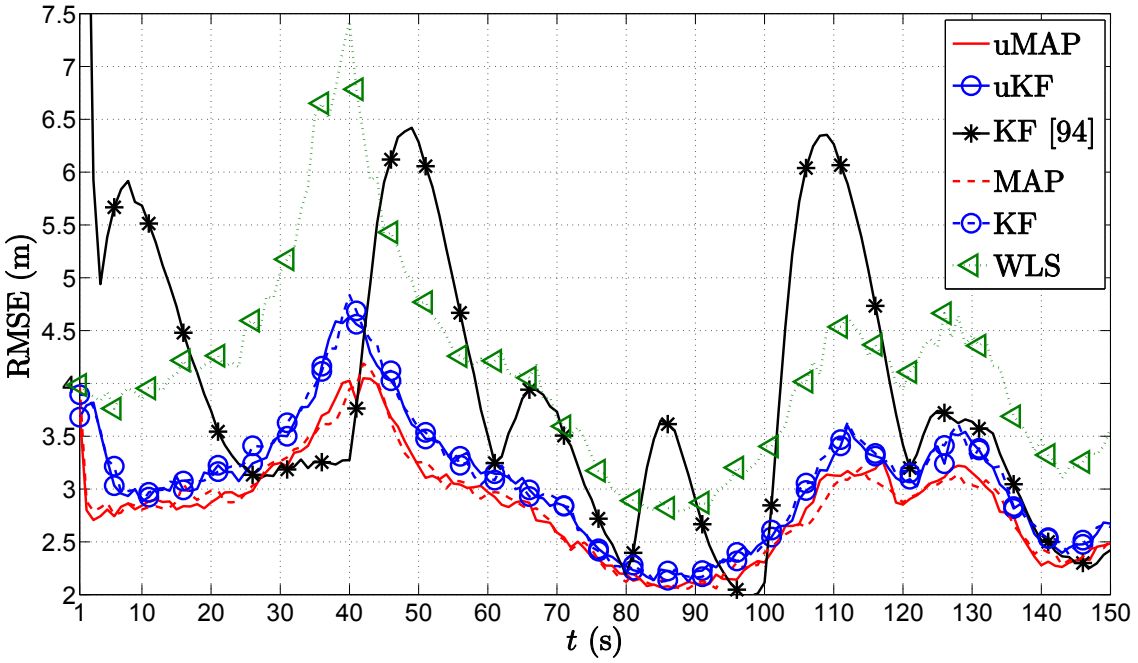

Figure 4.2: RMSE (m) versus t (s) comparison in the first scenario, when $N = 3$, $v_a = 0$ m/s, $\sigma_{n_i} = 9$ dB, $\sigma_{m_i} = 4\frac{\pi}{180}$ rad, $\gamma = 3$, $\gamma_i \sim \mathcal{U}[2.7, 3.3]$, $P_0 = -10$ dBm, $q = 2.5 \times 10^{-3}\,\mathrm{m}^2/\mathrm{s}^3$, $M_c = 1000$.

Table 4.1: $\overline{\text{RMSE}}$ (m) of the considered algorithms

Algorithm	uMAP	uKF	KF [95]	WLS	MAP	KF
Scenario 1	2.88	3.15	4.31	4.22	2.87	3.13
Scenario 2	2.97	3.22	4.14	4.30	2.97	3.22

Fig. 4.3 illustrates the RMSE (m) versus t (s) comparison of all considered approaches in the second scenario, for the static sensors case. From the figure, one can observe that the performance of all considered algorithms is significantly smoother in comparison with the first scenario. This behaviour is not surprising, since the target, although constantly changing its direction, is moving in a much smoother manner now. Fig. 4.3 exhibits also superior performance of the proposed algorithms in general, and robustness to not knowing the transmit power.

We present the average RMSE, $\overline{\text{RMSE}}$ (m), performance of the considered algorithms for static sensors setting in both scenarios in Table 4.1. From the table, we can see that the proposed uMAP algorithm performs best in both scenarios, and that the proposed *linearization* technique offers an improvement of roughly 1 m in both scenarios, in comparison with the existing one.

Fig. 4.4 illustrates a realization of the estimation process in the first scenario of the proposed (a) uMAP and (b) uKF algorithm, respectively, when sensor mobility is allowed. From hereafter, we only use $N = 2$ mobile sensors, and more particularly the first two

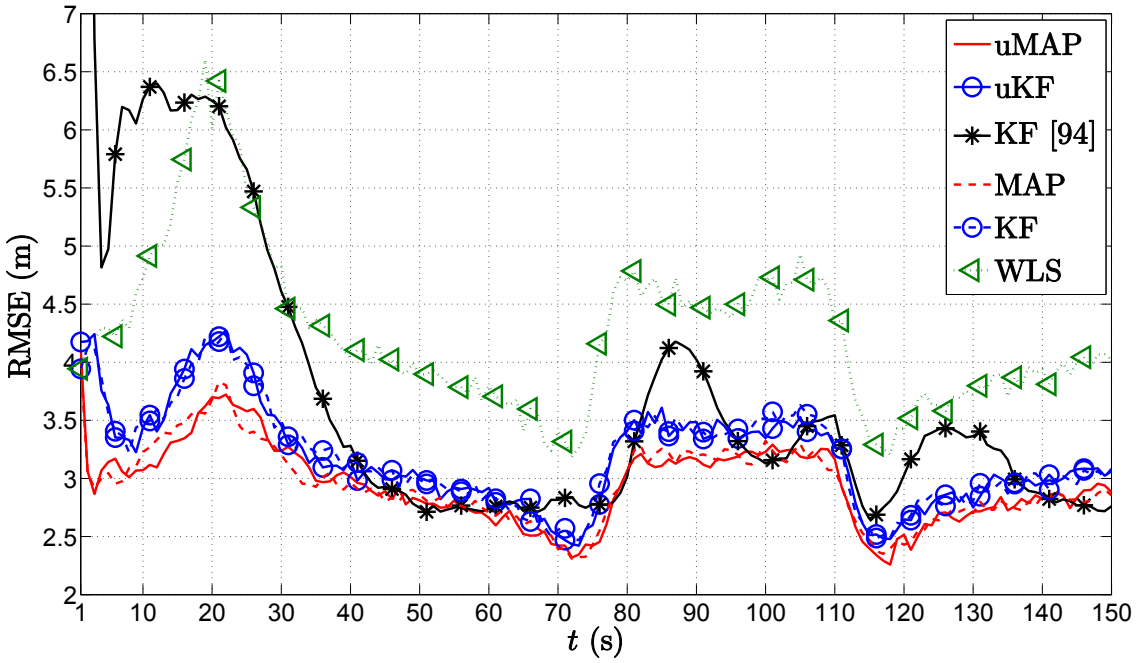

Figure 4.3: RMSE (m) versus t (s) comparison in the second scenario, when $N = 3$, $v_a = 0$ m/s, $\sigma_{n_i} = 9$ dB, $\sigma_{m_i} = 4\frac{\pi}{180}$ rad, $\gamma = 3$, $\gamma_i \sim \mathcal{U}[2.7, 3.3]$, $P_0 = -10$ dBm, $q = 2.5 \times 10^{-3}\,\mathrm{m}^2/\mathrm{s}^3$, $M_c = 1000$.

sensors from the original setting. From the figure, one can observe that both proposed algorithms solve very efficiently the target tracking problem with only $N = 2$ sensors, owing to their mobility.

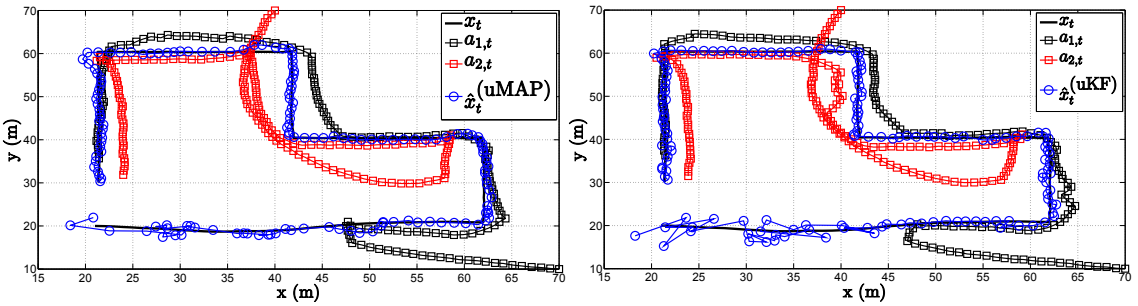

(a) uMAP (b) uKF

Figure 4.4: Illustration of the estimation process in the first scenario, when $N = 2$, $v_a = 1$ m/s, $\sigma_{n_i} = 9$ dB, $\sigma_{m_i} = 4\frac{\pi}{180}$ rad, $\gamma = 3$, $\gamma_i \sim \mathcal{U}[2.7, 3.3]$, $\tau = 5$ m, $P_0 = -10$ dBm, $q = 2.5 \times 10^{-3}\,\mathrm{m}^2/\mathrm{s}^3$.

Fig. 4.5 depicts the RMSE (m) versus t (s) performance comparison of the proposed algorithms in the first scenario for the mobile sensors case. As foreseen, the figure shows the poorest estimation accuracy in the first few time steps, which generally betters with time. This is because, in the first few time instants, the mobile sensors are far away from the target, and as they get closer to it, the performance improves in general. Essentially, only

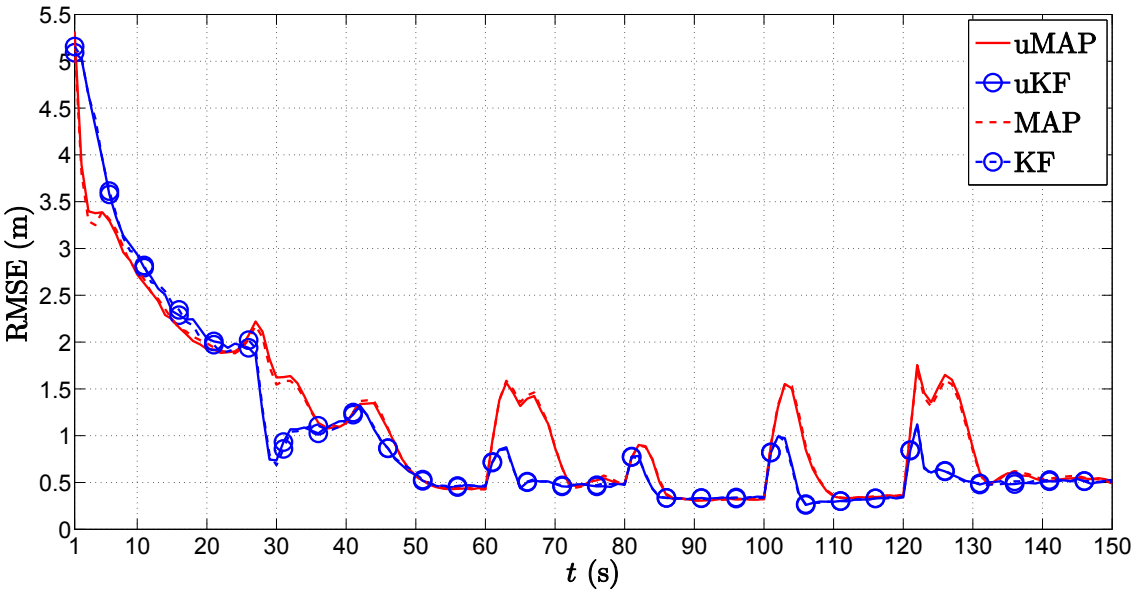

Figure 4.5: RMSE (m) versus t (s) comparison in the first scenario, when $N = 2$, $v_a = 1$ m/s, $\sigma_{n_i} = 9$ dB, $\sigma_{m_i} = 4\frac{\pi}{180}$ rad, $\gamma = 3$, $\gamma_i \sim \mathcal{U}[2.7,3.3]$, $\tau = 5$ m, $P_0 = -10$ dBm, $q = 2.5 \times 10^{-3}\,\mathrm{m}^2/\mathrm{s}^3$, $M_c = 1000$.

at the critical points at which the target takes sharp manoeuvres is where the impairments occur. However, even though we use only $N = 2$ sensors now, due to their mobility, we can see that these deteriorations are notably milder in comparison with the static sensors $N = 3$ case (Fig. 4.2). Moreover, the proposed uKF algorithm slightly outperforms the proposed uMAP. Lastly, the new algorithms show exceptional behaviour even for the case where the PLE and the true mobile sensors' locations are not perfectly known.

It might also be of interest for some applications to get an estimate of the target's transmit power. Hence, in Fig. 4.6 we show the average ML estimate of P_0, $\widehat{\bar{P}}_0$ (dBm), in the first scenario through time t (s) for the mobile sensors case. From Fig. 4.6, we can see that both proposed algorithms provide an excellent estimate of the transmit power in general. Similar with the case of location estimation, the only significant impairments in the power estimates occur at the critical points.

Fig. 4.7 illustrates a realization of the estimation process in the second scenario of the proposed (a) uMAP and (b) uKF algorithm, respectively, when sensor mobility is allowed. As in the first scenario, both proposed algorithms show exceptionally good performance.

Fig. 4.8 depicts the RMSE (m) versus t (s) performance comparison of the proposed algorithms in the second scenario for the mobile sensors case. The figure exhibits that both proposed algorithm require a certain amount of time before they *catch up* with the target, after which their estimation performance is outstanding and quite stable. Furthermore, a somewhat better performance of the proposed uKF can be detected in comparison with the uMAP.

In Fig. 4.9 we present the $\widehat{\bar{P}}_0$ (dBm) versus t (s) performance comparison in the second scenario for the mobile sensors case. Compared with the results in the first scenario, we

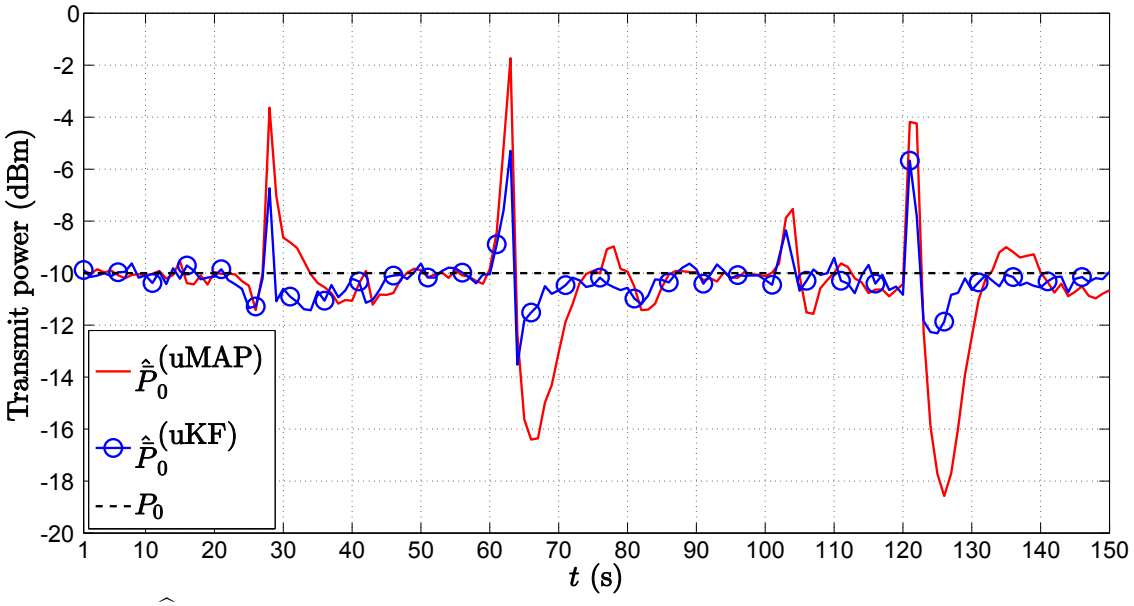

Figure 4.6: $\hat{\hat{P}}_0$ (dBm) versus t (s) comparison in the first scenario, when $N = 2$, $v_a = 0$ m/s, $\sigma_{n_i} = 9$ dB, $\sigma_{m_i} = 4\frac{\pi}{180}$ rad, $\gamma = 3$, $\gamma_i \sim \mathcal{U}[2.7, 3.3]$, $\tau = 5$ m, $P_0 = -10$ dBm, $q = 2.5 \times 10^{-3}\text{m}^2/\text{s}^3$, $M_c = 1000$.

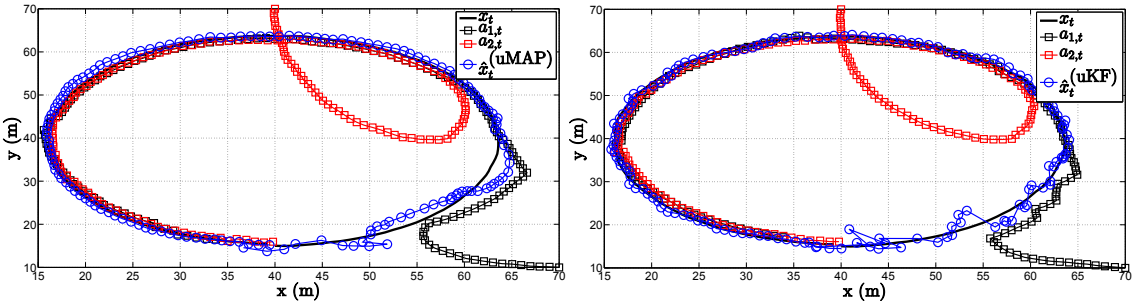

(a) uMAP (b) uKF

Figure 4.7: Illustration of the estimation process in the second scenario, when $N = 2$, $v_a = 1$ m/s, $\sigma_{n_i} = 9$ dB, $\sigma_{m_i} = 4\frac{\pi}{180}$ rad, $\gamma = 3$, $\gamma_i \sim \mathcal{U}[2.7, 3.3]$, $\tau = 5$ m, $P_0 = -10$ dBm, $q = 2.5 \times 10^{-3}\,\text{m}^2/\text{s}^3$.

can see that the estimation accuracy of P_0 is not as good. This result is interesting on its own, and it seems to be an outcome of the specificity of the target's trajectory (constant change of direction). Nonetheless, the detailed analysis of this phenomenon is beyond the scope of this work. Also, it can be noticed that a considerably better P_0 estimate is obtained through the proposed uKF.

It would also be interesting to investigate the influence of the mobile sensor's velocity on the performance of the proposed algorithms. Consequently, we present the $\overline{\text{RMSE}}$ (m) versus v_a (m/s) performance comparison for the first and the second scenario in Fig. 4.10 and Fig. 4.11, respectively. From the figures, it is obvious that the performance of the proposed algorithms depends on sensors' velocities, and one can notice that the performance of all algorithms betters as v_a (m/s) is increased. This is somewhat intuitive,

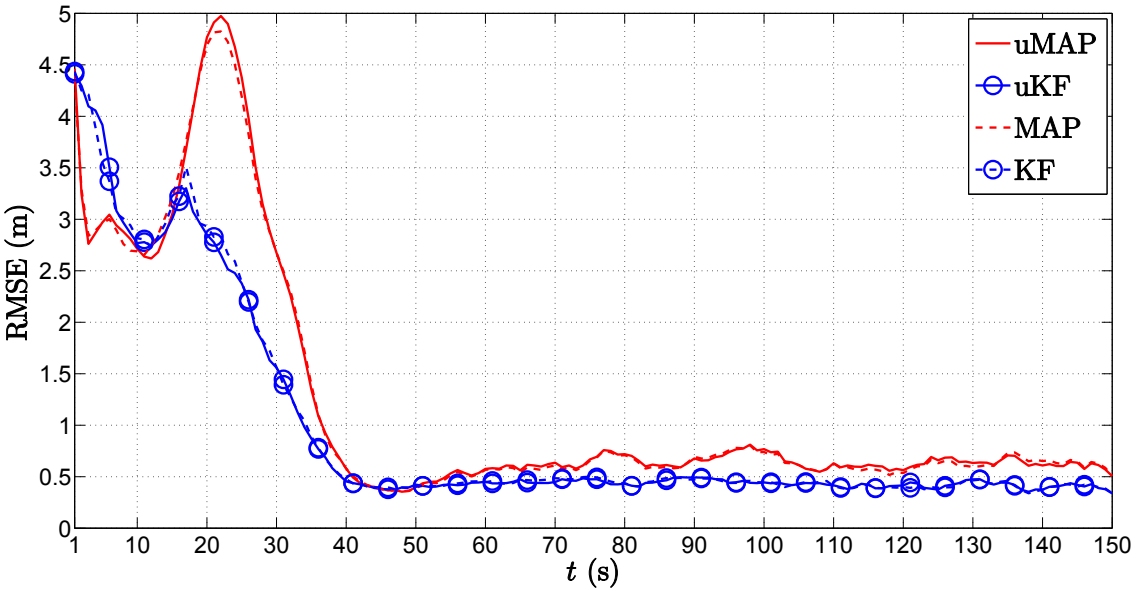

Figure 4.8: RMSE (m) versus t (s) comparison in the second scenario, when $N = 2$, $v_a = 1$ m/s, $\sigma_{n_i} = 9$ dB, $\sigma_{m_i} = 4\frac{\pi}{180}$ rad, $\gamma = 3$, $\gamma_i \sim \mathcal{U}[2.7, 3.3]$, $\tau = 5$ m, $P_0 = -10$ dBm, $q = 2.5 \times 10^{-3}\,\mathrm{m}^2/\mathrm{s}^3$, $M_c = 1000$.

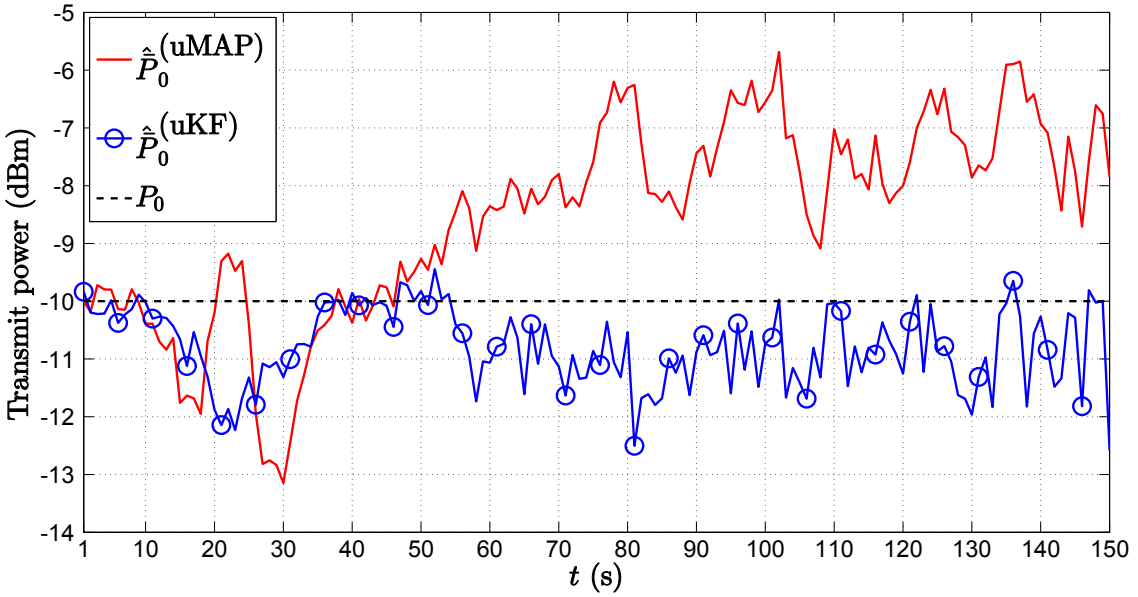

Figure 4.9: $\hat{\bar{P}}_0$ (dBm) versus t (s) comparison in the second scenario, when $N = 2$, $v_a = 0$ m/s, $\sigma_{n_i} = 9$ dB, $\sigma_{m_i} = 4\frac{\pi}{180}$ rad, $\gamma = 3$, $\gamma_i \sim \mathcal{U}[2.7, 3.3]$, $\tau = 5$ m, $P_0 = -10$ dBm, $q = 2.5 \times 10^{-3}\,\mathrm{m}^2/\mathrm{s}^3$, $M_c = 1000$.

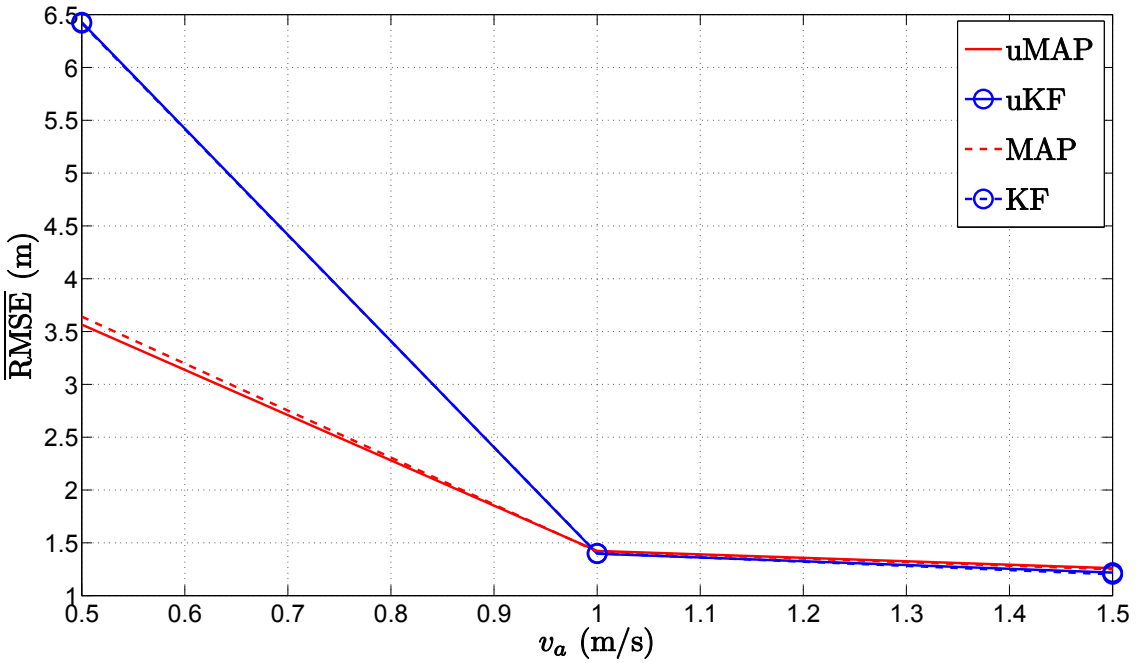

Figure 4.10: $\overline{\text{RMSE}}$ (m) versus v_a (m/s) comparison in the first scenario, when $N = 2$, $\sigma_{n_i} = 9$ dB, $\sigma_{m_i} = 4\frac{\pi}{180}$ rad, $\gamma = 3$, $\gamma_i \sim \mathcal{U}[2.7, 3.3]$, $\tau = 5$ m, $P_0 = -10$ dBm, $q = 2.5 \times 10^{-3}\,\text{m}^2/\text{s}^3$, $M_c = 1000$.

since the mobile sensors *catch* the target more rapidly as they move at higher velocity. Moreover, the overall performance of the proposed algorithms is very good, while for $v_a \geq \boldsymbol{v}_t$ their performance is remarkable.

4.6.2 Real Indoor Experiment

In this section, we assess the performance of our uMAP tracking algorithm through a real indoor experiment, based on the measurements performed in [81]. Fig. 4.12 illustrates the experimental setup of the target tracking scenario. The initial target location is indicated by a red circle and its direction by an arrow. The target passes through the hallways of the building, and at 23 different locations, observations were taken by $N = 7$ anchors, indicated by black squares.

In order to show the advantage of the employed Bayesian approach over the *traditional* ones, Fig. 4.13 illustrates the CDF of the LE (m) of our uMAP algorithm and the sequential WLS localization algorithm. The figure exhibits clearly the superiority of integrating the prior knowledge into an estimator. Our uMAP offers a median error of ME ≈ 2 m, and ME ≤ 3 m in almost 80% of the cases.

4.7 Conclusions

In this section, we have addressed the target tracking problem in WSN where sensor mobility was granted. The mobile sensors made use of not calibrated RSS measurements

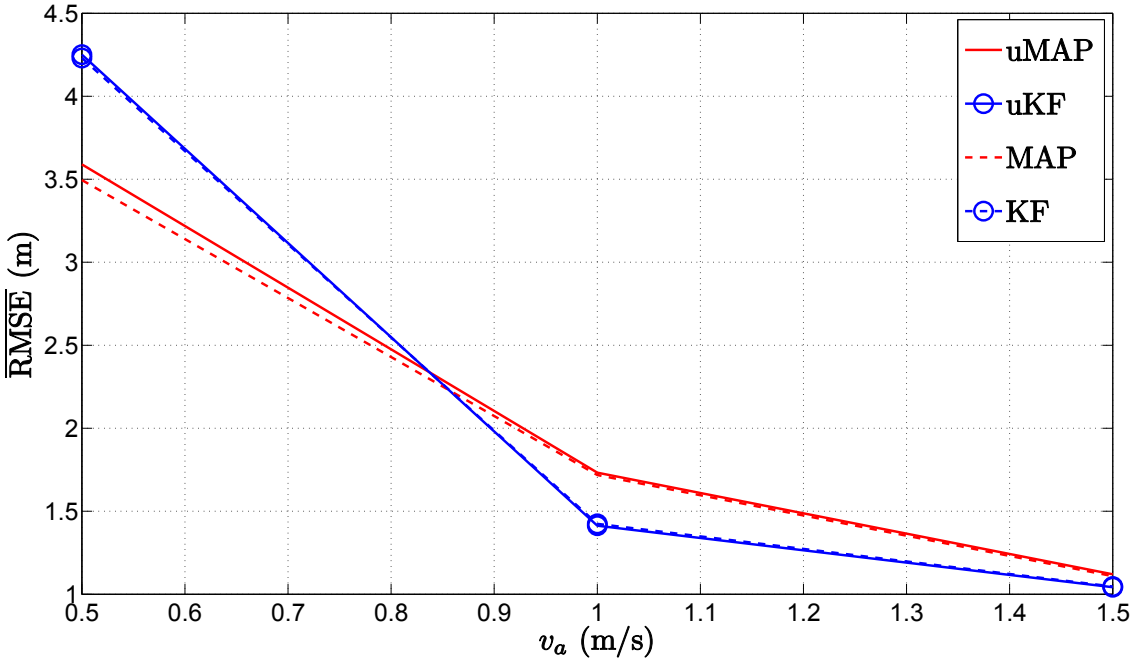

Figure 4.11: $\overline{\text{RMSE}}$ (m) versus v_a (m/s) comparison in the second scenario, when $N = 2$, $\sigma_{n_i} = 9$ dB, $\sigma_{m_i} = 4\frac{\pi}{180}$ rad, $\gamma = 3$, $\gamma_i \sim \mathcal{U}[2.7, 3.3]$, $\tau = 5$ m, $P_0 = -10$ dBm, $q = 2.5 \times 10^{-3}\,\text{m}^2/\text{s}^3$, $M_c = 1000$.

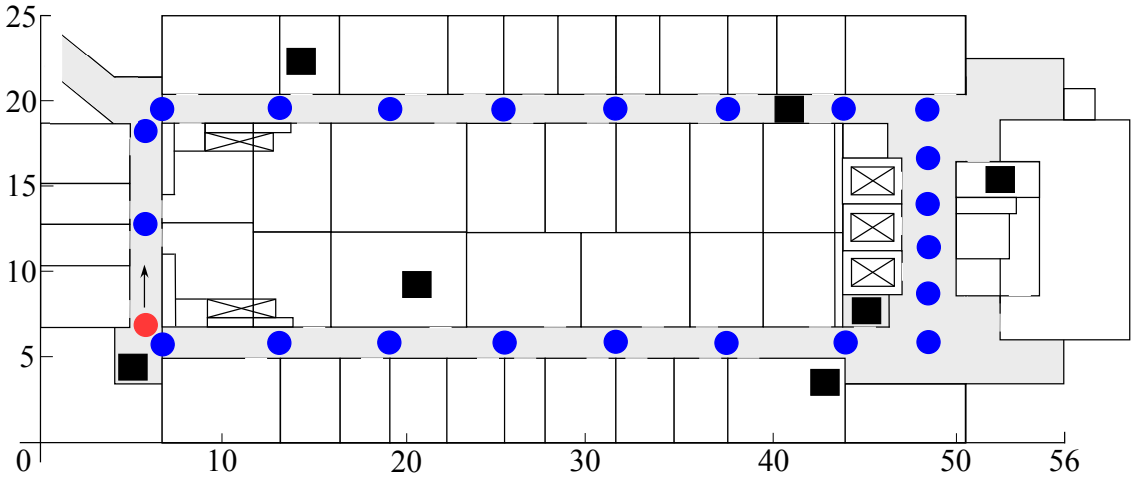

Figure 4.12: Experimental setup for target tracking; the starting point and the direction are indicated by a red circle and an arrow, respectively.

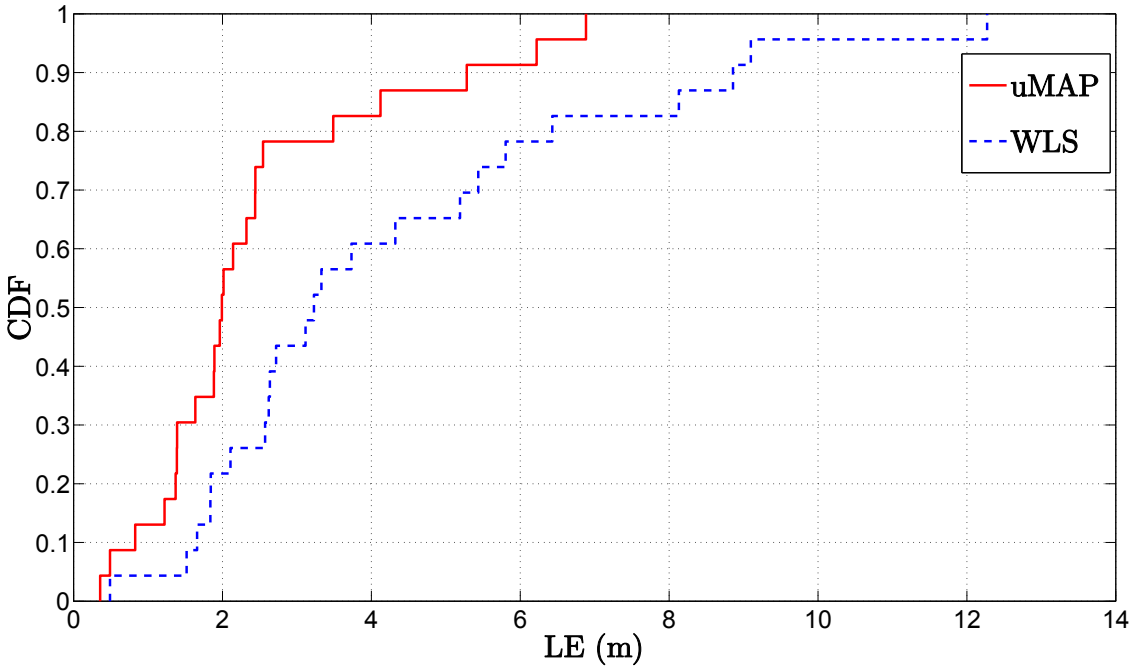

Figure 4.13: CDF of the LE (m) when $N = 7$.

with imperfect knowledge about the PLE and unknown target transmit power, which were combined with AoA observations. We have shown that this highly non-linear measurement model can be *linearized* by applying the described procedure. Then, by following the Bayesian methodology, we have managed to integrate the prior knowledge (extracted from the state transition model) with the observations in order to further ameliorate the estimation accuracy. As a result of our work, two novel tracking algorithms were proposed, namely uMAP and uKF. Furthermore, a simple navigation procedure was proposed, which even further improves the estimation accuracy of our algorithms. The new algorithms were compared with the existing KF algorithm and the classical localization algorithm which neglects the prior knowledge in two different scenarios: where the target took sharp manoeuvres and where the target followed a more smooth trajectory. Extensive simulations have been carried out, and the results have confirmed that incorporation of the prior knowledge into an estimator can significantly improve its estimation accuracy. Also, the simulation results showed that the proposed *linearization* technique offers significant error reduction in comparison with the existing one. Moreover, the simulation results corroborated the usefulness of the proposed mobile sensor navigation routine, demonstrating not only a remarkable improvement in the estimation accuracy, but doing so with a reduced number of sensors. Finally, the proposed algorithms exhibited robustness to not knowing transmit power, as well as to imperfect knowledge about the PLE and the true sensors' locations.

CHAPTER 5

Conclusions and Future Work

This chapter summarizes the major contributions and attained results of the thesis (Section 5.1) and discusses, in further detail, some foreseen directions for future research on this topic (Section 5.2).

5.1 Conclusions

This thesis has studied the problem of target localization in WSN. Two types of networks were considered, non-cooperative and cooperative, for two types of measurements, RSS and hybrid RSS-AoA. In the former type of networks, communication between a target and anchors is granted exclusively, while the latter type allows communication between a target and any sensor within its limited communication range. Also, two categories of algorithm conduction were addressed, centralized and distributed. The former category assumes existence of a central node which collects all information gathered in the network and performs all necessary processing, while in the latter category each target determines its own location by making use of local information only. Furthermore, the problem of tracking of a moving target was also investigated. Both cases of target tracking with static anchors and mobile sensors was of interest.

The common objective of the considered localization problems is to estimate the unknown location of the target by solving optimization problems that represent an excellent framework even under inopportune network configuration and strong measurement noise. A strong emphasis was made on convex relaxations and derivation of convex problems, whose global minima can be readily obtained through general-purpose solvers. Furthermore, the solution obtained through the algorithms could also be used as initial point for iterative methods, in which case the risk of convergence to local minima of these methods is minimized, and near-optimal performance can be obtained. The presented algorithms are

easy to implement and they offer exceptional estimation accuracy in a single (centralized) or just a few (distributed) iterations in general; thus, making them well suited for practical implementation.

An extensive set of simulation results was presented in the thesis, together with a detailed analysis of computational complexity. The simulation results corroborate the effectiveness of the presented algorithms, which not only represent an excellent trade-off between estimation accuracy and computational complexity, but also outperform the AoA in terms of estimation accuracy in general. Various network configurations were studied for a broad spectra of parameter settings, and in all of them the presented algorithms showed exceptional performance and robustness to not knowing additional parameters, beyond the target location. Also, it was shown that measurement fusion offers a significant improvement in terms of estimation accuracy in comparison with *traditional* approach. Moreover, it was shown that by exploiting prior knowledge, when it is possible, within an estimator can remarkably boost its performance. Finally, in the case of real-time target tracking, one could have seen that a simple navigation routine, used to manage sensor's movement, can lead to further error reduction, even when a lower number of sensors is employed for that task.

Finally, the performance of the algorithms presented within the thesis was tested with real indoor experimental data, and the results obtained suggest that our algorithms work well in the considered environment.

5.2 Future Work

There is a number of possibilities for future research. One interesting direction for future research might be development of new and adaptation of the presented algorithms to a more challenging scenarios of indoor localization in severe NLoS environments. NLoS can degrade significantly the localization accuracy, especially in the case where the configuration of the environment is not known, *i.e.*, when it is not known *a priori* which links are LoS and which are NLoS. Instead of trying to distinguish between LoS and NLoS links and disregarding the NLoS ones, because there is always a probability of false alarm or false detection, it would be of interest to exploit the property of positive NLoS bias, which is known to be much larger than the measurement noise.

In this thesis, a constant network topology during the computational phase was taken for granted. A more realistic scenario, where sensors and/or links can fail with a certain probability might be of interest in some applications, especially for distributed algorithms, which are carried out in an iterative fashion. Such a problem would represent a serious challenge for any localization algorithm, as it could lead to network disconnection or even isolated islands of sensors with no or very scarce information insufficient for *good* location estimation.

Similar to the last possibility, in large-scale WSNs, it might of interest to investigate the case where targets limit the number of cooperating nodes. In the case where a target has

a high number of neighbors, we might be interested in selecting only a certain number of its neighbors, by *e.g.*, choosing only the *nearest* ones such that the computational burden is decreased and that its estimation accuracy remains unaffected, or possibly even gets further improved (in the case where one or more very noise links are disregarded). The main challenge in such a problem would be to design an intelligent neighbor-selecting strategy, owing to noisy observations that might mislead a target to disregard a potentially good link and maintain a *bad* one.

In the case of distributed algorithm execution, the design of simple MAC protocols, such as the second-order coloring scheme used in this thesis, could be interesting as it might lead to error and time-execution reduction. This problem was not in the main scope of the thesis, and perhaps we did not exploit its full potential. By designing a more intelligent routine for operating hierarchy (*e.g.*, such that targets with the highest number of anchor neighbors work first) might produce better estimation accuracy and at the same time increase the convergence rate of an algorithm, since one would expect to obtain a *better* estimation for those targets which might propagate inside the network.

The thesis studied the target localization problem by using RSS and combined RSS and AoA measurements. Employing other types of measurements such as ToA, TDoA, frequency or phase of arrival, to name a few, or a combination of them to solve the localization problem might be of interest for future research as well.

For the case of target tracking, this thesis limited its discussion to tracking of a single target. Tracking of multiple targets simultaneously, possibly with sensor cooperation (if practical interest for such a setting exists), might be another direction for future research. Such a setting represents an extremely challenging problem, since many different aspects of the problem have to be taken into consideration, such as preventing physical collision of sensors, signal interference, and computational complexity of such algorithms to name a few.

Another possible direction for future research might be target navigation. By knowing the terrain configuration and by tracking the location of a mobile target, a relatively accurate target navigation could be done. Such an application might be of practical interest in search and rescue missions, exploration in hostile environments and robotics.

This thesis assumed omnidirectional antenna directivity such that the set of all possible solutions belongs to the area formed by an intersection of multiple circle-shaped contours. Although the presented methods work well in all considered scenarios, this assumption might be an oversimplification of the problem, since the antenna radiation pattern is non-isotropic in practice (*e.g.*, antenna radiation pattern depends on antenna geometry configuration - shape and dimension, dielectric material, combination (antenna array), and signal wavelength). Therefore, in practice, the set of all possible solutions belongs to the area formed by intersection of non-circular power contours determined by the antenna pattern. Hence, there seems to be some room for further improvement of the presented algorithms by taking the antenna pattern into consideration when deriving a localization scheme.

Lastly, validation of all potential algorithms and ideas for the described outline through experimental setup would be of great interest. In this thesis, we have used the measurements and scenario from another work, owing to unselfishness and kindness of our colleagues from Rutgers University. However, by doing so, we were very limited to that specific scenario and many times we were in doubt regarding the measurement setting. Thus, it would be of great personal interest for us to conduct an experiment by ourselves and be completely autonomous when validating our ideas.

APPENDIX A

CRB Derivation for RSS Localization

CRB provides a lower bound on the variance of any unbiased estimator, meaning that it is physically impossible to find an unbiased estimator whose variance is less than the bound. CRB offers us a benchmark against which we can compare the performance of any unbiased estimator. If the estimator attains the bound for all values of the unknown parameters, we say that such estimator is the minimum variance unbiased estimator [47].

Let $\boldsymbol{\theta} = \left[\boldsymbol{x}_k^T, P_0, \gamma\right]^T$, $k = 1, ..., M$, denote the $2M+2$ vector of all unknown parameters. According to [47], the variance of any unbiased estimator is lower bounded by $\text{var}(\hat{\boldsymbol{\theta}}_i) \geq \left[\boldsymbol{J}^{-1}(\boldsymbol{\theta})\right]_{ii}$, where $\boldsymbol{J}(\boldsymbol{\theta})$ is the $(2M+2) \times (2M+2)$ Fisher information matrix (FIM). The elements of the FIM are defined as $[\boldsymbol{J}(\boldsymbol{\theta})]_{i,j} = -E\left[\frac{\partial^2 \ln p(\boldsymbol{P}|\boldsymbol{\theta})}{\partial \boldsymbol{\theta}_i \partial \boldsymbol{\theta}_j}\right]$, where $i, j = 1, ..., (2M+2)$, and $p(\boldsymbol{P}|\boldsymbol{\theta})$ is the joint conditional probability density function (pdf) of the observation vector $\boldsymbol{P} = [P_1, ..., P_K]$, given $\boldsymbol{\theta}$.

The FIM is computed as:

$$\boldsymbol{J}(\boldsymbol{\theta}) = \frac{1}{\sigma^2} \sum_{(i,j):(i,j)\in\mathcal{A}} \boldsymbol{f}_{ij} \boldsymbol{f}_{ij}^T + \frac{1}{\sigma^2} \sum_{(i,k):(i,k)\in\mathcal{B}} \boldsymbol{f}_{ik} \boldsymbol{f}_{ik}^T, \tag{A.1}$$

where

$$\boldsymbol{f}_{ij} = \boldsymbol{\rho} - 10\boldsymbol{g} \log_{10} \frac{\|\boldsymbol{D}_i^T \boldsymbol{\theta} - \boldsymbol{a}_j\|}{d_0} + \frac{10\boldsymbol{g}^T \boldsymbol{\theta} d_0}{\ln(10)} \frac{\boldsymbol{D}_i \boldsymbol{D}_i^T \boldsymbol{\theta} - \boldsymbol{D}_i \boldsymbol{a}_j}{\|\boldsymbol{D_i}^T \boldsymbol{\theta} - \boldsymbol{a}_j\|^2},$$

$$\boldsymbol{f}_{ik} = \boldsymbol{\rho} - 10\boldsymbol{g} \log_{10} \frac{\|\boldsymbol{D}_i^T \boldsymbol{\theta} - \boldsymbol{D}_k^T \boldsymbol{\theta}\|}{d_0}$$

$$+ \frac{10\boldsymbol{g}^T \boldsymbol{\theta} d_0}{\ln(10)} \frac{\boldsymbol{D}_i \boldsymbol{D}_i^T \boldsymbol{\theta} - \boldsymbol{D}_i \boldsymbol{D}_k^T \boldsymbol{\theta} - \boldsymbol{D}_k \boldsymbol{D}_i^T + \boldsymbol{D}_k \boldsymbol{D}_k^T \boldsymbol{\theta}}{\|\boldsymbol{D}_i^T \boldsymbol{\theta} - \boldsymbol{D}_k^T \boldsymbol{\theta}\|^2},$$

and $\boldsymbol{\rho} = [\boldsymbol{0}_{2M\times 1}; 1; 0]$, $\boldsymbol{g} = \left[\boldsymbol{0}_{(2M+1)\times 1}; 1\right]$, $\boldsymbol{D}_i = [\boldsymbol{p}_{2i-1}, \boldsymbol{p}_{2i}]$, where $\boldsymbol{p}_i$ represents the i-th column of the identity matrix $\boldsymbol{I}_{2M+2}$.

Therefore, the CRB for the estimate of the source positions is computed as:

$$\mathrm{CRB} = \mathrm{tr}\left(\left[\boldsymbol{J}^{-1}(\boldsymbol{\theta})\right]_{1:2M,1:2M}\right), \tag{A.2}$$

where $[\boldsymbol{M}]_{a:b,c:d}$ represents the submatrix of the matrix $\boldsymbol{M}$ composed of the rows a to b and columns c to d of $\boldsymbol{M}$.

APPENDIX B

Indoor RSS-based Localization

In practice the attenuation in indoor environments is superior than that in outdoor environments due to additional deteriorating caused by obstacles (such as walls, floors and other objects) and multipath fading. Therefore, the propagation model (2.1) is not suitable for indoor localization, and hence, we adopt a different propagation model [51]:

$$P_i = P_0 - L_{w,i} - 10\gamma \log_{10} \frac{\|\boldsymbol{x} - \boldsymbol{s}_i\|}{d_0} + v_i,\ i = 1, ..., N, \tag{B.1}$$

where $L_{w,i}$ is the path-loss term that represents the attenuation caused by partitions and multipath fading. Like the model in [51], we assume that $L_{w,i} = n_{w,i}\gamma_w + u_i\Pi_w$, where $n_{w,i}$ represents the number of partitions that the signal passes through, γ_w is the partition attenuation factor, and $u_i = U\sin(2\pi t/t_u)$ is a random variable that models the varying indoor environment. The samples of t where drawn from the uniform distribution on the interval $[0, t_u]$. Π_w is the indicator function which indicates whether the signal passes through partitions or not, i.e.,

$$\Pi_w = \begin{cases} 0, & \text{if } n_{w,i} = 0; \\ 1, & \text{otherwise.} \end{cases}$$

Letting $\tilde{v}_i = u_i\Pi_w + v_i$ and $\tilde{P}_{0,i} = P_0 - n_{w,i}\gamma_w$, the following problem formulation is obtained

$$P_i = \tilde{P}_{0,i} - 10\gamma \log_{10} \frac{\|\boldsymbol{x} - \boldsymbol{s}_i\|}{d_0} + \tilde{v}_i,\ i = 1, ..., N. \tag{B.2}$$

In [51] it was shown that (B.2) can be expresses in a similar form as (2.1), using some approximations for $\tilde{v}_i$. Applying these approximations, the implementation of the described algorithms for the non-cooperative localization when P_T is known is straightforward for the case of indoor localization.

APPENDIX C

CRB Derivation for RSS-AoA Localization

Let $\boldsymbol{y} = [\boldsymbol{x}_k^T, P_0]^T, k = 1, ..., M$, denote the $3M+1$ vector of all unknown parameters. According to [32], the variance of any unbiased estimator is lower bounded by $\text{var}(\hat{\boldsymbol{y}}) \geq [\boldsymbol{J}^{-1}(\boldsymbol{y})]_{ii}$, where $\boldsymbol{J}(\boldsymbol{y})$ is the $(3M+1)\times(3M+1)$ FIM. The elements of the FIM are defined as $[\boldsymbol{J}(\boldsymbol{y})]_{i,j} = -\mathbb{E}\left[\frac{\partial^2 \ln p(\boldsymbol{\theta}|\boldsymbol{y})}{\partial \boldsymbol{y}_i \partial \boldsymbol{y}_j}\right]$, where $i, j = 1, ..., (3M+1)$, and $p(\boldsymbol{\theta}|\boldsymbol{y})$ is the joint conditional probability density function of the observation vector $\boldsymbol{\theta} = [\boldsymbol{P}^T, \boldsymbol{\phi}^T, \boldsymbol{\alpha}^T]$ ($\boldsymbol{P} = [P_{ij}^{\mathcal{A}}, P_{ik}^{\mathcal{B}}]^T$, $\boldsymbol{\phi} = [\phi_{ij}^{\mathcal{A}}, \phi_{ik}^{\mathcal{B}}]^T$, $\boldsymbol{\alpha} = [\alpha_{ij}^{\mathcal{A}}, \alpha_{ik}^{\mathcal{B}}]^T$), given $\boldsymbol{y}$.

Then, the FIM is computed as:

$$\boldsymbol{J}(\boldsymbol{y}) = \frac{1}{\sigma^2_{n_{ij}}} \sum_{(i,j):(i,j)\in\mathcal{A}} \boldsymbol{h}_{ij}\boldsymbol{h}_{ij}^T + \frac{1}{\sigma^2_{m_{ij}}} \sum_{(i,j):(i,j)\in\mathcal{A}} \boldsymbol{q}_{ij}\boldsymbol{q}_{ij}^T + \frac{1}{\sigma^2_{v_{ij}}} \sum_{(i,j):(i,j)\in\mathcal{A}} \boldsymbol{u}_{ij}\boldsymbol{u}_{ij}^T$$

$$+ \frac{1}{\sigma^2_{n_{ik}}} \sum_{(i,k):(i,k)\in\mathcal{B}} \boldsymbol{h}_{ik}\boldsymbol{h}_{ik}^T + \frac{1}{\sigma^2_{m_{ik}}} \sum_{(i,k):(i,k)\in\mathcal{B}} \boldsymbol{q}_{ik}\boldsymbol{q}_{ik}^T + \frac{1}{\sigma^2_{v_{ik}}} \sum_{(i,k):(i,k)\in\mathcal{B}} \boldsymbol{u}_{ik}\boldsymbol{u}_{ik}^T,$$

where

$$\boldsymbol{h}_{ij} = \boldsymbol{\rho} - \frac{10\gamma d_0}{\ln(10)} \frac{\boldsymbol{E}_i(\boldsymbol{E}_i^T\boldsymbol{y} - \boldsymbol{a}_j)}{\|\boldsymbol{E}_i^T\boldsymbol{y} - \boldsymbol{a}_j\|^2},$$

$$\boldsymbol{q}_{ij} = \frac{\boldsymbol{E}_i\boldsymbol{e}_2(\boldsymbol{e}_1^T\boldsymbol{E}_i^T\boldsymbol{y} - \boldsymbol{e}_1^T\boldsymbol{a}_j) - \boldsymbol{E}_i\boldsymbol{e}_1(\boldsymbol{e}_2^T\boldsymbol{E}_i^T\boldsymbol{y} - \boldsymbol{e}_2^T\boldsymbol{a}_j)}{(\boldsymbol{e}_1^T\boldsymbol{E}_i^T\boldsymbol{y} - \boldsymbol{e}_1^T\boldsymbol{a}_j)^2 + (\boldsymbol{e}_2^T\boldsymbol{E}_i^T\boldsymbol{y} - \boldsymbol{e}_2^T\boldsymbol{a}_j)^2},$$

$$\boldsymbol{u}_{ij} = \frac{\boldsymbol{E}_i(\boldsymbol{e}_3\|\boldsymbol{E}_i^T\boldsymbol{y} - \boldsymbol{a}_j\| - (\boldsymbol{E}_i^T\boldsymbol{y} - \boldsymbol{a}_j)(\boldsymbol{e}_3^T\boldsymbol{E}_i^T\boldsymbol{y} - \boldsymbol{e}_3^T\boldsymbol{a}_j))}{\|\boldsymbol{E}_i^T\boldsymbol{y} - \boldsymbol{a}_j\|^2\sqrt{\|\boldsymbol{E}_i^T\boldsymbol{y} - \boldsymbol{a}_j\|^2 - (\boldsymbol{e}_3^T\boldsymbol{E}_i^T\boldsymbol{y} - \boldsymbol{e}_3^T\boldsymbol{a}_j)^2}},$$

$$\boldsymbol{h}_{ik} = \boldsymbol{\rho} - \frac{10\gamma d_0}{\ln(10)} \frac{(\boldsymbol{E}_i - \boldsymbol{E}_k)(\boldsymbol{E}_i^T\boldsymbol{y} - \boldsymbol{E}_k^T\boldsymbol{y})}{\|\boldsymbol{E}_i^T\boldsymbol{y} - \boldsymbol{E}_k^T\boldsymbol{y}\|^2},$$

$$\boldsymbol{q}_{ik} = \frac{(\boldsymbol{E}_i - \boldsymbol{E}_k)(\boldsymbol{e}_2(\boldsymbol{e}_1^T\boldsymbol{E}_i^T\boldsymbol{y} - \boldsymbol{e}_1^T\boldsymbol{E}_k^T\boldsymbol{y}) - \boldsymbol{e}_1(\boldsymbol{e}_2^T\boldsymbol{E}_i^T\boldsymbol{y} - \boldsymbol{e}_2^T\boldsymbol{E}_k^T\boldsymbol{y}))}{(\boldsymbol{e}_1^T\boldsymbol{E}_i^T\boldsymbol{y} - \boldsymbol{e}_1^T\boldsymbol{E}_k^T\boldsymbol{y})^2 + (\boldsymbol{e}_2^T\boldsymbol{E}_i^T\boldsymbol{y} - \boldsymbol{e}_2^T\boldsymbol{E}_k^T\boldsymbol{y})^2},$$

$$\boldsymbol{u}_{ik} = \frac{(\boldsymbol{E}_i - \boldsymbol{E}_k)(\boldsymbol{e}_3\|\boldsymbol{E}_i^T\boldsymbol{y} - \boldsymbol{E}_k^T\boldsymbol{y}\| - (\boldsymbol{E}_i^T\boldsymbol{y} - \boldsymbol{E}_k^T\boldsymbol{y})(\boldsymbol{e}_3^T\boldsymbol{E}_i^T\boldsymbol{y} - \boldsymbol{e}_3^T\boldsymbol{E}_k^T\boldsymbol{y}))}{\|\boldsymbol{E}_i^T\boldsymbol{y} - \boldsymbol{E}_k^T\boldsymbol{y}\|^2\sqrt{\|\boldsymbol{E}_i^T\boldsymbol{y} - \boldsymbol{E}_k^T\boldsymbol{y}\|^2 - (\boldsymbol{e}_3^T\boldsymbol{E}_i^T\boldsymbol{y} - \boldsymbol{e}_3^T\boldsymbol{E}_k^T\boldsymbol{y})^2}},$$

and $\boldsymbol{\rho} = [\mathbf{0}_{1\times 3M}, 1]^T$, $\boldsymbol{E}_i = [\boldsymbol{e}_{3i-2}, \boldsymbol{e}_{3i-1}, \boldsymbol{e}_{3i}]$, where $\boldsymbol{e}_i$ represents the i-th column of the identity matrix $\boldsymbol{I}_{3M+1}$, and $\boldsymbol{e}_1 = [1, 0, 0]^T$, $\boldsymbol{e}_2 = [0, 1, 0]^T$ and $\boldsymbol{e}_3 = [0, 0, 1]^T$.

Therefore, the CRB for the estimate of the target positions is computed as:

$$\text{CRB} = \text{trace}\left(\left[\boldsymbol{J}^{-1}(\boldsymbol{y})\right]_{1:3M,1:3M}\right),$$

where $[\boldsymbol{M}]_{a:b,c:d}$ represents the sub-matrix of the matrix $\boldsymbol{M}$ composed of the rows a to b and the columns c to d of M.

APPENDIX D

Derivation of the State Transition Model

Consider the following continuous-time state transition model [103].

$$\dot{\boldsymbol{\theta}}(t) = \boldsymbol{A}\boldsymbol{\theta}(t) + \boldsymbol{D}\boldsymbol{u}(t) + \boldsymbol{B}\boldsymbol{r}(t), \;\; \boldsymbol{\theta}(t_0) = \boldsymbol{\theta}_0, \tag{D.1}$$

where $\boldsymbol{\theta}(t) \in \mathbb{R}^n$ is the state vector, $\boldsymbol{u}(t) \in \mathbb{R}^p$ is the vector containing any control inputs (steering angle, throttle setting, breaking force), $\boldsymbol{A} \in \mathbb{R}^{n\times n}$, $\boldsymbol{D} \in \mathbb{R}^{n\times p}$ and $\boldsymbol{B} \in \mathbb{R}^{n\times r}$ are the transition, input gain and noise gain matrices, respectively, and $\boldsymbol{r}(t)$ is a continuous-time process noise with covariance $\boldsymbol{Q}(t)$.

By using Euler's method or zero-order hold [104],[105], we can rewrite the continuous-time state transition model (D.1) for a time-invariant continuous-time system with sampling rate Δ, for initial time $t_0 = t\Delta$ and final time $t_f = (t+1)\Delta$, as

$$\boldsymbol{\theta}(t_f) = \exp\{\boldsymbol{A}(t_f - t_0)\}\boldsymbol{\theta}(t_0) + \int_{t_0}^{t_f} \exp\{\boldsymbol{A}(t_f - \tau)\}\left(\boldsymbol{D}\boldsymbol{u}(\tau) + \boldsymbol{B}\boldsymbol{r}(\tau)\right) d\tau,$$

which is equivalent to

$$\boldsymbol{\theta}(t+1) = \exp\{\boldsymbol{A}\Delta\}\boldsymbol{\theta}(t) + \int_{t\Delta}^{(t+1)\Delta} \exp\{\boldsymbol{A}((t+1)\Delta - \tau)\}\left(\boldsymbol{D}\boldsymbol{u}(\tau) + \boldsymbol{B}\boldsymbol{r}(\tau)\right) d\tau. \tag{D.2}$$

If we assume that the input $\boldsymbol{u}(t)$ changes slowly, relatively to the sampling period, we have $\boldsymbol{u}(t_f) \approx \boldsymbol{u}(t_0)$ for $t_0 \leq t \leq t_f$. Then by changing the variable of integration $\varphi = (t+1)\Delta - \tau$ such that $d\varphi = -d\tau$, (D.2) can be rewritten

$$\begin{aligned}\boldsymbol{\theta}(t+1) &= \exp\{\boldsymbol{A}\Delta\}\boldsymbol{\theta}(t) + \textstyle\int_{\Delta}^{0} \exp\{\boldsymbol{A}\varphi\}\boldsymbol{D}(-d\varphi)\boldsymbol{u}(t) \\ &\quad + \textstyle\int_{t\Delta}^{(t+1)\Delta} \exp\{\boldsymbol{A}((t+1)\Delta - \tau)\}\boldsymbol{B}\boldsymbol{r}(\tau)d\tau \\ &= \exp\{\boldsymbol{A}\Delta\}\boldsymbol{\theta}(t) + \textstyle\int_{0}^{\Delta} \exp\{\boldsymbol{A}\varphi\}\boldsymbol{D}d\varphi\boldsymbol{u}(t) + \int_{t\Delta}^{(t+1)\Delta} \exp\{\boldsymbol{A}((t+1)\Delta - \tau)\}\boldsymbol{B}\boldsymbol{r}(\tau)d\tau,\end{aligned} \tag{D.3}$$

and the state model (D.1) can be *discretized* as

$$\boldsymbol{\theta}_{t+1} = \boldsymbol{S}\boldsymbol{\theta}_t + \boldsymbol{G}\boldsymbol{u}_t + \boldsymbol{r}_t,$$

where

$$\boldsymbol{S} = \exp\{\boldsymbol{A}\Delta\}, \tag{D.4}$$

$$\boldsymbol{G} = \int_0^{\Delta} \exp\{\boldsymbol{A}\varphi\}\boldsymbol{D}d\varphi,$$

$$\boldsymbol{r}_t = \int_{t\Delta}^{(t+1)\Delta} \exp\{\boldsymbol{A}((t+1)\Delta - \tau)\}\boldsymbol{B}\boldsymbol{r}(\tau)d\tau. \tag{D.5}$$

The process noise, $\boldsymbol{r}(t)$, is assumed to be zero-mean and white Gaussian, and the *discretized* process noise, $\boldsymbol{r}_t$, retains the same characteristics [103], *i.e.*,

$$E[\boldsymbol{r}_t] = 0, \;\; E\left[\boldsymbol{r}_t \boldsymbol{r}_t^T\right] = \boldsymbol{Q}_t \delta_t,$$

where δ_t represents a Dirac impulse, and the covariance of the state process noise is given, according to (D.5), as

$$\boldsymbol{Q}_t = \int_0^{\Delta} \exp\{\boldsymbol{A}((t+1)\Delta - \tau)\}\boldsymbol{B}\boldsymbol{Q}\boldsymbol{B}^T \exp\left\{\boldsymbol{A}^T((t+1)\Delta - \tau)\right\}d\tau, \tag{D.6}$$

and $\boldsymbol{Q} = \mathrm{diag}([q, q])$, with q denoting a tuning parameter for the state process noise intensity.

Since this thesis assumes a 2-dimensional constant velocity model, the continuous-time target state model (D.1) can be simplified [103] as

$$\dot{\boldsymbol{\theta}}(t) = \boldsymbol{A}\boldsymbol{\theta}(t) + \boldsymbol{B}\boldsymbol{r}(t), \tag{D.7}$$

where

$$\boldsymbol{A} = \begin{bmatrix} 0 & 0 & 1 & 0 \\ 0 & 0 & 0 & 1 \\ 0 & 0 & 0 & 0 \\ 0 & 0 & 0 & 0 \end{bmatrix}, \; \boldsymbol{B} = \begin{bmatrix} 0 & 0 \\ 0 & 0 \\ 1 & 0 \\ 0 & 1 \end{bmatrix},$$

and $\boldsymbol{r}(t) \sim \mathcal{N}(\boldsymbol{0}, \boldsymbol{Q})$.

The discrete-time model equivalent to the above one is described by

$$\boldsymbol{\theta}_{t+1} = \boldsymbol{S}\boldsymbol{\theta}_t + \boldsymbol{r}_t, \tag{D.8}$$

where, by solving (D.4) and (D.6) respectively, we get

$$\boldsymbol{S} = \begin{bmatrix} 1 & 0 & \Delta & 0 \\ 0 & 1 & 0 & \Delta \\ 0 & 0 & 1 & 0 \\ 0 & 0 & 0 & 1 \end{bmatrix}, \; \boldsymbol{Q} = q \begin{bmatrix} \frac{\Delta^3}{3} & 0 & \frac{\Delta^2}{2} & 0 \\ 0 & \frac{\Delta^3}{3} & 0 & \frac{\Delta^2}{2} \\ \frac{\Delta^2}{2} & 0 & \Delta & 0 \\ 0 & \frac{\Delta^2}{2} & 0 & \Delta \end{bmatrix}.$$

Bibliography

[1] N. Patwari, "Location estimation in sensor networks", PhD thesis, University of Michigan, Jul. 2005.

[2] Y. Singh, S. Saha, U. Chugh, and C. Gupt, "Distributed event detection in wireless sensor networks for forest fires", in *UKSim*, Cambridge, UK, Apr. 2013, pp. 634–639.

[3] Z. Rongbai and C. Guohua, "Research on major hazard installations monitoring system based on WSN", in *ICFCC*, Wuhan, Hubei, China, May 2010, V1–741–V1–745.

[4] Z. Dai, S. Wang, and Z. Yan, "BSHM-WSN: a wireless sensor network for bridge structure health monitoring", in *ICMIC*, Wuhan, Hubei, China, Jun. 2012, pp. 708–712.

[5] L. Blazevic, J. Y. Le Boudec, and S. Giordano, "A location-based routing method for mobile ad hoc networks", *IEEE Trans. Mobile Computing*, vol. 4, no. 2, 97–110, 2005.

[6] L. Ghelardoni, A. Ghio, and D. Anguita, "Smart underwater wireless sensor networks", in *IEEEI*, Eilat, Israel, Nov. 2012, pp. 1–5.

[7] T. He, S. Krishnamurthy, J. A. Stankovic, T. Abdelzaher, L. Luo, R. Stoleru, T. Yan, and L. Gu, "Energy-efficient surveillance system using wireless sensor networks", in *MobiSys*, Boston, MA, USA, Jun. 2004, pp. 1–14.

[8] M. D. Dikaiakos, A. Florides, T. Nadeem, and L. Iftode, "Location-aware services over vehicular ad-hoc networks using car-to-car communication", *IEEE J. Selected Areas in Commun.*, vol. 25, no. 8, pp. 1590–1602, 2007.

[9] M. Faschinger, C. R. Sastry, A. H. Patel, and N. C. Tas, "An RFID and wireless sensor network-based implementation of workflow optimization", in *WoWMoM*, Helsinki, Finland, Jun. 2007, pp. 1–8.

[10] N. Deshpande, E. Grant, and T. C. Henderson, "Target-directed navigation using wireless sensor networks and implicit surface interpolation", in *ICRA*, Saint Paul, Minnesota, USA, May 2012, pp. 457–462.

[11] E. Xu, Z. Ding, and S. Dasgupta, "Target tracking and mobile sensor navigation in wireless sensor networks", *IEEE Trans. Mobile Comput.*, vol. 12, no. 1, pp. 177–186, 2013.

[12] N. Deshpande, E. Grant, and T. C. Henderson, "Target localization and autonomous navigation using wireless sensor networks–a pseudogradient algorithm approach", *IEEE Systems Journal*, vol. 8, no. 1, pp. 93–103, 2014.

[13] P. G. Kandhare and G. M. Bhandari, "Guidance providing navigation in target tracking for wireless sensor networks", *IJSR*, vol. 4, no. 6, pp. 2795–2798, 2015.

[14] Z. Sahinoglu, S. Gezici, and I. Güvenc, *Ultra-wideband Positioning Systems: Theoretical Limits, Ranging Algorithms, and Protocols*, 1st Ed. Cambridge University Press, NY, USA, 2008.

[15] L. Buttyán and J. P. Hubaux, *Security and Cooperation in Wireless Networks: Thwarting Malicious and Selfish Behavior in the Age of Ubiquitous Computing*, 1st Ed. Cambridge University Press, NY, USA, 2007.

[16] N. Patwari, J. N. Ash, S. Kyperountas, A. O Hero III, R. L. Moses, and N. S. Correal, "Locating the nodes: cooperative localization in wireless sensor networks", *IEEE Signal Process. Mag.*, vol. 22, no. 4, pp. 54–69, 2005.

[17] F. Bandiera, A. Coluccia, and G. Ricci, "A cognitive algorithm for received signal strength based localization", *IEEE Trans. Signal Process.*, vol. 63, no. 7, pp. 1726–1736, 2015.

[18] G. Destino, "Positioning in wireless networks: noncooperative and cooperative algorithms", PhD thesis, University of Oulu, Oct. 2012.

[19] J. He, Y. Geng, and K. Pahlavan, "Toward accurate human tracking: modeling time-of-arrival for wireless wearable sensors in multipath environment", *IEEE Sensors Journal*, vol. 14, no. 11, pp. 3996–4006, 2014.

[20] X. Qua and L. Xie, "An efficient convex constrained weighted least squares source localization algorithm based on TDoA measurements", *Elsevier Sign. Process.*, vol. 16, no. 119, pp. 142–152, 2016.

[21] J. Cota-Ruiz, J. G. Rosiles, P. Rivas-Perea, and E. Sifuentes, "A distributed localization algorithm for wireless sensor networks based on the solution of spatially-constrained local problems", *IEEE Sensors Journal*, vol. 13, no. 6, pp. 2181–2191, 2013.

[22] Y. Wang and K. C. Ho, "An asymptotically efficient estimator in closed-form for 3D AoA localization using a sensor network", *IEEE Trans. Wirel. Commun.*, vol. 14, no. 12, pp. 6524–6535, 2015.

[23] S. Tomic, M. Beko, and R. Dinis, "Distributed RSS-based localization in wireless sensor networks based on second-order cone programming", *MDPI Sensors*, vol. 14, no. 10, pp. 18 410–18 432, 2014.

[24] N. Salman, M. Ghogho, and A. H. Kemp, "Optimized low complexity sensor node positioning in wireless sensor networks", *IEEE Sensors Journal*, vol. 14, no. 1, pp. 39–46, 2014.

[25] N. Bulusu, J. Heidemann, and D. Estrin, "GPS-less low cost outdoor localization for very small devices", *IEEE Personal Commun. Mag.*, vol. 7, no. 5, pp. 28–34, 2000.

[26] A. Bahillo, S. Mazuelas, R. M. Lorenzo, P. Fernández, J. Prieto, R. J. Durán, and E. J. Abril, "Hybrid RSS-RTT localization scheme for indoor wireless networks", *EURASIP J. Advances in Sign. Process.*, vol. 10, no. 1, pp. 1–12, 2010.

[27] N. Alam and A. G. Dempster, "Cooperative positioning for vehicular networks: facts and future", *IEEE Trans. Intelligent Transportation Systems*, vol. 14, no. 9, pp. 1708–1717, 2013.

[28] U. Hatthasin, S. Thainimit, K. Vibhatavanij, N. Premasathian, and D. Worasawate, "The use of RTOF and RSS for a one base station RFID system", *IJCSNS*, vol. 10, no. 7, pp. 184–195, 2010.

[29] T. Gädeke, J. Schmid, J. J. M. Krüge and, W. Stork, and K. D. Müller-Glaser, "A bi-modal ad-hoc localization scheme for wireless networks based on RSS and ToF fusion", in *WPNC*, Dresden, Germany, Mar. 2013, pp. 1–6.

[30] K. Yu, "3-D localization error analysis in wireless networks", *IEEE Trans. Wireless Commun.*, vol. 6, no. 10, pp. 3473–3481, 2007.

[31] S. Wang, B. R. Jackson, and R. Inkol, "Hybrid RSS/AoA emitter location estimation based on least squares and maximum likelihood criteria", in *IEEE QBSC*, Kingston, ON, Canada, Jun. 2012, pp. 24–29.

[32] L. Gazzah, L. Najjar, and H. Besbes, "Selective hybrid RSS/AoA weighting algorithm for NLoS intra cell localization", in *IEEE WCNC*, Istanbul, Turkey, Apr. 2014, pp. 2546–2551.

[33] Y. T. Chan, F. Chan, W. Read, B. R. Jackson, and B. H. Lee, "Hybrid localization of an emitter by combining angle-of-arrival and received signal strength measurements", in *IEEE CCECE*, Toronto, ON, Canada, May 2014, pp. 1–5.

[34] S. Tomic, M. Marikj, M. Beko, R. Dinis, and N. Orfao, "Hybrid RSS-AoA technique for 3-D node localization in wireless sensor networks", in *IEEE IWCMC*, Dubrovnik, Croatia, Apr. 2015, pp. 1277–1282.

[35] C. Cheng, W. Hu, and W. P. Tay, "Localization of a moving non-cooperative RF target in NLoS environment using RSS and AoA measurements", in *IEEE ICASSP*, South Brisbane, Queensland, Australia, Apr. 2015, pp. 3581–3585.

[36] S. Tomic, M. Beko, and R. Dinis, "3-D target localization in wireless sensor network using RSS and AoA measurement", *IEEE Trans. Vehic. Technol.*, vol. 66, no. 4, pp. 3197–3210, 2017.

[37] A. Singh, S. Kumar, and O. Kaiwartya, "A hybrid localization algorithm for wireless sensor networks", in *ICRTC*, Ghaziabad India, Mar. 2015, pp. 1432–1439.

[38] S. Tomic, M. Beko, and R. Dinis, "Distributed RSS-AoA based localization with unknown transmit powers", *IEEE Wirel. Commun. Letters*, vol. 5, no. 4, pp. 392–395, 2016.

[39] S. Sundhar Ram, A. Nedić, and V. V. Veeravalli, "Distributed subgradient projection algorithm for convex optimization", in *IEEE ICASSP*, Taipei, Taiwan, Apr. 2009, pp. 3653–3656.

[40] I. Guvenc and C. C. Chong, "A survey on ToA based wireless localization and NLoS mitigation techniques", *IEEE Commun. Survey and Tutorials*, vol. 11, no. 3, pp. 107–124, 2009.

[41] J. Blumenthal, R. Grossmann, F. Golatowski, and D. Timmermann, "Weighted centroid localization in zigbee-based sensor networks", in *WISP*, Alcala de Henares, Spain, Oct. 2007, pp. 1–6.

[42] M. Brunato and R. Battiti, "Statistical learning theory for location fingerprinting in wireless LANs", *Elsevier, J. Computer Networks*, vol. 47, no. 6, pp. 825–845, 2005.

[43] Y. Chen, "Network localization and navigation: theoretical framework, efficient operation, and security assurance", PhD thesis, Massachusetts Institute of Technology, Jun. 2014.

[44] D. E. Manolakis, "Efficient solution and performance analysis of 3-D position estimation by trilateration", *IEEE Trans. Aerospace and Electronic Systems*, vol. 32, no. 4, pp. 1239–1248, 1996.

[45] A. H. Sayed, A. Tarighat, and N. Khajehnouri, "Network-based wireless location", *IEEE Sign. Process. Mag.*, vol. 22, no. 40, pp. 24–40, 2005.

[46] B. T. Fang, "Simple solutions for hyperbolic and related position fixes", *IEEE Trans. Aerospace and Electronic Systems*, vol. 26, no. 5, pp. 748–758, 1990.

[47] S. M. Kay, *Fundamentals of Statistical Signal Processing: Estimation Theory*, 1st Ed. Prentice Hall Upper Saddle River, NJ, USA, 1993.

[48] X. Li, "Collaborative localization with received-signal strength in wireless sensor networks", *IEEE Trans. Veh. Technol.*, vol. 56, no. 6, 3807–3817, 2007.

[49] K. W. K. Lui, W. K. Ma, H. C. So, and F. K. W. Chan, "Semi-definite programming algorithms for sensor network node localization with uncertainties in anchor positions and/or propagation speed", *IEEE Trans. Signal Process.*, vol. 57, no. 2, pp. 752–763, 2009.

[50] R. W. Ouyang, A. K. S. Wong, and C. T. Lea, "Received signal strength-based wireless localization via semidefinite programming: noncooperative and cooperative schemes", *IEEE Trans. Veh. Technol.*, vol. 59, no. 3, pp. 1307–1318, 2010.

[51] G. Wang and K. Yang, "A new approach to sensor node localization using RSS measurements in wireless sensor networks", *IEEE Trans. Wireless Commun.*, vol. 10, no. 5, pp. 1389–1395, 2011.

[52] R. M. Vaghefi, M. R. Gholami, and E. G. Ström, "RSS-based sensor localization with unknown transmit power", in *IEEE ICASSP*, Prague, Czech Republic, Apr. 2011, pp. 2480–2483.

[53] H. Chen, G. Wang, Z. Wang, H. C. So, and H. V. Poor, "Non-line-of-sight node localization based on semi-definite programming in wireless sensor networks", *IEEE Trans. Wireless Commun.*, vol. 11, no. 1, pp. 108–116, 2012.

[54] G. Wang, H. Chen, Y. Li, and M. Jin, "On received-signal-strength based localization with unknown transmit power and path loss exponent", *IEEE Wireless Commun. Letters*, vol. 1, no. 5, pp. 536–539, 2012.

[55] S. Tomic, M. Beko, R. Dinis, and V. Lipovac, "RSS-based localization in wireless sensor networks using SOCP relaxation", in *IEEE ICASSP*, Darmstadt, Germany, Jun. 2013, pp. 749–753.

[56] R. M. Vaghefi, R. M. B. M. R. Gholami, and E. G. Ström, "Cooperative received signal strength-based sensor localization with unknown transmit powers", *IEEE Trans. Signal Process.*, vol. 61, no. 6, pp. 1389–1403, 2013.

[57] S. Boyd and L. Vandenberghe, *Convex Optimization*, 1st Ed. Cambridge University Press, Cambridge, UK, 2004.

[58] T. S. Rappaport, *Wireless Communications: Principles and Practice*, 1st Ed. Prentice Hall Upper Saddle River NJ, USA, 1996.

[59] M. L. Sichitiu and V. Ramadurai, "Localization of wireless sensor networks with a mobile beacon", in *IEEE MASS*, Fort Lauderdale, FL, USA, Oct. 2004, pp. 174–183.

[60] N. Patwari, R. J. O'Dea, and Y. Wang, "Relative location in wireless networks", in *IEEE VTC*, Birmingham, AL, USA, May 2001, pp. 1149–11 153.

[61] P. Oguz-Ekim, J. Gomes, J. Xavier, and P. Oliveira, "A convex relaxation for approximate maximum-likelihood 2D source localization from range measurements", in *IEEE ICASSP*, Dallas, TX, USA, Mar. 2010, pp. 1–4.

[62] M. Grant and S. Boyd, *CVX: matlab software for disciplined convex programming*, 2003. [Online]. Available: `http://cvxr.com/cvx`.

[63] I. Pólik and T. Terlaky, *Interior point methods for nonlinear optimization*, 2010.

[64] J. Lofberg, "Dualize it: software for automatic primal and dual conversions of conic programs", *Optim. Meth. Softw*, vol. 24, no. 3, pp. 313–325, 2009.

[65] J. F. Sturm, "Using SeDuMi 1.02, a MATLAB toolbox for optimization over symmetric cones", *Optim. Meth. Softw*, vol. 11, no. 1, pp. 625–653, 1999.

[66] N. Salman, M. Ghogho, and A. H. Kemp, "On the joint estimation of the RSS-based location and path-loss exponent", *IEEE Wireless Commun. Lett.*, vol. 1, no. 1, pp. 34–37, 2012.

[67] B. Béjar and S. Zazo, "A practical approach for outdoor distributed target localization in wireless sensor networks", *EURASIP J. Advances in Sign. Process.*, vol. 12, no. 95, pp. 1–11, 2012.

[68] A. Bel, J. L. Vicario, and G. Seco-Granados, "Localization algorithm with on-line path loss estimation and node selection", *MDPI Sensors*, vol. 11, no. 7, pp. 6905–6925, 2011.

[69] S. C. Ergen and P. Varaiya, "TDMA scheduling algorithms for wireless sensor networks", *Wireless Networks*, vol. 16, no. 4, 985–997, 2010.

[70] J. F. C. Mota, J. M. F. Xavier, P. M. Q. Aguiar, and M. Püschel, "D-ADMM: a communication-efficient distributed algorithm for separable optimization", *Wireless Networks*, vol. 61, no. 10, 2718–2723, 2013.

[71] L. Xiao and S. Boyd, "Fast linear iterations for distributed averaging", in *IEEE CDC*, Chiba-shi, Japan, Dec. 2003, pp. 4997–5002.

[72] A. J. Martin, "Towards an energy complexity of computations", *Information Process. Letters*, vol. 77, no. 2-4, 181–187, 2001.

[73] S. Tomic, M. Beko, and R. Dinis, "RSS-based localization in wireless sensor networks using convex relaxation: noncooperative and cooperative schemes", *IEEE Trans. Veh. Technol.*, vol. 64, no. 5, pp. 2037–2050, 2015.

[74] P. Biswas, T. C. Lian, T. C. Wang, and Y. Ye, "Semidefinite programming based algorithms for sensor network localization", *ACM Trans. Sensor Networks*, vol. 2, no. 2, pp. 188–220, 2006.

[75] R. Fletcher, *Practical Methods of Optimization*, 1st Ed. John Wiley & Sons, Chichester, UK, 1987.

[76] P. Biswas, H. Aghajan, and Y. Ye, "Semidefinite programming algorithms for sensor network localization using angle of arrival information", in *Asilomar Conference on Signals, Systems, and Computers*, Pacific Grove, CA, USA, Oct. 2005, pp. 220–224.

[77] M. B. Ferreira, *Hybrid indoor localization based on ranges and video*, MSc Thesis, Universidade Técnica de Lisboa, 2014.

[78] M. B. Ferreira, J. Gomes, and J. P. Costeira, "A unified approach for hybrid source localization based on ranges and video", in *IEEE ICASSP*, South Brisbane, Queensland, Australia, Apr. 2015, pp. 2879–2883.

[79] M. B. Ferreira, J. Gomes, C. Soares, and J. P. Costeira, "Collaborative localization of vehicle formations based on ranges and bearings", in *UComms*, Lerici, Italy, Apr. 2016, pp. 1–5.

[80] Z. Xiang and U. Ozguner, "A 3-D positioning system for off-road autonomous vehicles", in *IEEE IV*, Las Vegas, NV, USA, Jun. 2005, pp. 130–134.

[81] D. Niculescu and B. Nath, "VOR base stations for indoor 802.11 positioning", in *ACM MobiCom*, Philadelphia, PA, USA, Sep. 2004, pp. 58–69.

[82] I. J. Myung, "Tutorial on maximum likelihood estimation", *J. Mathematical Psychology*, vol. 47, no. 1, pp. 90–100, 2003.

[83] A. Beck, P. Stoica, and J. Li, "Exact and approximate solutions of source localization problems", *IEEE Trans. Signal Process.*, vol. 56, no. 5, pp. 1770–1778, 2008.

[84] J. J. More, "Generalization of the trust region problem", *Optim. Meth. and Soft.*, vol. 2, no. 3-4, pp. 189–209, 1993.

[85] A. F. Molisch, *Wireless Communications*, 2nd Ed. John WIley & Sons Ltd., Chichester, UK, 2011.

[86] T. Eren, O. Goldenberg, W. Whiteley, Y. R. Yang, A. S. Morse, B. D. Anderson, and P. N. Belhumeur, "Rigidity, computation, and randomization in network localization", in *INFOCOM*, Hong Kong, Mar. 2004, pp. 2673–2684.

[87] G. Oliva, F. Pascucci, S. Panzieri, and R. Setola, "Sensor network localization: extending trilateration via shadow edges", *IEEE Trans. Autom. Control*, vol. 60, no. 10, pp. 2752–2755, 2015.

[88] A. Sahin, Y. S. Eroglu, I. Guvenc, N. Pala, and M. Yuksel, "Accuracy of AoA-based and RSS-based 3D localization for visible light communications", in *IEEE VTC*, Boston, MA, USA, Sep. 2015, pp. 1–5.

[89] B. D. S. Muswieck, J. L. Russi, and M. V. T. Heckler, "Hybrid method uses RSS and AoA to establish a low-cost localization system", in *SASE/CASE*, Buenos Aires, Argentina, Aug. 2013, pp. 1–6.

[90] E. Elnahrawy, J. A. Francisco, and R. P. Martin, "Adding angle of arrival modality to basic RSS location management techniques", in *ISWPC*, San Juan, PR, USA, Feb. 2007, pp. 1–6.

[91] D. Dardari, P. Closas, and P. M. Djuric, "Indoor tracking: theory, methods, and technologies", *IEEE Trans. Vehic. Technol.*, vol. 64, no. 4, pp. 1263–1278, 2016.

[92] J. P. Beaudeau, M. F. Bugallo, and P. M. Djuric, "RSSI-based multi-target tracking by cooperative agents using fusion of cross-target information", *IEEE Trans. Sign. Process.*, vol. 63, no. 19, pp. 5033–5044, 2015.

[93] E. Masazade, R. Niu, and P. K. Varshney, "Dynamic bit allocation for object tracking in wireless sensor networks", *IEEE Trans. Sign. Process.*, vol. 60, no. 10, pp. 5048–5063, 2012.

[94] S. Tomic, M. Beko, R. Dinis, M. Tuba, and N. Bacanin, "Bayesian methodology for target tracking using RSS and AoA measurements", *submitted to Elsevier Ad Hoc Networks*, vol. PP, no. 99, pp. 1–1, 2016.

[95] M. W. Khan, A. H. Kemp, N. Salman, and L. S. Mihaylova, "Tracking of wireless mobile nodes in the presence of unknown path-loss characteristics", in *Fusion*, Washington DC, USA, Jul. 2015, pp. 104–111.

[96] M. W. Khan, N. Salman, A. Ali, A. M. Khan, and A. H. Kemp, "A comparative study of target tracking with kalman filter, extended kalman filter and particle filter using received signal strength measurements", in *ICET*, Peshawar, Pakistan, Dec. 2015, pp. 1–6.

[97] B. K. Chalise, Y. D. Zhanga, M. G. Amina, and B. Himed, "Target localization in a multi-static passive radar system through convex optimization", *Elsevier Sign. Process.*, vol. 14, no. 102, pp. 207–215, 2014.

[98] S. Tomic, M. Beko, R. Dinis, and P. Montezuma, "Distributed algorithm for target localization in wireless sensor networks using RSS and AoA measurements", *Elsevier Perv. Mobile Comput.*, vol. 37, no. 1, pp. 63–77, 2017.

[99] S. K. Meghani, M. Asif, and S. Amir, "Localization of WSN node based on time of arrival using ultra wide band spectrum", in *WAMICON*, Cocoa Beach, Florida, USA, Apr. 2012, pp. 1–4.

[100] S. Tomic, M. Beko, R. Dinis, and P. Montezuma, "A closed-form solution for RSS/AoA target localization by spherical coordinates conversion", *IEEE Wirel. Commun. Letters*, vol. 5, no. 6, pp. 680–683, 2016.

[101] Y. Zou and K. Chakrabarty, "Distributed mobility management for target tracking in mobile sensor networks", *IEEE Trans. Mobile Comput.*, vol. 6, no. 8, pp. 872–887, 2007.

[102] G. Wang, Y. Li, and M. Jin, "On MAP-based target tracking using range-only measurements", in *CHINACOM*, Guilin, China, Aug. 2013, pp. 1–6.

[103] J. B. B. Gomes, *An overview on target tracking using multiple model methods*, MSc Thesis, Universidade Técnica de Lisboa, 2008.

[104] R. G. Brown and P. Y. C. Hwang, *Introduction to Random Signals and Applied Kalman Filtering*, 3rd Ed. WIley, NY, USA, 1997.

[105] Y. Bar-Shalom and X. R. Li, *Estimation with Applications to Tracking and Navigation*, 1st Ed. John WIley & Sons Inc., NY, USA, 2001.